Stimuli-Responsive Self-Assembly and Spatial Functionalization of Organic Cages Based on Tribenzotriquinacenes

Dissertation zur Erlangung des

naturwissenschaftlichen Doktorgrades

der Julius-Maximilians-Universität Würzburg

vorgelegt von

Ayan Dhara

aus Singarkone, Indien

Würzburg 2017

Eingereicht bei der Fakultät für Chemie und Pharmazie am:

 11.09.2017

Gutachter der schriftlichen Arbeit:

1. Gutachter: Priv.-Doz. Dr. Florian Beuerle

2. Gutachter: Prof. Dr. Frank Würthner

Prüfer des öffentlichen Promotionskolloquiums:

1. Prüfer: Priv.-Doz. Dr. Florian Beuerle

2. Prüfer: Prof. Dr. Frank Würthner

3. Prüfer: Prof. Dr. Udo Radius

Datum des öffentlichen Promotionskolloquiums:

 27.10.2017

Doktorurkunde ausgehändigt am:

Dedicated

To

My beloved

Parents

List of Abbreviations

BARF	Tetrakis(3,5-bis(trifluoromethyl)phenyl)borate
BET	Brunauer-Emmett-Teller
CCDC	Cambridge Crystallographic Data Center
COF	Covalent Organic Framework
CTV	Cyclotriveratrylene
D	Diffusion Coefficient
DABCO	1,4-Diazabicyclo[2.2.2]octane
DCC	Dynamic Covalent Chemistry
DCM	Dichloromethane
DCTB	*trans*-2-[3-(4-*tert*-Butylphenyl)-2-methyl-2-propenylidene]malononitrile
DIBAL-H	Di-*iso*-butylaluminium hydride
DMSO	Dimethylsulfoxide
DOSY	Diffusion-Ordered Spectroscopy
EA	Elemental Analysis
EM	Effective Molarity
G	Gibbs Free Energy
H	Enthalpy
ITC	Isothermal Titration Calorimetry
K_a	Association Constant
k_B	Boltzmann Constant
K_i	Intrinsic Binding Constant
K_σ	Statistical Factor
MALDI	Matrix-Assisted Laser Desorption/Ionization
MOF	Metal Organic Framework
MOMCl	Methoxymethyl chloride
MS	Mass Spectrometry
N_A	Avogadro constant
NBS	*N*-Bromosuccinimide

NMR	Nuclear Magnetic Resonance
OAc	Acetoxy
OMIM	Organic Monomer with Intrinsic Microporosity
ORTEP	Oak Ridge Thermal Ellipsoid Plot
OTf	Trifluoromethanesulfonate
PIM	Polymer with Intrinsic Microporosity
PM6	Parameterization Method 6
ppm	Parts Per Million
p-**TsOH**	*para*-Toluenesulfonic acid
Q	Heat Change
R	Gas Constant
r	Radius
R$_f$	Retention factor
rt	Room Temperature
S	Entropy
TBAF	Tetra-*n*-butylammonium fluoride
TBTQ	Tribenzotriquinacene
TES	Triethylsilyl
TFA	Trifluoroacetic acid
THC	Tetrahedral Character
THF	Tetrahydrofuran
TLC	Thin Layer Chromatography
TMS	Trimethylsilyl
TOF	Time of flight
tpt	2,4,6-Tri(4-pyridyl)-1,3,5-triazine
η	Viscosity
ρ	Density
σ	Symmetry Number
σ$_{ext}$	External Symmetry Number
σ$_{int}$	Internal Symmetry Number

Table of Contents

CHAPTER 1

●

Aim of the Thesis

"...imagine putting automotive parts in a large box, shaking it, and finding an assembled car when you look inside!"[1]

This metaphor beautifully captures the essence of self-assembly, which is defined as the spontaneous arrangement of building components into ordered patterns without any external intervention.[2] Self-assembly is the central process in many natural systems. It is involved in constructing a countless number of functional architectures from protein to virus with dimensions ranging from the sub-nanometer scale to several hundred nanometers.[3] The importance of self-assembly in nature has ignited an interest among scientists for artificial self-assembly to control the relative organization of the individual molecular components into a designed pattern endowed with a desired functionality. Among all the self-assembled systems, the study of cage assemblies has received particular attention due to its attractive features such as modulation of catalytic reactions,[4] stabilization of reactive species,[5] selective encapsulation of molecular guests[6] resembling properties of biological receptors. The structural pattern of cage compounds is basically encoded in two parameters: geometry of the building units and binding interactions. For further applications, functionality of cages needs to be programmed in a defined manner, which sets two important goals in current research on cages: *i)* control of assembly/disassembly by external stimuli and *ii)* spatial control of functional sites within cage assemblies. Molecular self-assembly typically involves non-covalent[7] or dynamic covalent[8] interactions. On one hand, these interactions are required to be strong enough (compared to thermal energy, k_BT) to induce the assembly of the molecular building units in solution.[9] On the other hand, the interactions must be reversible in order to achieve ordered nanostructures, since the reversibility of the binding interactions among molecules allows correction of errors and the formation of one single organized aggregate as the main product.[3] Furthermore, the interactions should also be sufficiently directional and selective so that the final self-assembled structure forms as the singular thermodynamic product out of the many alternatives in an equilibrated system.[9] In this context, the dative boron-nitrogen bond

formed by the Lewis acidic boron center and the Lewis basic nitrogen have all the above properties such as reversibility, high directionality with an added advantage of facile tunability of the bond-strength by varying the substituents on the individual molecular components.[10] However, boron-nitrogen dative bonds are still relatively less explored in the molecular self-assembly due to the difficulty in obtaining a well-defined supramolecular aggregate of high kinetic stability in solution. In this respect, the noncovalent synthesis[11] of an organic cage based solely on boron-nitrogen bonds that is stable in solution and can be studied as a monodisperse species is highly desirable since it will allow an in-depth study on how multiple boron-nitrogen bonds can promote cooperativity, which finally induces the specific organization of the building blocks to form the desired structure. Of equal importance is the development of stimuli-responsive systems so that both assembly and disassembly processes can be manipulated by changing external parameters such as temperature or pH.[2] Such a comprehensive study on the formation as well as the thermodynamic parameters of a well-defined aggregate would add the boron-nitrogen dative bond to the arsenal of supramolecular chemists for the design of artificial nanoarchitectures.
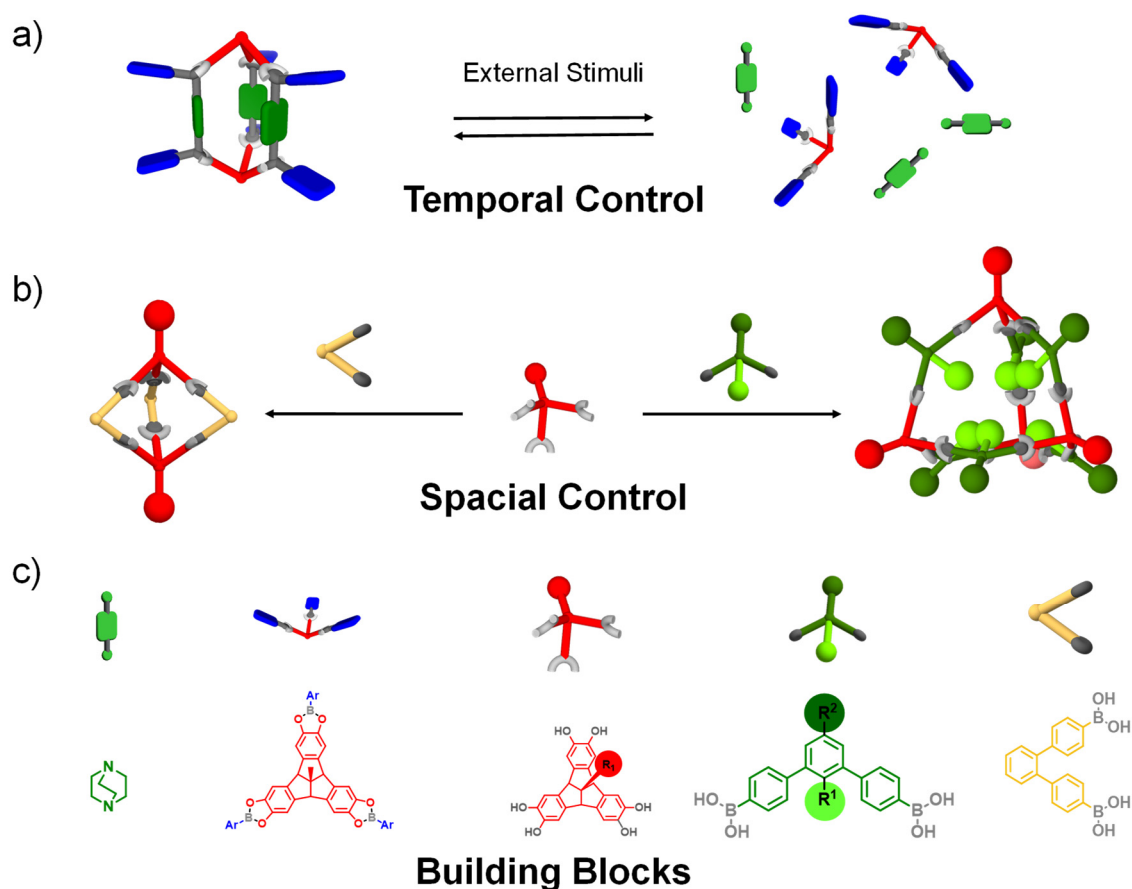

Figure 1 | Molecular self-assembly: **a)** control of assembly/disassembly of cages by external stimuli; **b)** spatial control of functionalities within cage assemblies. **c)** Schematic representations of molecular building units described in this thesis.

Molecular self-assembly depends not only on the binding interactions involved, but also on the chemical information encoded within the individual building units, which ultimately determines the final topology of the self-assembled structure.[9] Apart from defining the size and shape of the aggregate, a suitable molecular building block also provides possibility of situating functional groups at intended positions of the final self-assembled architecture. This spatial control of functionality within a self-assembled system can be achieved by synthesizing molecular building blocks with at least two independently addressable functional groups - one type being involved in self-assembly process, whereas the other one determining the spatial orientation of the functionality in the final nanostructure. In this context, the tribenzotriquinacene[12] (TBTQ), which is a rigid, tripodal bowl-shaped molecular building unit, is worth exploring, since it can be integrated in different types of self-assemblies ranging from discrete cage structures to polymeric materials.[13] In recent years, specific functionalization at selective positions of the TBTQ scaffold has been extensively studied. In particular, catechol-functionalized TBTQ derivatives have been introduced as versatile building blocks for the efficient formation of bipyramidal, tetrahedral and cubic cage assemblies upon reaction with diboronic acids having different bite angles.[14]

To address the issue of spatial control for functionality within such aggregates, the TBTQ building block needs to possess another functional group in addition to the catechol groups. Since the apical position of the TBTQ molecule reside on the convex surface of the cage compounds, the incorporation of apically functionalized TBTQ units would give access to organic cages possessing external functionality. However, the facile apical functionalization of the TBTQ scaffold was still unattainable by any state-of-the-art synthetic route. Hence, the development of a new synthetic protocol of the apically functionalized TBTQ derivatives is a prerequisite for the formation of exohedrally functionalized TBTQ-based cages. In order to functionalize the interior of TBTQ-cage assemblies, a suitable building block with concave functionality needs to be designed. In this regard, *meta*-diboronic acids with additional functionalities in the 2-position was chosen as the target molecule. Ultimately, the co-condensation of building blocks that are suitable for exohedral and endohedral functionalization might lead to organic cage assemblies, that enable an elegant spatial control of functionalities on both the exterior as well as the interior of cage compounds.

With these goals in mind, this thesis has been outlined in six chapters. In Chapter **2**, an account of the supramolecular assemblies based on boron-nitrogen dative bonds is provided in Section **2.1**. Next, a brief review of the geometry, synthesis and functionalization of TBTQ derivatives is discussed in Section **2.2**. Finally, the examples of cage structures with additional functionalities (either exohedral or endohedral) are discussed in Section **2.3** to put a perspective on the importance of functionalized organic cage compounds. The results of this thesis are discussed in Chapter **3**. It starts with the description of the formation and an in-depth study of solution-stable organic cages *via* boron-nitrogen dative bonds in Section **3.1**. Afterwards, a facile synthetic route for the apical functionalization of TBTQ derivatives is described in Section **3.2**. The versatile modularity of this new approach is also showcased by introducing various functional groups at the apical positions of TBTQs. Based on the new apically functionalized TBTQ derivatives, the synthesis of exohedrally functionalized organic cages is documented in Section **3.3**. Furthermore, this section reports the elegant design and synthesis of a new divergent diboronic acid with concave functionality along with the implementation of the new molecular building blocks for the formation of cages with both external and internal functionalities. Chapter **4** and Chapter **5** summarize the work of this thesis in English and German, respectively. Finally, the experimental details describing all applied methods and materials, new synthetic routes are reported in Chapter **6**.

CHAPTER 2

●

Literature Survey

2.1 Boron-Nitrogen Dative Bonds in Supramolecular Assemblies

The well-defined internal organization of molecular building units into extended architecture is a fundamental requirement for the formation of functional materials with desired properties. In this regard, self-assembly plays a pivotal role in controlling the spatial orientation of each molecular component to construct well-defined nanomaterials. In nature, there are numerous impressive examples of such assemblies, *e.g.* the formation of one highly sophisticated icosahedral Norwalk virus capsid from 180 identical proteins.[15] This has inspired supramolecular chemists to utilize the self-assembly of small molecular building units for the design and synthesis of complex multicomponent supramolecular systems. Non-covalent interactions, *e.g.* van der Waals, electrostatic, hydrophobic and hydrogen bonding interactions[2, 16] or dynamic covalent reactions, *e.g.* imine bond, boronate ester formation, alkyne metathesis and thiol oxidation[17] have been used for molecular self-assembly. Using these bonding motifs, a vast number of complex nanostructures has been successfully synthesized such as synthetic analogues of enzyme-like catalysts,[18] knots,[19] mechanically interlocked systems,[20] framework materials[21] and many more with intricate complexity.[22] To simplify, any type of self-assembled systems may be classified into four categories such as zero-dimensional objects (cages), one-dimensional fibres (polymers), two-dimensional layers (self-assembled nanosheets) and three-dimensional solids (covalent organic frameworks).[23] In order to be able to predict the final topology of a self-assembled supramolecular entity, the interactions among molecular components should be sufficiently reversible as well as highly directional. Therefore, the dynamic system can converge into a well-defined singular thermodynamic product.[24] The efficient control of both assembly and disassembly - ideally induced by specific external stimuli - is highly desirable not only to understand the processes that dictate the formation of self-assembled aggregates but also to facilitate on-demand switching or controlled release of encapsulated guests from self-assembled structures. Since the majority of molecular systems

reported so far are based on either metallasupramolecular[25] or dynamic covalent bond[17b, 26] formation, the precise control of the assembly processes is, in most cases, hampered by kinetic effects, moisture-dependent hydrolysis, or harsh reaction conditions. By contrast, weaker interactions, *e.g.* hydrogen bonding[27] or hydrophobic interactions[28] should be more suitable for reversible self-assembly, but tuning the bond strengths of these interactions is much more difficult in order to obtain the desired thermodynamic and kinetic stabilities of the self-assembled systems. In this respect, boron-nitrogen dative bonds that are formed by Lewis acid/base interactions between electrophilic boron centers and nitrogen nucleophiles can act as a suitable motif for supramolecular self-assembly. The following section will examine how the bond strengths of boron-nitrogen dative bonds can be tuned by changing the electronic properties of both electro- and nucleophilic moieties. In this context, a discussion about the geometry around the boron center in boron-nitrogen adducts will be presented. Finally, the utilization of boron-nitrogen dative bonds for the formation of a variety of supramolecular assemblies will be described. Supramolecular aggregates based on boron-nitrogen dative bonds can be classified into two types: *i)* Structures stabilized by boron-nitrogen dative bonds, *i.e.* the boron-nitrogen bonds act as a secondary non-covalent interaction needed either to form or to stabilize the assembly. In other words, cleavage of the boron-nitrogen bonds in these structures will not end up in disassembling the self-assembled system into individual small building blocks and *ii)* Supramolecular structures can intrinsically be based on boron-nitrogen dative bonds, *i.e.* the molecular components self-assemble through the boron-nitrogen bonds as a primary bonding interaction. In the latter case, the self-assembly occurs solely due to the boron-nitrogen dative bonds and cleavage of these bonds results in disassembly into individual subcomponents.

2.1.1 Geometry and Stability of Boron-Nitrogen Dative Bonds

The basic principle of the boron-nitrogen dative bond is that the Lewis acidic boron center of a boronate ester, which can be formed by condensation of boronic acids with suitable diols with loss of two water molecules, can form an adduct with a nitrogen donor ligand such as pyridine or amine bases (see Figure 2a). Upon formation of this adduct, the trigonal planar geometry at the boron center changes to tetrahedral environment. The bond length of boron-nitrogen dative bond may vary from 1.57 Å (boron-nitrogen bond length in cubic boron nitride) to 2.91 Å (sum of the van der Waals radii for boron and nitrogen atoms).[29] The relationship between the tetrahedral character of the boron center in a boron-nitrogen adduct (*THC*) and the bond angles around the boron center of boron-nitrogen adduct (*θ*) has been extensively studied by Höpfl based on crystallographic solid-state data and he established an empirical equation which correlates the two aforementioned parameters - *THC* and *θ* (see Figure 2b).[30] Figure 2c shows a plot of the boron-nitrogen bond length as a function of the corresponding *THC* values for boron-nitrogen adducts. In general, decrease in the length of a boron-nitrogen dative bond results in an increase of the tetrahedral character of the boron center.
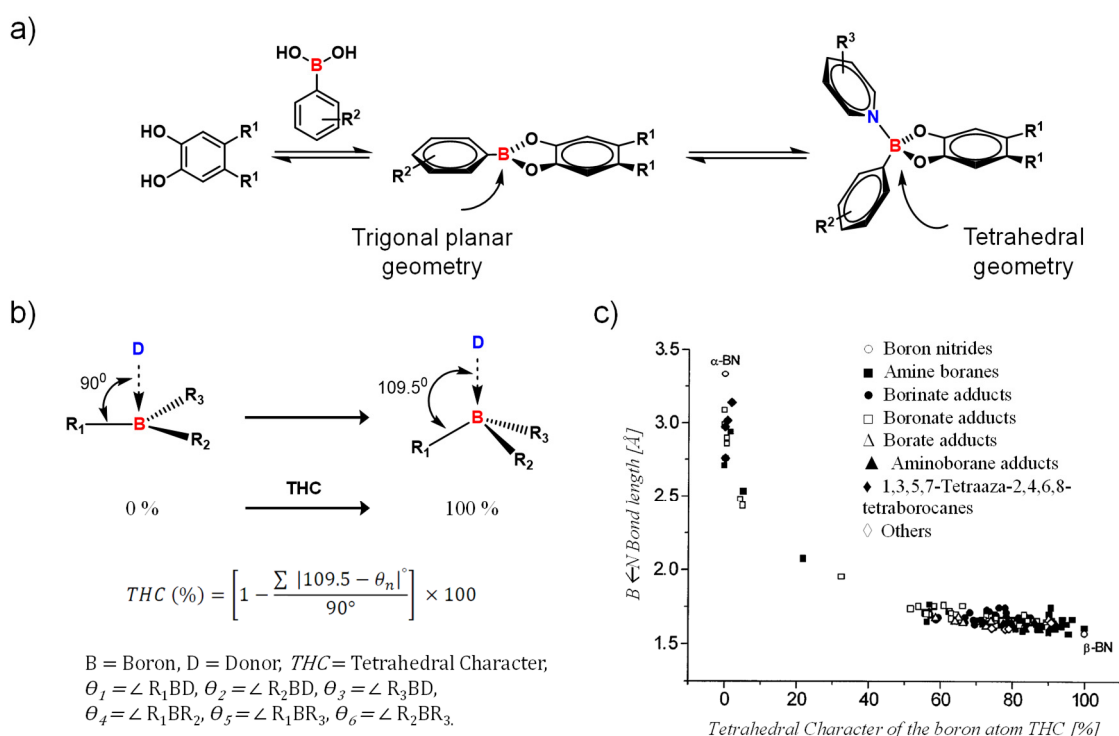

Figure 2 | a) The formation of a boron-nitrogen dative bond between a monoboronate ester and a pyridyl ligand, **b)** the change in bond angles upon binding of the donor molecule with the boron atom and the equation to calculate the tetrahedral character (*THC*) of the boron center of the boron-nitrogen adduct. **c)** The correlation between the tetrahedral character of the boron atom and the boron-nitrogen bond length for different compounds. Adapted with permission from ref. 30. Copyright 1999 Elsevier.

The equation shown in Figure 2b:

$$THC\,(\%) = \left[1 - \frac{\sum |109.5 - \theta_n|^\circ}{90°}\right] \times 100$$

B = Boron, D = Donor, *THC* = Tetrahedral Character,
$\theta_1 = \angle R_1BD$, $\theta_2 = \angle R_2BD$, $\theta_3 = \angle R_3BD$,
$\theta_4 = \angle R_1BR_2$, $\theta_5 = \angle R_1BR_3$, $\theta_6 = \angle R_2BR_3$.

For a better understanding of the factors that determine the bond strength of a boron-nitrogen dative bond, Severin and coworkers carried out a detailed study on monoboronate ester-pyridine adducts by either ^{1}H-NMR titration experiment or isothermal titration calorimetry (ITC) depending on the association constant for the individual binding event.[10a] The boron-nitrogen bond strength varies from 13.6 kJ mol^{-1} ($K_a = 10^2$ M^{-1}) to 33.0 kJ mol^{-1} ($K_a = 10^5$ M^{-1}) in chloroform (Figure 3). Stronger boron-nitrogen dative bonds were formed when either the Lewis acidity of the boronate ester or the Lewis basicity of the pyridyl components was increased due to electron withdrawing substituents at the boronate ester or electron donating groups at the pyridyl ligands, respectively. It was also observed that in benzene the bonding energies are usually enhanced by 1-6 kJ mol^{-1} compared to chloroform confirming the increase in the boron-nitrogen bond strength in less polar solvents.
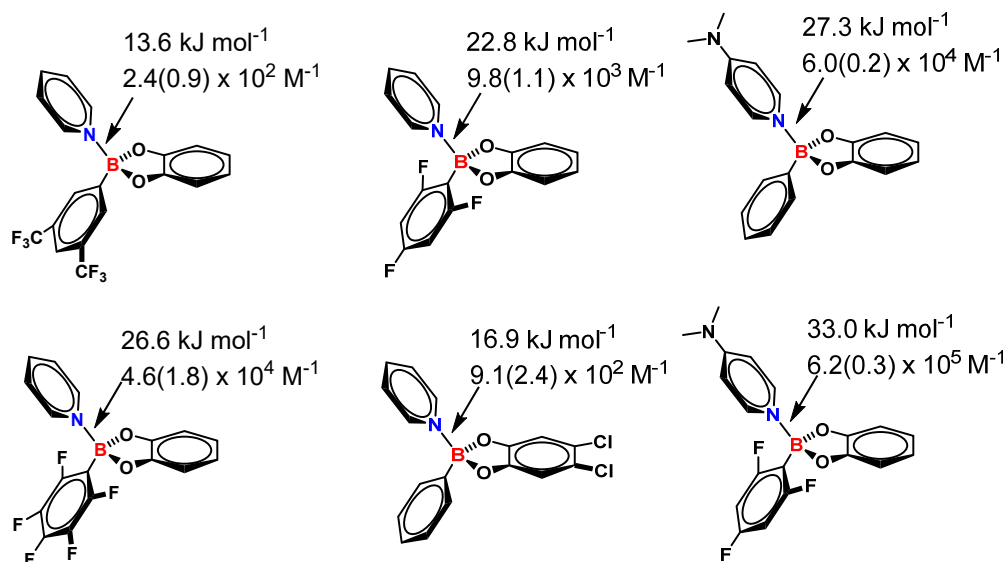

Figure 3 | Association constants and Gibbs free energies for different monoboronate ester-pyridyl adducts.

Apart from the bond strengths and the bond lengths of boron-nitrogen dative bonds, knowledge about dihedral angles among different aromatic planes of the molecular motif constituted by catechol, boronic acid and *N*-donor ligand may be useful to design supramolecular aggregates with much higher precision. In this context, Severin and coworkers recently analyzed the available data of all boronate ester-pyridyl adducts deposited in the Cambridge Crystallographic Data Center (CCDC). In this analysis all molecular and polymeric structures and also aromatic rings with different substituents have been thoroughly considered.[10b] As it is depicted in Figure 4, the catecholate plane **c** is almost exclusively oriented perpendicularly to the reference

plane **a**, whereas for the angle between planes **a** and **b**, a statistical distribution was observed. A nearly orthogonal arrangement of the planes **d** and **a** was detected in most cases.
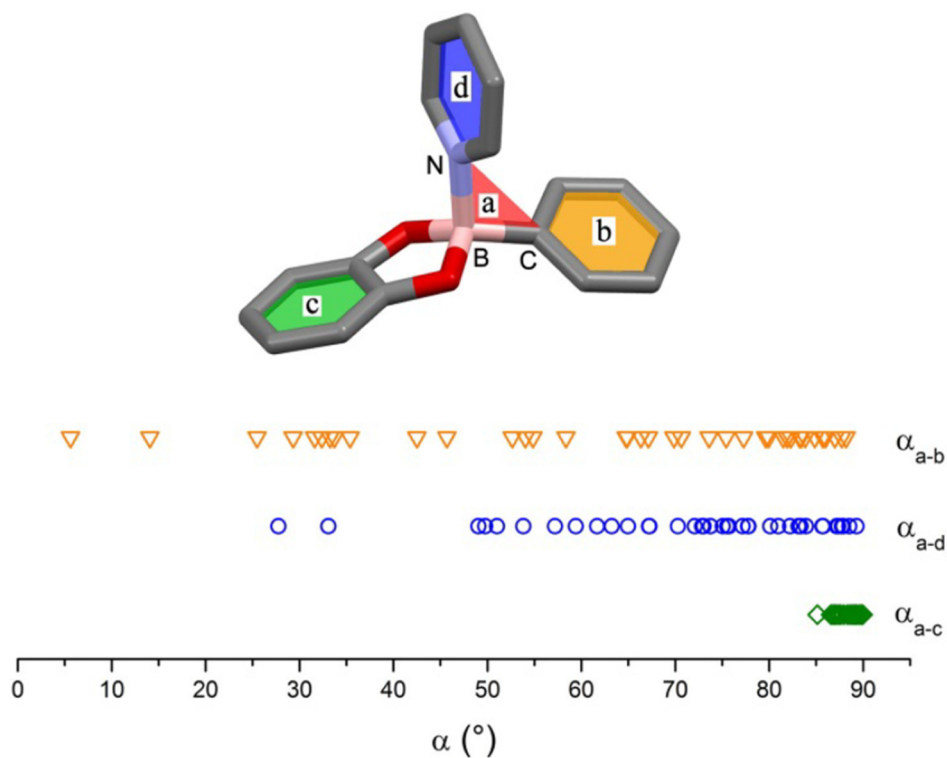

Figure 4 | Angles between the planes defined by the aromatic rings of the arylboronate ester (yellow, **b**), the pyridyl ligand (blue, **d**) or the catecholate (green, **c**) with respect to the reference plane defined by the adjacent N-B-C atoms (**a**). Adapted with permission from ref. 10b. Copyright 2016 American Chemical Society.

## 2.1.2 Boron-Nitrogen Dative Bonds as Secondary Interactions

Höpfl and coworkers have reported various macrocyclic oligoboronates, in which boron-nitrogen dative bonds provide both rigidity as well as the required stability to form the macrocyclic scaffold.[31] Reaction of tridendateimine ligands synthesized from salicylaldehyde and aminoalcohols with boronic acids results in the formation of macrocycles **1** (see Scheme 1). The same group has also studied the condensation of 3-aminophenylboronic acid with substituted salicylaldehydes to form trimeric macrocycles **2**. These macrocycles can form host-guest complexes upon inclusion of different primary amines as well as ammonium chloride derivatives. The macrocycle **3** has been successfully achieved by [3+3]-condensation of 2,6-dimethanolpyridine with phenylboronic acid.
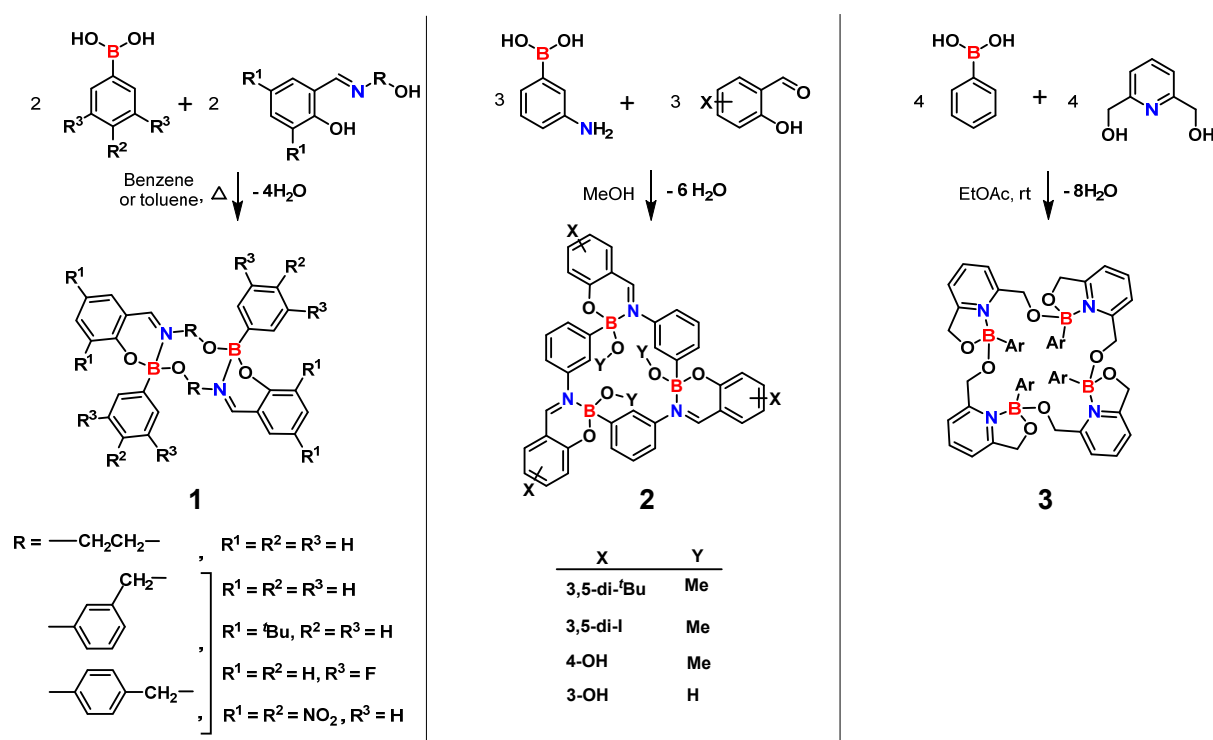
Scheme 1 | The formation of macrocycles stabilized by tetracoordination at the boron center.

Nitschke and coworkers have reported on multicomponent architectures such as macrocycles and cages based on an iminoboronate ester motif formed by a reversible B-O and C=N bond formation among diols, amines and 2-formylboronic acids. The condensation of 2-formylboronic acid, pentaerythrol and 1,4-diaminobenzene in dimethylformamide has resulted in the formation of the [4+2+2]-macrocycle **4** along with a number of unidentified soluble side products after two days in the NMR tube (see Scheme 2a). Both geometry and stability of macrocycle **4** are dictated by boron-nitrogen dative bonds. Using this concept of iminoboronate

subcomponent assembly, the quantitative formation of organic cage **5** has been achieved by [6+3+2]-condensation of 2-formylphenylboronic acid, *meta*-xylenediamine and cyclotricatechylene derivative in an NMR experiment in deuterated DMF (Scheme 2b).[32]
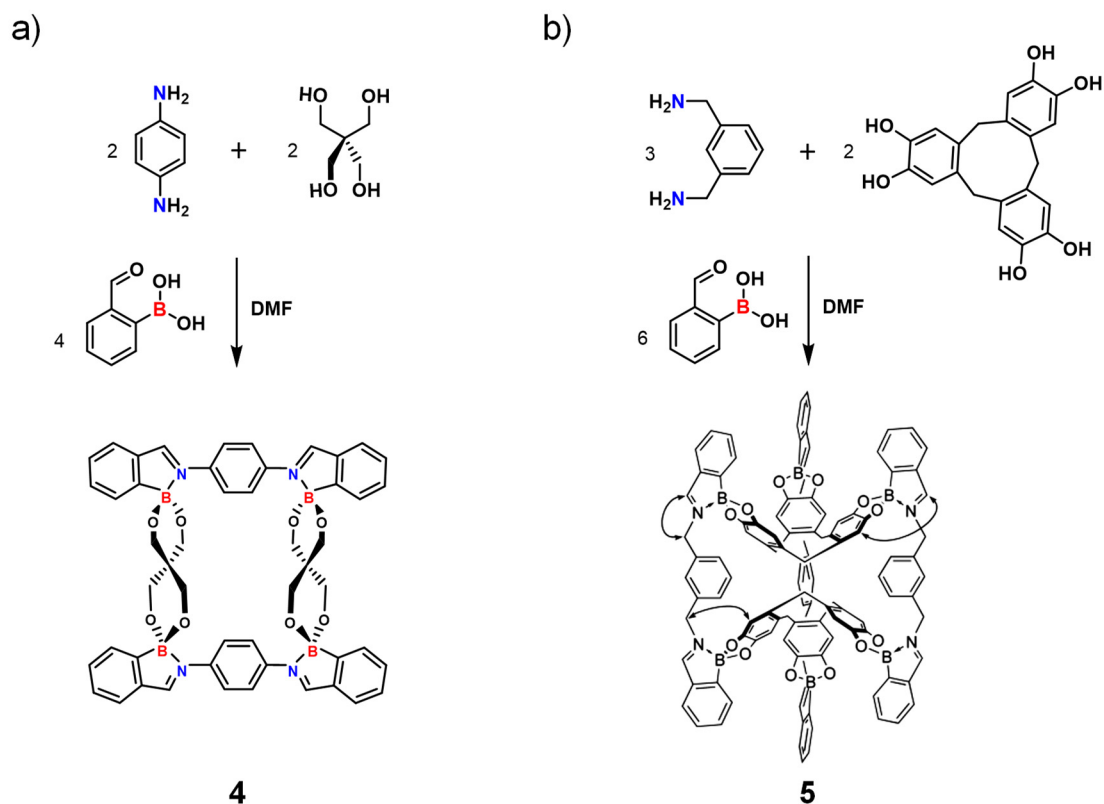
Scheme 2 | The formation of **a)** macrocycle **4** and **b)** organic cage **5** based on iminoboronate esters. The picture of cage **5** is adapted with permission from ref. 32. Copyright 2008 WILEY-VCH Verlag GmbH & Co. KGaA, Weinheim.

A different type of an ion-pair-driven heterodimeric capsule from a bowl-shaped trisboronic acid of hexahomotrioxacalix[3]arene **6** and a cyclotricatechylene **7** has been reported by Kataoka and coworkers. In protic solvents, **6** does not react with **7**, but in the presence of tetraethylammonium acetate, the formation of [1+1]-heterodimeric organic capsule **8** occurs quantitatively (see Scheme 3). In this case, the capsule is stabilized by the encapsulation of a tetraethylammonium ion and the pyramidalization at the boron center through B-O dative bonds from acetate counter ions. Almost immediately, AcO-B (sp^3) dative bond is subject to solvolysis in methanol, which leads to the substitution of acetate ions by methoxy groups. Given the reversible formation of boronate esters, the formation of capsule **8** can be dynamically controlled by changing pH of the solution. Upon treatment with HCl, the capsule collapses resulting in the removal of triethylammonium ion from its cavity. Subsequent addition of base, namely NaHCO$_3$, re-assembles the cage by the encapsulation of a triethylammonium ion, therefore rendering controlled capsule assembly by the pH switching. The similar heterodimeric

capsule **9** is formed by using tri-*n*-butylamine utilizing B-N dative bonds, which are also replaced by B-O dative bonds from methoxy groups upon solvolysis in methanol to form cage **10**. The advantage of this organic capsule **10** is that the conjugated acid $HN^nBu_3^+$ from the solvolysis reaction cannot enter the internal cavity due to its bigger size than the $HNEt_3^+$ ion. Hence, capsule **10** can accommodate other guests such as Et_4N^+, Me_4N^+, Me_4P^+, Cs^+ and THF.[33]
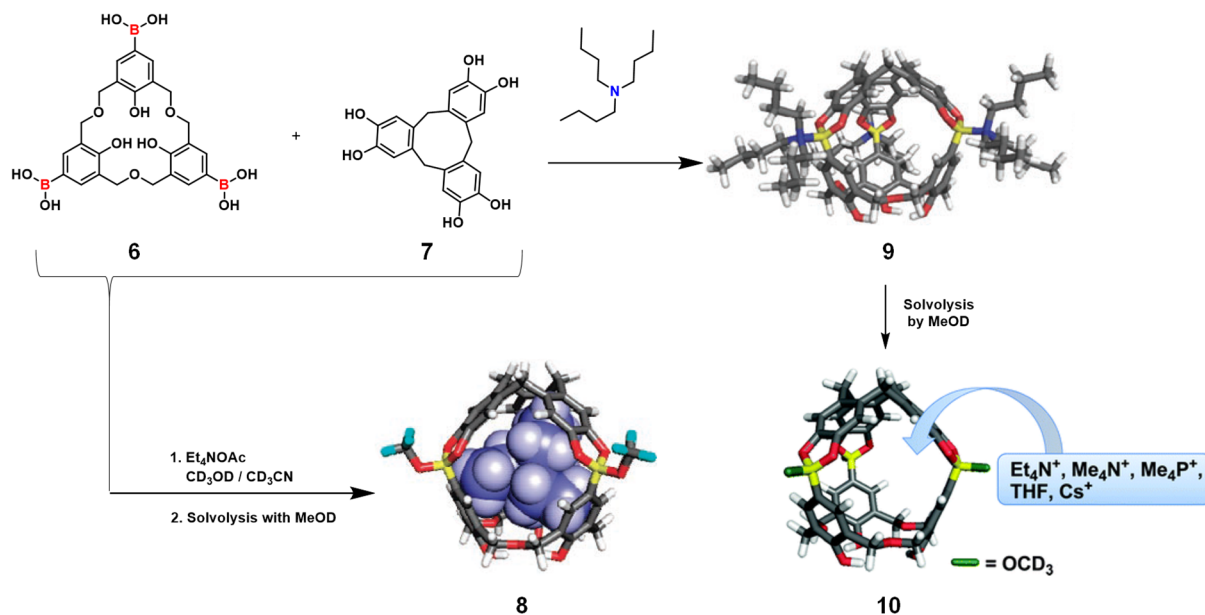
Scheme 3 | Anion-assisted self-assembled organic cages. Adapted with permission from ref. 33a (Copyright 2016 American Chemical Society) and ref. 33b (Copyright 2009 The Royal Society of Chemistry).

Galbraith and coworkers have reported the quantitative formation of stable Schiff base macrocycles **11** by the reaction of 2-formylarylboronic acids with 1,2-aminoalcohols (Scheme 4). Macrocycles **11** contain bridging boron-oxygen-boron units, whereas the boron-nitrogen bonds between boron centers of boracycles and imine nitrogens stabilize the macrocyclic structures.[34]
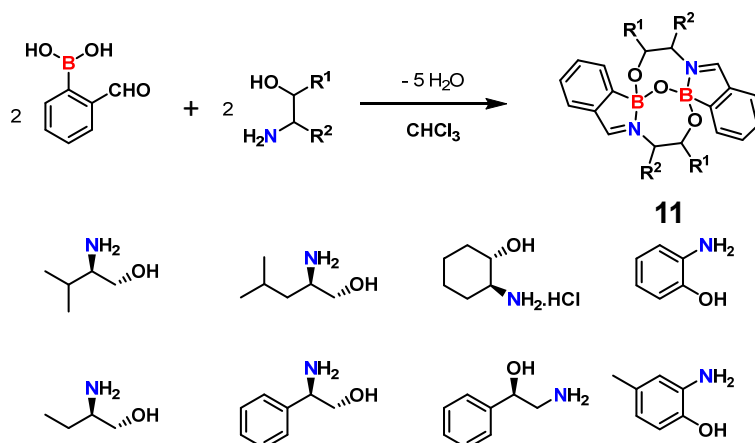
Scheme 4 | Schiff base macrocycles **11** stabilized by boron-nitrogen dative bonds.

12

2.1.3 Boron-Nitrogen Dative Bonds as Primary Interactions

Several examples are known in literature where boron-nitrogen dative bonds constitute the backbone of the supramolecular structures such as macrocycles, cages, rotaxane and also some polymeric materials. Severin and coworkers have explored the formation of both macrocyclic pentamer **12** and tetramer **13** by the reaction of different boronic acids with 3,4-dihydroxypyridine and 2,3-dihydroxypyridine, respectively (see Scheme 5a).[35] This is remarkable considering the fact that when the aryl boron center is replaced by the analogous (π-ligand) metal centers (Ru, Ir, Rh), the formation of only trimeric macrocycle occurs, no matter which dihydroxypyridyl ligand (2,3- or 3,4-dihydroxypyridine) is used.[36] This underlines the strong directionality of the boron-nitrogen dative bond, which is beneficial to the formation of well-defined supramolecular structures.
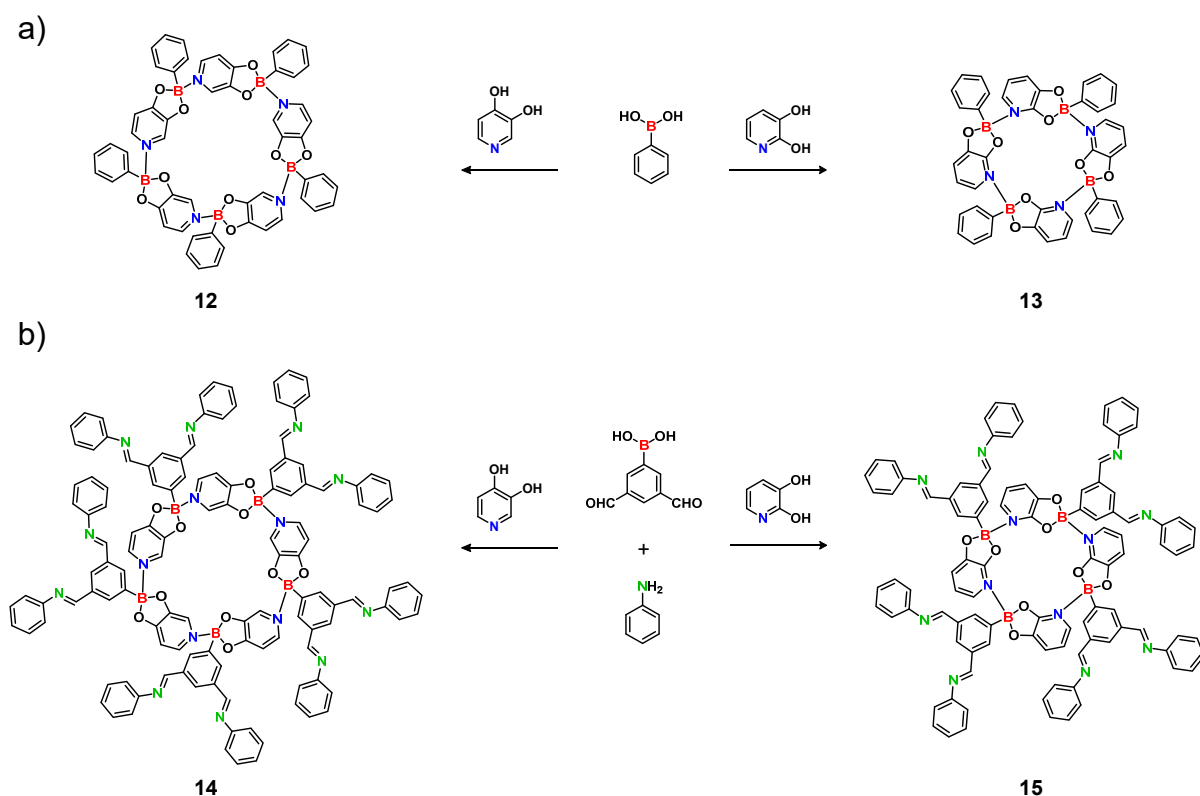

Scheme 5 | Representative examples of the self-assembled macrocyclic structures based on **a)** boron-nitrogen dative bonds and **b)** simultaneous imine condensation and boronate ester formation along with boron-nitrogen dative bonds.

Both pentameric and tetrameric macrocycles can act as scaffolds to build dendritic architectures.[37] Condensation of 3,5-diformylphenylboronic acid with 3,4-dihydroxypyridine and primary amines provides pentameric dendrimer **14**. Similarly, when 2,3-dihydroxypyridine

is used as the bridging ligand, tetrameric dendrimer **15** is formed (Scheme 5b). The fact that the aldehyde-amine condensation does not interfere with the formation of boron-nitrogen dative bonds, opens up the possibility to use building blocks with three chemically distinct functional groups (boronic acid, amine and aldehyde) for orthogonal multicomponent self-assembly.

As a proof of this concept, the macrocycle **16** with both B-N bond and C=N bond as separate structural motifs has been reported by the Severin group (Scheme 6).[38] Benzene-1,4-diboronic acid reacts with catechol to form a 1,4-bisboronate ester in parallel to the imine condensation of 4-pyridinecarboxyaldehyde with 4-picolineamine for the *in situ* generation of a ditopic pyridyl ligand. This bidendate pyridyl ligand aggregates with the 1,4-bisboronate ester by eight boron-nitrogen dative bonds resulting in the formation of the tetrameric macrocycle **16**.


16
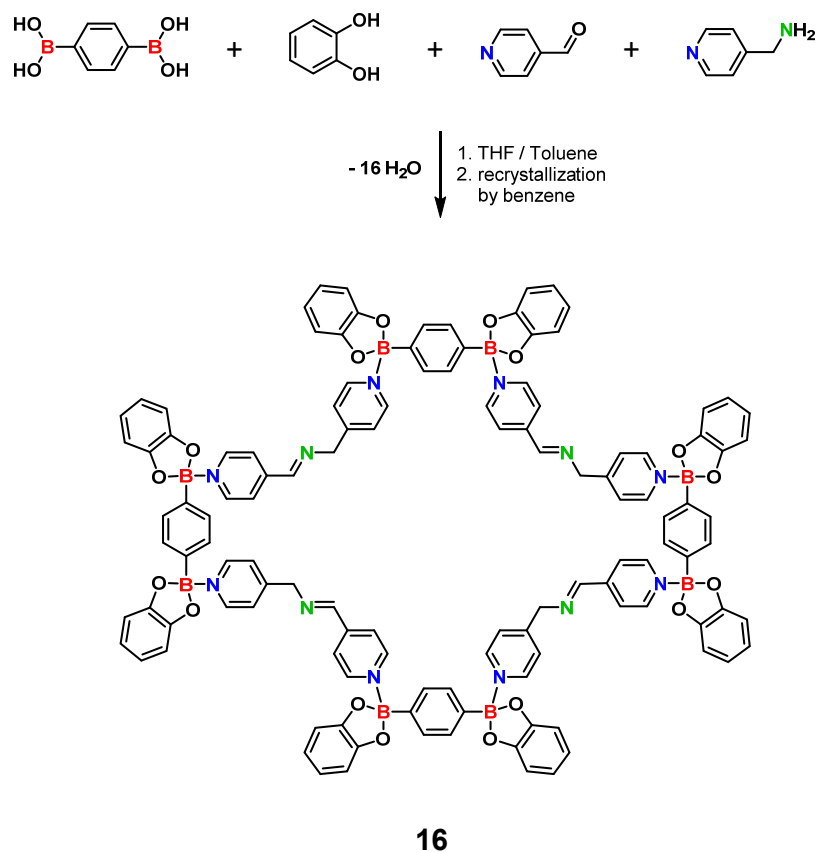
Scheme 6 | The multi-component synthesis of macrocycle **16** formed by eight boron-nitrogen dative bonds.

The Severin group has also presented the boron-based rotaxane **17** from a multicomponent assembly of a dipyridyl linker, two arylboronic acids, two catechols and one crown ether (Scheme 7).[39] The boronate esters act not only as Lewis acids to coordinate with the dipyridyl ligands by boron-nitrogen bonds but also as stoppers at both ends of the rotaxane.
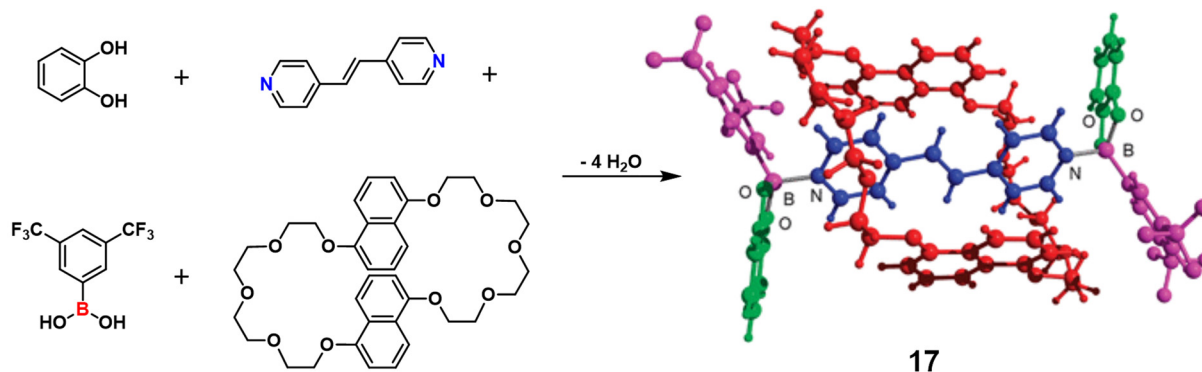
Scheme 7 | The formation of rotaxane **17** linked by boron-nitrogen dative bonds. The single crystal X-ray structure has been adapted with permission from ref. 39. Copyright 2008 Royal Society of Chemistry.

Although this rotaxane has been characterized by single crystal X-ray diffraction in solid-state, solution-studies revealed that the self-assembled rotaxane falls apart in solution due to the highly dynamic nature of the boron-nitrogen dative bonds. On the other hand, the labile boron-nitrogen dative bonds can be conceived as an advantageous bonding motif for the construction of a highly ordered crystalline framework material based on boron-nitrogen bonds. Wagner and coworkers have adopted this concept to report one of the first examples of single crystal X-ray structures for the one-dimensional polymer **18** based on boron-nitrogen dative bonds formed by the reaction of borylated ferrocenes with pyrazines (Scheme 8).[40] When 4,4′-bipyridine has been used as the bidendate ligand, a microcrystalline polymer has been obtained.
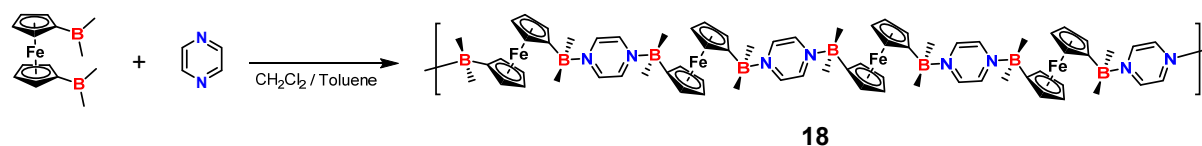
Scheme 8 | One dimensional supramolecular polymer **18** based on boron-nitrogen dative bonds.

An interesting property of this type of crystalline polymers is their intense color in solid-state, which arises due to strong charge-transfer interactions between the electron-rich ferrocene fragments and electron-poor pyrazine or bipyridyl bridges within a polymeric strand. Similar

type of intrastrand charge-transfer transition is responsible for the deep-purple color of the one-dimensional polymer **19** (Scheme 9). This linear polymer **19** has been obtained *via* a three-component reaction of phenylboronic acid with 1,2,4,5-tetrahydoxybenzene and 1,2-bis(4-pyridyl)ethylene or 4,4′-bipyridine upon simultaneous boronic acid-diol condensations with dative boron-nitrogen interactions as reported by the Severin group.[41] They have exploited this type of multicomponent assembly to obtain the two-dimensional network **20** by the condensation of tritopic boronic acids with 4-*tert*-butylcatechols in parallel with dative boron-nitrogen bonds by ditopic pyridyl ligands.[42]
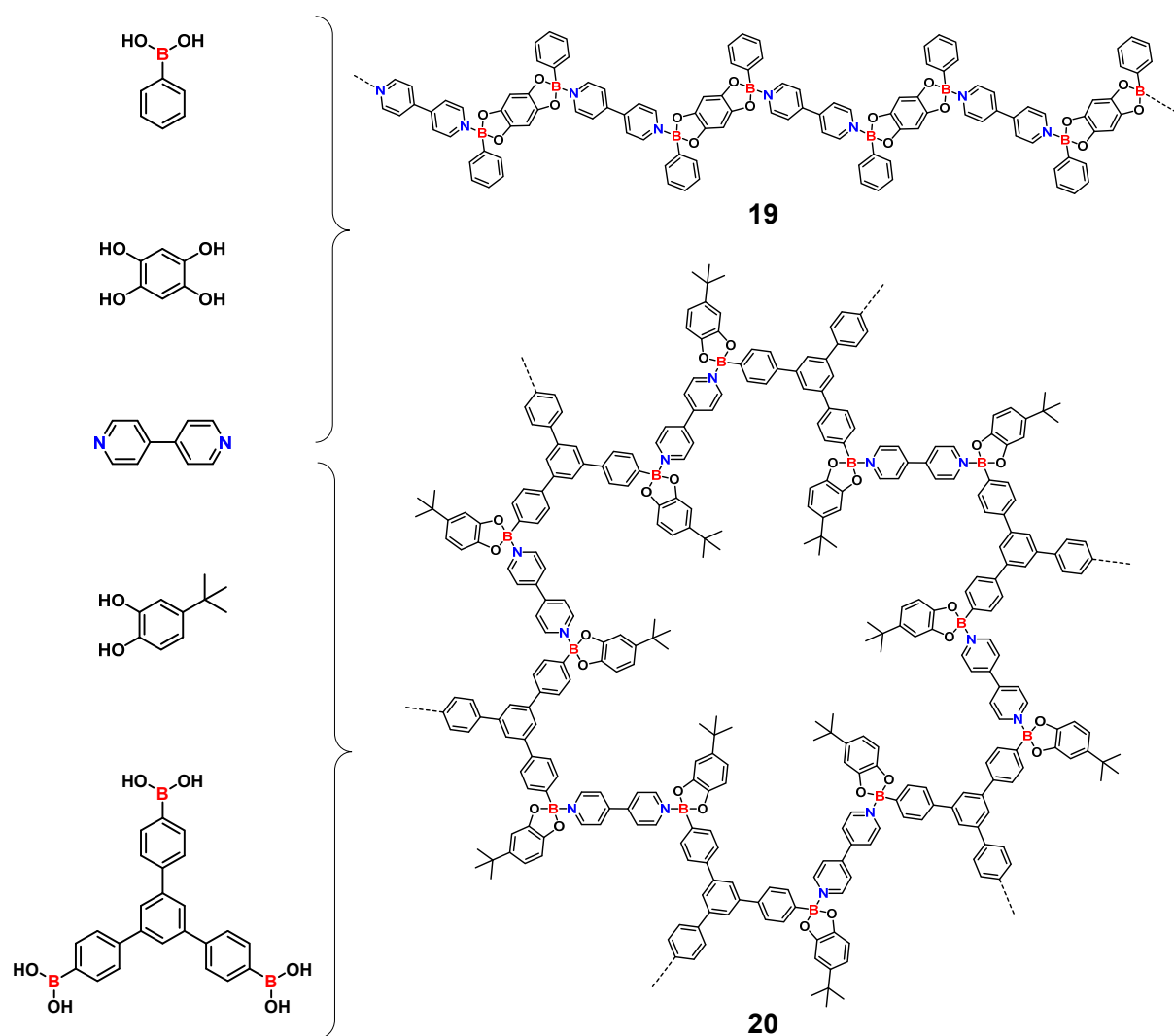
Scheme 9 | The formation of one-(**19**) and two-dimensional (**20**) supramolecular polymers based on suitable boronate esters connected by boron-nitrogen dative bonds.

These polymers dissociate in toluene upon heating due to the cleavage of boron-nitrogen dative bonds. When these hot solutions are slowly cooled to room temperature, the polymers crystallize. In general, the weak boron-nitrogen bonds are easily broken at higher temperatures

and subsequent slow cooling induces the crystallization of supramolecular assemblies. Instead of using two building units, *i.e.* boronic acids and *N*-donor ligands individually, the Höpfl group have employed self-complementary boronic acids containing both Lewis acidic borons and nitrogen-donor sites to the formation of self-assembled network structures based on boroxines or boronate esters through boron-nitrogen dative bonds. For example, the auto-condensation of 3-pyridylboronic acid leads to the formation of a nanometer sized-boroxine cage **21**, whereas two dimensional and three dimensional networks **22** and **23** have been obtained by the reaction of pentaerythritol with 4-pyrdineboronic acid and 5-isoquinolineboronic acid, respectively (Scheme 10).[43]
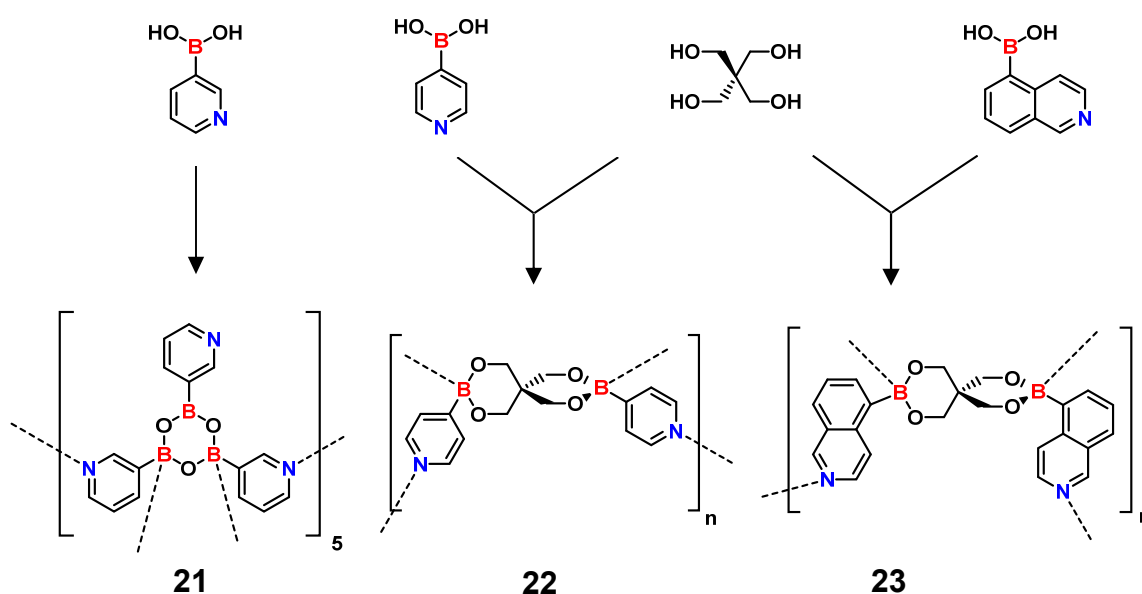
Scheme 10 | Supramolecular structures linked through boron-nitrogen dative bonds based on self-complementary boronic acids possessing both Lewis acidic boron centers and Lewis basic nitrogen atoms.

Although the reversibility of boron-nitrogen dative bonds allows for a so-called `error-correction´ while forming crystalline networks, one significant limitation is the low bond-strength of boron-nitrogen bonds, which hampers the predictable design of supramolecular boron-nitrogen adducts. As a consequence, it remains unclear if the observed solid-state structures are primarily formed due to packing effects. For example, a trigonal prismatic molecular cage **24** was obtained by the co-crystallization of a diboronate ester based on 4,5-dichlorocatechol with the tritopic 2,4,6-tri(4-pyridyl)-1,3,5-triazine (tpt) ligand (see Scheme 11).[38, 44] However, co-crystallization of the diboronate ester based on unsubstituted catechol with the same tpt ligand resulted in formation of macrocycle **25**. Performing the same co-crystallization in the presence of corronene led to the formation of one-dimensional polymeric

chains **26**.[38] The mutual formation of either macrocycle **25** or polymeric chain **26** can be rationalized by the lower Lewis acidity of the boronate ester from 4,5-dichlorocatechol in comparison to the boronate ester of unsubstituted catechol, that ensures strong boron-nitrogen dative bonds which, in turn, stabilizes cage **24** in solid state. However, due to this subtle effects on boron-nitrogen bond strength, no solution-stable supramolecular cage based solely on boron-nitrogen dative bonds has been reported so far.
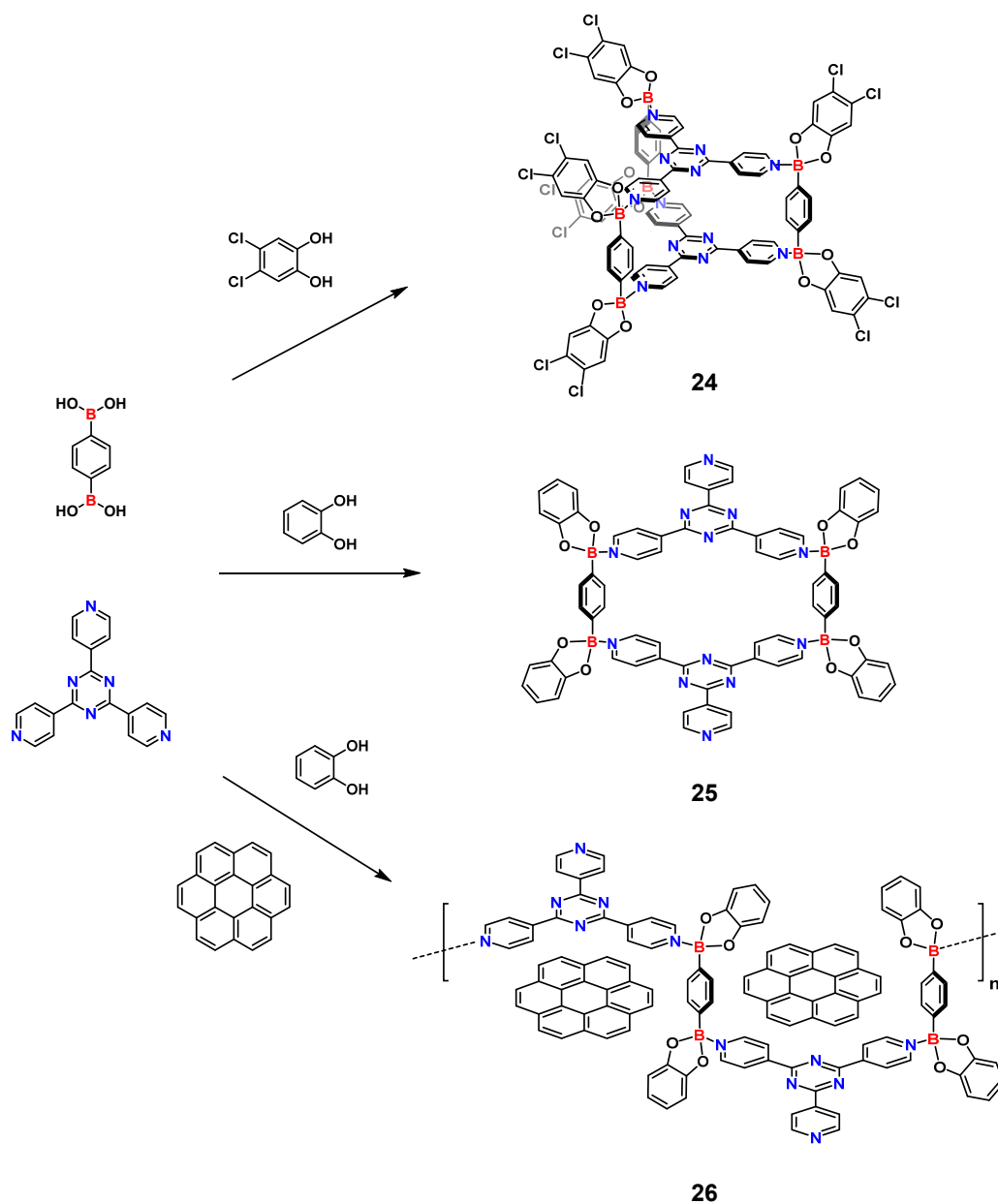
Scheme 11 | The selective formation of cage **24**, macrocycle **25** and polymer **26** depending on the Lewis acidity of the boron center of the boronate ester and also the template used for crystallization.

2.2 Tribenzotriquinacene

Bowl-shaped molecules[45] define a suitable rigid platform for either the spatially well-defined attachment of functional units,[46] convex/concave π-interactions,[47] or the formation of cyclic[48] and cage-type[13a, 49] architectures. Prominent examples for such molecular scaffolds include calixarenes,[50] cyclotriveratrylenes[51] (CTVs), cyclodextrins,[52] corannulenes,[53] subphthalocyanines,[54] or tribenzotriquinacenes (TBTQ).[55] Both TBTQ and subphthalocyanine differ from other bowl-shaped molecules due to the possibility of attaching a functional group at the apical position. In contrast, the apex for most of the other known molecules with convex-concave topology are either flat, for example, corannulenes, or possess narrow orifices, for example, calixarenes and CTVs. In addition, the rigidity, well-defined cavity and all-carbon framework make TBTQ and derivatives thereof promising candidates for molecular assemblies.[55] TBTQ belongs to the centropolyindane family with its core consisting of triquinacene unit (Figure 5).[55] The parent triquinacene **27** was first synthesized by Woodward and coworkers in 1964.[56] It possesses a conformationally rigid structure with three-fold symmetrical architecture, but it suffers from the intrinsic instability and the high reactivity due to its polyolefinic character. In this respect, the extension of each side arm of a triquinacene molecule by benzene rings provides better stability and controllable reactivity than the triquinacene itself while retaining the inherent geometrical features, which was first demonstrated by Dietmar Kuck in 1984.[57]
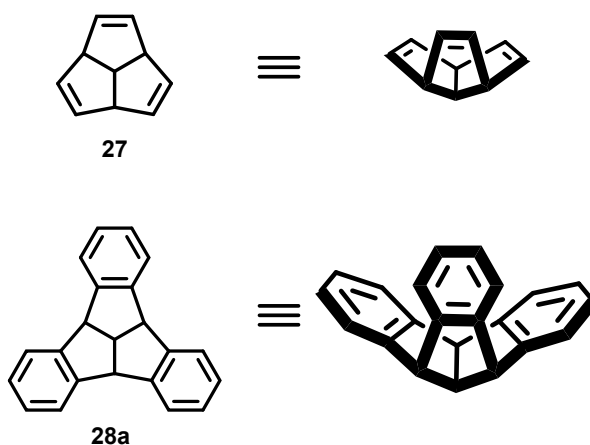

Figure 5 | The structures of triquinacene **27** and tribenzotriquinacene **28a**.

The unique geometry of TBTQ **28a** renders it an attractive building block for covalent or supramolecular architectures. For example, suitable derivatives of TBTQ have been implemented in covalent organic cage compounds,[14, 58] supramolecular aggregates,[13b, 59] metallosquares,[48] cryptophanes[60] or fullerene receptors,[61] thus showcasing the versatility of TBTQ as a curved aromatic building unit. This section will therefore summarize the most important geometrical and structural aspects of this class of compounds, followed by an overview over general synthetic strategies for both the TBTQ backbone and facile functionalization at specific positions. Figure 6 highlights four different positions suitable for functionalization namely, bridgehead, outer rim, *ortho*- and apical positions.
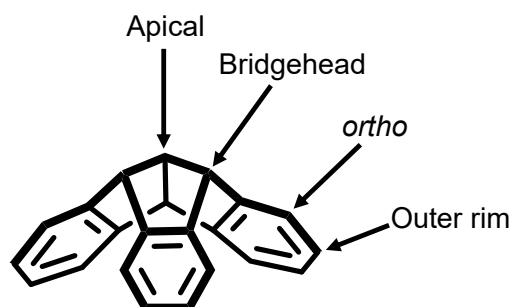

Figure 6 | The four different positions of the T̲ri̲B̲enzo̲T̲ri̲Q̲uinacene (TBTQ) scaffold.

Each type of functionalization offers a unique opportunity to encode functionality to the TBTQ scaffold. For example, both apical and bridgehead substituents can control the solubility of TBTQs or exohedral functionalization of the molecular architecture based on TBTQ building blocks while retaining the inherent bowl-shaped structural geometry of the TBTQ framework (see section 2.2.3). The outer-rim functionalization gives access to a variety of self-assembled molecular systems either based on solely TBTQs[13b] or by crosslinking TBTQs with other molecular building units[13a, 14a, 58]. Also the extension of each arm upon outer rim functionalization of the TBTQ scaffold provides a perfect platform with large concave molecular surface to form host-guest complexes with molecules of complementary shape such as C_{60} and C_{70}[61]. Functionalization at the *ortho* positions of a TBTQ unit and subsequent cross-linking with the neighboring aromatic ring can lead to the formation of a polycyclic aromatic system with curved π-surface[62], which can serve as a stepping stone towards the synthesis of warped nanographenes.

2.2.1 Structural Analysis

The basic structure of the parent TBTQ **28a** features the orthogonal arrangement of three annulated indane wings, which provides a rigid, C_{3v}-symmetrical molecular scaffold (Figure 7). A thorough analysis of the solid-state structures of the tribenzotriquinacene **28a** and its *centro*-methyl derivative **28b** reported by Kuck and coworkers provides insight into important structural parameters of typical TBTQ derivatives (see Figure 7).[63] As expected, the presence of a *centro*-methyl group does not alter the molecular structure significantly. In both cases, all carbon atoms of each of the three indane rings are within one plane with a mean deviation of around 0.01 Å. The three axes generated from the central carbon atom to the centroids of the peripheral phenyl rings are almost orthogonal to each other (87.7° for TBTQ **28a** and 87.2° for TBTQ **28b**). These almost 90° angles are quite unique for an organic building block, considering the most common arrangements of bonds around a carbon atom are tetrahedral, triangular and linear with bond angles 109°28′, 120° and 180° for sp^3-, sp^2- and sp-hybridized carbons, respectively. This remarkable geometrical feature of perpendicular orientation of each arm of the TBTQ scaffold is the key information required to design molecular assemblies using TBTQ derivatives as molecular building blocks.
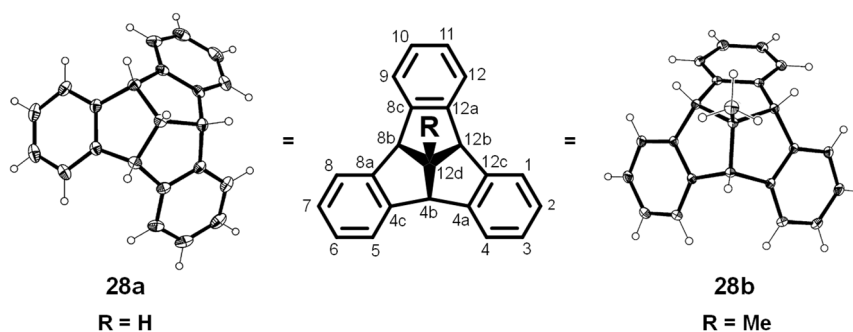

Figure 7 | Single crystal X-ray structures of tribenzotriquinace **28a** and 12d-methyltribenzotriquinacene **28b** and the atom-numbering of the TBTQ backbone. The single crystal molecular structures are adapted with permission from ref. 63. Copyright 2013 WILEY-VCH Verlag GmbH & Co. KGaA, Weinheim.

2.2.2 Synthesis of the TBTQ Scaffold

Kuck has first synthesized the TBTQ **28b** successfully in 1984.[57] Later, his group also presented the synthesis of parent TBTQ **28a**.[64] Their general synthesis usually starts with the C-C coupling of benzhydrol (**29**) and suitable indane-1,3-dione derivatives such as **30** (Scheme 12). Afterwards, reduction of the 2-substituted indane-1,3-dione (**31**) followed by a two-fold dehydrocyclization in the presence of an acid catalyst (see Scheme 13a for the mechanism of this step) leads to the formation of the desired TBTQ molecule (**28b**).
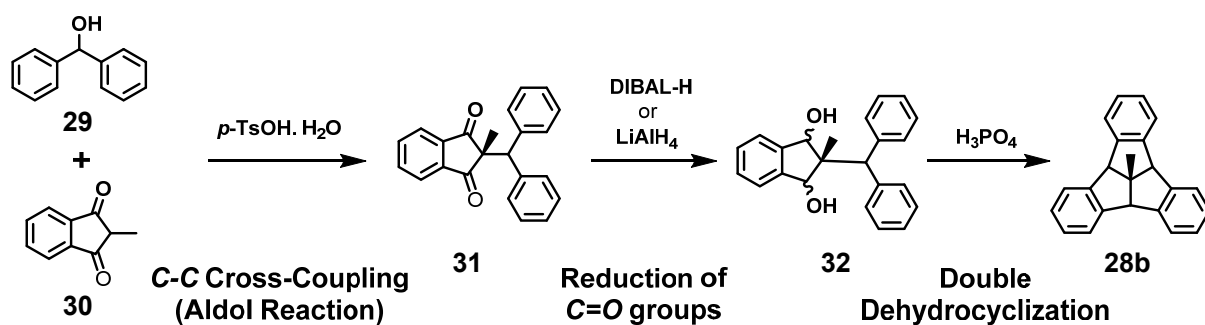
Scheme 12 | The typical synthetic strategy towards the formation of TBTQ **28b** developed by Kuck and coworkers.

In the case of alkylated derivatives such as **28b**, the overall yield was acceptable. However, for the synthesis of prototypical TBTQ **28a**, the yield went down drastically. In this case, the undesired elimination of water involving the proton at the 2-position of indane-1,3-diol,[64] which would otherwise end up at the apical position of the TBTQ can occur during cyclization (Scheme 13b). This side reaction lowers the yield significantly.
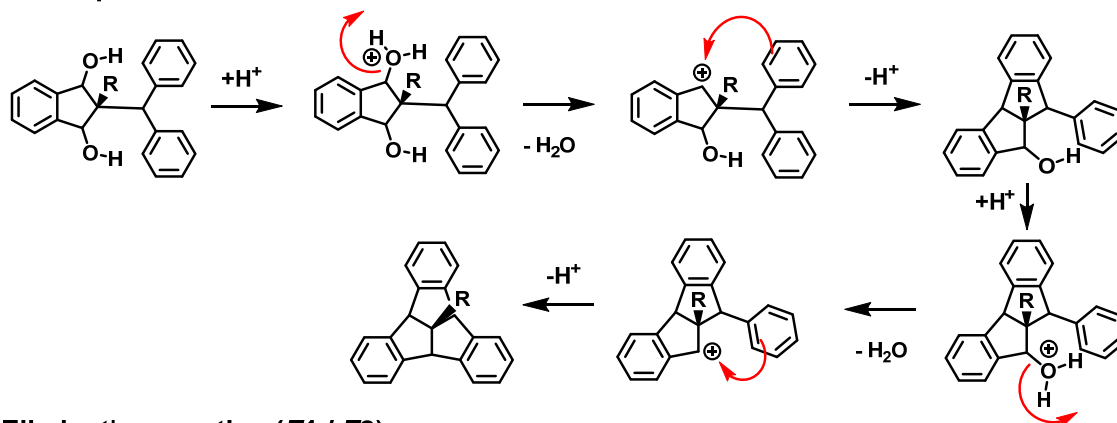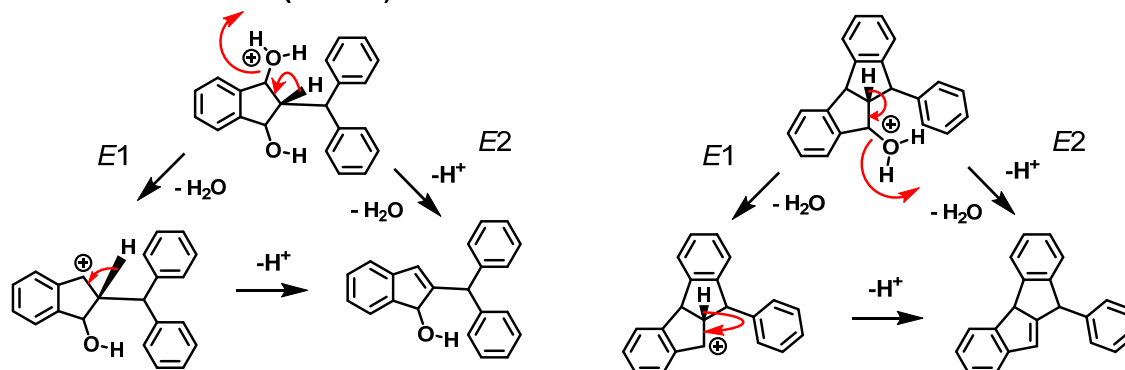

Scheme 13 | a) The proposed mechanism of the final twofold dehydrocyclization for the formation of the TBTQ scaffold; **b)** undesired side reactions during the formation of the unfunctionalized TBTQ **28a** while following Kuck´s synthetic method.

To solve this problem, an alternative synthetic pathway was developed by Hopf and coworkers.[65] This route increased the yield of the last dehydrocyclization step to 32 % giving access to TBTQ **28a** in gram quantities. Initially, synthesis of the benzylidene propanedione **35** *via* a Knoevenagal condensation followed by reduction leads to the diastereomeric diols **36** and subsequent cyclization by polyphosphoric acid as dehydrating agent finally results in the formation of TBTQ **28a** in reasonable yield (see Scheme 14). This method also allows easy functionalization at the *ortho*-positions of TBTQs.
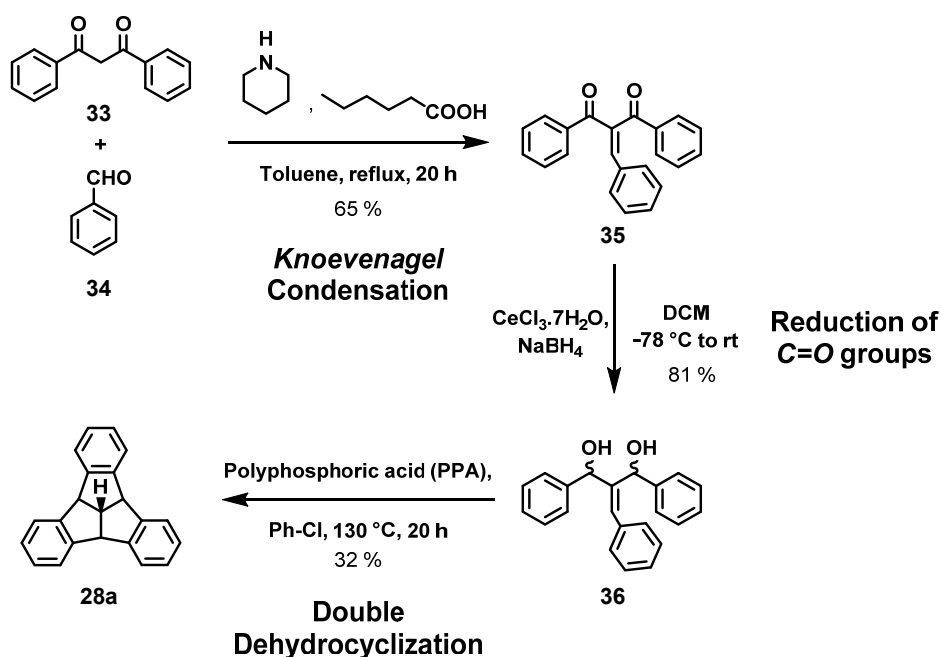

Scheme 14 | The synthesis of TBTQ **28a** following a procedure described by Hopf and coworkers.

2.2.3 Bridgehead-Functionalization

Since the initial report on the 12d-methyl derivative **28b** in 1984 by Kuck, the selective functionalization at different sites has been intensively studied in recent years. Among all the positions of TBTQ, the high reactivity of benzhydrilic bridgehead protons results in TBTQ-derivatives with different types of substituents at these positions.[12, 66] In most cases, the key intermediate is the tribromo-substituted TBTQ **37** that can be synthesized by free radical bromination using elemental bromine in carbon tetrachloride (Scheme 15).[12] As an alternative, Mastalerz and Beaudoin have recently used *N*-bromosuccinimide (NBS) in conjunction with benzoyl peroxide as the initiator to effect bromination at the bridgehead positions of TBTQ in relatively benign conditions.[66a] Hereafter, the facile S_N1-type substitution of the bromine atoms leads to a variety of TBTQ-derivatives, where the bridgehead positions are functionalized

by different functional groups through the formation of either carbon-carbon bond or carbon-heteroatom bond involving halogen, oxygen, sulfur, phosphorus or nitrogen as heteroatom.[12, 66a, 67] One of the benefits of the bridgehead functionalization for TBTQs is the pronounced increase in solubility in common organic solvents upon introduction of alkyl or ether groups at the convex surface of the TBTQ-framework without affecting the geometry of the concave bowl of the TBTQ-scaffold.[68]
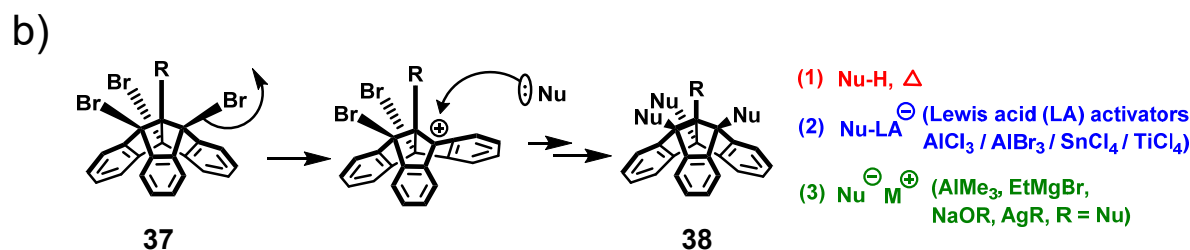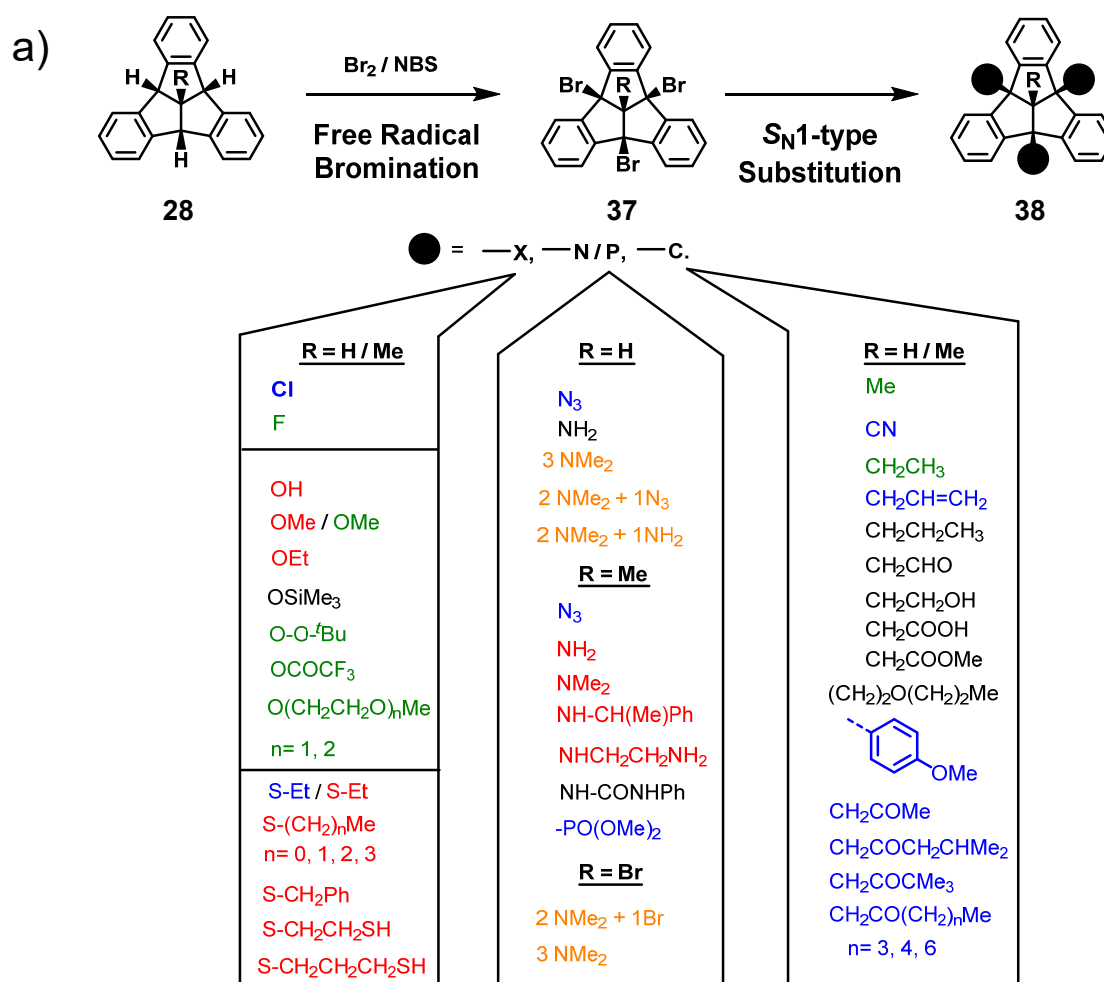
Scheme 15 | a) Bridgehead-functionalization of TBTQs and **b)** a tentative mechanism for the S_N1-type substitution of TBTQ **37**. The color of the functional group in list (a) corresponds with the color of the type of nucleophilic attack in the scheme (b), *e.g.* The -OEt groups at the bridgehead positions can be obtained by refluxing **37** in EtOH (1). The substituents colored black in list (a) are obtained by the post-synthetic modification of other bridgehead functional groups. The mechanism for installing the functional groups colored in yellow such as –NMe₂ is discussed in Scheme 16.

Treatment of TBTQ **37a** (R=H) with secondary amine does not result in the usual three-fold bridgehead-substitution, instead *E*1-type elimination of hydrogen bromide leads to the formation of an air-stable and crystalline compound **39** (Scheme 16a).[69] Due to the remarkable out-of-plane distortion of the double bond, alkene **39** undergoes facile electrophilic addition reactions to yield TBTQ derivatives with different bridgehead substitutions (see Scheme 16d). Interestingly, TBTQ **37a** provides triamine derivative **40** when treated with ammonia in benzene.[69] It has been proposed that the chelate complex formed between intermediate **41** and one ammonium ion facilitates the electrophilic attack of ammonium proton to the double bond, which ultimately results in the formation of **40** (Scheme 16c).
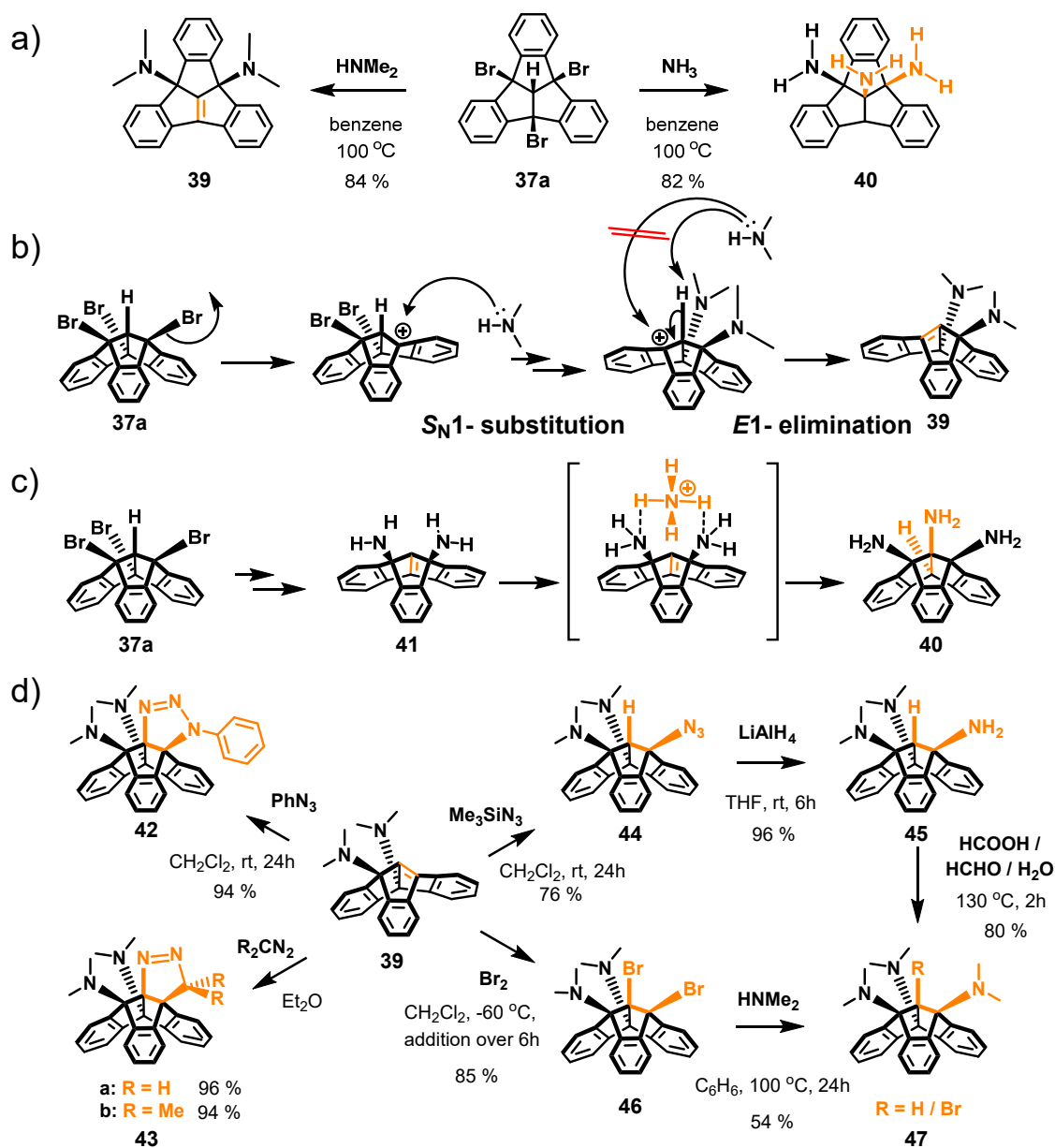
Scheme 16 | a) Synthesis of **39** and **40**; **b)** a proposed mechanism for the aminolysis of **37a** when reacted with dimethylamine; **c)** provisional explanation for the formation of **40**; **d)** the different types of derivatives which are accessible from the versatile intermediate **39** upon electrophilic addition reactions to the unsaturated C=C bond.
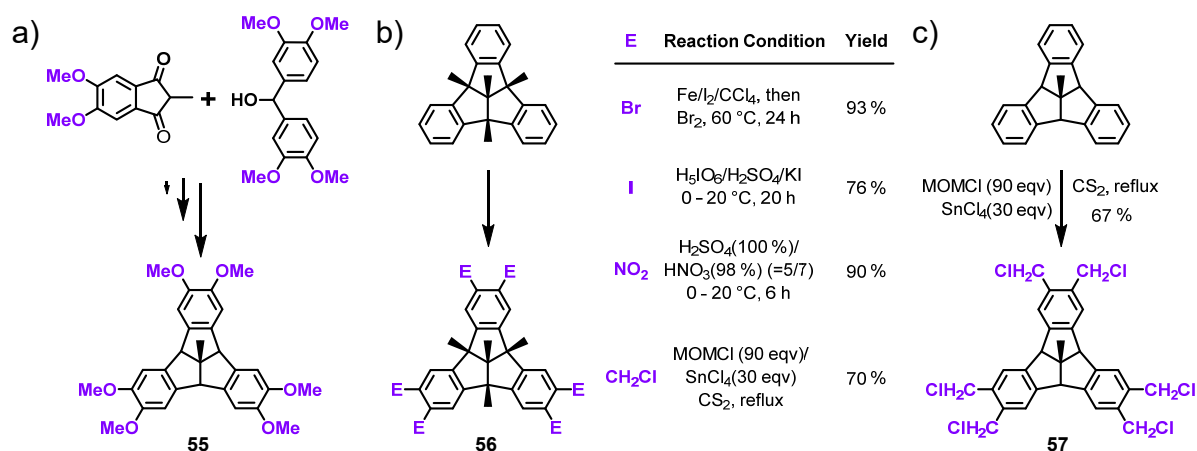
Instead of three-fold substitution, partial halogenation of benzhydrilic C-H bonds can occur, when is treated with sub-equivalents of bromine or *N*-bromosuccinimide at low temperature, although the reaction leads to mixtures of all possible halogenated derivatives along with the starting TBTQ.[12] Therefore, a tedious column chromatography is necessary to separate the product mixture. Nevertheless, the same S_N1-type substitution on any of these brominated derivatives leads to partial bridgehead functionalization of TBTQs.[12, 66a, 69] Apart from the usual bromination followed by nucleophilic substitution, an alternative route has been described in literature. It involves the formation of a tribenacepentalene dianion **48** by treating TBTQ **28** with strong bases and subsequent reaction of **48** with different electrophiles to provide a variety of disubstituted tribenzodihydroacepentalenes **49**. Upon treating **48** with water at −78 °C and warming to room temperature, dimer **51** is formed through intermediate **50**. Several Diels-Alder adducts have also been obtained from **50** (see Scheme 17).[70]
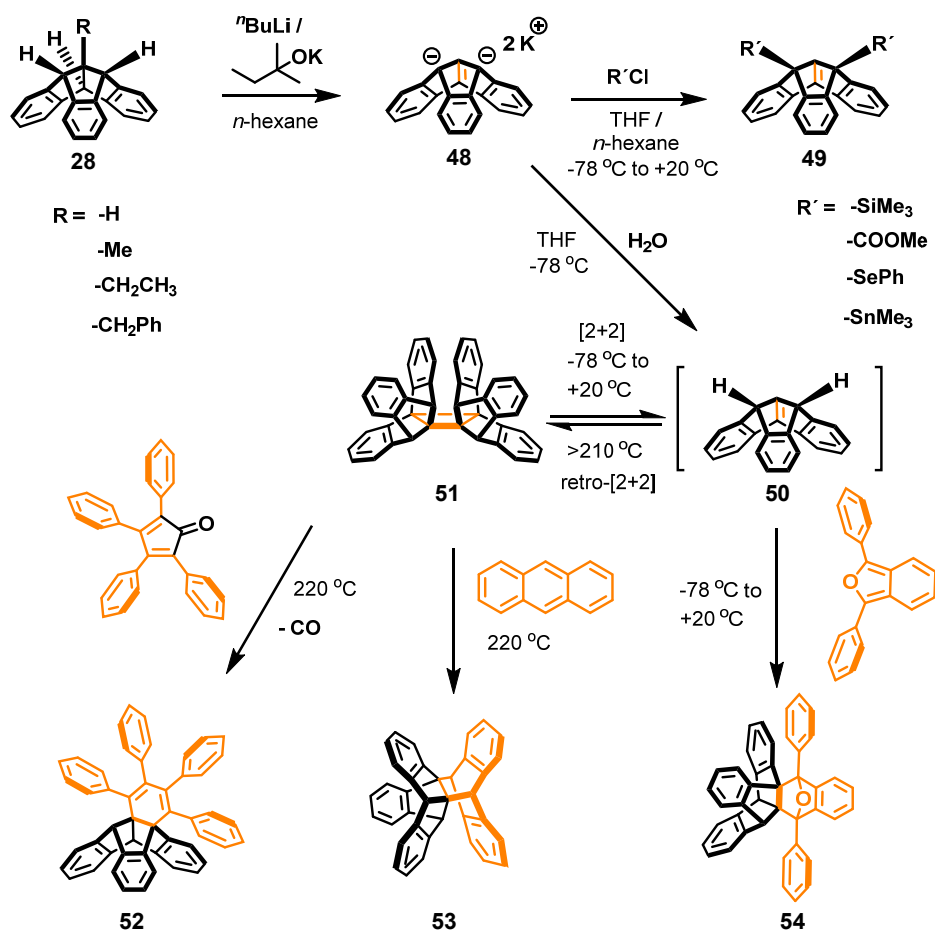
Scheme 17 | Synthesis of tribenzodihydroacepentalene derivatives **49** and Diels-Alder adducts **52-54**.

2.2.4 Outer rim-Functionalization

The outer-rim functionalization of TBTQs allows the extension of each arm of the TBTQ-backbone, which can act as a host to C_{60} and C_{70} fullerene guests with varied binding affinities depending on the extending part on the outer rim of a TBTQ-scaffold.[61a, 61b, 61d, 61e] The functional groups at the outer rim positions of TBTQs can also dictate the formation of complex self-assembled nanoarchitectures from organic cages[13a] to supramolecular polymers.[13b] How are the outer rim positions of TBTQs functionalized? Basically, two different approaches to functionalize the outer rim of TBTQ scaffold are feasible. At first hand, a suitable choice of starting materials with the substituents already however positioned appropriately so that after formation of the TBTQ scaffold the functional groups end up at the desired outer rim positions. One such example is the synthesis of the versatile hexamethoxyderivative **55** (Scheme 18a).[13c, 71] This direct approach is limited by the fact that the functional groups introduced in the starting materials are required to survive all the reaction conditions employed to form the TBTQ-framework. This limits the type of functional groups that can be placed at the outer rim positions *via* this route. Otherwise, the following indirect approach is much more suitable. In this case, outer rim substituents are introduced by electrophilic aromatic substitution at the phenylene side arms. In most cases, the high reactivity of the bridgehead positions makes a protection of these protons necessary (Scheme 18b).[12, 72] But if the bridgehead C-H protons do not interfere with the reaction condition for the desired electrophilic aromatic substitution, it is not necessary to protect the bridgehead positions before performing the outer-rim functionalization at a TBTQ molecule (Scheme 18c).

E	Reaction Condition	Yield
Br	Fe/I_2/CCl_4, then Br_2, 60 °C, 24 h	93 %
I	H_5IO_6/H_2SO_4/KI 0 - 20 °C, 20 h	76 %
NO_2	H_2SO_4(100 %)/ HNO_3(98 %) (=5/7) 0 - 20 °C, 6 h	90 %
CH_2Cl	MOMCl (90 eqv)/ $SnCl_4$(30 eqv) CS_2, reflux	70 %

Scheme 18 | The outer rim functionalized TBTQ derivatives **a)** synthesized from pre-functionalized precursor molecules; **b)** obtained by electrophilic aromatic substitutions after protecting the bridgehead positions and **c)** without protecting the bridgehead positions (see text).

The functional groups that have been installed at the outer-rim positions in **55**, **56** and **57** can be modified post-synthetically to other suitable functional groups desired for any specific purpose (Figure 8). For example, **55** can be deprotected to hexahydroxyderivative **58b**, which can act as organic building units for the synthesis of organic cages.[14a, 59] Several TBTQ-based receptors such as **60-64** can be achieved by extending each arm of **56** to form host-guest complexes with fullerenes.[61a, 61b, 61d, 61e]
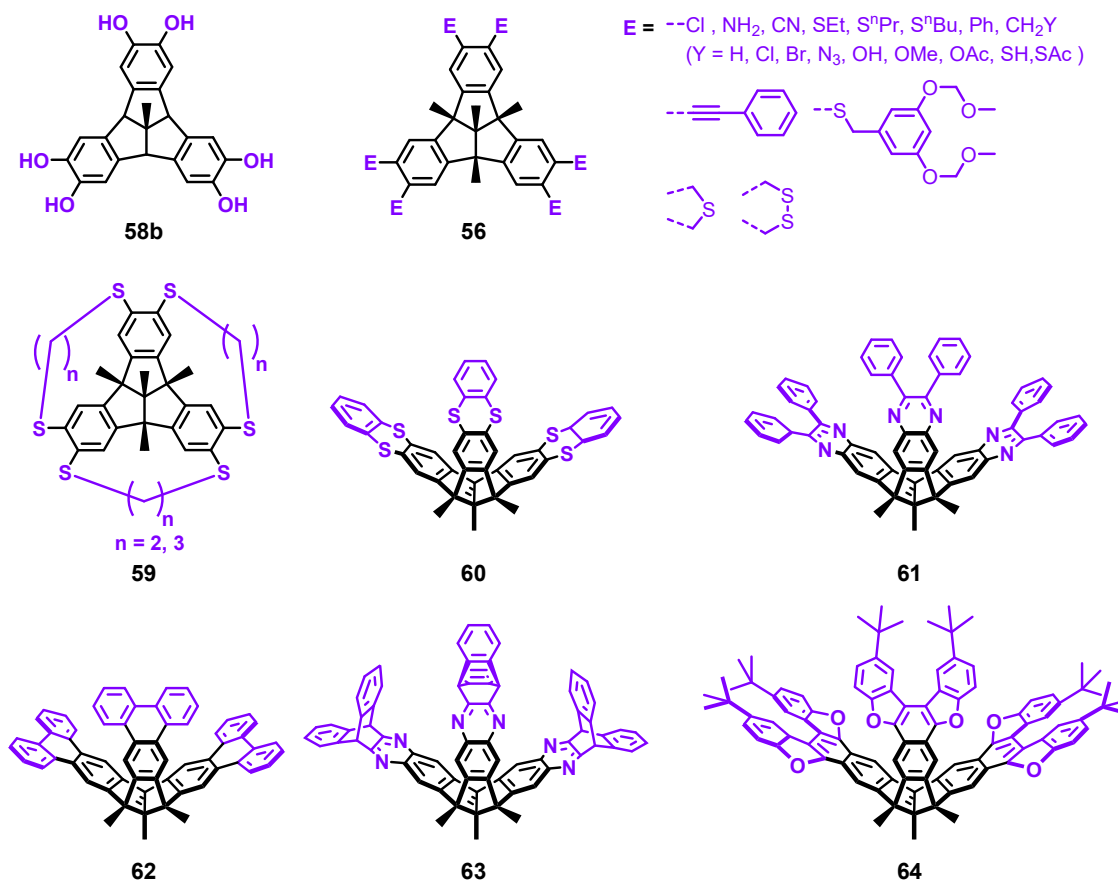

Figure 8 | The outer rim functionalized TBTQ derivatives with a range of functional groups by post-synthetic modification of TBTQ **55** and **56**.

Compared to the six-fold functionalization, mono-, di- or tri-substitution is much more difficult to achieve.[73] In this regard, the synthetic route developed by Hopf and co-workers gives access to the regiospecific synthesis of monofunctionalized as well as chiral C_3-TBTQ derivatives (**67**) utilizing the first approach, *i.e.* by choosing the precursor molecules functionalized properly (Figure 9).[65] To obtain enantiomerically pure TBTQ derivatives, resolution of the racemic mixture can be achieved by preparative HPLC on chiral columns,[48, 74] by using chiral auxillaries to form separable diastereomers[75] or by enzyme-catalyzed kinetic resolution (Figure 9).[76]
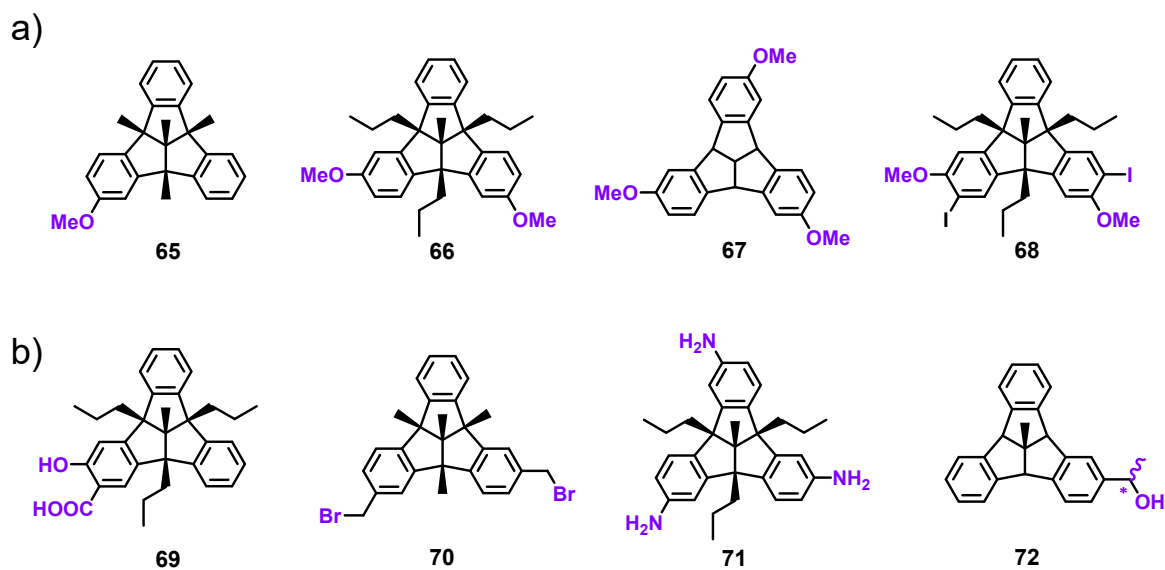
a)

b)

Figure 9 | a) Partial outer rim functionalization of TBTQs;[48, 65, 74] **b)** the TBTQ derivatives isolated in enantiomerically pure forms by chiral HPLC (**69**)[75a] or by forming diasteriomers using chiral auxillaries such as BINOL (1,1´-Bi-2-naphthol) (**70**),[75b] dibenzoyl-*L/D*-tartaric acid (**71**)[75c] or by employing enzyme catalysis (**72**).[76]

The chiral purity of TBTQ-derivatives is of immense importance due to its influence over the final topology of TBTQ-based self-assembled systems. For example, the enantiomerically pure (+) - (*P*) - **73** self-assembles into an octameric hydrogen-bonded organic capsule by exploiting the strategy of chirality-assisted synthesis, whereas its racemate forms ill-defined aggregate in solution and hydrogen-bonded network in solid-state (Figure 10).[13b]
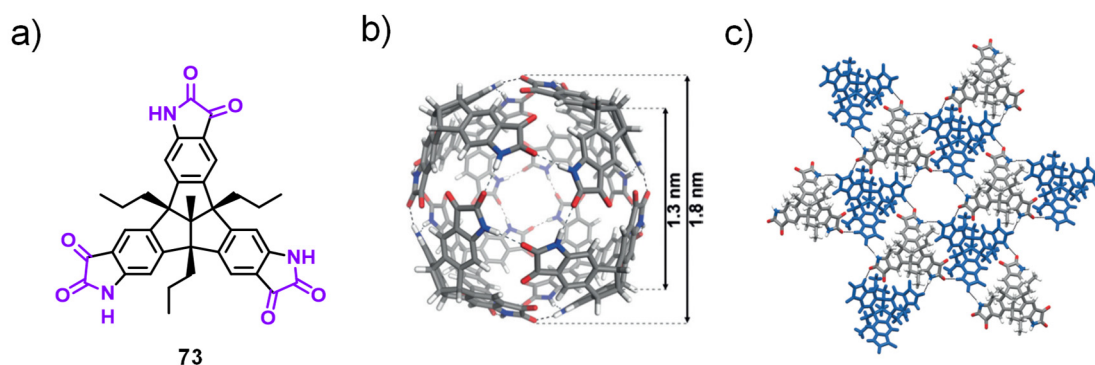
a)   b)   c)

Figure 10 | a) Structure of tris(isatin) **73**; **b)** self-assembly of (+) - (*P*) - **73** into an octameric hydrogen-bonded cube-shaped capsule; **c)** representation of the partial corrugated hydrogen-bonded sheet of the crystal structure of (±) - **73**. Adapted with permission from ref. 13b. Copyright 2016 WILEY-VCH Verlag GmbH & Co. KGaA, Weinheim.

2.2.5 *Ortho*-Functionalization

Unlike the facile outer rim functionalization of TBTQ, installation of functional groups at the *ortho*-positions is not easily accessible *via* electrophilic aromatic substitution even under harsh reaction conditions, because the orthogonal arrangement of phenylene units is severely distorted due to significant steric interactions. However, *ortho*-functionalization of TBTQs provides promising building blocks for subsequent cyclizations yielding expanded π-systems containing odd-membered rings. In an interesting reaction, an *ortho*-derivative was obtained upon addition of nucleophile at one of the *ortho*-positions from the electrophilically activated metal carbonyl complex of 12d-methyltribenzotriquinacene (Scheme 19a).[77] To end up with a TBTQ bearing methyl groups at all *ortho*-positions, Krüger and coworkers chose suitably methylated starting materials and followed Kuck's protocol, but due to severe steric crowding, a Wagner-Meerwein rearrangement occurred that resulted in the predominant formation of the rearranged product and the desired six-fold *ortho*-methylated tribenzotriquinacene could only be isolated in very low yield of 1 % (Scheme 19b).[78] In this respect, the synthetic scheme that has been developed by Hopf and coworkers gives access to regiospecific syntheses of various *ortho*-derivatives of tribenzotriquinacenes (Scheme 19c).[65]
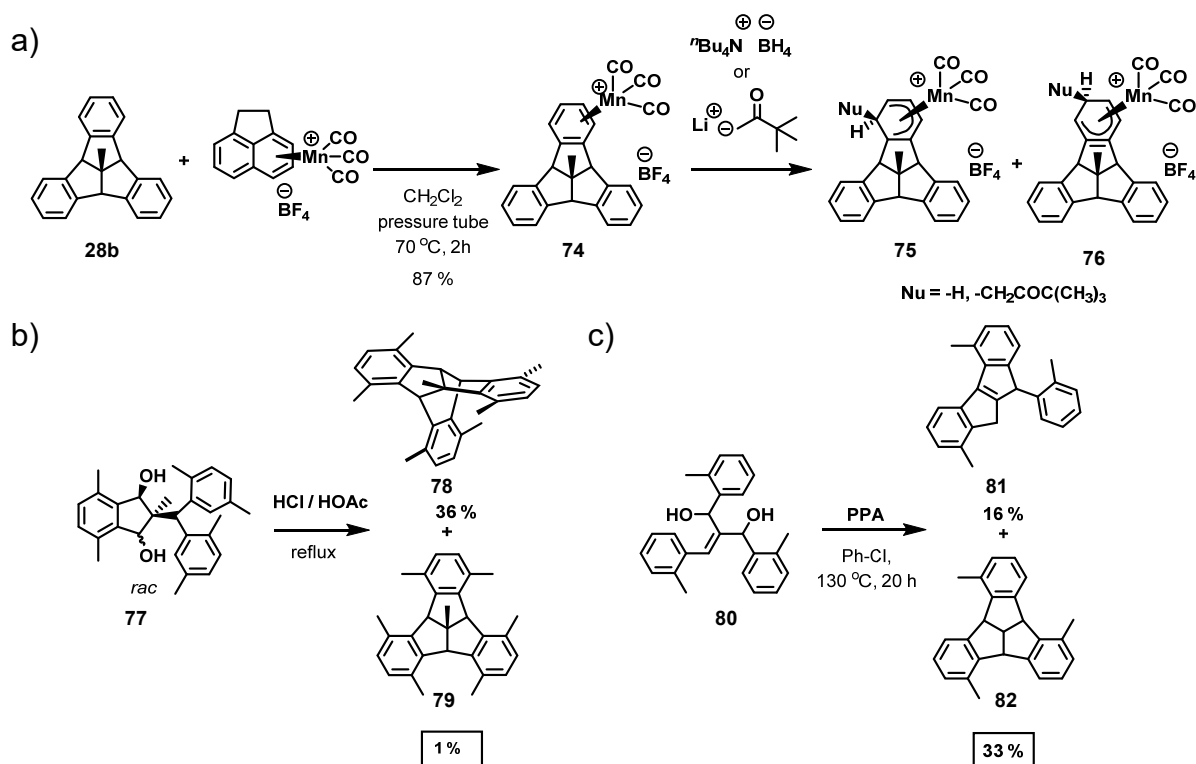
Scheme 19 | a) Synthesis of manganese tricarbonyl complex **74** followed by the addition of nucleophiles to afford an inseparable mixture of isomers **75** and **76**; **b)** the formation of rearranged product **78** as the major isomer along with the desired TBTQ **79** as the minor product; **c)** the regiospecific synthesis of **82** reported by Hopf and coworkers.

In another example, Kuck and Mughal reported the formation of a cycloheptatriene ring between two opposing *ortho*-positions of a TBTQ framework *via* a Scholl reaction (Scheme 20a).[79] Instead of only one cycloheptatriene ring, a remarkable three-fold Scholl-type cycloheptatriene ring-formation was recently reported by Kuck and coworkers for the synthesis of a wizard hat-shaped TBTQ derivative **88** with all the *ortho*-positions substituted, which is an interesting model-system for investigations of distorted graphene systems containing 5-7 defects (Scheme 20b).[62, 80]
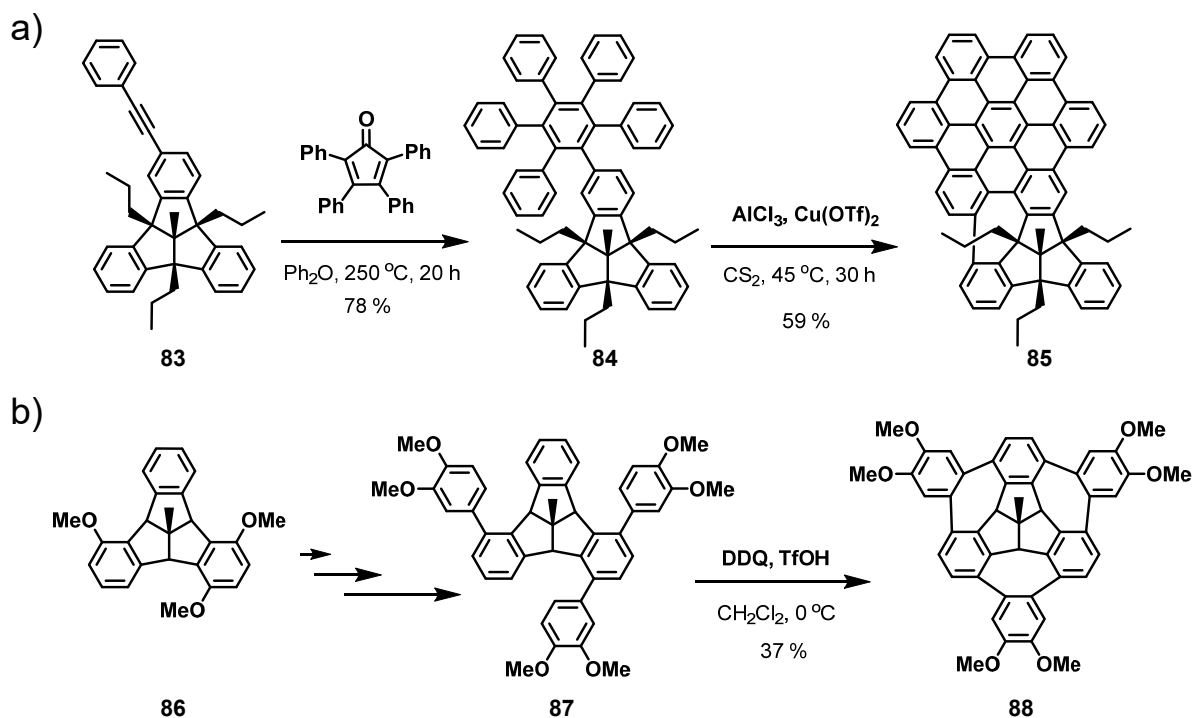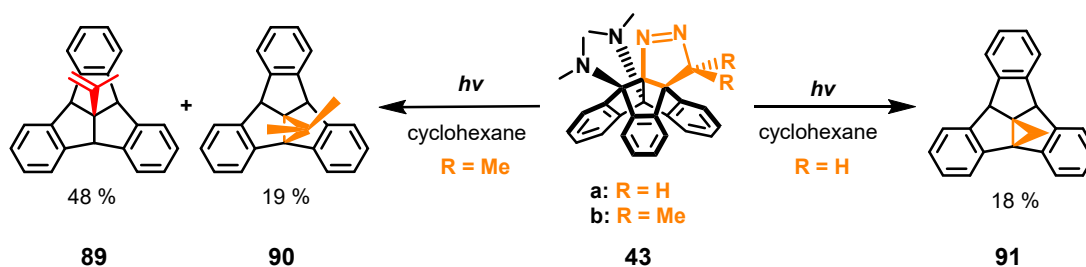

Scheme 20 | a) Synthesis of TBTQ **85** by the formation of a bay-bridging cycloheptatriene ring merging a TBTQ core with a hexabenzocoronene; **b)** the threefold Scholl-type oxidative cycloheptatriene ring formation to synthesize TBTQ **88**.

2.2.6 Apical-Functionalization

Analogous to bridgehead functionalization, substitution at the apical 12d-position offers the possibility of introducing functionality on the convex surface without interference with the concave bowl or the orthogonality of three side arms. The functionalization at the apical position of TBTQ is, however, very limited to date. A few alkyl substituents, namely methyl, ethyl, benzyl, *n*-butyl or *iso*-propyl have been implemented to enhance solubility in organic solvents.[13c, 14a, 64] Each of these alkyl groups is installed prior to the formation of the TBTQ backbone. The post-synthetic insertion of an apical group at a TBTQ framework has been

achieved by the electrophilic addition to tribenzodihydroacepentalene **39**, *e.g.* the simultaneous addition of amino or bromo groups at the apical and bridgehead positions (see Scheme 16d). Scheme 16d has also shown the quantitative formation of triazole **42**, tetracyclic dihydropyrazoles **43a** and **43b** upon addition of phenyl azide, diazomethane and 2-diazopropane, respectively to alkene **39**. Upon irradiation of a suspension in cyclohexane at room temperature, adduct **43a** undergoes photolytic deamination to form tetracycle **91** (Scheme 21). Interestingly, the photolytic deamination of *cyclo*-adduct **43b** furnishes the tetracycle **90** along with the formation of ring-opened 10-(propen-2-yl)tribenzotriquinacene **89** as the major product. TBTQ **89** is the first TBTQ-derivative with an unsaturated substituent at the apical position.[69]

Scheme 21 | Synthesis of tetracyclic TBTQ derivatives **90**, **91** and the formation of TBTQ **89** with an *iso*-propenyl functional group at the apical position.

An attempt to obtain an apical functional group directly from 12d-methyl derivative **28b** under strong oxidizing conditions has led to the oxidation of the apical methyl group to a carboxyl group accompanied with three-fold oxyfunctionalization at bridgehead positions.[81] However, the final product was neither fully purified nor characterized due to volatility and very poor solubility. Apart from that, no further examples for apical functionalization of TBTQs have been reported in literature. Considering the fact that some of the diverse tasks, such as better control of solubility of TBTQs, attachment of other functional building blocks at geometrically very specific orientation, immobilization on solid support, exohedral functionalization of organic cages can be achieved from apically functionalized TBTQs, a facile route for apical functionalization of TBTQs can unquestionably give access to novel functional material of sophisticated design and desired properties.

2.3 Framework Materials

Framework materials are an important class of functional architecture with widespread application in gas adsorption and separation, catalysis, purification, sensing, light harvesting, energy storage and production.[82] Although zeolites[83] have been well-developed and commercialized over the years, there are different types of functions that cannot be performed by these purely inorganic porous materials. This prompted chemists to explore other classes of framework materials. Figure 11 summarizes the whole family of currently developed synthetic porous materials.
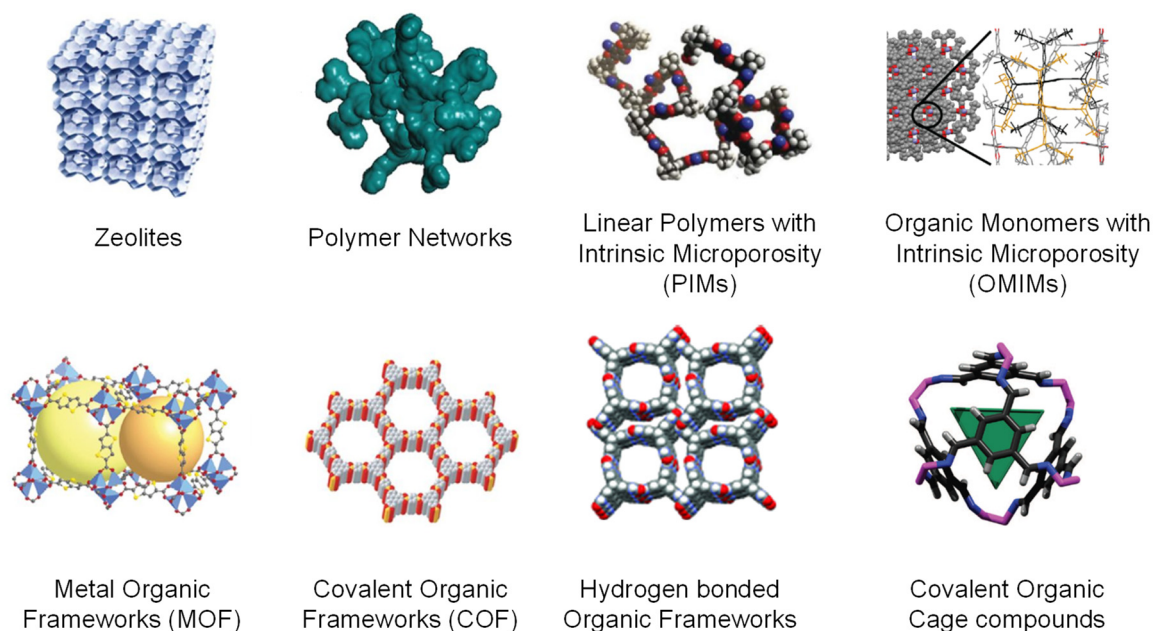

Figure 11 | Different types of framework materials. The pictures are adapted with permission from ref. 82 (Copyright 2015 Science AAAS), ref. 88 (Copyright 2016 WILEY-VCH Verlag GmbH & Co. KGaA, Weinheim) and ref. 89 (Copyright 2012 WILEY-VCH Verlag GmbH & Co. KGaA, Weinheim).

Metal organic frameworks (MOFs)[21c, 84] and covalent organic frameworks (COFs)[85] utilize metal-ligand coordination and dynamic covalent reactions, respectively, to form crystalline porous solids. The ordered crystallinity is responsible for the porosity of either of the above materials similar to the zeolites. On the other hand, porous polymer networks[86] are generally amorphous materials formed from rigid building units through strong covalent bonds, which leads to excellent hydrothermal stability of these materials. All these three-dimensional networks or polymeric frameworks are insoluble solids which render them difficult for solution-processing. In this respect, polymers with intrinsic microporosity (PIM),[87] where the frustrated solid-state packing due to structural rigidity results in the microporosity of these materials, can

be processed from solution. The same concept has been utilized to develop organic monomers with intrinsic microporosity (OMIMs).[88] For OMIMs, the bulky substituents at the periphery of a molecular adduct formed from rigid structural building units prevents the molecules to pack efficiently in solid-state which, in turn, gives rise to the microporosity of the materials. Another way to obtain a porous material from discrete organic molecules is to design a molecule with proper geometry and with hydrogen bonding functionalities so that extrinsically porous crystalline materials[89] can be obtained by the directional intermolecular hydrogen bonding interactions among different molecular building blocks. In contrast to the extrinsic porous molecules, porous organic cage compounds[90] are the molecules possessing intrinsic cavities inside the rigid shape-persistent molecular structure. Unlike the extended porous frameworks, these organic cages are usually synthesized in solution and characterized by standard analytical techniques used for small organic molecules and finally assembled in the solid-state to form porous materials. The solubility of the organic cage molecules in common organic solvents offers a significant advantage over the insoluble organic and inorganic polymeric framework to process these materials from solution. This solution-processability as well as the defined shape and size of the cage compounds also facilitates easy functionalization either at the periphery or in the confined space to encode the desired functionalities predictably thereby forming porous materials with specific properties.

2.3.1 Covalent Organic Cage Compounds

Organic cage compounds can be synthesized *via* irreversible or reversible pathways. Metal-catalyst assisted carbon-carbon cross-coupling,[91] nucleophilic aromatic substitution[92] and azide-alkyne Huisgen cycloaddition[93] are some examples for the irreversible reactions utilized to synthesize porous organic cage structures. Irreversible synthetic routes generally involve linear sequences of reaction steps with the necessity of purification for each intermediate resulting in poor yields for the final cage-type assembly. In this respect, reversible bond forming reactions provide a dynamic equilibrium system which minimizes the formation of kinetic side products and allows error correction to form the thermodynamically most stable cage compound. This synthetic approach by means of dynamic covalent chemistry (DCC)[94] enhances both the yield as well as the reliability to obtain the cage as the only product. Some examples for widely-used reversible reactions are boronate ester[14, 44, 95] or boroxine formation,[96] imine condensation[49a, 90, 97] and alkyne metathesis[17c, 98] among suitable building units to the preferential formation of closed-shell organic cages (see Scheme 22).

a)

b)

c)

92

58

93

C = Catalyst

5 mol% [Mo] /
Ph₃SiOH

[Mo] =

94

95

96
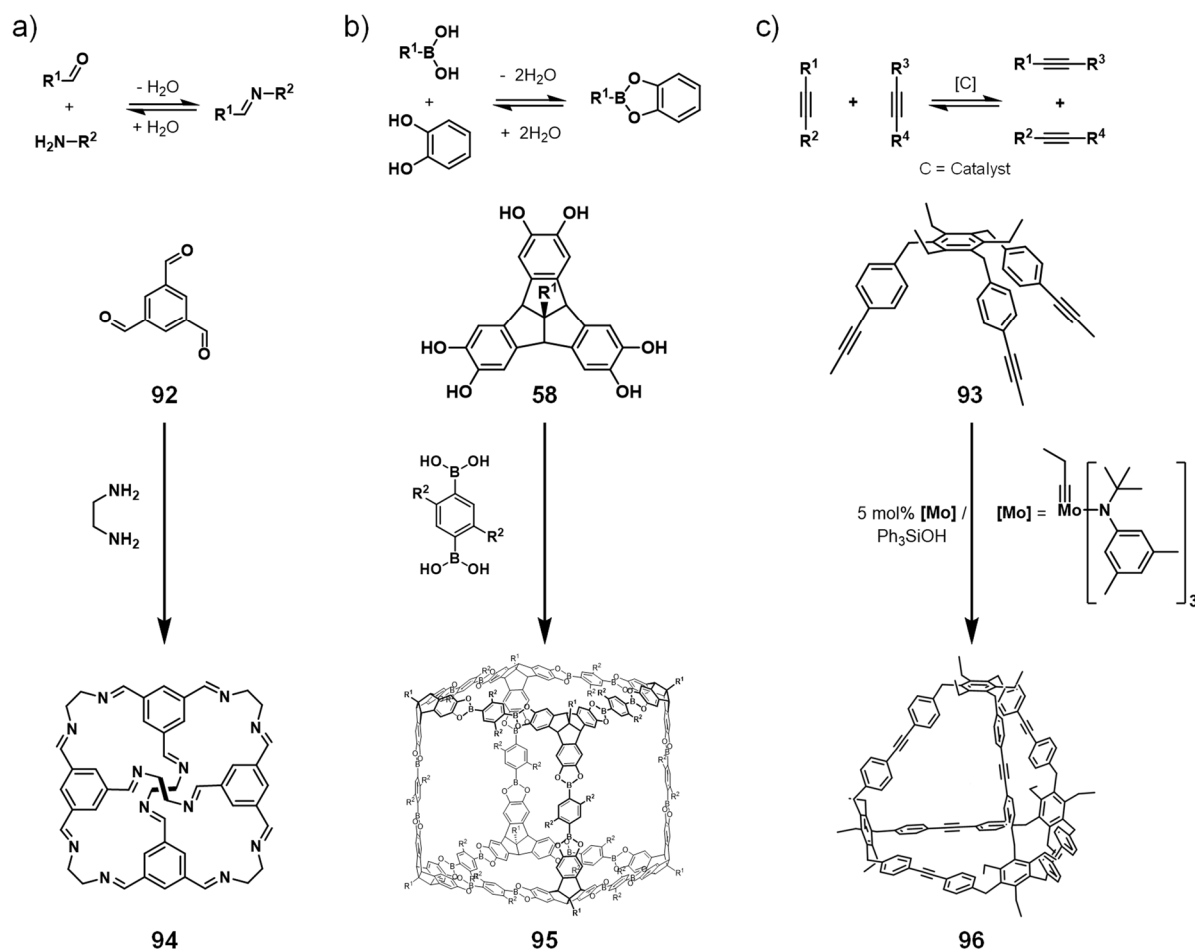
Scheme 22 | Different dynamic covalent reactions utilized for the formation of covalent organic cage compounds by dynamic covalent reactions: **a)** imine condensation to synthesize **94**, **b)** reversible boronic acid-diol reactions to form boronate ester cage **95** and **c)** metal-catalyzed alkyne metathesis to yield tetrahedral cage **96**.

Structure and topology of the self-assembled cages are usually determined by the geometry of the subcomponents and the angles between the bond-forming functionalities. One of the building blocks has to be capable of cross-linking in at least three directions in order to form a cage structure. Most of the cages reported so far are constructed by a combination of either tri- or tetratopic building units with ditopic linkers. Scheme 23 summarizes the elegant shape-selective formation of trigonal bipyramidal, tetrahedral or cubic cages reported by the Beuerle group.[14] In these organic cages, the hexahydroxy-TBTQ **58c** acts as the corner piece and depending on the bite angles of the linking functional groups for the diboronic acid counterpart, different types and shapes of boronate ester cages are obtained.
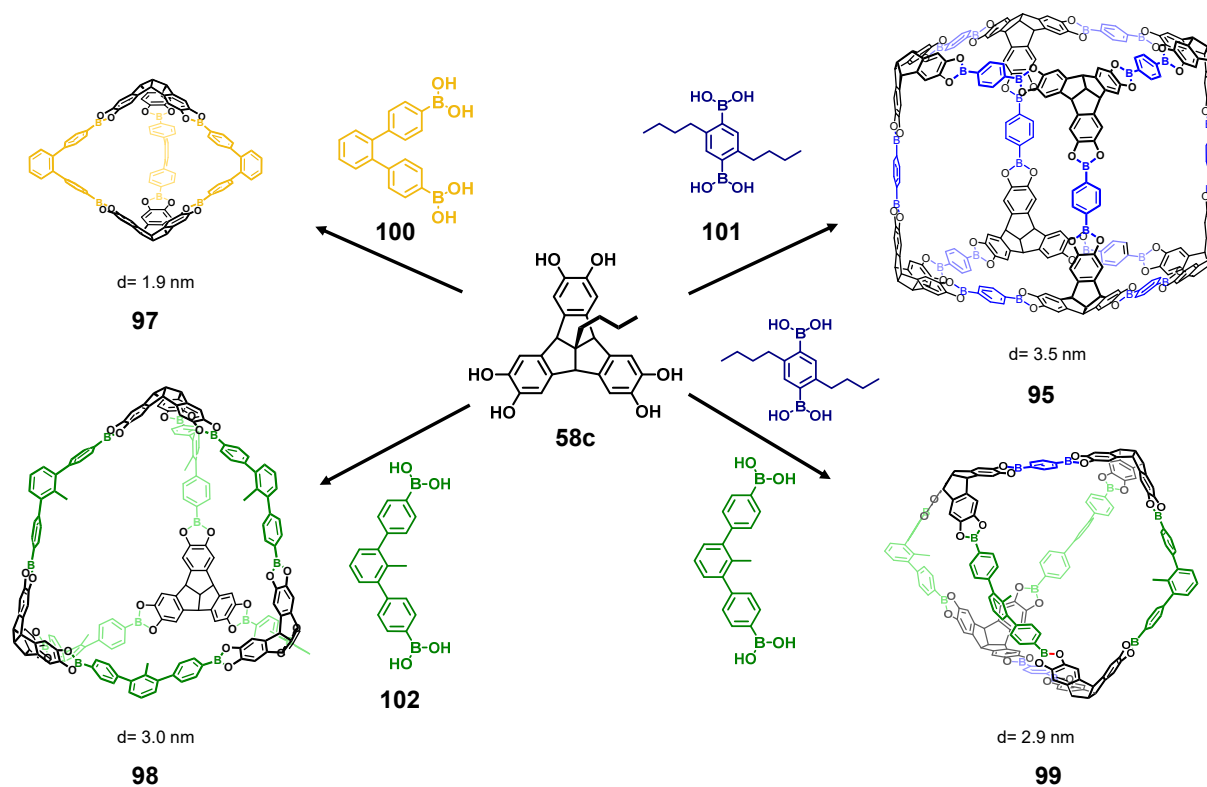
Scheme 23 | Shape-selective synthesis of molecular cages of different sizes and shapes from the orthogonal tritopic TBTQ derivative **58c** and phenylene diboronic acids with suitable bite angles between the two boronic acid units. The hydrodynamic diameter for each cage molecule are given as obtained from Stokes-Einstein equation from DOSY-NMR data. The alkyl groups (except methyl) on the cage compounds are not shown for visual clarity.

Interestingly, a mixed cage assembly **99** can be synthesized as the sole product from a ternary mixture of TBTQ unit **58c** with two different types of diboronic acids (**101** and **102**). This example underlines how the shape and structure of organic cages can be predicted elegantly by the rational control over the geometry and the bite angles among the reactive sites of the building blocks as long as the cage is the most stable thermodynamic product from the precursor molecular units.

2.3.2 Endohedral Functionalization of Covalent Organic Cage Compounds

Such rigid organic cage compounds usually possess highly-defined molecular pores that can selectively be functionalized to understand structure-property relationships of the cage materials, provided a proper functional group is pointing inwards the cage compound. Figure 12 shows a [4+6]-imine cage **105**, which offers the potential for functionalization of the cage

cavity through reactions at the hydroxyl groups.[99] The Mastalerz group explored the post-synthetic modification of the hydroxyl groups of cage **105** by Williamson ether synthesis using different alkyl halides.
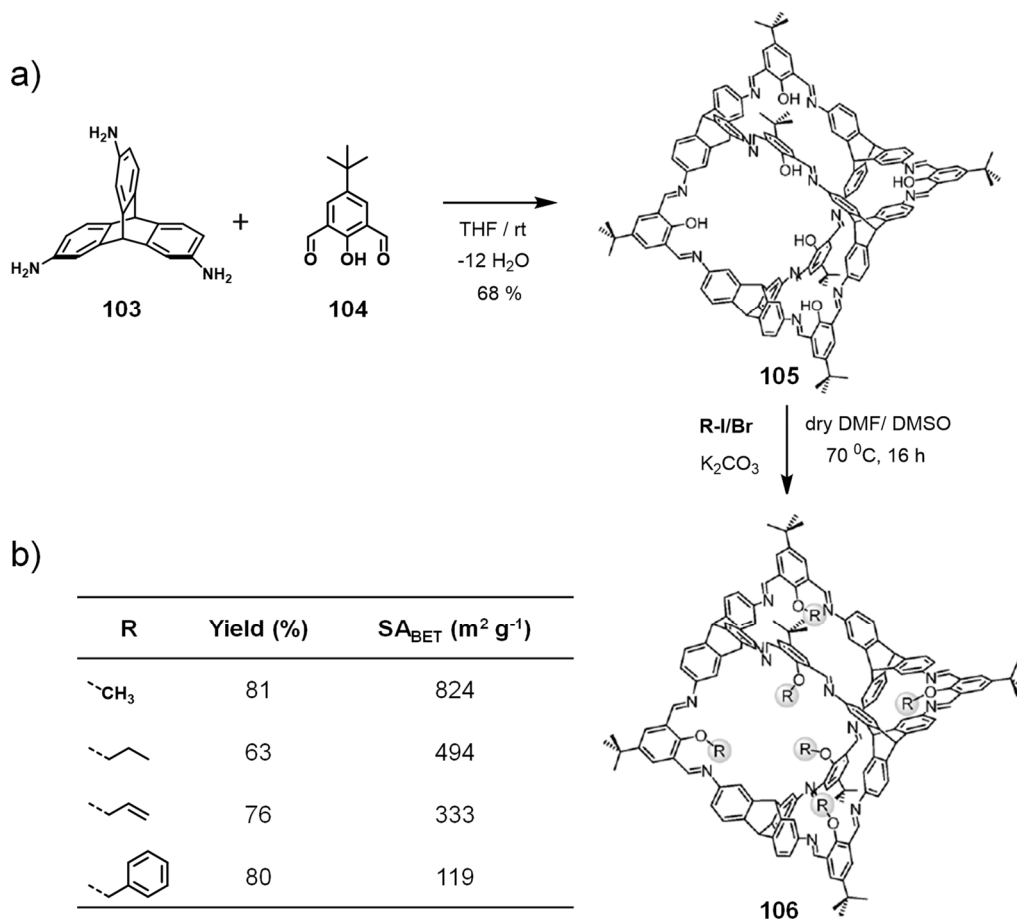

Figure 12 | a) The dynamic imine condensation to synthesize organic cage **105** followed by the post-synthetic modification of hydroxyl groups by the six-fold Williamson etherification; **b)** isolated yields and specific surface areas of the endohedrally functionalized different cage compounds. The BET surface area was determined by nitrogen adsorption at 77 K. Adapted with permission from ref. 99. Copyright 2013 WILEY-VCH Verlag GmbH & Co. KGaA, Weinheim.

All endohedrally modified cage compounds have been subjected to gas-adsorption studies. It has been found that with increased steric demand of the substituents introduced in the interior of the cage, a lowering of the specific surface area of the cage solids was observed as determined by the Brunauer-Emmett-Teller (BET) model (Figure 12b). The alkyl groups occupy the intrinsic cavity of the cage molecule thereby blocking the gas molecules to have access the pores of the cage solids and hence, low specific surface area. Apart from this work, no other examples for endohedrally functionalized covalent organic cage compounds have been reported in the literature so far.

2.3.3 Exohedral Functionalization of Covalent Organic Cage Compounds

In addition to the `intrinsic porosity´ of covalent organic cage compounds, which is determined by the shape, size and internal functionalization of molecular cavities, organic cages can also exhibit `extrinsic porosity´ depending on the solid-state packing of molecular cages.[97a] For example, the Cooper group has reported on various tetrahedral [4+6]-cages formed by cycloimination reactions of 1,3,5-triformylbenzene with different 1,2-diamines.[90] Cage **107** derived from the cyclohexane-1,2-diamine crystallizes in a window-to-window fashion, which interconnects the internal voids of cage molecules in the solid material. This diamondoid 3D pore network leads to highly porous solids. On the other hand, in the single crystal, Cage **94** derived from ethylenediamine stacks in a window-to-arene orientation generating isolated pore volumes which, in turn, makes the intrinsic pores of the cage molecules unavailable for gas adsorption. This clearly shows the effect of exohedral functionalization of the isostructural organic cage molecules on the solid-state packing thereby affecting the porosity of the material in bulk-state. This concept was recently further verified by the Cooper group after synthesizing different isostructural tetrahedral cages by reacting 1,3,5-triformylbenzene with diamine building blocks containing various external functionalities on the periphery.[100]
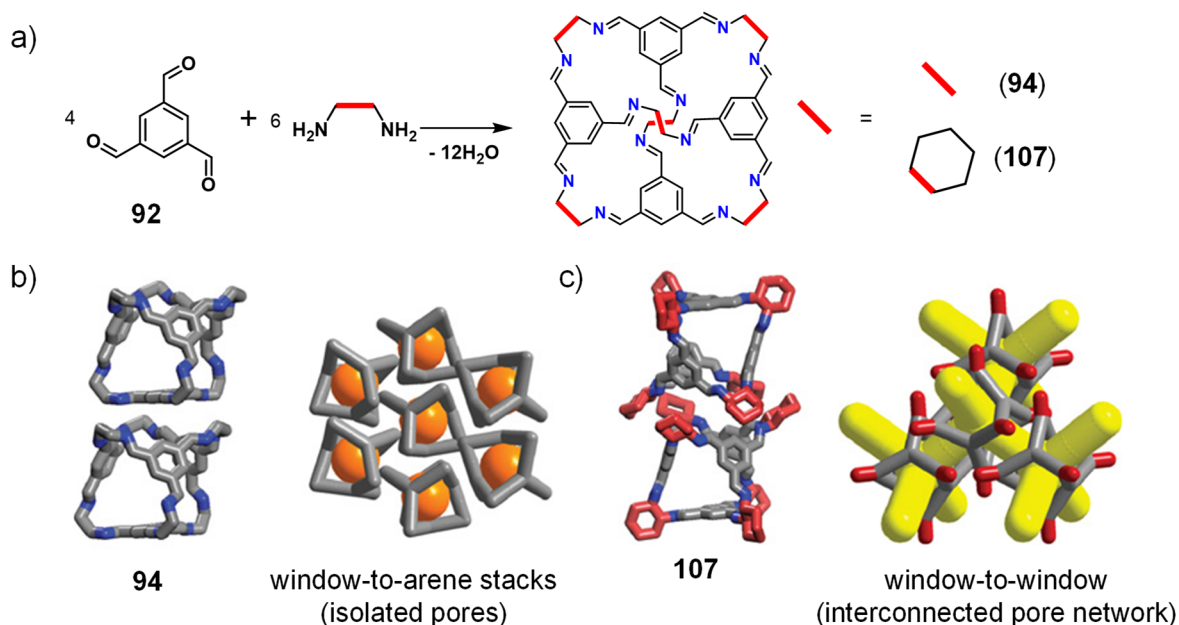

Figure 13 | a) Synthesis of organic cage compounds **94** and **107**; **b)** influence of the extrinsic functionalities on the solid-state packing of the cage molecules: Cage **94** packs in a window-to-arene fashion leading to isolated pores in the solid-state, the window-to-window stack of cage **107** results in the interconnectivity of cage cavities. Adapted with permission from ref. 90. Copyright 2009 Nature Publishing Group.

Other physical properties such as solubility or melting points of the cage compounds can also be tuned by designing and attaching appropriate ligands onto the cage exterior. When the cage periphery was functionalized by multiple alkyl groups, the porous solid melts at a certain temperature, *e.g.* the melting point of cage **108** was reported to be as low as 50 °C (Figure 14b).[101] The similar imine-linked cage **107** shows no melting point, instead it decomposes at higher temperatures above >300 °C (Figure 14a). However, the microporosity of cage **108** was drastically reduced due to the penetration of the long alkyl chain into the cavities of adjacent cages in the solid state. By installing a looped oligoether chain instead of linear alkyl groups, the Cooper group was able to construct the first example of liquids with permanent porosity when this cage was mixed with 15-crown-5 as solvent.[102] The cyclic oligoether chains on the periphery of cage **109** and also the solvent molecules cannot enter the cage cavity resulting in retaining the microporosity which enhances the bulk solubility of gases and other solutes in the liquid state (Figure 14c). A significant increase in the solubility of organic cages can also be achieved by preparing the so-called `scrambled cages´, *i.e.* a mixture of organic cage compounds with different peripheral functionalities from respective mixtures of different building blocks. Porous liquids based on these `scrambled cages´ also increased gas intake when the solvent molecules are too big to occupy the intrinsic cavities of organic cages.
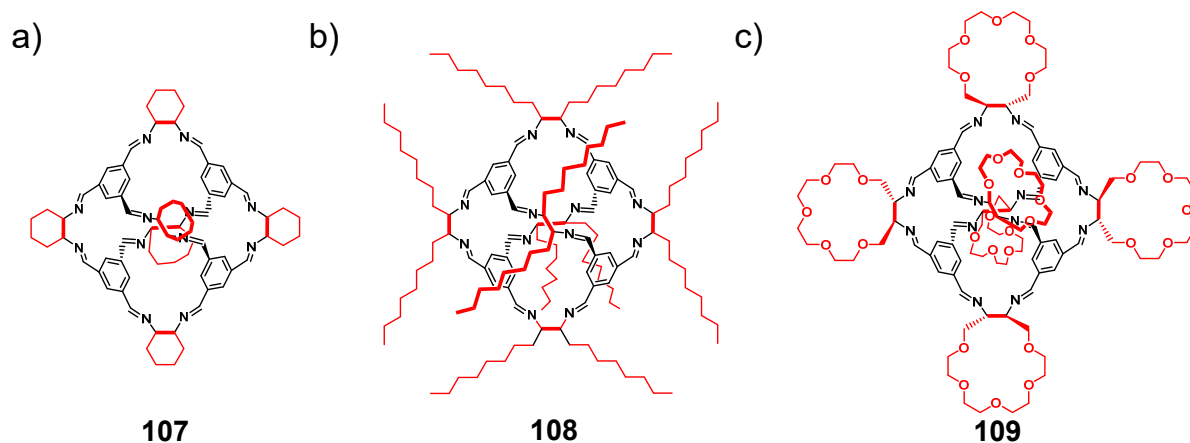

Figure 14 | Impact of the extrinsic functionality of a cage molecule on its physical state: **a)** crystalline porous solid, **b)** non-porous neat liquid (at 50 °C) and **c)** porous liquid at room temperature.

It is obvious from the above examples how the properties of organic cage compounds can be controlled by either endohedral or exohedral functionalization of the cage molecules with proper design. Hence, the benefit of synthesizing a cage molecule with both the external and the internal functional groups is undeniable. In this regard, molecular building units with functional groups installed at the proper positions need to be designed precisely so that after the formation of the cage compounds the desired functional groups are precisely located both inside the molecular void and at the periphery of the cage skeleton.

CHAPTER 3

●

Results and Discussion

## 3.1 An Organic Cage Linked by Boron-Nitrogen Dative Bonds[‡]

The reversible nature and directionality of the boron-nitrogen dative bond, as it was discussed in section **2.1**, renders it a suitable bonding motif for efficient formation of self-assembled supramolecular architectures derived from small organic building blocks. However, the formation of supramolecular cage structures based on boron-nitrogen dative bonds that are stable and can be investigated as discrete species in solution has remained elusive so far. The following section will discuss about the design and synthesis of a trigonal bipyramidal [2+3]-supramolecular cage structure assembled by boron-nitrogen dative bonds. Furthermore, the thermodynamic equilibria of cage formation have been studied by isothermal titration calorimetry (ITC) and reversible cage opening/reassembly has been investigated by variable-temperature NMR spectroscopy.

3.1.1 Design Principle

The reversible reaction between a boronic acid and a catechol leads to the formation of a boronate ester. Subsequently, the directed Lewis acid/base interaction of this three-coordinate boronate ester with a nitrogen nucleophile results in the formation of a boron-nitrogen dative bond accompanied by pyramidalization at the now four-coordinate boron center (Scheme 24a). Utilizing this concept, a supramolecular cage can, in principle, be formed assembling triboronate esters with ditopic nitrogen donor ligands. The stability of the self-assembled cage depends on the strength of the coordinating boron-nitrogen dative bonds. In this regard, any boronate ester with a high Lewis acidic boron center and any nitrogen donor linker with high

---

Lewis basicity will strengthen the dative boron-nitrogen bonds. Therefore, building blocks with appropriate electronic properties need to be considered to ensure high stability as well as the enduring formation of a supramolecular cage structure. Therefore, boronic acid **110** possessing strong electron-withdrawing substituents was singled out for obtaining the desired electron-deficient boronate ester (Scheme 24b). On the other hand, 1,4-diazabicyclo[2.2.2]octane (**111**) was chosen as the ditopic nitrogen donor ligand due to its strong nucleophilicity and rigid structure. Among all bowl-shaped molecules reported so far, tribenzotriquinacene (TBTQ) scaffold sets itself apart thanks to its unique geometry that offers a rigid curved π-surface formed by three orthogonally annulated indane wings. The rigid nature of the TBTQ backbone provides a suitable platform for its derivatives to be suitable candidates for supramolecular interactions. Hence, the formation of a supramolecular [2+3]-assembly with bipyramidal shape can be envisaged after interaction of the trigonal trisboronate ester of TBTQ **58b** with linear bifunctional linkers **111** (Scheme 24b).
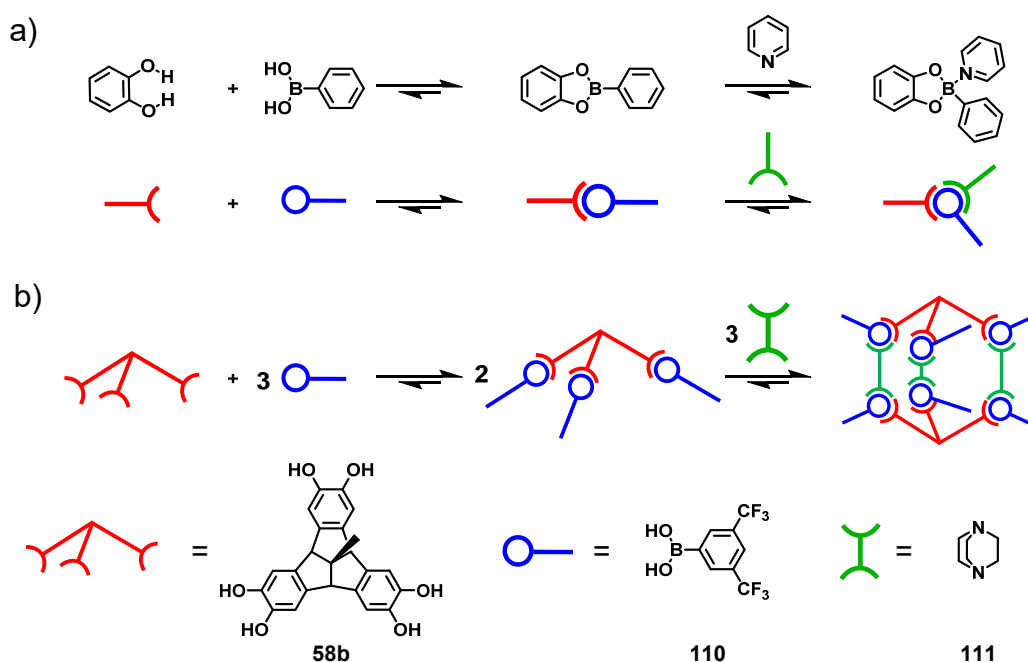
Scheme 24 | a) The formation of a boron-nitrogen dative bond between a monoboronate ester and pyridine; **b)** the design principle to the formation of a supramolecular cage based on boron-nitrogen dative bonds.

3.1.2 Model System

As a simplified model system to probe the Lewis acid/base interactions between **111** and electron-deficient boronate esters, the supramolecular complexation of **111** with monoboronate ester **112** was investigated as a reference (Figure 15a). Monoboronate ester **112** was synthesized from catechol and 3,5-bis(trifluoromethyl)phenylboronic acid following the procedure described by Severin and coworkers.[39] Stock solutions of **111** and **112** were prepared in CDCl$_3$ and ^{1}H-NMR spectra were measured at various molar ratios with a constant total concentration of 9.89×10^{-3} M (Figure 15b). Variations in the molar fractions led to gradual changes of chemical shifts, which indicated lack of kinetic stability of individual species at least on the NMR time scale implying fast exchange between aggregated and non-aggregated species. As shown in Figure 15c, Job plot analysis confirmed the presence of a 1:1 complex [(**112**)·(**111**)] as the predominate species in solution, which implies very low second binding constant compared to the first binding constant of **111** with **112**.
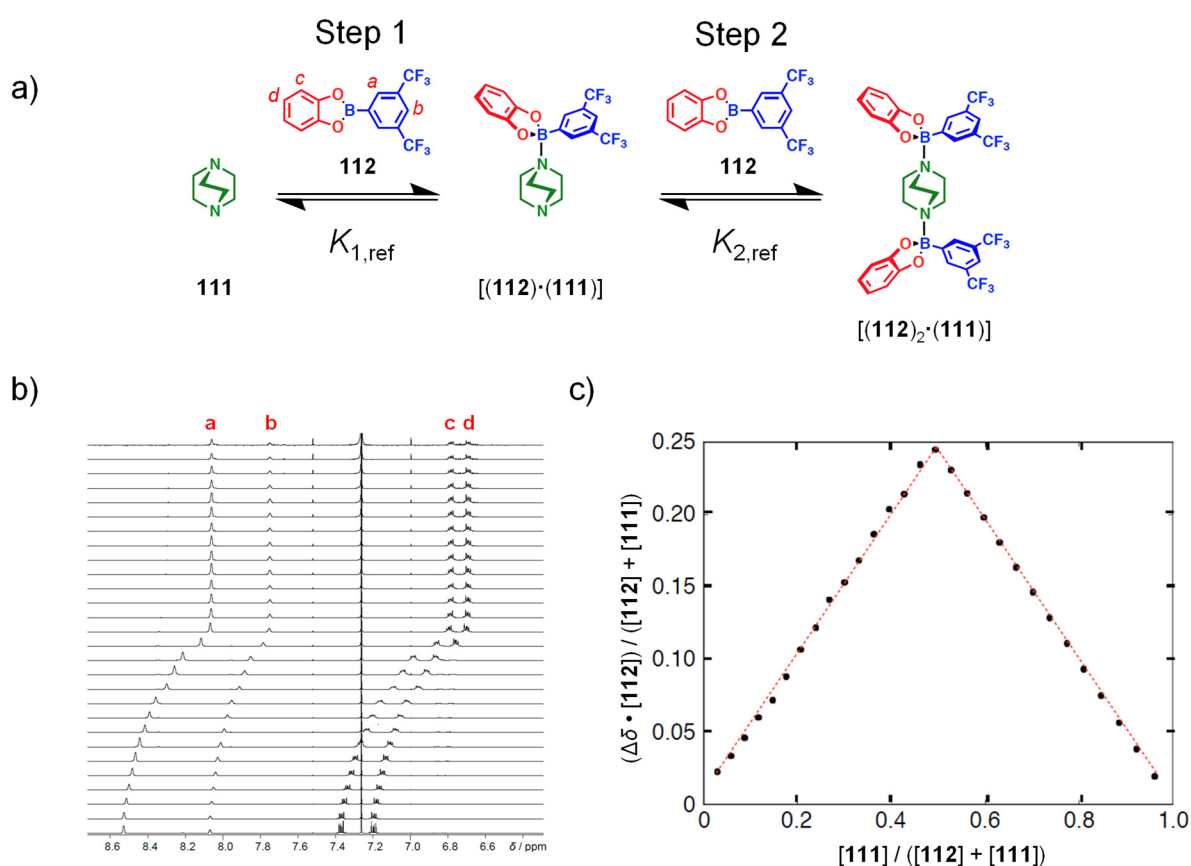

Figure 15 | a) Supramolecular complex formation between bifunctional nucleophile **111** and monoboronate ester **112**; **b)** ^{1}H-NMR (400 MHz, CDCl$_3$, rt) spectra for titration of **112** with **111** (increasing from bottom to top); **c)** Job plot for the shifts of the boronate *o*-protons (a) of **112** showing a maximum at 0.5 molar fraction which indicates formation of the [1+1]-complex as the dominant species.

Determination of the thermodynamic binding constants was not possible based on these NMR data since K was presumably higher than 10^5 M^{-1}.[103] Hence, Isothermal Titration Calorimetry (ITC) is a more suitable analytical technique to obtain thermodynamic information for this model system. ITC measurements were carried out for the stepwise injection of 2 μL solution of **112** (20.2 mM in CDCl$_3$) at a rate of 0.5 μL/s into the calorimeter cell containing a solution of **111** (1.43 mL, 1.08 mM in CDCl$_3$) at 293 K. The time spacing between consecutive injections was 120 seconds (Figure 16a).

For fitting with the [1:1]-model, equations for single set of identical sites were used (Figure 16b) and parameters n (stoichiometry), K, ΔH and ΔH_{corr} were optimized. For fitting with the [2:1]-model, equations

$$(1) \quad [112]_{total} = [112] + K_{1,ref}\cdot[112]\cdot[111] + 2\cdot K_{1,ref}\cdot K_{2,ref}\cdot[112]^2\cdot[111] \quad \text{and}$$

$$(2) \quad [111]_{total} = [111] + K_{1,ref}\cdot[112]\cdot[111] + K_{1,ref}\cdot K_{2,ref}\cdot[112]^2\cdot[111]$$

were solved numerically and heat changes for each titration step were calculated according to

$$(3) \quad Q_i = V\cdot(\Delta H_{1,ref}\cdot K_{1,ref}\cdot[112]_i\cdot[111]_i + \Delta H_{2,ref}\cdot K_{1,ref}\cdot K_{2,ref}\cdot[112]_i^2\cdot[111]_i).$$
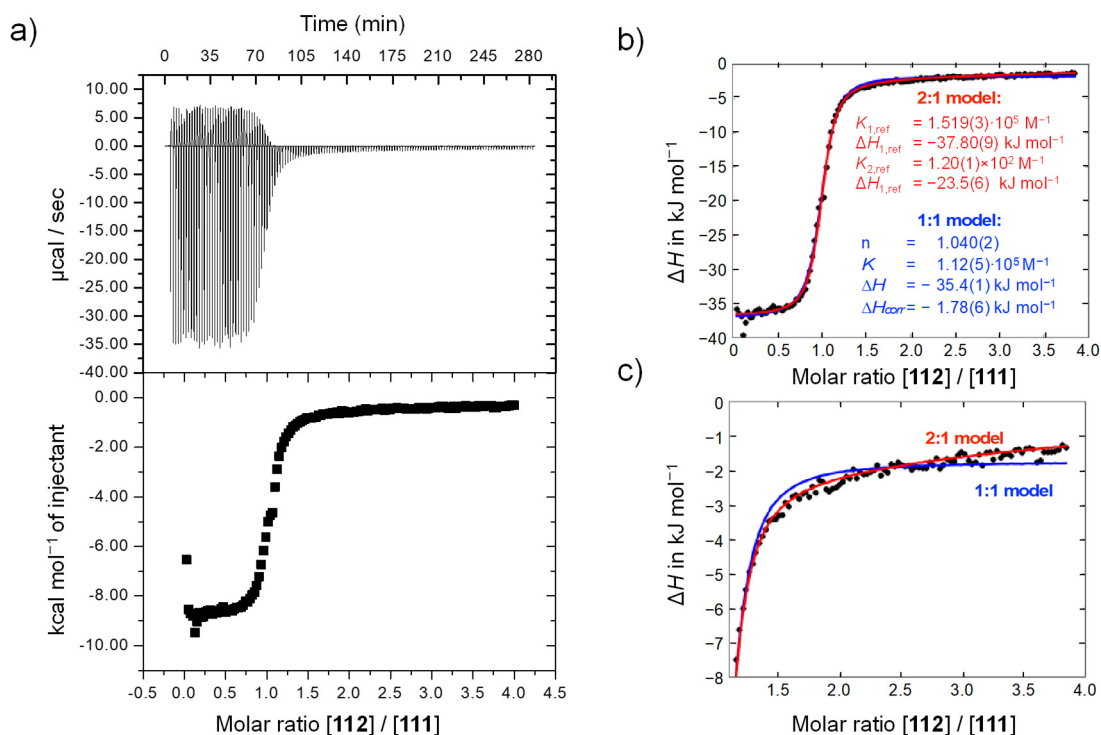

Figure 16 | a) Isothermal Titration Calorimetry (ITC) data for model system [(**112**)$_n$ · (**111**)]; **b)** Fitting of heat/mole curve for ITC experiment of model system [(**112**)$_n$ · (**111**)] to [1:1]-model (single set of identical sites, blue line) and to [2:1]-model (red line); **c)** region of excess **112** showing differences for [1:1] and [2:1]-model.

Initial assignment of $K_{1,ref}$ and $K_{2,ref}$ was followed by iterative optimization of $\Delta H_{1,ref}$, $K_{1,ref}$, $\Delta H_{2,ref}$ and $K_{2,ref}$. Better fitting of the experimental data was obtained considering the 2:1 binding model (see Figure 16c), which provided association constants of $K_{1,ref} = 1.519(3) \times 10^5\,M^{-1}$ and $K_{2,ref} = 1.20(1) \times 10^2\,M^{-1}$ and molar enthalpies of $\Delta H_{1,ref} = -37.80(9)\,kJ\,mol^{-1}$ and $\Delta H_{2,ref} = -23.5(6)\,kJ\,mol^{-1}$, respectively.

From these K-values, ΔG for each step at 293 K can be calculated from equation 4. Now, plugging the values of molar enthalpies obtained from the fitted ITC-data to equation 5, the other important thermodynamic constant, ΔS can be obtained.

$$(4) \quad \Delta G = - RT \ln K$$

$$(5) \quad \Delta G = \Delta H - T\Delta S$$

T = absolute temperature = 293 K
R = gas constant = 8.314 J mol^{-1} K^{-1}

Table 1 | Thermodynamic parameters of the two steps for the equilibrium between **112** and **111**.

	K (M^{-1})	ΔG (kJ mol^{-1})	ΔH (kJ mol^{-1})	ΔS (kJ mol^{-1}K^{-1})
Step 1	1.5×10^5	−29.0	−37.8	−0.0300
Step 2	1.2×10^2	−11.7	−23.5	−0.0403

The experimentally determined association constants (K_{exp}) of a generic equilibrium (equation 6) can be factorized into an intrinsic binding constant K_i and a statistical factor K_σ. According to Benson's symmetry number method,[104] K_σ can be calculated by the ratio of the product of all symmetry numbers for reactants and products of all symmetry numbers of all products in an equilibrium.

$$(6) \quad aA + bB \rightleftharpoons cC + dD$$

$$(7) \quad K_i = \frac{K_{exp}}{K_\sigma}, \text{ where } K_\sigma = \frac{\prod_i \sigma_{i,react}}{\prod_i \sigma_{i,prod}}$$

This approach stems from the fact that the symmetry number of a molecule (σ) influences the rotational entropy by a factor $-R \ln \sigma$. Now, σ is the product of external (σ_{ext}) and internal symmetry numbers (σ_{int}). The external symmetry factor σ_{ext} is the number of different but indistinguishable conformational arrangements that can be obtained by rotating any given molecule. This number can be determined from the corresponding point group of the molecule.[104d] Similarly, the internal symmetry factor σ_{int} is defined by the number of different but indistinguishable atomic arrangements obtainable by internal rotation of single bonds. This

factor σ_{int} corresponds to the product of the rotation axes of the rotors involved. For the reference system a two-step binding model between monoboronate ester **112** and **111** is considered, where the first step involves the formation of [(**112**)·(**111**)] followed by further addition of **112** leading to the 2:1 complex [(**112**)$_2$·(**111**)] (Figure 15). To assess the cooperativity for both steps, statistical factors for each step have been calculated using Benson´s approach (see Table 2) and then intrinsic bindings constants $K_{1,ref}$ and $K_{2,ref}$ have been evaluated from apparent association constants which have been obtained experimentally by ITC.

Table 2 | Internal, external and total symmetry numbers for each species.

| Component	Point Group	σ_{ext}	σ_{int}	σ
112	C_{2v}	2	1	2
111	D_{3h}	6	1	6
[(**112**)·(**111**)]	C_s	1	3	3
[(**112**)$_2$·(**111**)]	C_{2v}	2	3	6

Step 1	**Step 2**
$K_{\sigma(1)} = (2 \times 6) / 3 = 4$	$K_{\sigma(2)} = (3 \times 2) / 6 = 1$
$K_{1,ref} = 1.5 \times 10^5 \, M^{-1}$	$K_{2,ref} = 1.2 \times 10^2 \, M^{-1}$
$K_{i(1,ref)} = (1.5 \times 10^5) \, M^{-1} / 4 = 3.8 \times 10^4 \, M^{-1}$	$K_{i(2,ref)} = (1.2 \times 10^2) \, M^{-1} / 1 = 1.2 \times 10^2 \, M^{-1}$

The statistically corrected values of the association binding constants for the formation of [(**112**)·(**111**)] and [(**112**)$_2$·(**111**)] are $3.8 \times 10^4 \, M^{-1}$ and $1.2 \times 10^2 \, M^{-1}$, respectively.

Since $K_{i(1,ref)} \gg K_{i(2,ref)}$, the interaction between **112** and **111** can be considered as heterotopic allosteric anti-cooperativity. So, the binding of one boronate ester molecule decreases the affinity of **111** to bind with another boronate ester significantly. Hence, the fully bound state [(**112**)$_2$·(**111**)] is never populated in solution. Most probably, the significant decrease in the nucleophilicity after formation of the first boron-nitrogen dative bond is the reason for this large difference between these two binding constants. This also correlates well with the substantial difference between the two pK_a values for **111** (2.70 and 8.79 in water).[105] Severin and coworkers also observed similar differential binding affinities for dipyridyl axles utilized in the rotaxane formation.[39] This might be responsible for the usually fast exchange and low stability of complex supramolecular architectures mediated by boron-nitrogen dative bonds in solution. However, chelate cooperativity effects might still favor the formation if the distinct binding sites are well-organized within a rigid framework.
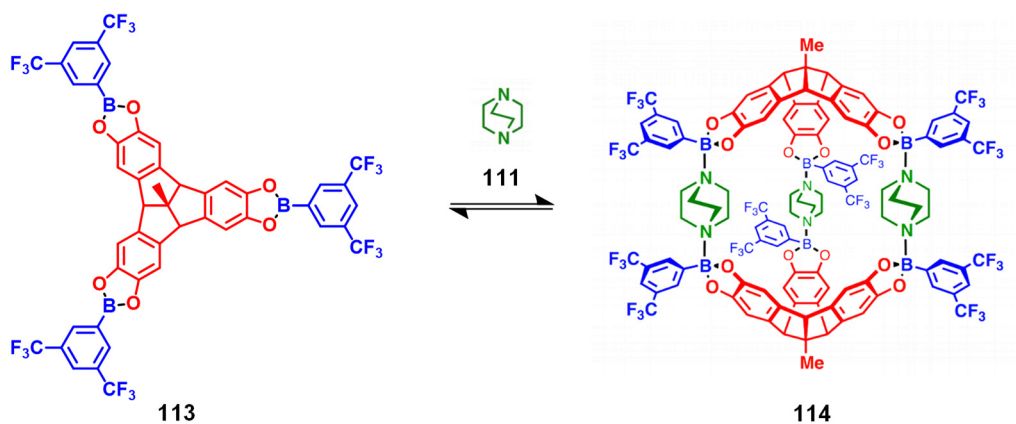
3.1.3 Supramolecular Cage Based on Boron-Nitrogen Dative Bonds

Synthesis of the trigonal trisboronate ester **113** was achieved by the reaction of TBTQ derivative **58b** with monoboronic acid **110** in reasonable yields.
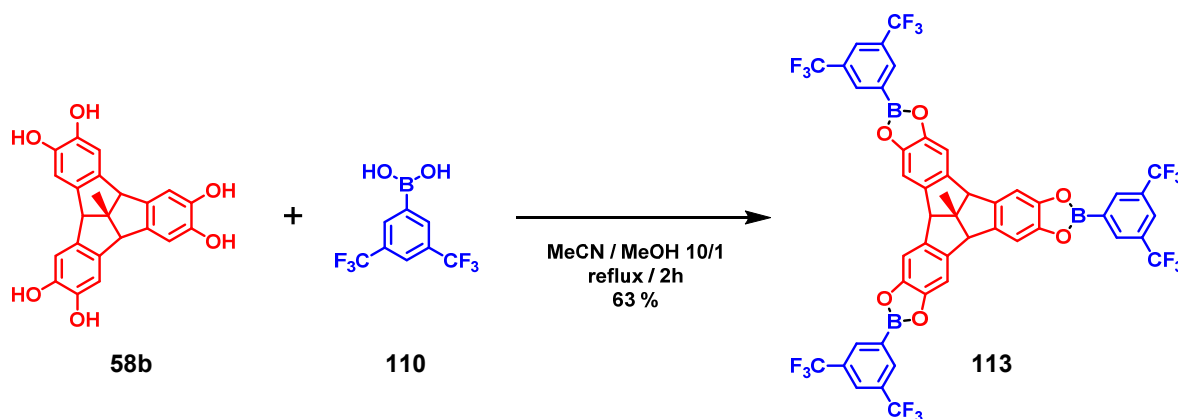
Scheme 25 | Synthesis of trisboronate ester **113** from TBTQ **58b** and boronic acid **110**.

The reaction between **113** and **111** was investigated by measuring ^{1}H-NMR spectra at different equivalents of the two compounds (Scheme 26). Therefore, stock solutions of trisboronate ester **113** (1.204×10^{-3} M) and **111** (1.204×10^{-3} M) in CDCl$_3$ were prepared and ^{1}H-NMR spectra were recorded for varying molar ratios between **113** and **111** (Figure 17). Interestingly, in contrast to the reference system [(**112**)$_n$·(**111**)], the accumulation of a new species, in addition to free **113**, with increasing amounts of **111** was observed with full conversion being reached at a molar ratio of 2:3 (Figure 17d).

Scheme 26 | The supramolecular cage-assembly based on boron-nitrogen dative bonds.
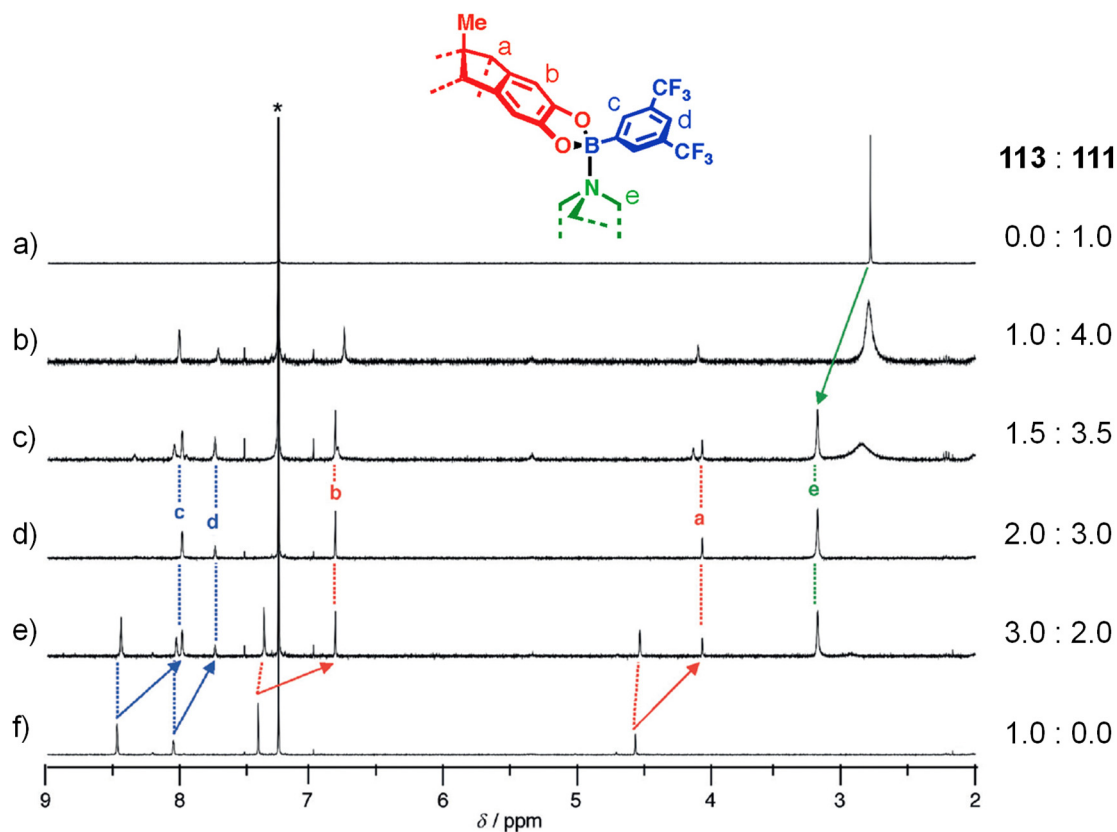
Figure 17 | ¹H-NMR spectra (400 MHz, CDCl₃, rt) of **a) 111**, **b)** and **c)** decomposition products in the case of excess **111**, **d)** supramolecular cage **114** (molar ratio **113/111** 2:3), **e)** co-existence of cage **114** and excess **111** (molar ratio **113/111** 3:2) and **f)** trisboronate ester **113**.

DOSY NMR spectroscopy measurements for the nonstoichiometric 3:2 mixtures (Figure 17e) confirmed the presence of two distinct species with different diffusion coefficients (Figure 18). For the assembled species, a hydrodynamic diameter of 1.9 nm was calculated with the Stokes–Einstein equation 8. This finding is in good agreement with a PM6-optimized model[106] (Figure 18, inset) for the proposed bipyramidal [2+3]-cage compound **114**.

$$(8) \qquad D = \frac{k_\mathrm{B}T}{6\pi\eta r}$$

T = temperature = 303.6 K

k_B = Boltzmann constant = 1.4×10^{-23} J K^{-1}

$\eta(\mathrm{CDCl_3^{pure}})$ = viscosity = 0.539 cP

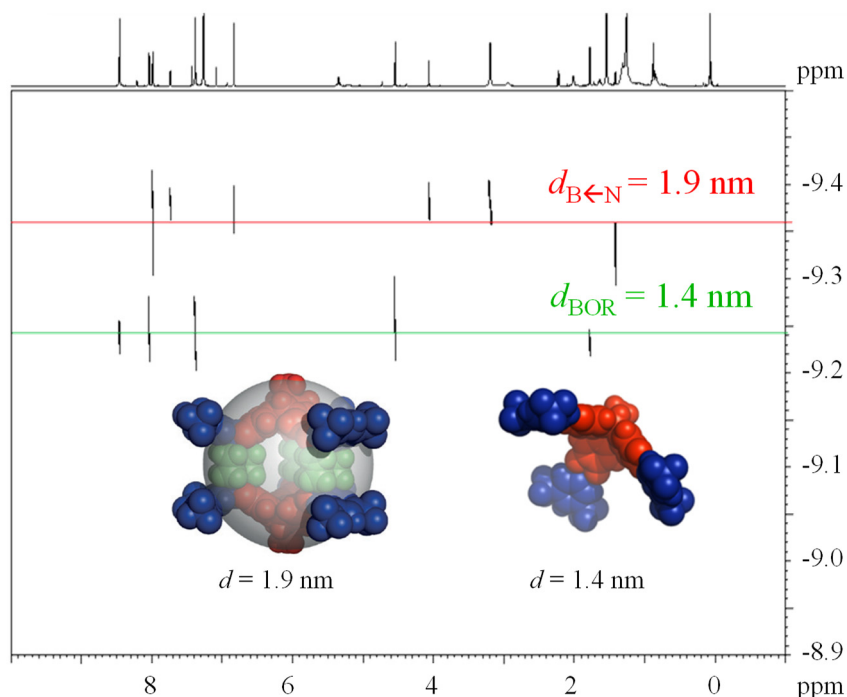D = diffusion coefficient

r = hydrodynamic radius

Figure 18 | 2D-DOSY-NMR (600 MHz, CDCl₃, rt) spectrum of solution containing supramolecular cage **114** and boronate ester **113** (molar ratio **113/111** 3:2). The hydrodynamic diameter for the PM6-optimized space-filling model of **114** is indicated as a semi-transparent grey sphere.

Unfortunately, the determination of the molecular mass of **114** by mass spectrometry failed since both ESI and MALDI-TOF measurements gave either no signals or resulted in decomposition under ionizing conditions. However, the molecular mass of **114** could be estimated by referencing the diffusion coefficient for the assembled species to free boronate ester **113** as an internal standard under the assumption that both cage **114** and boronate ester **113** possessed the same density ρ as a sphere-like particle within the Stokes–Einstein approximation (Figure 18). The calculated value of 2427.2 g mol⁻¹ is in very good agreement with the molar mass 2448.6 g mol⁻¹ for **114**.

$$(9) \quad M = \frac{4\pi r^3 \rho N_A}{3}$$

$$(10) \quad \frac{M_{114}}{M_{113}} = \frac{r_{114}^3}{r_{113}^3}$$

M = molecular weight
ρ = density
r = radius
N_A = Avogadro constant

M_{113} = 1056.07 g mol⁻¹

$\Rightarrow$ M_{114} = 2427.1 (calculated from DOSY)

M_{114} = 2448.6 g mol⁻¹

Therefore, all NMR spectroscopy data provide convincing evidence for the highly efficient and fast formation of cage **114**. Self-assembly takes place instantaneously after mixing the precursors, and the aggregates possess a surprisingly high kinetic stability because both **114** and **113** coexist with no exchange, at least on the NMR timescale, for substoichiometric amounts of **111**. However, for excess of **111**, decomposition of **114** occurs, which results in species with a higher content of **111**, for example, [(**113**)·(**111**)$_3$], as the most plausible final products (see Figure 17b and c).

The determination of thermodynamic association parameters for the formation of the aforementioned [2+3]-supramolecular cage is of immense importance in order to understand the underlying equilibrium processes that govern the self-assembly of the organic building units into supramolecular cage structure through boron-nitrogen dative bonds. So, to gain more insight into the association equilibria and to estimate binding constants for the individual steps, ITC measurements for the stepwise addition of **111** into a stock solution of **113** was performed in CHCl$_3$ at 293 K. The curve shape clearly indicates two distinct processes and both steps could be fitted individually to a sequential binding model that revealed stoichiometries of 1.5 and 2.5, as well as molar enthalpies of –124.0 kJ mol^{-1} and –45.7 kJ mol^{-1}, respectively (see Figure 19a). For all following fits, concentrations of **111** were adjusted in order to reach a stoichiometry of 1.5 for the assembly step (most probably due to impurities or partial decomposition of the boronate ester **113**).
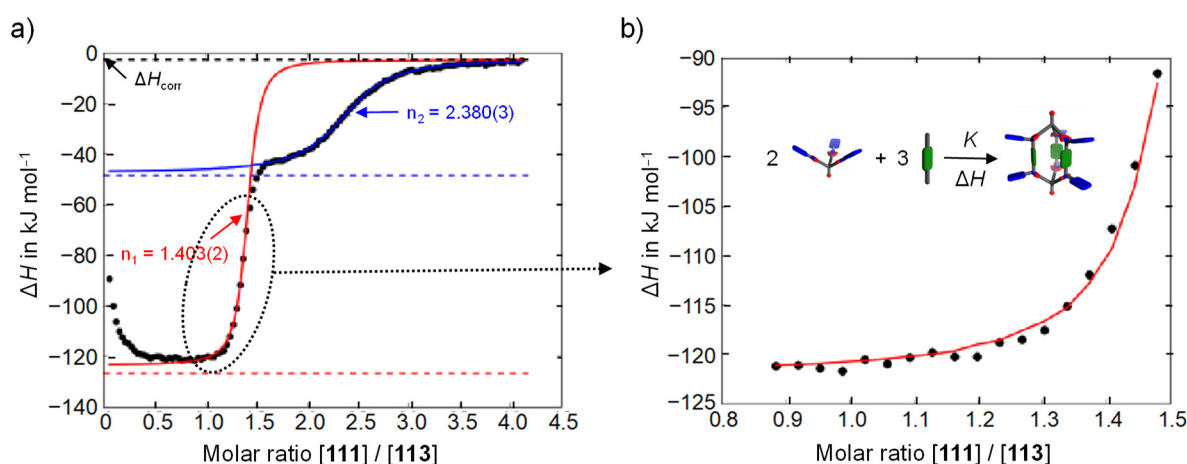

Figure 19 | Isothermal Titration Calorimetry (ITC) data for the formation of supramolecular cage **114**; **a)** fitting of both cage formation (first step, red line) and disassembly (second step, blue line) to one set of identical binding sites; parameters n and ΔH_{corr} were optimized; **b)** fitting of heat/mole curve for [**111**]/[**113**] from 0.9 to 1.5 to [2:3]-model (red line).

For molar ratios [**111**]/[**113**] in the range of 0.9 to 1.5, the stepwise addition of **111** leads to the cooperative formation of cage **114**. For fitting with a [2:3]-model, equations

(11) $[\mathbf{113}]_{total} = [\mathbf{113}] + 2 \cdot K \cdot [\mathbf{113}]^2 \cdot [\mathbf{111}]^3$ and

(12) $[\mathbf{111}]_{total} = [\mathbf{111}] + 3 \cdot K \cdot [\mathbf{113}]^2 \cdot [\mathbf{111}]^3$

were solved numerically and heat changes for each titration step were calculated according to

(13) $Q_i = V \cdot \Delta H \cdot K \cdot [\mathbf{113}]_i^2 \cdot [\mathbf{111}]_i^3$.

After an initial guess for ΔH and K, iterative optimization of ΔH and K was performed which provided an apparent association constant of $K = 8.43(2) \times 10^{22}\,\mathrm{M^{-4}}$ and a reaction enthalpy of $\Delta H = -368.2(7)\,\mathrm{kJ\,mol^{-1}}$. Therefore, the contribution of each boron-nitrogen dative bond to the bonding enthalpy of the cage formation is $61.4\,\mathrm{kJ\,mol^{-1}}$.

To simulate the ITC experiment, a simplified model depicted in Figure 20 is proposed. The initial slope in the binding isotherm for the first addition steps of **111** to an excess amount of **113** can most probably be attributed to the initial formation of small amounts of the (1:1)-complex [(**113**)·(**111**)]. With ongoing addition of **111**, efficient assembly of cages **114** takes place until full conversion at optimum stoichiometry. In the presence of excess **111**, decomposition occurs, which results in the formation of the [(**113**)$_2$·(**111**)$_5$] assembly as the final product. All other intermediates depicted in gray in Figure 20 are presumably populated only in trace amounts and are therefore not incorporated in the model. However, the formation of [(**113**)·(**111**)$_3$] with higher excesses of **111** cannot be completely excluded, but if so, no significant heat exchange is observed for this transformation.
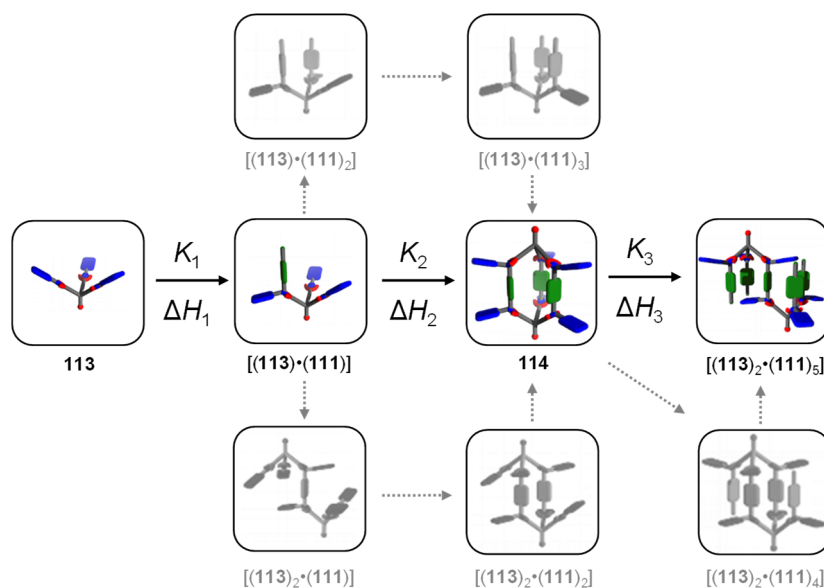

Figure 20 | Proposed model for the assembly and the disassembly of supramolecular cage **114**.

Based on this four-component model, simulation of the titration curve and fitting of the experimental data was done with a python script.[107] For fitting with the four-component model, equations

(14) $[113]_{total} = [113] + K_1 \cdot [113] \cdot [111] + 2 \cdot K_1 \cdot K_2 \cdot [113]^2 \cdot [114]^3 + 2 \cdot K_1 \cdot K_2 \cdot K_2 \cdot [113]^2 \cdot [111]^5$

(15) $[111]_{total} = [111] + K_1 \cdot [113] \cdot [111] + 3 \cdot K_1 \cdot K_2 \cdot [113]^2 \cdot [111]^3 + 5 \cdot K_1 \cdot K_2 \cdot K_2 \cdot [113]^2 \cdot [111]^5$

were solved numerically and heat changes for each titration step were calculated according to

(16) $Q_i = V \cdot (\Delta H_1 \cdot K_1 \cdot [113]_i \cdot [111]_i + (\Delta H_1 + \Delta H_2) \cdot K_1 \cdot K_2 \cdot [113]_i^2 \cdot [111]_i^3 + (\Delta H_1 + \Delta H_2 + \Delta H_3)$
$\cdot K_1 \cdot K_2 \cdot K_3 \cdot [113]_i^2 \cdot [111]_i^5$

Values of ΔH_1, $(\Delta H_1 + \Delta H_2)$ and ΔH_3 were fixed to -37.8 kJ mol^{-1} (derived from model compound $[(112) \cdot (111)]$), -368.2 kJ mol^{-1} (derived from [2:3]-model) and -45.7 kJ mol^{-1} (derived from fit for disassembly process), respectively. $K_1 \cdot K_2$ was fixed to $8.43 \cdot 10^{22}$ M^{-4} (derived from [2:3]-model) whereas K_1 and K_3 were fitted to the experimental data according to the four-component model independently in order to match respective parts of the binding isotherm. The simulated heat release is shown as a red line in Figure 21a. Based on these K values, the concentrations for all species at each titration step could be calculated and the mole fractions depending on the total concentration of **113** are depicted in Figure 21b.
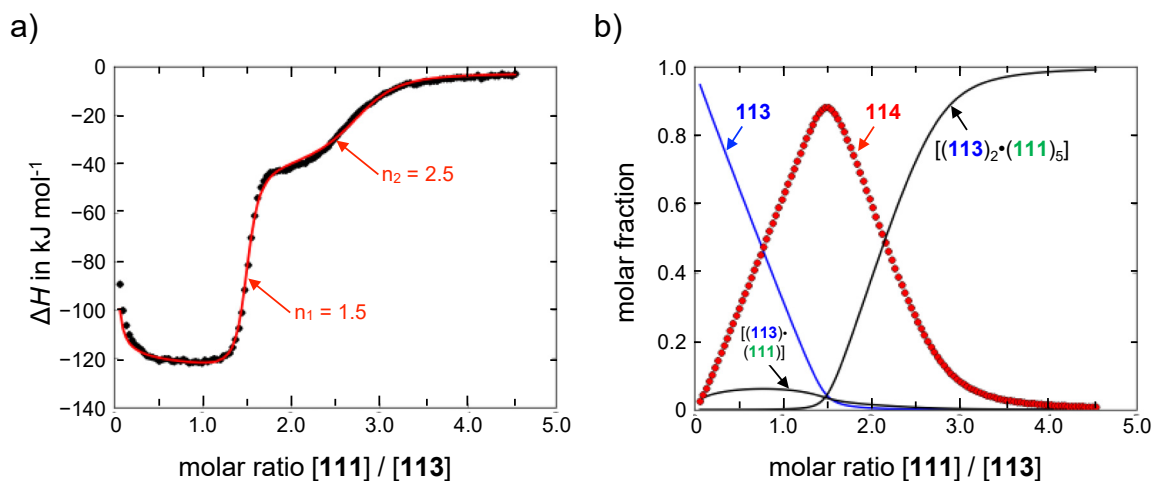

Figure 21 | a) Heat/mole curve for ITC after stepwise addition of **111** to a solution of **113** in CHCl$_3$ at 293 K; the curve shape indicates two independent processes with stoichiometries of n$_1$=1.5 and n$_2$=2.5, respectively (fitting according to the four-component model is indicated as a red line); **b)** variation of the mole fractions of relevant species calculated from the obtained K values as a function of the molar ratio [**111**]/[**113**].

From the values of association constants K and ΔH all other thermodynamic constants can be calculated for these binding events following equations 4 and 5.

Table 3 | Thermodynamic parameters of the three steps for equilibrium between **113** and **111** at 293 K.

K	ΔG (kJ mol^{-1})	ΔH (kJ mol^{-1})	ΔS (kJ mol^{-1}K^{-1})
2.5×10^5 M^{-1}	−30.3	−37.8	−0.0256
3.4×10^{17} M^{-3}	−98.3	−330.4	−0.7922
4.6×10^9 M^{-2}	−54.2	−45.7	+0.0290

Similar to the model system, the experimentally obtained association constants have been deconvoluted onto statistical factors and intrinsic binding constants for each step.

Table 4 | Internal, external and total symmetry numbers for each species.

Component	Point Group	σ_{ext}	σ_{int}	σ
113	C_{3v}	3	1	3
111	D_{3h}	6	1	6
[(**113**)·(**111**)]	C_s	1	3	3
[(**113**)$_2$·(**111**)$_3$]	D_{3h}	6	3^3	162
[(**113**)$_2$·(**111**)$_5$]	C_{2h}	2	3^6	1458
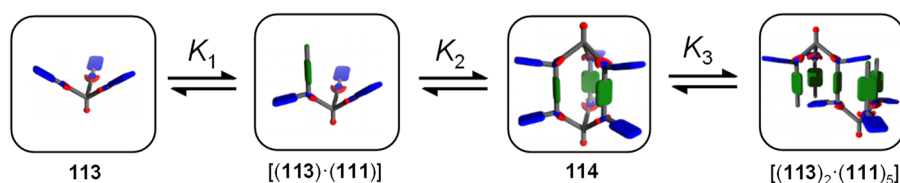
$$K_{\sigma(1)} = \frac{3 \times 6}{3} = 6$$
$$K_1 = 2.5 \times 10^5 \text{ M}^{-1}$$
$$K_{i(1)} = \frac{2.5 \times 10^5}{6} \text{ M}^{-1} = 4.2 \times 10^4 \text{ M}^{-1}$$

$$K_{\sigma(2)} = \frac{3 \times 3 \times 6^2}{162} = 2$$
$$K_2 = 3.4 \times 10^{17} \text{ M}^{-3}$$
$$K_{i(2)} = \frac{3.4 \times 10^{17}}{2} \text{ M}^{-3} = 1.7 \times 10^{17} \text{ M}^{-3}$$

$$K_{\sigma(3)} = \frac{162 \times 6^2}{1458} = 4$$
$$K_3 = 4.6 \times 10^9 \text{ M}^{-2}$$
$$K_{i(3)} = \frac{4.6 \times 10^9}{4} \text{ M}^{-2} = 1.2 \times 10^9 \text{ M}^{-2}$$

By comparing the values of the intrinsic association constants of the model system with the formation of cage **114**, it can be observed:

$$K_{i(1)} \approx K_{i(1,\text{ref})} \approx 4 \times 10^4 \text{ M}^{-1}$$

The fact that the intrinsic equilibrium constant $K_{i(1)}$ of the four-component model and $K_{i(1,ref)}$ of the model system are same suggests that the binding of **111** to one of the boronate esters of **113** is not affected by the other two boronate esters, which do not participate in binding with **111** while the formation of [(**113**)·(**111**)]. Hence, it can be assumed that the thermodynamic parameters associated with two-step binding of **111** with monobonate ester **112** for the reference system remain same for the three-step equilibrium between **113** and **111**, if we consider the following conditions:

A. Once one **111** molecule is bound to one of the boronate ester units of **113**, it does not influence the binding of a second **111** molecule to other boronate ester of the same **113**.

B. The association constant of one boronate ester unit of **113** with one boronate ester-bound **111** is equal to the intrinsic binding constant $K_{i(2,ref)}$ of the model system multiplied by the statistical factor of that step.

Considering these assumptions, we can propose the following extended model for the formation of cage **114**.
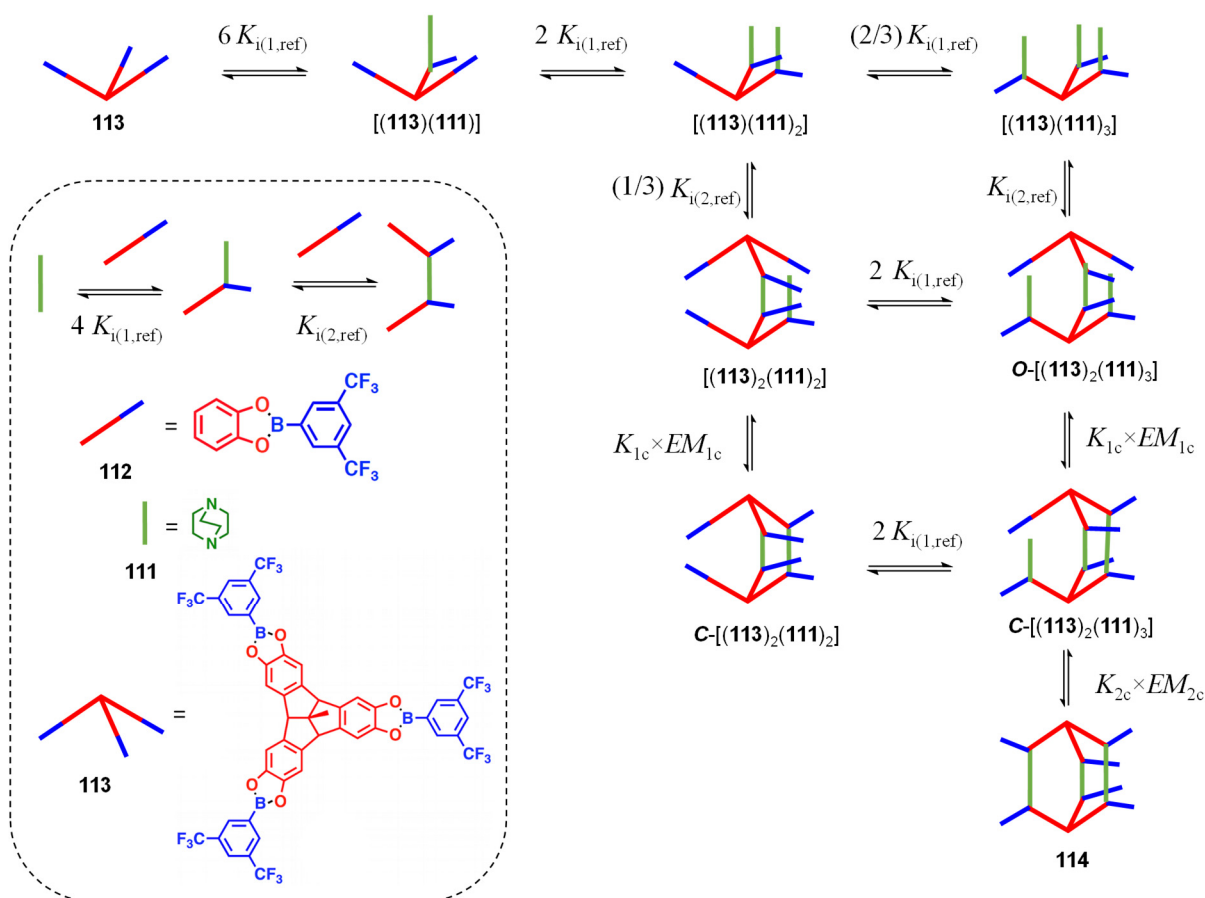

Figure 22 | The extended model for the assembly of cage **114**. EM_c = Effective molarity for each cyclization step.

To understand the intramolecular cooperativity[108] during cage formation, the competition between ring closure to cage **114** and formation of open oligomer starting from the "open" [2+3]-assembly O-[(**113**)$_2$·(**111**)$_3$] has to be considered, if Anderson and Hunter´s approach is followed.[109] The positive cooperativity would shift the equilibrium towards the cage structure, while the negative cooperativity will lead to the formation of mixture of oligomers. According to this model, thermodynamic association constant for the formation of "open" complex O-[(**113**)$_2$·(**111**)$_3$] from individual **113** and **111** building units can be expressed as the following equation:

(17) $K(O\text{-}[(\mathbf{113})_2 \cdot (\mathbf{111})_3]) = 6 \times 2 \times (2/3) \times [K_{i(1,\text{ref})}]^3 \times [K_{i(2,\text{ref})}] = 8 \times (4 \times 10^4)^3 \times 1.2 \times 10^2 \text{ M}^{-4}$

$\Rightarrow$ $K(O\text{-}[(\mathbf{113})_2 \cdot (\mathbf{111})_3]) = 6.1 \times 10^{16} \text{ M}^{-4}$

The binding constant for the formation of **114** from the individual **113** and **111** (Table 3) can be calculated by:

(18) $K(\mathbf{114}) = K_1 \times K_2 = (2.5 \times 10^5 \text{ M}^{-1}) \times (3.4 \times 10^{17} \text{ M}^{-3}) = 8.5 \times 10^{22} \text{ M}^{-4}$

According to the extended model (Figure 22), the association constant for the formation of "closed" **114** cage from **113** and **111** can be expressed as the following equation:

(19) $K(O\text{-}[(\mathbf{113})_2 \cdot (\mathbf{111})_3]) \times (K_{1c} \times EM_{1c}) \times (K_{2c} \times EM_{2c}) = K(\mathbf{114})$, EM = effective molarity

$\Rightarrow$ $(K_{1c} \times EM_{1c}) \times (K_{2c} \times EM_{2c}) = \dfrac{K(\mathbf{114})}{K(O[(\mathbf{113})_2 \cdot (\mathbf{111})_3]} = \dfrac{8.5 \times 10^{22} \text{M}^{-4}}{6.1 \times 10^{16} \text{M}^{-4}} = 1.4 \times 10^6$

Most probably, $EM_{2c} > EM_{1c}$ because the complex C-[(**113**)$_2$·(**111**)$_3$] is more pre-organized than the complex O-[(**113**)$_2$·(**111**)$_3$] for cyclization. For simplicity, if we consider $EM_{1c} = EM_{2c}$, then $(K \times EM_c) = \sqrt{1.4 \times 10^6} = 1.2 \times 10^3 \gg 1$. This implies high chelate cooperativity for the formation of cage **114**, which results in all-or-nothing population of cage **114**.[109]

Therefore, despite no allosteric cooperativity with respect to the multiple binding sites of **113** along with allosteric anti-cooperativity regarding the two-fold binding of **111**, strong chelate cooperativity favors the formation of cage **114** while closing the rings of open oligomers. However, for molar ratios [**111**]/[**113**] higher than 1.5 (see Figure 21b), the intermolecular interaction of excess **111** with **113** competes with chelate cooperativity for the formation of cage **114**, which finally leads to the denaturation of cage **114**.

3.1.4 Stimuli-Responsive Switching

Owing to the supramolecular nature of boron-nitrogen dative bonds, the stability of cage **114** is expected to be strongly dependent on temperature and pH. Therefore, reversible cage opening at higher temperatures and reassembly upon cooling to room temperature can be envisaged.
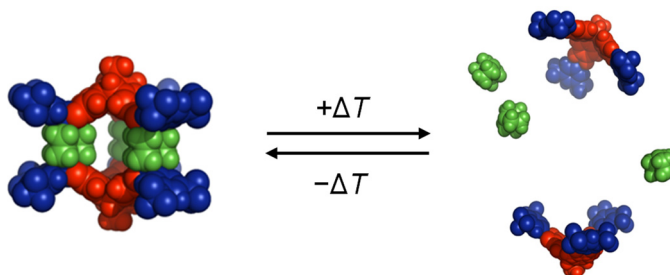

Figure 23 | Temperature-dependent on-off switching of the supramolecular [2+3]-cage **114**.

Based on the ITC-derived ΔH and ΔS values (Table 3), temperature-dependent equilibrium constants have been calculated in the range from 290 K to 430 K for all species of the four-component model (Figure 20) utilizing equations 4 and 5 by assuming the values of ΔH and ΔS are independent of ΔT. Based on the K values, concentrations of all relevant species have been calculated for a 1.9 mM solution of cage **114** at different temperatures. The calculated molar fractions of all species as a function of temperature are depicted in Figure 24.
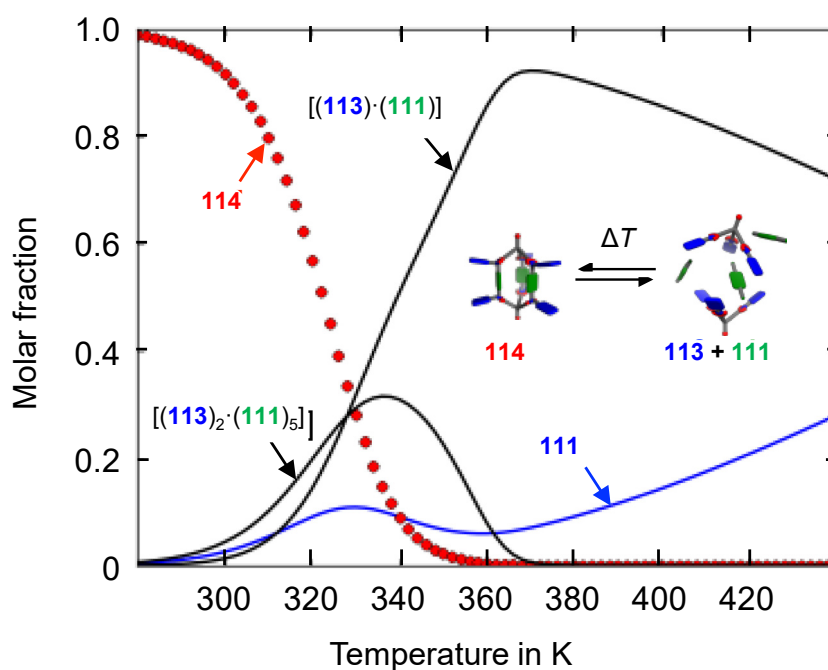

Figure 24 | Temperature-dependent simulation of mole fractions for equilibrium species of a 1.9 mM solution of **114**.

Figure 24 predicts that at higher temperatures disassembly of cage **114** leads to the formation of the 1:1 complex as the predominant species that slowly disassembles into individual building blocks at temperatures higher than 420 K. To verify these assumptions experimentally, temperature-dependent ^{1}H-NMR spectroscopy measurements in 1,2-dichlorobenzene in the range of 293 K to 416 K (see Figure 25a–g) has been performed. Increasing temperature results in the decomposition of **114**, reaching coalescence at around 360 K. These observations are in good agreement with the simulated temperature dependence, which indicates an entropically driven disassembly starting at around 320 K. Interestingly, the intermediate appearance of sharp signals for the boronic acid moiety was observed for temperatures in the range of 350 K - 400 K (Figures 25c,d). Because the chemical shifts are similar to free **113**, these signals might be attributed to the partial presence of species such as [(**113**)$_2$·(**111**)$_2$] that are not considered in the four-component model but might still be populated significantly at these temperatures. For temperatures higher than 400 K, complex [(**113**)·(**111**)] and **113** became the dominant species with the ratio shifting towards **113** at higher temperatures. Due to fast exchange between the protons of [(**113**)·(**111**)] and **113** in the NMR time scale, an average shift of each proton has been observed even at temperature as high as 416 K. This is the reason that shifts are not the same as free **113**. After cooling again to room temperature, quantitative reformation of cage **114** was observed (see Figure 25g), thus proving a fully reversible disassembly/assembly process with increasing/decreasing temperature. Therefore, the predicted temperature dependence could be verified by NMR measurements.
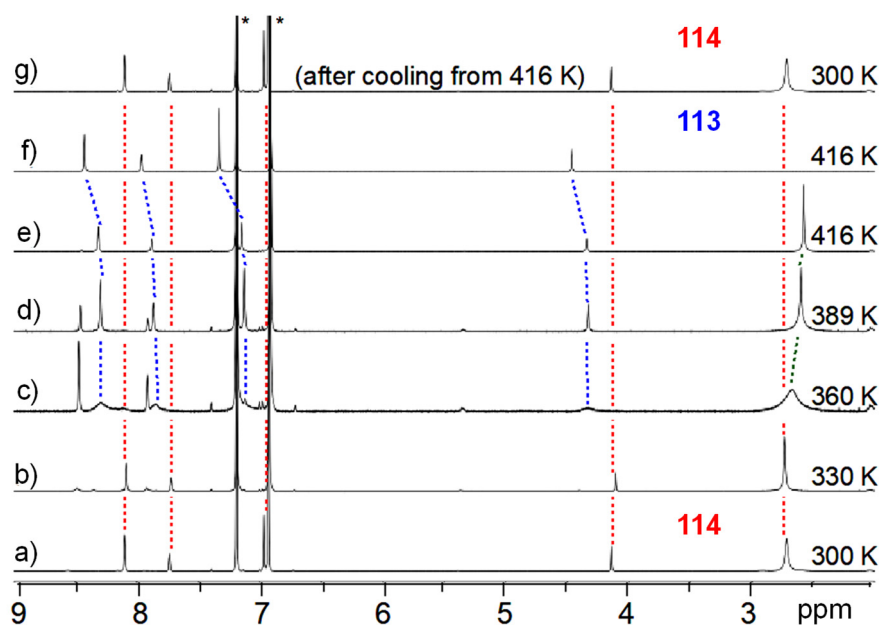

Figure 25 | Temperature-dependent ^{1}H-NMR spectra (1,2-C$_6$D$_4$Cl$_2$, 400 MHz) of a 1.9 mM solution of **114** at **a)** 300 K, **b)** 330 K, **c)** 360 K, **d)** 389 K **e)** 416 K, **f)** **113** at 416 K and **g)** **114** at 300 K after heating to 416 K.

As another possibility for cage opening, disassembly of cage **114** upon protonation of **111** under acidic conditions can be envisaged. The addition of trifluoroacetic acid (TFA) to a solution of **114** in CDCl₃ resulted in quantitative cage opening, as evidenced by the formation of free **113** and a broad signal for protonated **111** (Figure 26).
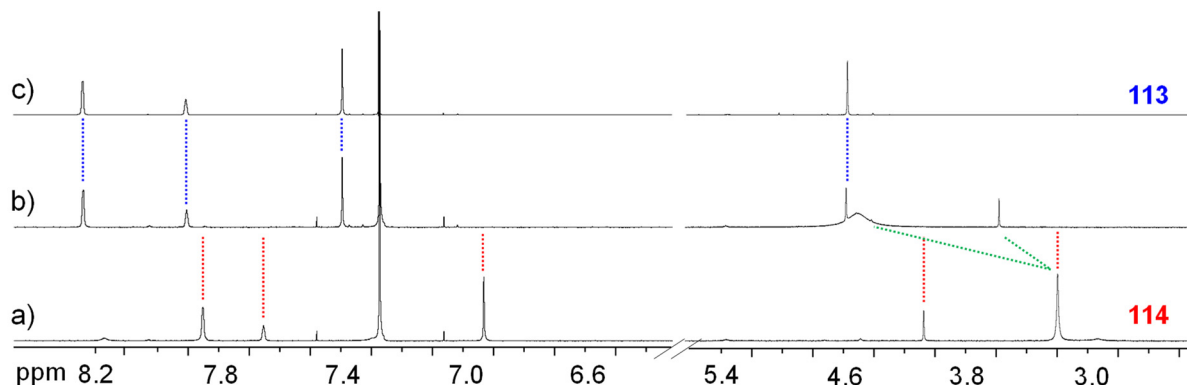

Figure 26 | ^{1}H-NMR spectra (CDCl₃, 400 MHz, rt) of **a) 114**, **b)** a solution showing disassembly of cage **114** to **113** and protonated **111** after the addition of TFA and **c) 113**.

For a reversible reassembly, free **111** has to be recovered under basic conditions. However, the pronounced proneness of boronate esters towards hydrolytic cleavage poses difficulty in reassembling cage **114** under these conditions such as K₂CO₃, K₂CO₃+18-crown-6, DBU, P₁-^{t}Bu in either CDCl₃ or 1,2-C₆D₄Cl₂. Nevertheless, the addition of Cs₂CO₃ led to the partial reformation of cage **114** when 1,2-C₆D₄Cl₂ was used as a solvent (see Figure 27). It should be noted that when trifluoroacetic acid was added to the solution of **114** in 1,2-C₆D₄Cl₂, a white precipitate appeared immediately at the bottom of the NMR tube. The precipitate was most probably the trifluoroacetate salt of protonated **111**, since no signal corresponding to the protons of **111** was observed in the ^{1}H-NMR spectrum of the solution. However, adding Cs₂CO₃ to the solution leads to partial reassembly of cage **114** along with some decomposition products due to the cleavage of the boronate ester bonds (Figure 27e).
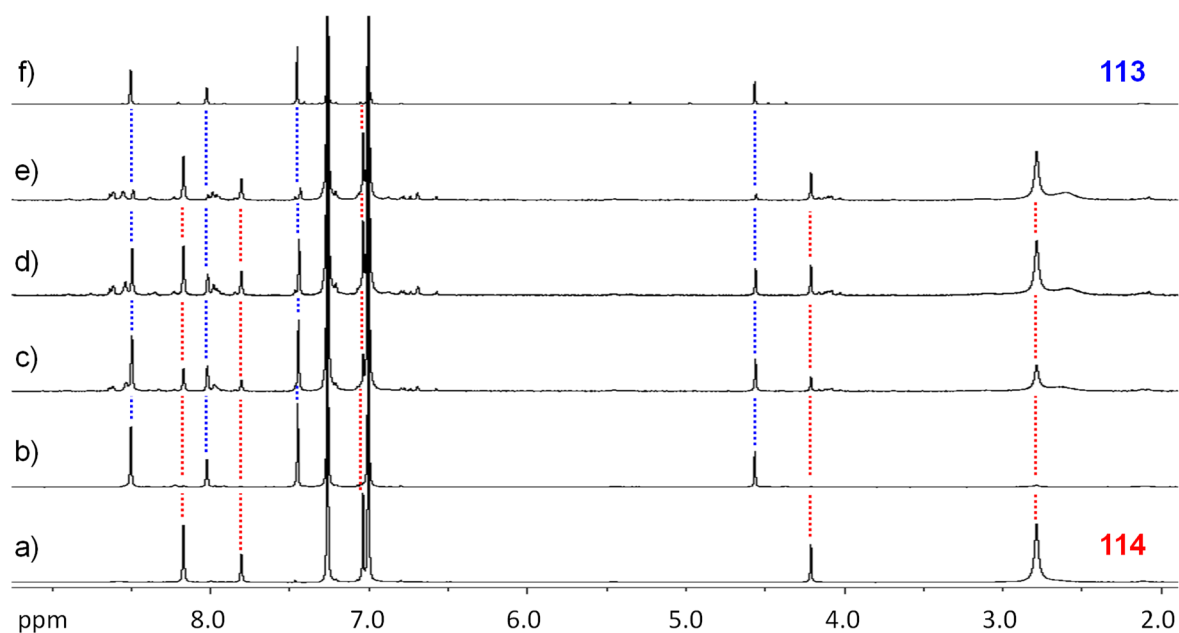
Figure 27 | ^{1}H-NMR spectra (1,2-$C_6D_4Cl_2$, 400 MHz, rt) of **a)** **114**, **b)** a solution after the addition of TFA to **114** showing quantitative cage opening and solutions upon consecutive addition of TFA and Cs_2CO_3 measured after **c)** 16 hours, **d)** 23 hours, **e)** 41 hours after the addition of Cs_2CO_3 showing partial reassembly of cage **114** and **f)** **113**.

An elegant fully reversible opening and reassembly of cage **114** has been presented with change of temperature, which can reliably be predicted based on the ITC-data for the formation of cage **114**. This temperature-dependent switching between assembly and disassembly of cage **114** makes cage **114** all the more unique among other cage structures. Furthermore, the complete dissociation of cage **114** into individual building units upon addition of acid and partial reassembly by addition of base features the remarkable pH-responsiveness of cage **114**. Having established this prototypical cage, the next generation of supramolecular cages based on boron-nitrogen dative bonds can be envisaged by extending each wing of **113** to form a cage with its cavity large enough to encapsulate desired guest molecules.

3.2 Apical Functionalization of Tribenzotriquinacene[‡]

Tribenzotriquinacene offers a suitable tripodal (C_{3v}-) symmetrical closed molecular scaffold for the well-defined spatial orientation of functional substituents (see section **2.2**). The functional groups can selectively be installed at different positions such as *ortho-*, bridgehead- and outer rim positions to obtain the desired TBTQ derivatives. However, functionalization at the apical position of a TBTQ molecule was challenging for a long time as it has been stated by Dietmar Kuck almost a decade ago … "*introduction of a single functional group at the central carbon atom is a synthetically difficult task but an important challenge because this could offer a central point to connect larger building blocks*".[55] The following section will describe the easy and scalable synthesis of TBTQ **115**, which possesses an alkyne unit directly attached to the central carbon atom of the TBTQ core. Subsequent demethylation of the methoxy groups without intermediate protection of the terminal alkyne unit, postsynthetic modifications by utilizing the azide–alkyne click reaction and Sonogashira cross-coupling exemplarily showcase the tempting potential of apically attached acetylenes as privileged intermediates in TBTQ synthesis.
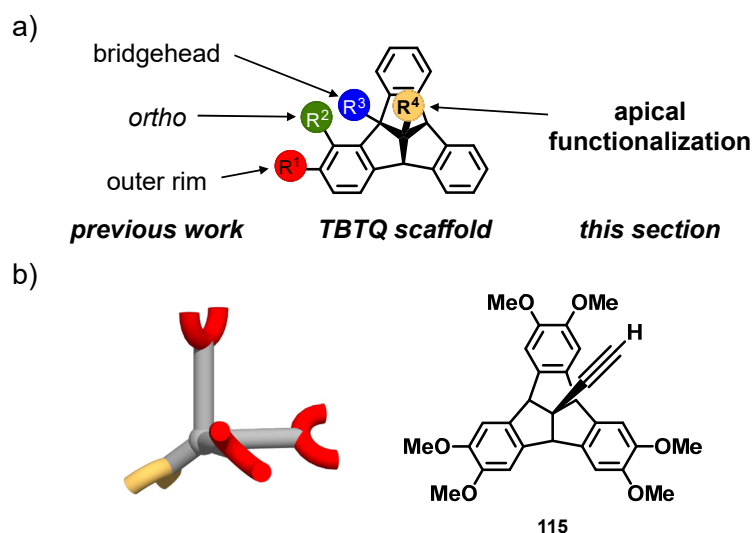

Figure 28 | a) Different positions for functionalization of the TBTQ scaffold; **b)** schematic representation of multifunctional TBTQ derivatives capable of both wing extension (red) as well as apical modification (yellow) with different functional groups and TBTQ **115** as a prototypical example for such rigid building blocks.

3.2.1 Design Principles

Generally, the synthesis of parent TBTQ and derivatives thereof is accomplished by either Kuck´s method[57] or the protocol developed by Hopf and coworkers[65] (see section **2.2.2**). All TBTQ derivatives, that can be accessed by Hopf´s protocol, cannot have any functional group at the apical position as a result of the pathway, followed to synthesize the TBTQ-framework (see Scheme 14). Hence, Hopf´s synthetic route is not suitable for the apical functionalization of a TBTQ unit. On the other hand, Kuck´s synthetic protocol involves an acid-catalyzed coupling of benzhydrol and indanedione derivatives to diketo compounds, which are ultimately transformed into TBTQs through reduction and subsequent cyclodehydration. The group at the 2-position of the indanedione derivative ultimately ends up at the apical position of the TBTQ molecule (Scheme 12). This substituent is usually introduced *via* the corresponding 2-substituted malonic acid. However, while trying to attach sterically more demanding groups providing higher solubility, *e.g.* branched alkyl chains, significantly lower yields for both benzhydrol coupling as well as the final cyclization step were obtained accompanied with significant byproduct formation during cyclization due to undesired rearrangements (see Scheme 19b).[78] For a more suitable and modular approach, alternative reaction pathways have to be considered fulfilling the following criteria: *i*) reduced steric demand for higher yields in key steps, *ii*) introduction of the apical substituents in late steps along the synthetic route, *iii*) retention of the inherent threefold symmetry, which is actually not the case for elongated alkyl substitutents due to the tetrahedral geometry of sp^3-hybridized carbon and *iv*) the potential for versatile post-synthetic modification. Based on these considerations, a sterically less demanding alkyne moiety has been identified as a suitable functional moiety at the apical position featuring a linear extension off the convex face and the potential of several well-established reaction pathways for subsequent transformations. Based on earlier work by Kuck and coworkers, regarding the direct C-H functionalization of the central carbon atom,[55] comparable reactivities for C-H bonds at both bridgehead and apical positions may however hamper the formation as well as the yield to synthesize apically functionalized TBTQ derivatives by functionalization of the parent TBTQ scaffold. Taking all these factors into account, an alternative retrosynthetic analysis has been proposed to obtain an apically functionalized TBTQ (Figure 29).
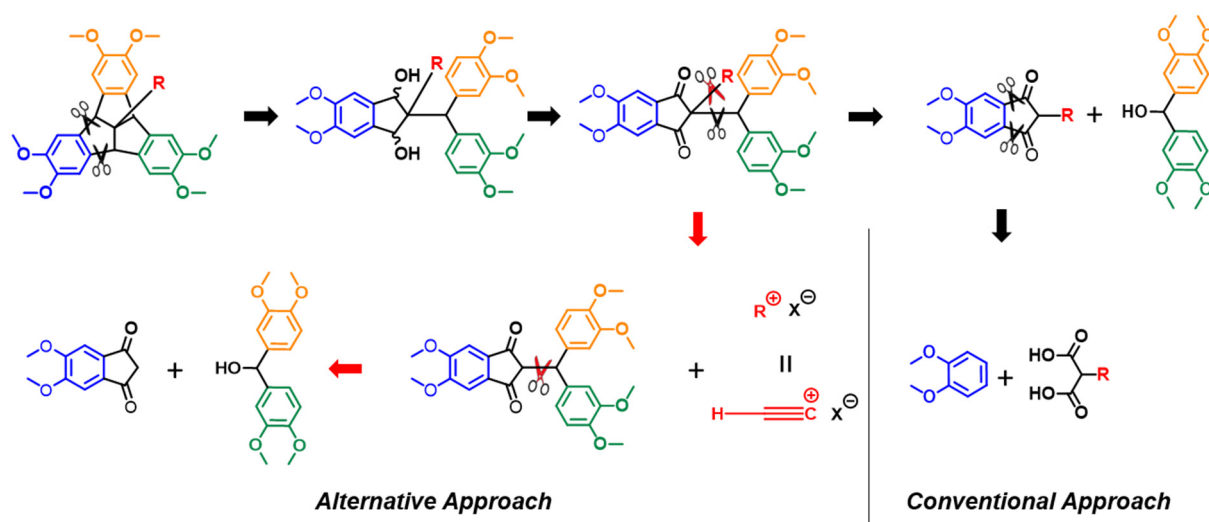
Figure 29 | Two different retrosynthetic analyses of tribenzotriquinacene derivatives.

In this approach, the introduction of a terminal alkyne group at the 2-position of the indanedione derivative requires *umpolung* reactivity of acetylene. Therefore, an electrophilic alkynyl synthon needs to be considered because the all-carbon quarternary center containing a triple bond cannot be easily accessed by using a conventional acetylide nucleophile.[110] Hence, the introduction of the alkyne unit prior to cyclodehydration but after coupling between benzhydrol and indanedione precursors was envisioned to be the most logical step along the synthetic route.
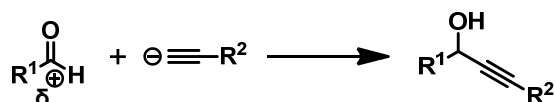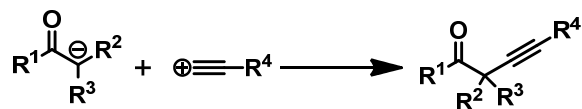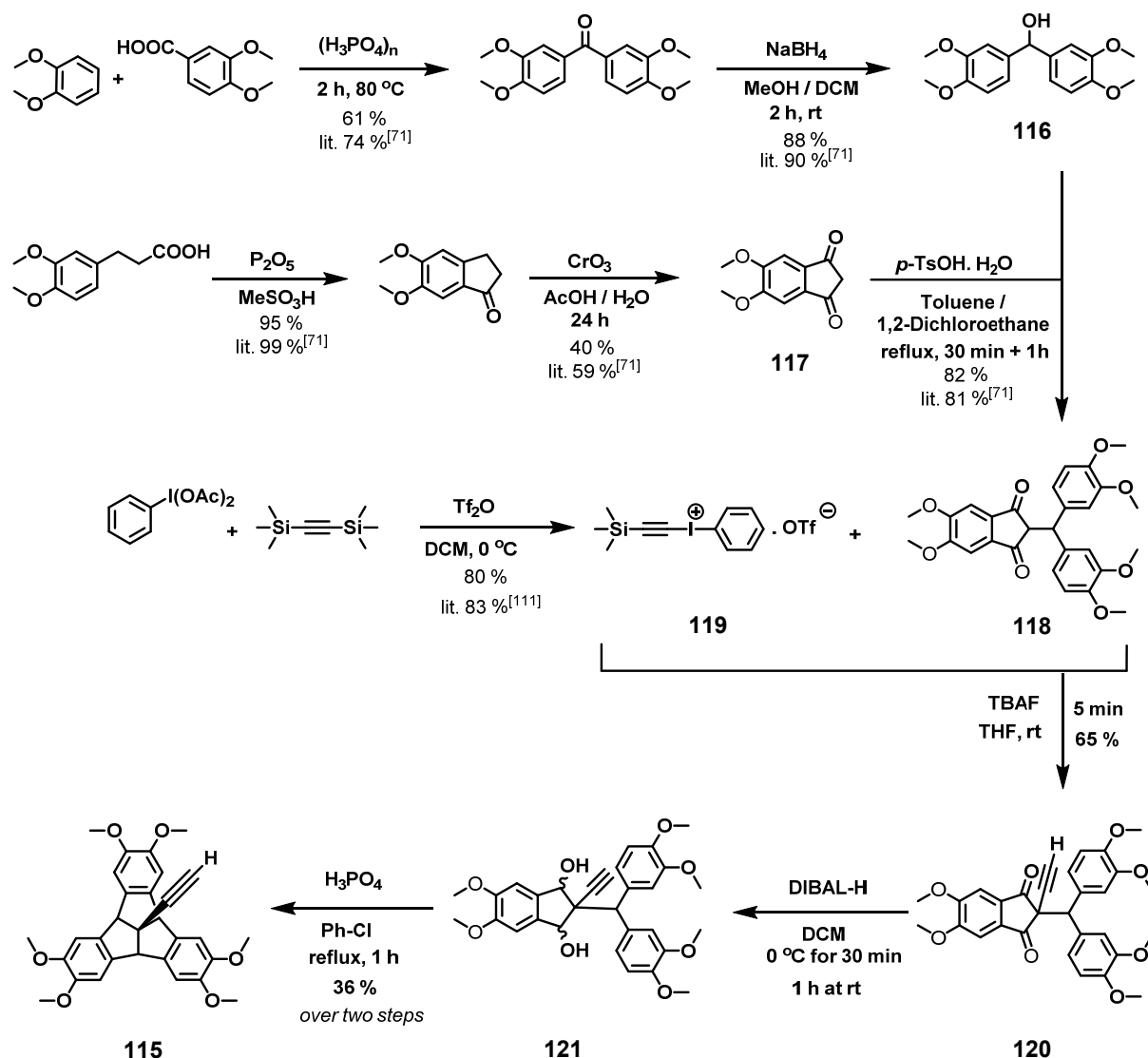

Scheme 27 | **a)** Classical and **b)** non-conventional (*umpolung*) reactivity of carbonyl compounds.

3.2.2 Synthesis of Apically Functionalized Tribenzotriquinacene

The target **115** was synthesized according to the procedure depicted in Scheme 28.

Scheme 28 | Synthesis of the alkyne-functionalized TBTQ **115** (compounds **118** and **119** were synthesized according to reported synthetic procedures). DIBAL-H=di-*iso*-butylaluminiumhydride, OAc=acetoxy, OTf=trifluoromethanesulfonate, Tf$_2$O= trifluoromethanesulfonic anhydride, TBAF=tetra-*n*-butylammonium fluoride, TMS=trimethylsilyl, *p*-TsOH=*para*-toluenesulfonic acid.

In order to obtain diketone **118**, benzhydrol **116** and indanedione **117** were synthesized following literature known procedures.[71] Benzhydrol **116** was synthesized by Friedel-Crafts acylation of veratrole with 3,4-dimethoxybenzoic acid in polyphosphoric acid followed by reduction of the benzophenone derivative with sodium borohydride in good yields. On the other hand, the synthesis of 5,6-dimethoxyindane-1-one from 3,4-dimethoxyhydrocinnamic acid

with Eatons reagent followed by the oxidation with chromium oxide led to the formation of indanedione **117** in acceptable yield. Diketone **118** was synthesized by proton-catalyzed C-C coupling of **116** and **117** as reported by Kuck and coworkers.[71] The following reaction conditions were necessary to follow for a better yield of **118** while performing the reaction: *i*) Short duration of the reaction to minimize the dialkylation of **117** since it processes two enolizable protons and *ii*) the dropwise addition of the solution of benzhydrol **116** in the refluxing reaction mixture to suppress disproportionation reaction of benzhydrol **116** in acidic media as well as formation of some condensation products.[71] Instead of chromatographic separation, simple precipitation from hot methanol gave **118** in sufficient purity for the next reaction. For this step, trimethylsilyl protected hypervalent iodonium salt **119**[111] was chosen as an electrophilic alkyne synthon for the coupling with diketone **118**. Mild and scalable reaction conditions were achieved after optimizing this step varying different parameters, *e.g.* base, temperature, duration of reaction etc. (see Table 5).

Table 5 | Reaction optimization for the synthesis of **120** *via* electrophilic alkynylation

	Reaction Condition	**Work-up**	**Result**
1	KO^{t}Bu, THF, −78 ^{0}C, 24h at rt	aqueous quench at rt	decomposition
2	KO^{t}Bu / TBAF, THF, −78 ^{0}C, 24h at rt	direct evaporation	33 % yield (^{1}H-NMR)
3	KO^{t}Bu / TBAF, THF, −78 ^{0}C, 1h	direct evaporation	71 % yield (^{1}H-NMR), 100 mg
		aqueous quench at rt	decomposition
		aqueous quench at +10 ^{0}C	17 % yield (^{1}H-NMR), 1.0 g
4	TBAF, THF, −78 ^{0}C, 1h	aqueous quench at +10 ^{0}C	52 % yield (1.0 g scale) not reproducible
5	**TBAF, THF, rt, 5 min**	**aqueous quench at rt**	**Yield varies from 62-71 % yield (reproducible)**

At first, an early report by Ochiai and co-workers[112] was followed that utilized enolization of diketone **118** in the presence of strong bases such as potassium *tert*-butoxide followed by addition of **119**. Unfortunately, this procedure resulted in complete decomposition of the reagents. Waser and coworkers observed that the acetylene-transfer ability was strongly increased when using the desilylated alkynyl iodine reagent instead of the silyl protected one. Therefore, tetra-*n*-butyl ammonium fluoride (TBAF)[110b] was added for an *in-situ* deprotection of the silyl group to facilitate facile acetylene transfer to the corresponding enolate generated

from diketone **118**. Although the desired product could be obtained following this procedure (entry 2 in Table 5), the yield was very low along with decomposed material. Variations of duration of the reaction or quenching methods proved to be unsuccessful to obtain **120** in a scalable way. Since TBAF is known to act as both activating agent and base, the reaction was then performed without the use of any additional strong base (entry 4 in Table 5). Though the reaction worked decently under these conditions, the yield was very difficult to reproduce. Finally, reaction of **118** and **119** in presence of TBAF at room temperature for five minutes, followed by aqueous quenching led to the formation of alkyne derivative **120** in decent yield in a reproducible way. Longer reaction time only resulted in the increased formation of unidentifiable decomposition products. The purification of **120** was achieved by means of flash column chromatography either by n-hexane/EtOAc (1:1) or n-hexane/Et$_2$O (6:1, 8:1, 10:1). A tentative mechanism for this electrophilic alkynylation reaction is proposed in Scheme 29.
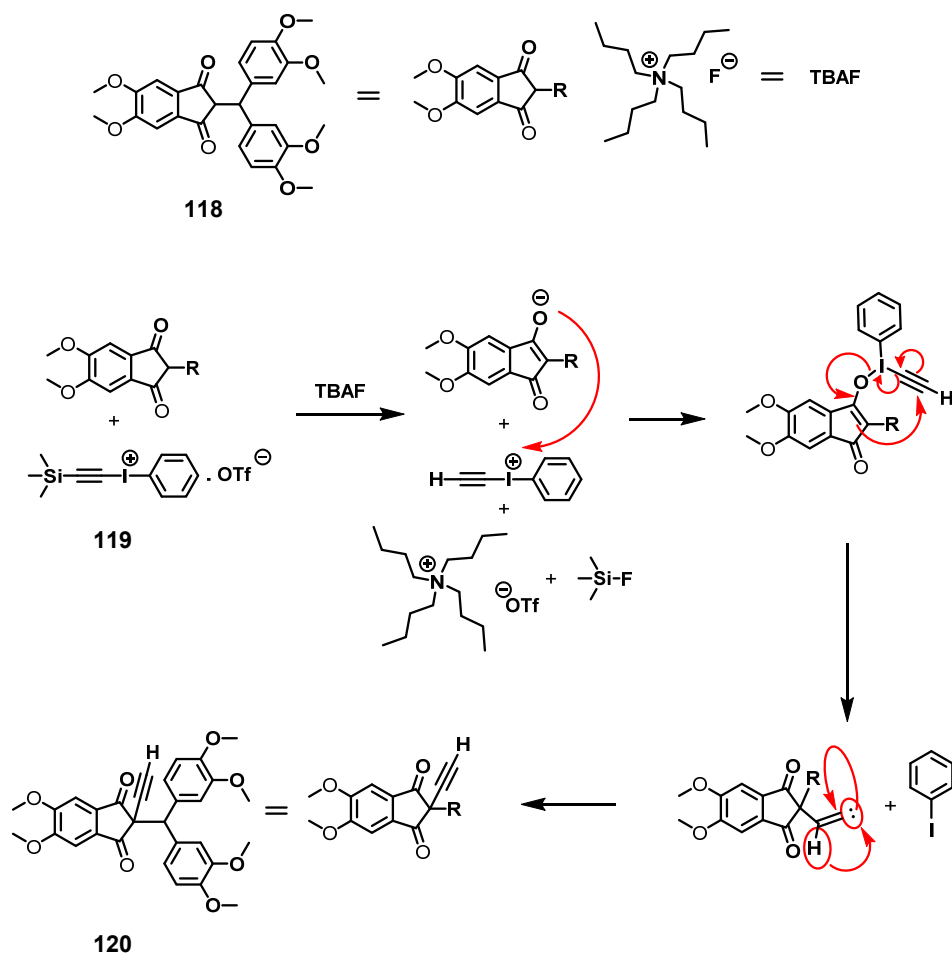
Scheme 29 | A proposed mechanism for the electrophilic alkynylation of **118**.

Single crystals of **120** suitable for X-ray diffraction could be grown by slow evaporation of 1:1 *n*-hexane/Et₂O solution overnight. Indanedione **120** crystallized in the triclinic space group $P\bar{1}$ (Figure 30), and the obtained crystal structure provided additional evidence for the successful attachment of the alkyne moiety.
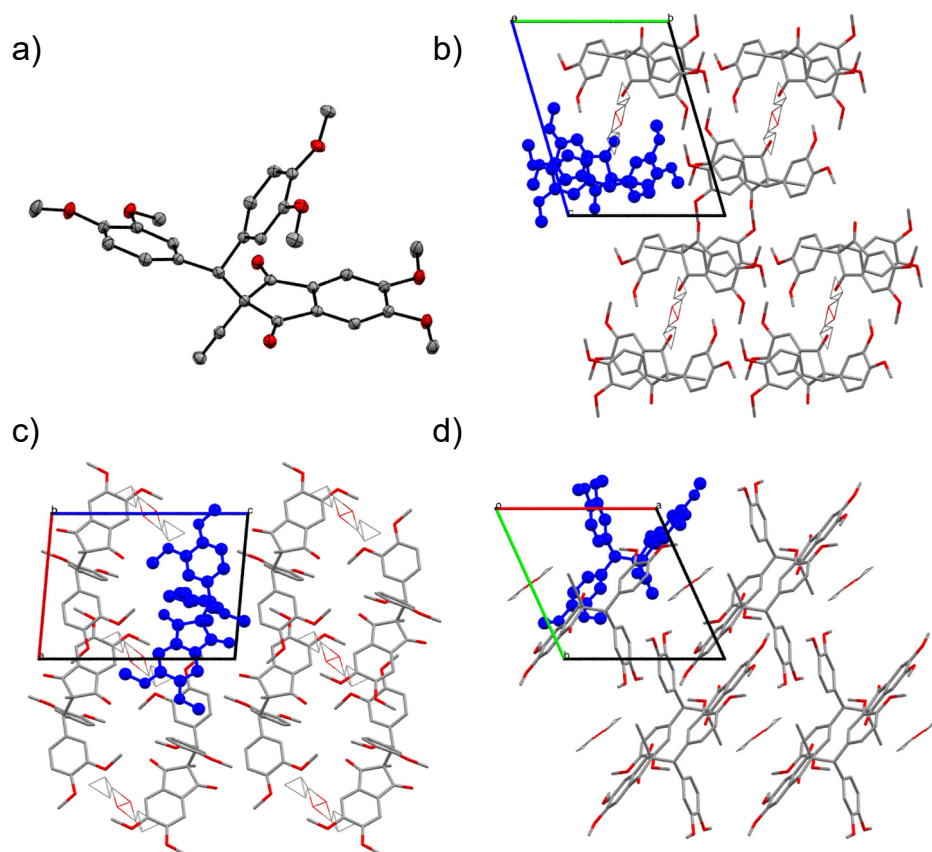

Figure 30 | Single-crystal X-ray structure of diketone **120**: **a)** ORTEP representation of single molecule of **120** (thermal ellipsoids set to 50% probability, carbon grey, oxygen red, hydrogen atoms omitted for clarity); crystal packing with views along the crystallographic **b)** a, **c)** b and **d)** c-axis (single molecule of **120** is highlighted in blue).

Subsequent reduction of the carbonyl groups with DIBAL-H resulted in the quantitative formation of two diastereomeric indanediols **121** in an 83:17 ratios (Scheme 28). For apical alkyl substitutents of hexamethoxy derivatives, it has been revealed that only the all-*cis* isomer is formed.[71] For sterically less-demanding alkyne groups however, the X-ray structure in Figure 30 might indicate that hydride attack from the opposite carbonyl face becomes more feasible, thus resulting in the formation of the observed isomeric mixture. Separation of the diastereomers is just about possible, but not necessary because exposure of the crude mixture of **121** to a solution of orthophosphoric acid in chlorobenzene under refluxing condition resulted in the efficient formation of the apically functionalized TBTQ **115** with a total yield of 36 % after both reduction and cyclization. The ¹H-NMR spectrum of **115** in deuterated chloroform in

Figure 31 clearly shows the characteristic signal pattern of a C_{3v}-symmetric TBTQ-derivative confirming the formation of the desired **115** (Figure 31a). Again, single crystals suitable for X-ray studies could be obtained after recrystallization from EtOH. Hexamethoxy-TBTQ **115** crystallized in the tetragonal space group $I4_1/a$, and an ORTEP representation of the molecular structure is depicted in Figure 31b.
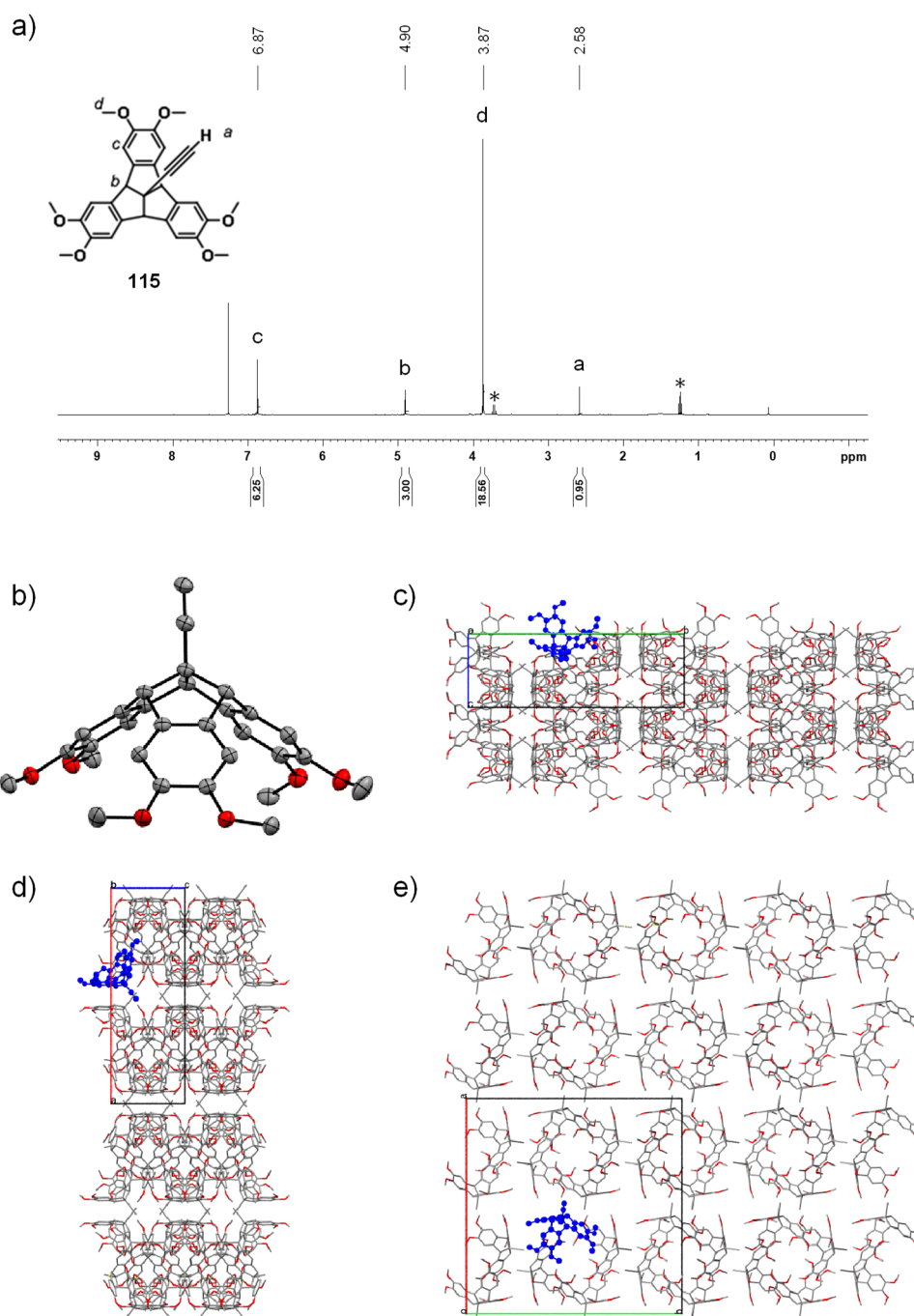

Figure 31 | a) ^{1}H-NMR spectrum (400 MHz, CDCl$_3$, rt) of **115** (∗ indicates EtOH); single-crystal X-ray structure of TBTQ **115**: **b)** ORTEP representation of single molecule of **115** (thermal ellipsoids set to 50% probability, carbon grey, oxygen red, hydrogen atoms omitted for clarity); crystal packing with views along the crystallographic **c)** a, **d)** b and **e)** c axis (single molecule of **115** is highlighted in blue).

From this X-ray structure, it is clearly evident that the apical alkyne substituent is spatially well-separated at the convex face and points away from the bowl-shaped TBTQ scaffold, thus coinciding with the molecular axis. In total, **115** can be conveniently synthesized from readily available starting materials **116** and **117** in only four steps in 20 % overall yield. Because none of the steps requires tedious chromatographic purification, gram quantities of **115** can be easily obtained within two weeks, thus making this apically functionalized TBTQ derivative a very versatile building block for further chemical transformations.

3.2.3 Deprotection of Methoxy Groups

To highlight the potential of the TBTQ derivative **115** as a divergent molecular unit, both the deprotection of the methoxy groups for further functionalization at the outer rim and subsequent reactions at the apical alkyne moiety are worthwhile goals. However, the seemingly simple deprotection of all six methoxy groups in TBTQ **115** turned out to be very difficult to execute in an efficient way. Conventional deprotection with BBr$_3$, routinely used to deprotect other alkyl functionalized TBTQs,[13c, 14a] was unsuccessful. Most probably, reaction of BBr$_3$ with the terminal alkyne[113] at the apical position of **115** resulted in the decomposition of the starting material and no product formation could be observed. In addition, the use of other Lewis acids, *e.g.* BCl$_3$, AlCl$_3$ (also in presence of tetra-*n*-butylammonium iodide)[114], or Me$_3$SiI[115] did not result in efficient deprotection either. Similar obstacles during the attempted deprotection of methoxy groups in the presence of terminal alkyne groups have been reported by other groups.[116] Therefore, silylation of the alkynes prior to methoxy deprotection followed by final removal of the silyl groups is usually applied.[116] As a more straightforward alternative, herein is reported an elegant two-step process with an initial exchange of the protective groups from methyl to triethylsilyl groups under reductive conditions followed by acidic cleavage of the silylated intermediate without the need for protection of the terminal alkyne. Indeed, the reaction of **115** with triethylsilane in the presence of trispentafluorophenylborane as a Lewis acidic catalyst[117] smoothly exchanged protective groups, thus yielding silylated derivative **122** (see Scheme 30). Quenching of trispentafluorophenylborane by an appropriate base turned out to be essential before isolating pure **122** since a complex mixture was obtained possibly due to decomposition of **122** in the presence of strong Lewis acidic borane. Interestingly, passing the reaction mixture through either silica or alumina pads did not effectively quench the borane thereby resulting in the decomposition of **122**. Conversely, the reaction was efficiently quenched when triethylamine was added to the solution after completion of the reaction.
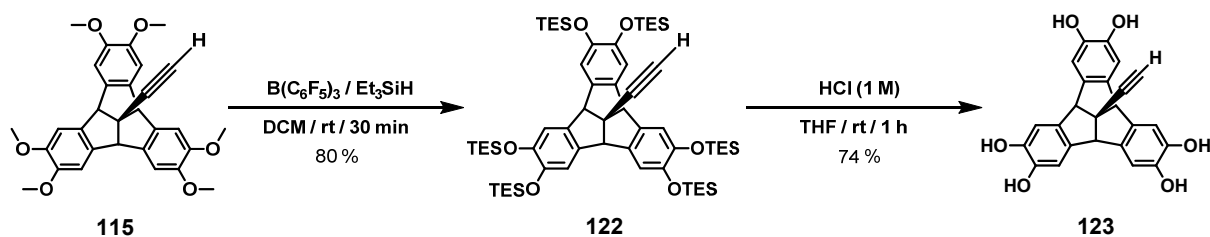
Scheme 30 | Deprotection of methoxy groups of **115** by exchanging methyl to triethylsilyl groups followed by desilylation of **122** under acidic condition.

Silylated TBTQ derivative **122** possesses very good solubility in common organic solvents. Hence, this intermediate can be considered as another versatile precursor for further transformations at the alkyne position. Desilylation under standard conditions, *i.e.* TBAF in THF suffered from extensive decomposition most probably due to the instability of hexahydroxy derivative **123** in basic medium. As an alternative, acidic treatment of **122** in THF resulted in the smooth formation of triscatechol **123**. The possibility of orthogonal functionalization of the outer rim through the catechol units and the convex face through alkyne chemistry makes this TBTQ derivative a valuable and unique building block among all the bowl-shaped molecules.

3.2.4 Apically Functionalized Tribenzotriquinacenes

To further showcase the potential for facile apical functionalization, two test reactions were performed, namely an azide–alkyne Huisgen cycloaddition and a Sonogashira cross-coupling reaction for the straightforward apical attachment of readily available azides or aromatic halides, respectively. As an initial experiment, triscatechol **123** was used as the substrate for a click reaction with benzyl azide in the presence of $CuSO_4$ (0.2 eqv) and sodium ascorbate (0.5 eqv) in a THF/H_2O mixture to obtain triazole **124** in moderate yield of 60 %. Since this reaction is catalyzed by Cu(I) formed by reduction of Cu(II) as precatalyst, excess of sodium ascorbate (10.0 eqv) was needed for complete conversion of **123** to triazole **124** in excellent yield of 90 % (see Scheme 31). The fact that unprotected **123** could be directly used for this transformation highlights once again the advantages of the synthetic approach. Based on this modular strategy, fast and easy access to a great variety of substituted derivatives can be envisioned, while avoiding recurring optimization of catechol deprotection. In addition, such derivatives can serve as versatile building blocks by themselves for subsequent dynamic

covalent reactions with boronate esters, supramolecular interactions involving hydrogen bonding or other chemical transformations. The observation of supramolecular complexation between DCTB matrix molecules and free catechol **123** in MALDI-TOF measurements (see Figure A17 in the section Appendix) might be a first indication towards this direction.
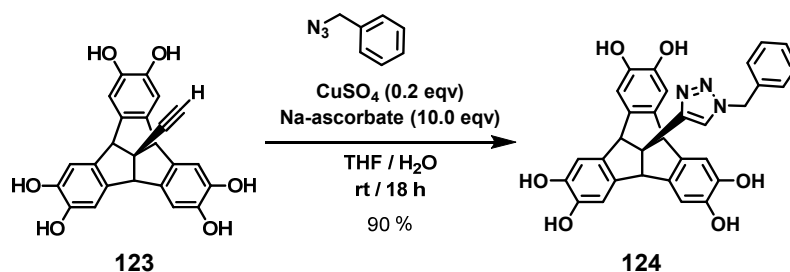
Scheme 31 | Synthesis of **124** by azide-alkyne Huisgen cycloaddition reaction.

With the aim of retaining the inherent threefold symmetry of the TBTQ backbone after apical functionalization, a Sonogashira cross-coupling between **115** and 1-bromo-4-iodobenzene was also performed. The reaction in toluene and in the presence of 4 mol % Pd(dppf)Cl$_2$ and CuI as a co-catalyst under basic conditions resulted in the clean formation of the alkynyl-phenyl derivative **125** in 69 % yield (Scheme 32). Afterwards, the deprotection of methoxy groups of **125** was investigated for further functionalization at the outer rim positions. The direct deprotection with BBr$_3$ under the standard condition led to the decomposition of **125**. This is somehow surprising considering that the internal alkyne does not generally get affected by BBr$_3$. Therefore, the reaction was performed at lower temperatures (at –70 °C instead of 0 °C). Unfortunately, the decomposition of the material hampered smooth deprotection of the methoxy groups of **125**. Hence, the previously introduced two-step strategy involving the exchange from methyl to triethylsilyl groups followed by an acidic cleavage of the silyl groups was employed for the demethylation of **125**. The synthesis of silyl derivative **126** worked well, although the purification of crude **126** by sonication in methanol led to partial decomposition of the product. However, the usual acidic cleavage of **126**, which was proven to be quite efficient for the desilylation of **122**, did not proceed efficiently. To understand the unexpected decomposition of **126**, desilylation of **126** was performed in an NMR tube and followed by ^{1}H-NMR spectroscopy with time. The ^{1}H-NMR spectrum, taken after 5 minutes of acidic treatment to **126** in THF-d$_8$, showed quantitative deprotection of silyl groups. The ^{1}H-NMR spectrum of the same solution recorded after 48 hours showed major decomposition of the product **127**. Therefore, the instability of **127** resulted in the observed decomposition while executing the

demethylation of methoxy groups either with BBr$_3$ or by the two-step deprotection strategy. Nevertheless, compound **127** could be obtained in an acceptable purity by washing the crude product with copious amounts of dichloromethane and diethyl ether (see Scheme 32). In this regard, an *in situ* deprotection of **126** may be a useful strategy for further transformation of **127** such as boronate ester based cage formation. However, the purification of the final assembly may be difficult to achieve. Interestingly, analysis by MALDI-TOF mass spectrometry of **127** reveals the presence of one ion-peak at around *m/z* = 2217.2 which can be ascribed to a tetrameric self-assembled cage based on **127** (Figure A29 in section Appendix). In this regard, a strategy for the exclusive formation of the tetrameric hydrogen-bonded organic capsule based on TBTQ can be envisaged by introducing solubilizing groups at the apical position of **127** to increase its solubility in non-polar solvents, which usually favors the formation of hydrogen bonded organic capsules.[27a]
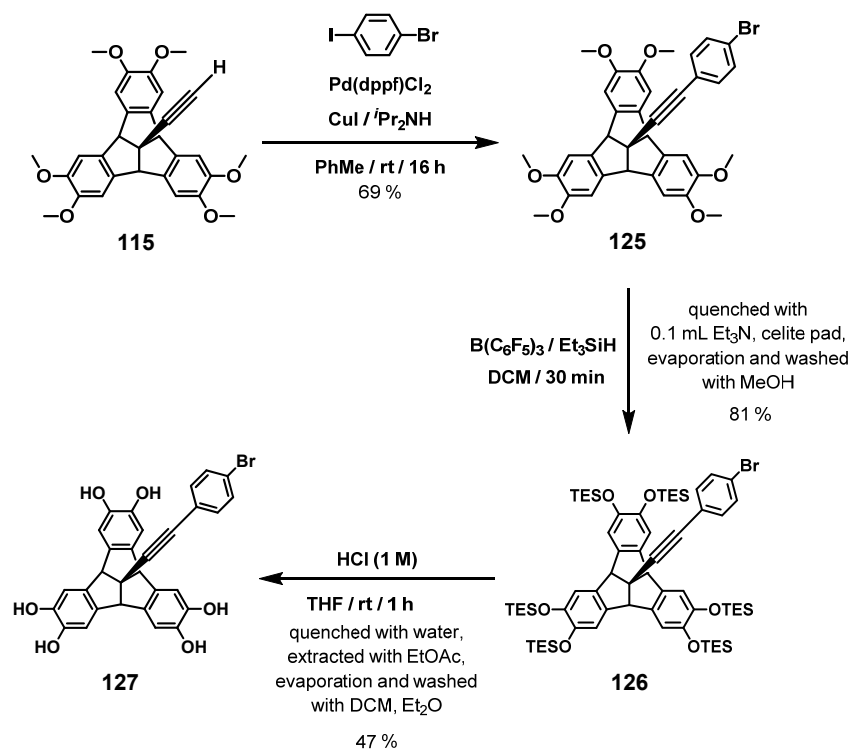
Scheme 32 | Synthesis of **127** *via* Sonogashira cross-coupling at the apical position of **115** followed by deprotection of methoxy groups at the outer rim positions.

Scheme 33 summarizes all the post-synthetic modifications of **115**. It features facile synthesis of various apically functionalized TBTQ derivatives by two versatile reactions namely, azide-alkyne Huisgen cycloaddition and Sonogashira cross-coupling at the terminal alkyne of **115**. Furthermore, the mild two-step deprotection sequence that has been employed for efficient demethylation of protected catechols of both **115** and **125** shows the wide applicability of this deprotection strategy of methoxy groups.
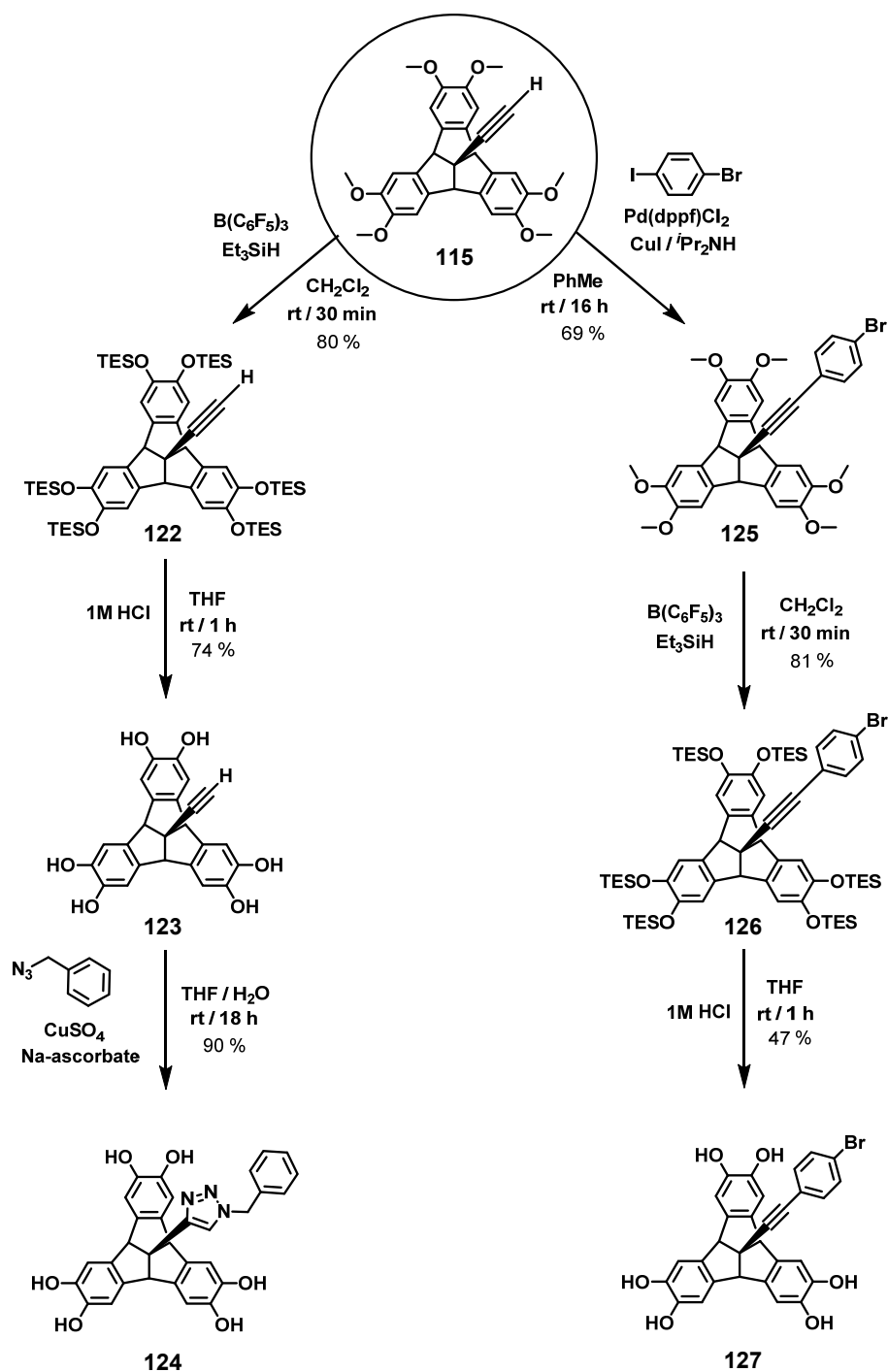
Scheme 33 | Modular deprotection and apical functionalization of TBTQ derivatives. dppf = 1, 1´-bis(diphenylphosphino)ferrocene, TES = triethylsilyl.

3.3 Functionalized Organic Cages

The introduction of suitable functional groups either at the periphery or in the internal cavity of porous organic cage molecules is highly desirable to fine-tune materials properties such as solubility, melting point, crystallinity or porosity as it has been already discussed in chapter **2.3**. In previous work from the Beuerle group, TBTQ molecular scaffold was introduced as a versatile tritopic building unit for the formation of cages with different sizes and shapes.[14] For all these TBTQ-based cages, the alkyl groups at the apical position of the TBTQ subcomponents are located at the outer periphery of the cages. Therefore, any TBTQ molecule with proper apical functionalization could, in principle, lead to the formation of an organic cage with external functionality. The first part of this section will describe syntheses of two exohedrally functionalized bipyramidal [2+3]-organic cages based on different apically functionalized TBTQ molecules. This establishes alkynyl-functionalized TBTQs as suitable building blocks for exohedral cage functionalization. On the other hand, to functionalize the interior void of organic cages, a new building unit has to be developed. In this respect, the synthesis of an angled diboronic acid with additional substituents between two reactive sites is worthwhile goal, since co-condensation with the apically functionalized TBTQ derivative may lead to the formation of a covalent organic cage with both internal and external functionalities which is unprecedented in literature. Therefore, the synthesis of a new diboronic acid with a pyridyl group substituent in 2-position will be described in the second part of this section, followed by initial investigations regarding the implementation of this building block into covalent organic cage compounds.

3.3.1 Exohedral Cage Functionalization

In the following section, the design and synthesis of two covalent organic cage compounds will be discussed possessing the same trigonal bipyramidal shape but with different functionalities on the cage periphery. These cages consist of diboronic acids with bite angles 60° between the two reactive boronic acids and two catechol-functionalized tribenzotriquinacenes with varying apical functionalization. Recently, the Beuerle group has optimized reaction conditions for the formation of boronate ester cages.[14] Generally, tritopic TBTQ molecules and suitable boronic acids are dissolved in the correct molar ratio in THF-d$_8$ at room temperature and the progress of the reaction is monitored by ^{1}H-NMR spectroscopy. Molecular sieves (4 Å) are added to significantly shift the equilibrium towards the higher condensation products so that the desired

boronate ester cage forms ultimately as the single thermodynamic product. TBTQ **123** was chosen as a candidate for cage formation because the peripheral terminal alkyne group provides the opportunity for further functionalization by post-synthetic modification (Figure 32a). The synthesis of TBTQ **123** was already described in chapter **3.2.3**. For the cage formation, TBTQ **123** and diboronic acid **100** were dissolved in THF-d8 and to this solution, properly oven-dried molecular sieves (4 Å) were added. Progress of the reaction was followed by ^{1}H-NMR spectroscopy over time. After four days, ^{1}H-NMR spectrum of the reaction mixture showed only one set of signals for the individual protons indicating the quantitative formation of a highly symmetrical product as depicted in Figure 32c.
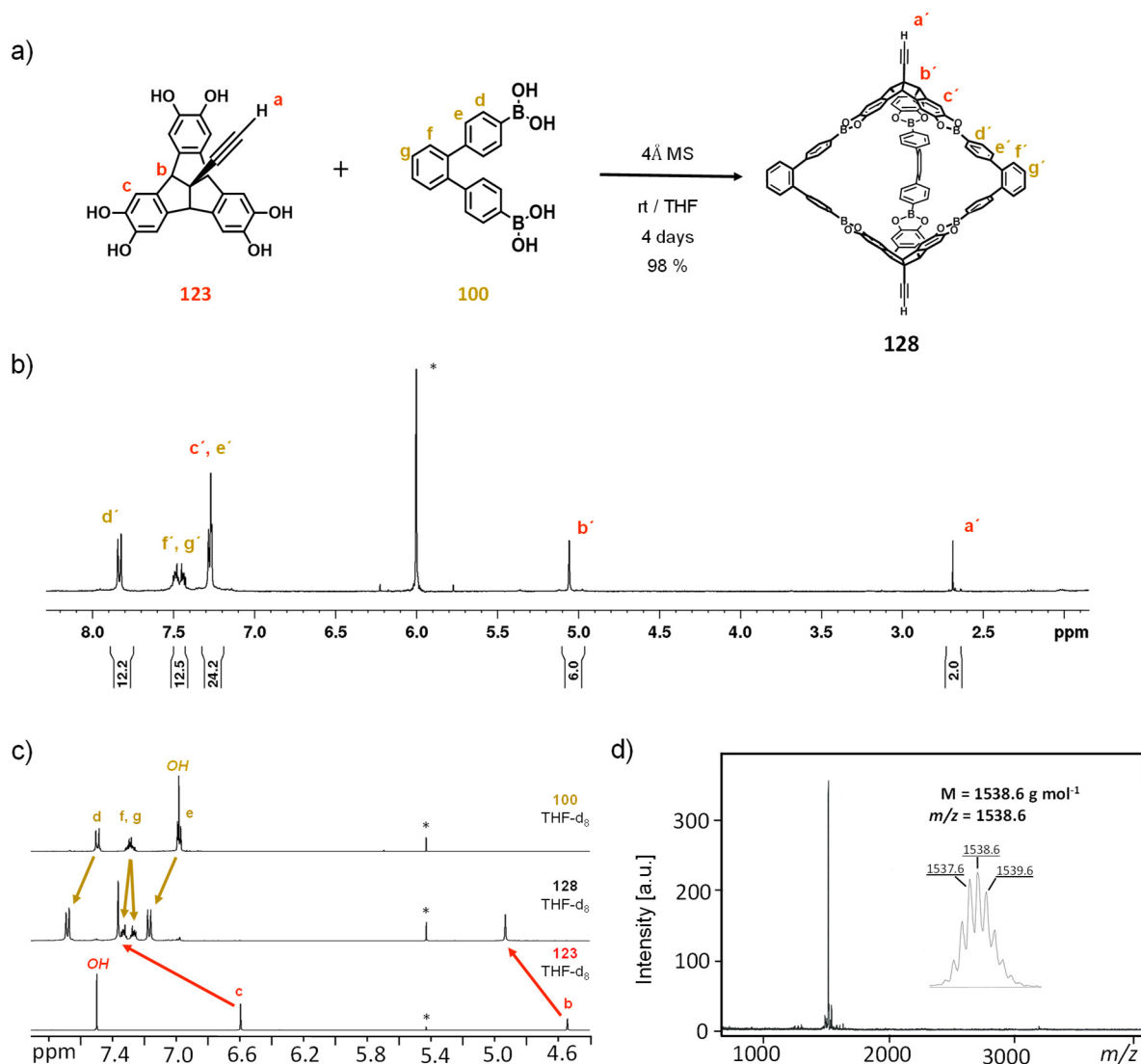

Figure 32 | a) Synthesis of [2+3]-organic cage **128** from TBTQ derivative **123** and diboronic acid **100** under water-removing conditions; **b)** ^{1}H-NMR spectrum (400 MHz, 1,1,2,2-$C_2D_2Cl_4$, rt) of the isolated cage **128**, ∗ indicates residual solvent peak; **c)** ^{1}H-NMR spectra (400 MHz, THF-d8, rt) of tritopic TBTQ derivative **123** (bottom), diboronic acid **100** (top) and cage **128** (middle), ∗ = CH_2Cl_2; **d)** MALDI-TOF MS (DCTB, $CHCl_3$) of trigonal bipyramidal cage **128**.

The expected downfield shift of both the aromatic protons and the methine protons upon conversion to the boronate ester suggests the formation of a trigonal bipyramidal covalent organic cage. Furthermore, analysis by MALDI-TOF mass spectrometry reveals a molecular ion peak at $m/z = 1538.6$ as the only detectable species, which correlates well with the formation of [2+3]-cage structure (Figure 32d). The THF solution was evaporated by blowing nitrogen gas at room temperature to obtain cage **128** as amorphous precipitates with small crystalline domains in 98 % yield. The precipitate is soluble in 1,1,2,2-tetrachloroethane, a solvent where neither of the molecular precursors is soluble. A ^{1}H-NMR spectrum of the isolated material in deuterated 1,1,2,2-tetrachloroethane also confirms the formation of the cage (Figure 32b). According to both NMR and MS results, the formation of a trigonal-bipyramidal organic cage with peripheral terminal alkyne groups has been successfully achieved. Unfortunately, any attempt to obtain single crystals of the cage by means of slow evaporation of THF or 1,1,2,2-$C_2H_2Cl_4$, layering between THF/n-hexane or vial-in-vial crystallization from THF/n-hexane or 1,1,2,2-$C_2H_2Cl_4$/n-hexane did not succeed.

To further probe the idea that the cage formation does not interfere with the apical functionality of the TBTQ building block, another catechol-functionalized TBTQ **127** with different apical substituent was selected for the formation of another organic cage with same geometrical shape (Figure 33a). Thereby, TBTQ **127** possessing (4-bromophenyl)ethynyl groups was again chosen to facilitate X-Ray analysis of boronate ester cages. According to previous reports by the Beuerle group, the obtained crystals for cages based on TBTQs with alkyl substituents are either too small to get the X-ray diffraction data of sufficient quality or no diffraction is observed due to the lack of presence of heavy atoms in those cage compounds.[14a] This phenomenon is still a common challenge in the organic cage community as it has been recently pointed out by Mastalerz.[17b] In this respect, it was hoped that the rigidity of TBTQ **127** may lead to an efficient solid-state packing of the cages. In addition, the incorporation of heavy atoms, namely bromine at the periphery of the organic cage may provide diffraction data of better quality to solve the cage structure. TBTQ **127** and diboronic acid **100** were subjected to the same optimized reaction conditions as applied for the formation of the [2+3]-organic cage **128**. ^{1}H-NMR spectra of the respective building units **127** and **100** as well as of the reaction mixture after cage formation are shown in Figure 33b. Analysis by MALDI-TOF mass spectrometry also confirms the desired cage structure (Figure 33c). Removal of the solvent followed by drying under vacuum resulted in amorphous precipitate of cage **129** in 89 % yield. Unlike the previous cage **128**, the precipitate obtained after evaporation of the THF solution of

cage **129** appeared to be insoluble in any chlorinated solvent such as chlorobenzene, chloroform, dichloromethane or 1,1,2,2-tetrachloroethane. The similar difficulty was also encountered by other groups while dissolving the solid precipitate of organic cages.[14a, 95a] However, neither slow evaporation of the THF solution nor layering between THF/*n*-hexane resulted in the formation of single crystals.
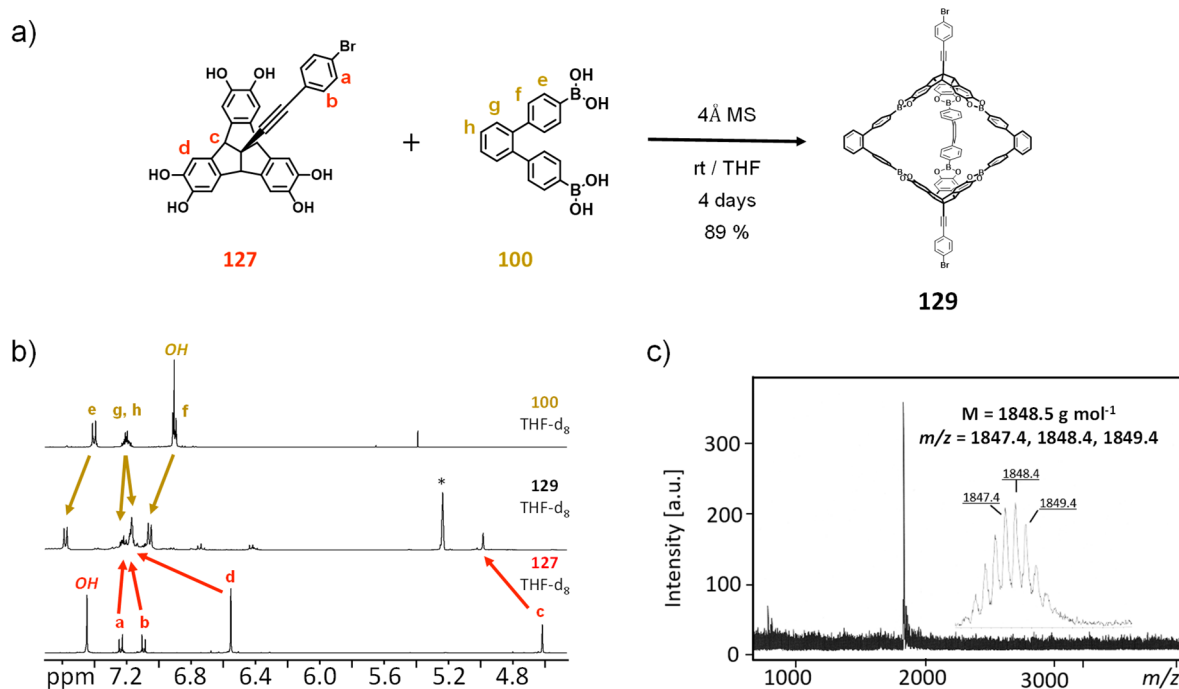

Figure 33 | a) Synthesis of organic cage **129** from TBTQ derivative **127** and diboronic acid **100** in THF in the presence of 4 Å molecular sieves; **b)** ^{1}H-NMR spectra (400 MHz, THF-d$_8$, rt) of **127** (bottom), diboronic acid **100** (top) and cage **129** (middle), ∗ = CH$_2$Cl$_2$; **c)** MALDI-TOF MS (DCTB, CHCl$_3$) of cage **129**.

These two examples clearly underline how the TBTQ building units with chemically modifiable terminal alkyne groups at the apical position strongly influence the solid-state packing of the isostructural organic cages, which affects the solubility of the cages as it has been discussed above. However, formation of large single crystals still remains elusive and either crystal growth conditions need to be further optimized or novel substituents, *e.g.* trityl groups[118] need to be considered. Furthermore, both the organic cages, which have exohedral functional groups, could act as the promising ligands for synthesis of extended framework materials by post-synthetic modifications.

3.3.2 Synthesis of a 2-Substituted-*meta*-diboronic Acid

To functionalize the interior of shape-persistent organic cage compounds, the synthesis of a building block with suitable internal functionality has been envisaged. The basic design principle is to attach a functional group to the molecule in such way that upon formation of the cage, the group will eventually point inwards the cage cavity. In this regard, the ditopic diboronic acid with *meta*-relationship between the two boronic acid groups has been selected as the molecular precursor for the cage formation. Figure 34 shows the structure of diboronic acid **130** which satisfies all the design criteria for a perfect molecular precursor for internal functionalization of an organic cage.
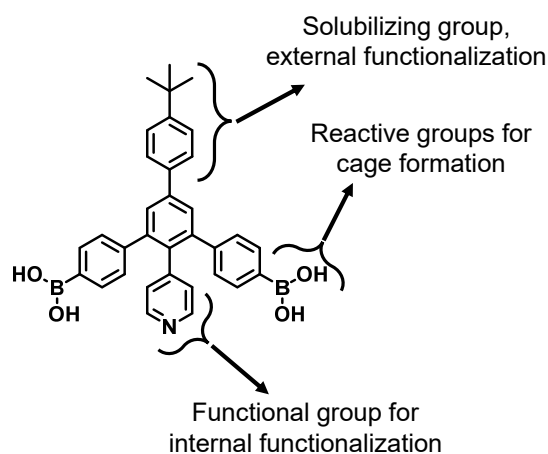

**Figure 34 |** Design principle for diboronic acid **130**.

The chosen synthetic route for the synthesis of diboronic acid **130** is depicted in Scheme 34. As a suitable starting material, compound **132** was synthesized following a procedure described by Höger and coworkers.[119] The key step for the formation of **132** is the transformation of the 2,4,6-triarylpyrilium salt **131** to the corresponding 2-substituted-arene **132** by reacting it with sodium salt of 4-pyridylacetic acid as it was originally described by Zimmermann and Fischer.[120] With the dihalogenated derivative in hand, the double borylation reaction of compound **132** was investigated.
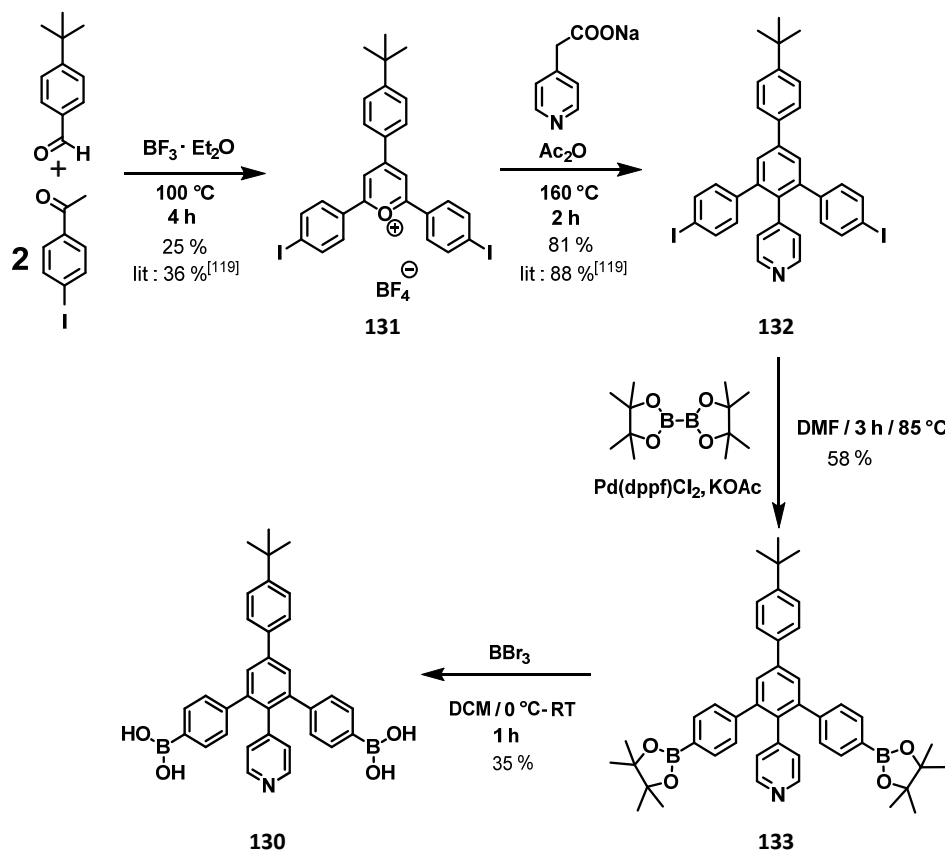
Scheme 34 | Synthesis of diboronic acid **130**.

Initially, a recently-developed photochemical borylation of the aryl iodide was attempted due to its attractive features such as high yields, broad functional group tolerance or metal-free mild reaction conditions.[121] Unfortunately, no conversion of the starting material was observed (Table 6). Therefore, the well-known palladium-catalyzed Suzuki-Miyauara borylation of aryl halides has been employed for the synthesis of diborylated derivative **133**.[122] A profound solvent effect was observed with DMF being the ideal solvent for the borylation reaction. The duration of the reaction was also crucial for the success of the two-fold cross-coupling with both aryl iodide moieties. Reaction of **132** with bis(pinacolato)diboron in dry DMF at 85 °C for 90 minutes led to the formation of compound **133** along with partially borylated derivative **134**, which was hard to detect due to its comparable R_f value on TLC when eluted with DCM/MeOH 95:5. Coincidently, both mono-borylated compound **134** and bis-borylated species **133** have the same molecular weight. Hence, confirmation of the purity of the compound by MALDI-TOF measurements was fruitless, since it only revealed the presence of one molecular ion-peak at around $m/z= 691.4$ as the only detectable species even for mixtures of **134** and **133**. On the other hand, separate signals for all protons corresponding to both **133** and **134** were obtained in ¹H-NMR spectra. Initially, the signals for the mono-borylated species **134** were mistakenly

assigned to a partially deprotected species that might have been formed while passing the reaction mixture through a short silica column. This wrong assumption led to the attempt to obtain pure product **133** by quenching the reaction mixture by water and then extraction by diethyl ether, instead of purification by column chromatography. However, no differences in the ^{1}H-NMR spectra of the crude product were observed. Therefore, the duration of the reaction was increased in order to exclusively get diborylated **133**. Although the desired product could be obtained after chromatographic purification, the yield of the reaction went down significantly, most probably due to the formation of oligomers *via* Suzuki coupling between iodo-aryl and borylated aryl species. However, this optimized procedure provides compound **133** in acceptable amount and high purity for the next deprotection reaction.
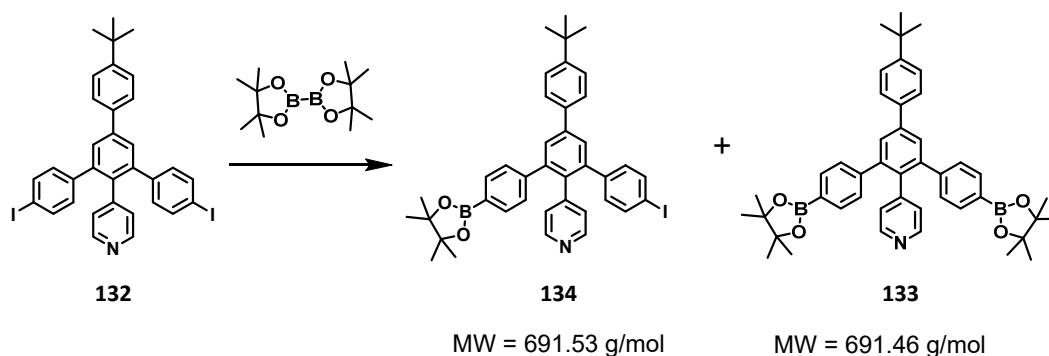
| Reagents	Solvent	Temperature	Duration	Result
UV light	CH$_3$CN, MeOH, CH$_3$COCH$_3$	rt	1 h	No conversion
Pd(dppf)Cl$_2$, KOAc	THF	reflux	3 h	No conversion
	Dioxane	85 °C	24 h	**132: 134: 133** = 5: 3: 2
	DMF	85 °C	90 min[†]	**134: 133** = 1: 9 (combined yield = 78 %)
	DMF	85 °C	90 min[‡]	**134: 133** = 1: 9 (combined yield = 81 %)
	DMF	85 °C	3 h[#]	Only **133** (Yield = 57-60 %)

Table 6 | Optimization of the double borylation reaction. († = reaction mixture was filtered through a pad of silica; ‡ = reaction mixture was quenched by water and then extracted with Et$_2$O; # = reaction mixture was either passed through a short silica pad or quenched with water).

For the deprotection of the pinacolyl boronate esters, the widely-used strategy of oxidative cleavage with sodium periodate was initially employed.[123] Surprisingly, this reaction did not proceed as anticipated rather led to the cleavage of the C-B bonds resulting in the undesired diphenol **135**. There may be a bit of ambiguity regarding the MALDI-TOF spectrum of compound **135**, since the molecular peak could also be assigned to the desired compound **130** with the loss of a tertiary butyl group. But this would be very unlikely, given the very mild conditions applied for the ionization for MALDI technique.
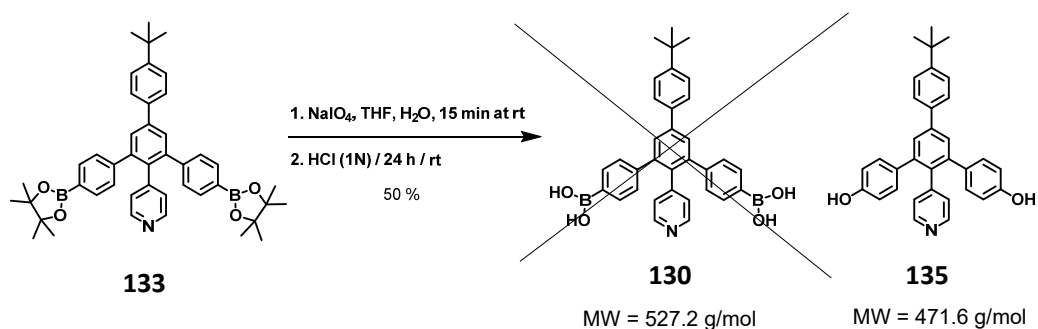
Scheme 35 | The formation of **135** instead of **130** upon oxidative deborylation of **133**.

To overcome this setback, different strategies to synthesize the desired compound **130** have been evaluated. Treatment of **133** with hydrochloric acid in THF without the addition of any oxidizing agent, which was proven to be successful for the deprotection of some pinacol-protected boronate esters,[124] did not result in any deprotection of the compound **133**. In an attempt to directly transform diiodo-derivative **132** to diboronic acid **130**, compound **132** was treated with ^{n}BuLi for a lithium-iodide exchange followed by the addition of trimethyl borate and quenching of the reaction mixture with acidic water. However, this also resulted in the formation of diol derivative **135** instead of diboronic acid **130**.
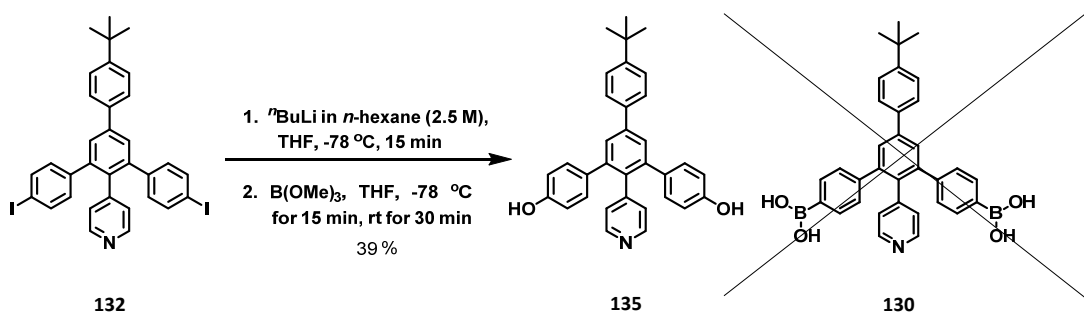
Scheme 36 | Synthesis of **135** upon lithiation-borylation reaction of **132**.

Ultimately, the pinacol groups of **133** could be successfully removed by treating **133** with boron tribromide. Diboronic acid **130** has been fully characterized by ^{1}H-NMR, ^{13}C-NMR spectroscopy and MALDI-TOF spectrometry.
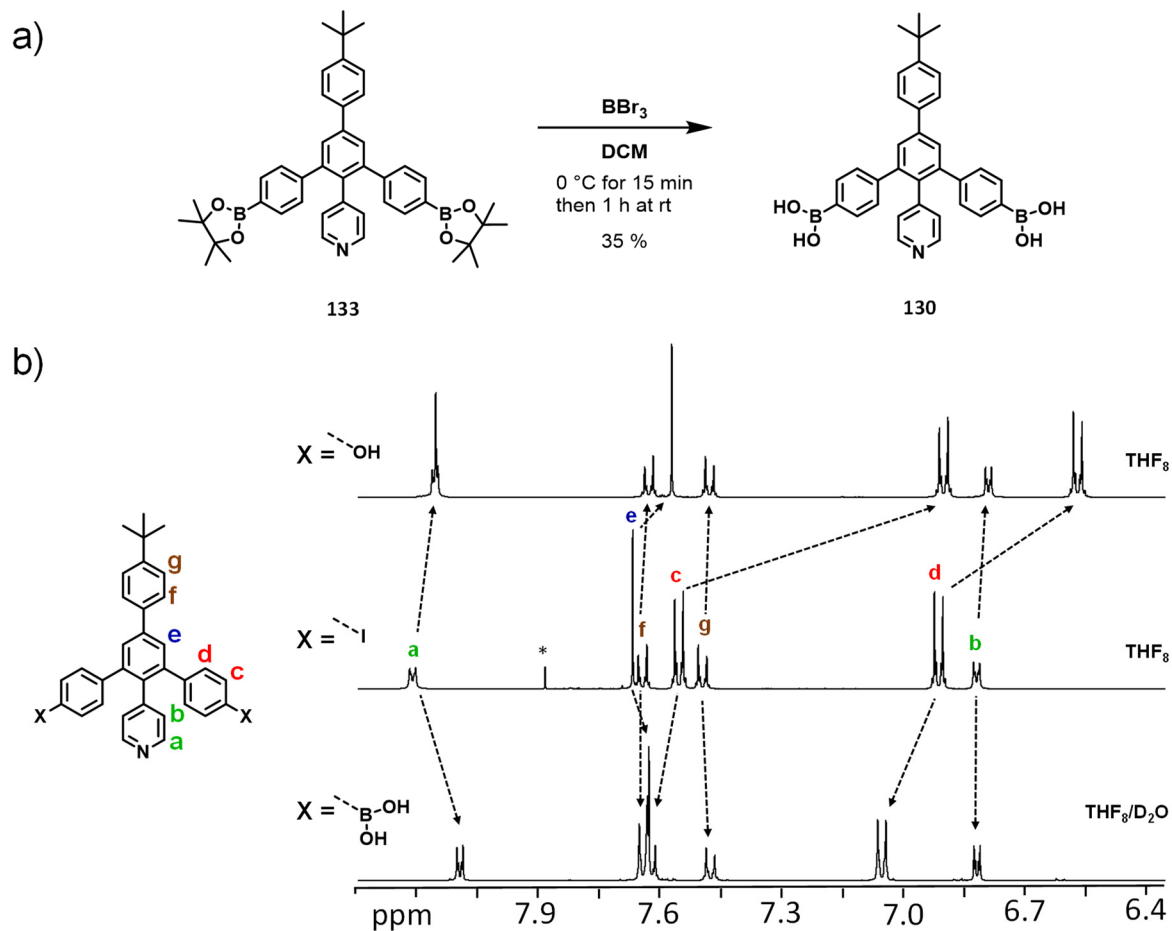

Figure 35 | a) Synthesis of the desired diboronic acid **130** upon deprotection of the pinacolyl boronate esters; **b)** ^{1}H-NMR spectra (400 MHz, rt) of *m*-terphenylene derivatives doubly substituted by -OH (THF-d$_8$, top), -I (THF-d$_8$, middle) and -B(OH)$_2$ (THF-d$_8$/D$_2$O, bottom) groups; ∗ = CHCl$_3$.

In this context, the solubility profile of diboronic acid **130** is worth noting since it differs significantly from the isostructural diboronic acid **102** previously synthesized by the Beuerle group (see Figure 36).[14b] Whereas methyl derivative **102** is soluble in polar solvents such as THF, MeOH and DMSO, pyridine containing diboronic acid **130** is insoluble in THF, MeOH but only soluble in DMSO.
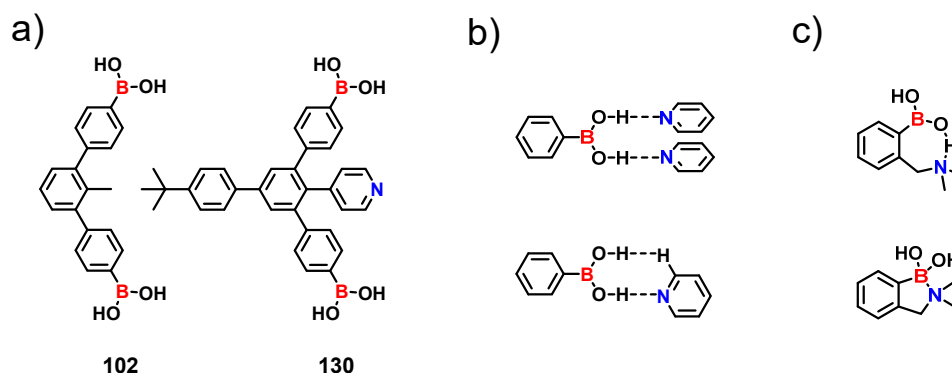
Figure 36 | a) The two isostructural diboronic acids; **b)** the observed hydrogen-bonding patterns for the adducts formed between pyridyl and boronic acid building blocks found in the solid-state; **c)** the representative conformers of *o*-(*N*,*N*-dimethylaminomethyl)phenylboronic acid based on the intramolecular B-O-H⋯N hydrogen bond and B⋯N dative bond.

This remarkable difference in solubility of both diboronic acids may seem surprising, given the structural similarity between them. It may stem from the formation of boron-nitrogen dative bonds in solid-state, which results in difficulty to solubilize compound **130** unlike boronic acid **102**. Also there is another possibility of the formation of hydrogen bonds between boronic acids and pyridyl groups in the solid-state of diboronic acid **130** as it has been reported in literature by Höpfl and coworkers for the solid-state adducts formed from pyridine and different boronic acids (Figure 36b).[125] A comprehensive computational study by Larkin and coworkers on *o*-(*N*,*N*-dialkylaminomethyl)aryl boronic acid recently indicated that in vacuum the calculated B-O-H⋯N hydrogen-bonded form is slightly lower in energy (~ 1 kcal mol^{-1}) than the corresponding B⋯N dative bonded structure (Figure 36c).[126] Due to this small difference in energy between those conformers, it can be reasonably assumed both boron-nitrogen dative bonds and hydrogen bonds may contribute to the overall stability resulting in variation of solid-state arrangements of **130**, thus leading to different solubilities when compared to **102**.

Altogether, the synthesis of a building block possessing the desired concave functionalization has been successfully accomplished. Given the variety of possible further reactions of the boronic acids, *e.g.* boronate ester formation or cross-coupling reactions, this diboronic acid may serve as a diverse building unit in supramolecular chemistry as well as in polymer science in the future.

3.3.3 Towards the Formation of Cages Possessing Both Interior and Exterior Functionalities

This section describes the initial synthetic efforts towards the formation of an organic cage from building units having both intrinsic and extrinsic functionalities individually. Figure 37 shows the basic concept for the synthesis of a boronate ester-based tetrahedral [4+6]-cage by condensing the tritopic TBTQ **123** with the ditopic linker **130**. The intrinsic pyridyl groups can be exploited to tune the property of the cage cavity and the protruding terminal alkyne groups offer the potential for exohedral functionalization of the cage by post-synthetic modification. These features render the preparation of the designed [4+6]-cage **136** an attractive target to pursue.
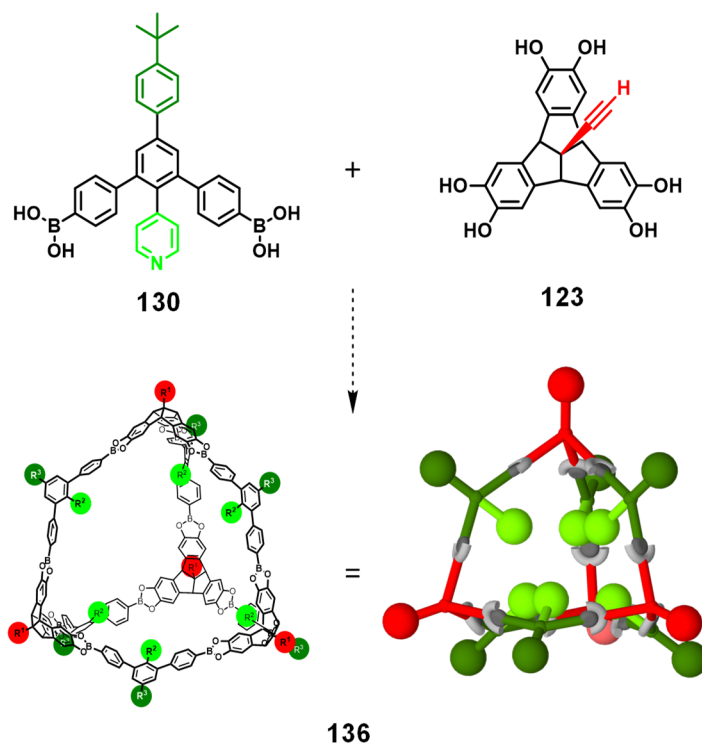

Figure 37 | The strategy to synthesize a covalent organic cage based on boronate esters with the possibility of both exohedral and endohedral functionalization.

Previously, the Beuerle group reported the synthesis of tetrahedral [4+6]-covalent organic cage **98** by condensation reactions of catechol-functionalized TBTQ **58c** with *n*-butyl group at the apical position and aromatic diboronic acid **102** with *meta*-relationship between the two boronic acid groups (Figure 38a).[14b] This reaction was performed under usual conditions, *i.e.* dissolving TBTQ **58c** and diboronic acid **102** in THF-d$_8$ in 2:3 ratio, addition of 4 Å molecular sieves and monitoring the reaction by ^{1}H-NMR spectroscopy until quantitative cage formation.

The first hurdle to apply this reaction condition for the formation of the desired [4+6]-cage **136** is the insolubility of diboronic acid **130** in THF-d$_8$ as it has been discussed in the previous section. Hence, a solution of 1:1 THF-d$_8$/DMSO-d$_6$ was chosen as the reaction medium and after addition of molecular sieves ^{1}H-NMR spectra were measured over time (Figure 38b). At the beginning, sharp NMR signals were observed corresponding to the protons of the starting materials. After one day however, broad and overlapping ^{1}H-NMR signals appeared. As a matter of fact, assigning and integrating any NMR signals became improbable. The NMR spectrum did not further change over the course of three days even after the addition of more molecular sieves. Also no precipitation was observed in the NMR tube.
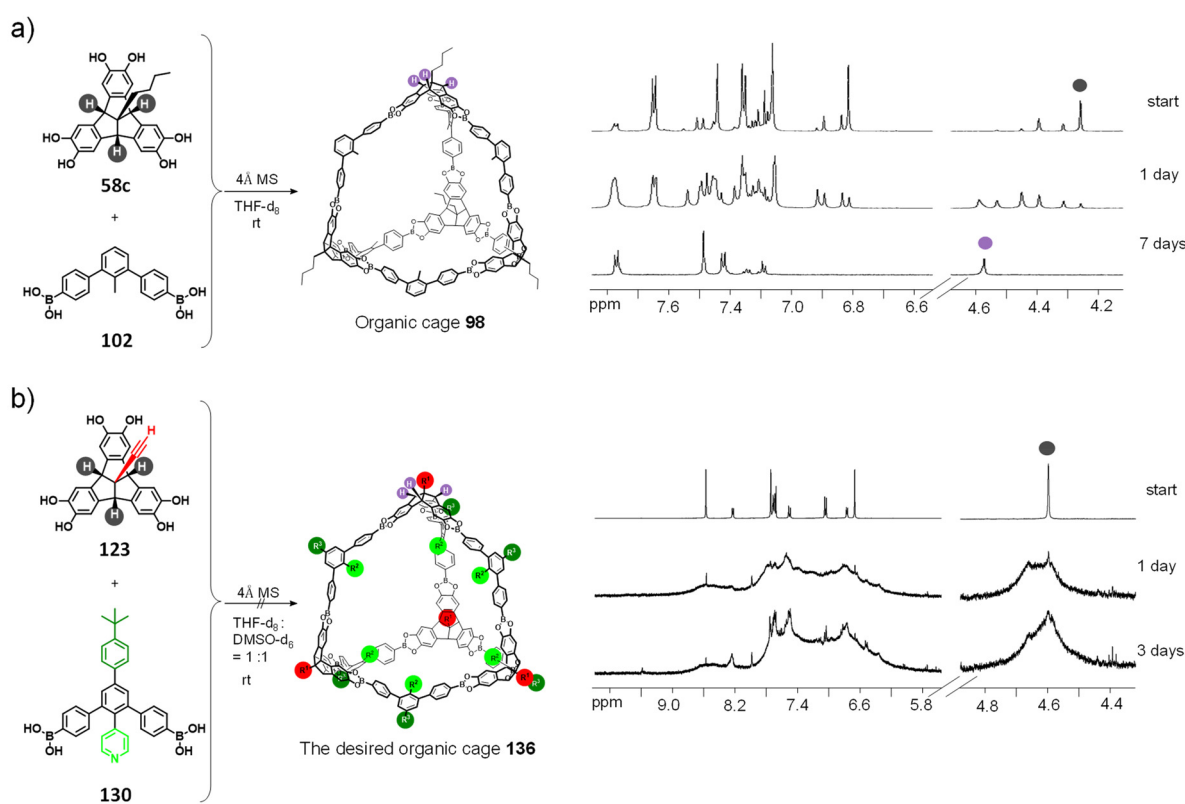

Figure 38 | a) Reaction procedure to synthesize organic cage **98** and monitoring of the reaction by ^{1}H-NMR spectra (400 MHz, THF-d$_8$, rt) periodically till the end of the reaction; **b)** reaction condition for the formation of organic cage **136** and measurement of ^{1}H-NMR spectra (400 MHz, THF-d$_8$/DMSO-d$_6$, rt) at regular time-interval to follow the progress of the reaction.

This observation raises the question: Why did not the reaction go to completion to form the desired cage **136** like the reported [4+6]-cage **98**? The working principle behind the syntheses of all reported boronate ester cages is that at first, a dynamic reaction mixture consisting of multiple kinetic oligomers exists and over time, this oligomeric mixture equilibrates towards the thermodynamically most stable cage compound due to the dynamic nature of the boronate

ester bonds. For the formation of cage **136** however, there is the additional possibility that these kinetic intermediates might be trapped by the formation of boron-nitrogen dative bonds between pyridyl group and boronate esters. Furthermore, the geometry around boron centers changes upon formation of boron-nitrogen dative bonds as it was extensively discussed in chapter **3.2**. This alters the bite angles among the reactive sites of the building blocks necessary for the formation of covalent organic cage compounds. Most probably, this unwanted boron-nitrogen dative bond formation causes the system not to reach the thermodynamic minimum, ultimately leading to trapped oligomers and broad signals in ^{1}H-NMR spectra.

Hence, the obvious solution would be to block the pyridyl nitrogen atom, thereby preventing the formation of boron-nitrogen dative bonds ensuing the synthesis of the desired cage. With this in mind, trifluoromethanesulfonic acid was added to the suspension of diboronic acid **130** in THF-d$_8$. The solid material slowly became soluble in THF-d$_8$ upon formation of the triflate salt of **130**. To this THF-solution of the diboronic acid with protonated pyridyl group, TBTQ **123** was added in 2:3 molar ratio at room temperature and a ^{1}H-NMR spectrum was instantly measured (Figure 39a). Afterwards, 4 Å molecular sieves were added to the NMR tube and the reaction progress was monitored by ^{1}H-NMR spectroscopy. Basically, boronate ester formation withdraws electron density from TBTQ core, which resulted in increasing down-field shifts for the aromatic protons of both TBTQ **123** and diboronic acid **130** as well as the aliphatic protons of TBTQ after successive ester formation. In this regard, the ^{1}H-NMR signal of the methine protons of TBTQ provides useful insights into the progress of the reaction since the signature of this signal is directly related to the symmetry of the TBTQ molecule. When single- or double-condensation products of TBTQ are formed, the methine protons are no longer chemically equivalent resulting in splitting into two signals with a 2:1 integral ratio (Figure 39). Figure 39c shows the shift in equilibrium towards the thermodynamically stable triply condensed product with time.
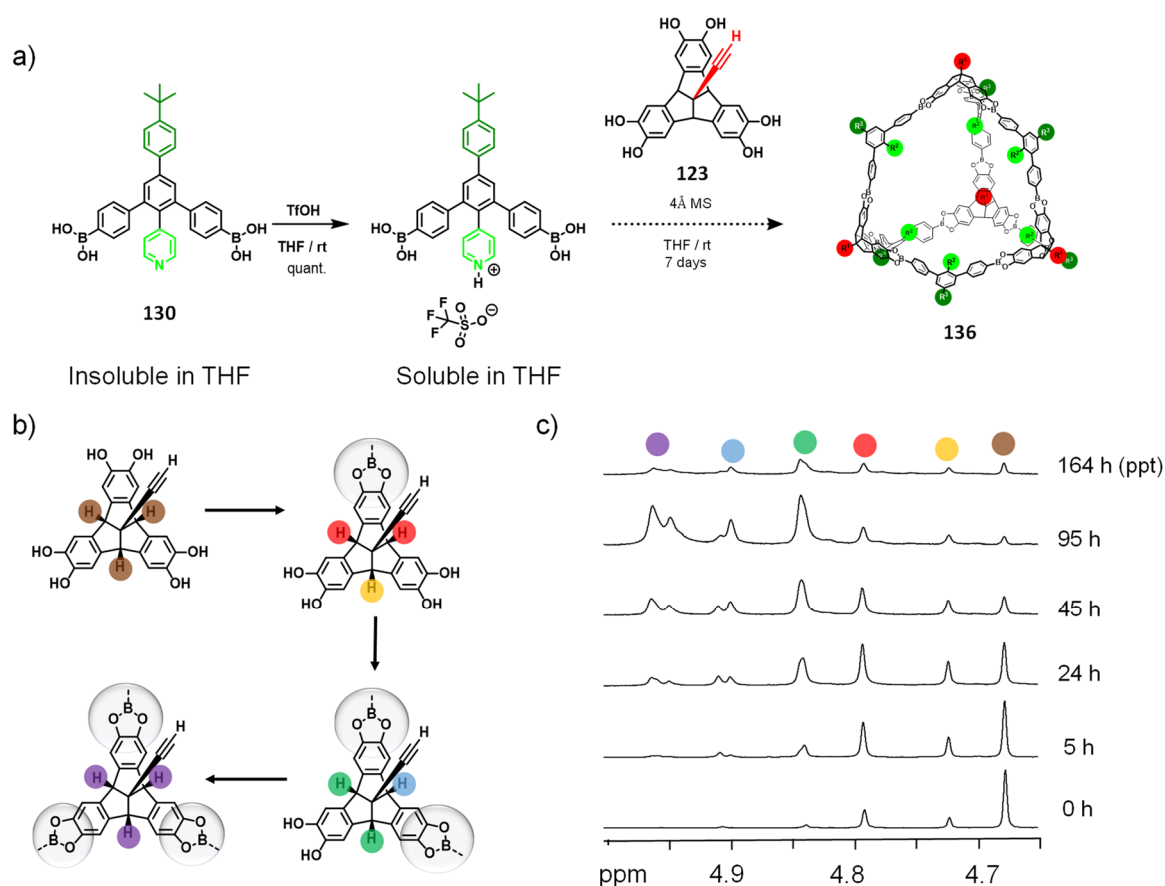
Figure 39 | a) Formation of the pyridinium triflate salt upon addition of triflic acid to diboronic acid **130** followed by the addition of **123** for synthesis of organic cage **136**; **b)** The expected reaction intermediates for the formation of the cage structure; **c)** Evolution of the ^{1}H-NMR signal (400 MHz, THF-d$_8$, rt) of methine protons of the TBTQ-derivative with progress of the reaction. (ppt = precipitate).

After seven days, white precipitates appeared at the bottom of the NMR tube. The precipitate was insoluble in any chlorinated solvent such as chlorobenzene, chloroform, dichloromethane or 1,1,2,2-tetrachloroethane. Hence, the formation of the expected cage compound could not be confirmed by NMR spectroscopy. This may seem quite unprecedented considering the fact that no precipitate appeared while formation of [4+6]-cage **98**.[14b] The only solubilizing groups, that cage **98** have, are four *n*-butyl groups at the apical positions of the TBTQ molecules (Figure 38a), whereas the expected cage **136** would possess six *tert*-butylbenzyl groups at the periphery, if formed. The coulombic interaction between the cationic pyridium ion with the triflate anions may be the reason for the precipitation of condensation products from the THF-solution. In line with this argument, a far less weakly coordinating anion than triflate ion may not interfere with the chemical equilibrium to the formation of the desired cage molecule. Hence, use of the pyridinium salt of diboronic acid **130** with the well-known BARF anion,[127] as the building block to synthesize the desired cage molecule is put forward as an outlook of the project.

CHAPTER 4

●

Summary

In conclusion, the aim to control over the function of organic cages has been successfully addressed by developing well-defined, discrete self-assembled organic cages based on building units of desired functionalities. On one hand, the control over assembly/disassembly by change of external parameters, *e.g.* temperature and pH has been achieved by utilization of the dynamic nature of boron-nitrogen dative bonds of cage assemblies. On the other hand, the incorporation of newly-synthesized functional molecular building units such as the apically functionalized TBTQs and the 2-substituted *meta*-diboronic acids into the cage framework provides the necessary spatial control over functionalities of covalent organic cage compounds.

In the first part, boron-nitrogen dative bonds have been exploited for the synthesis of the well-defined bipyramidal [2+3]-cage **114** from tribenzotriquinacene trisboronate ester **113** and 1,4-diazabicyclo[2.2.2]octane **111** (Figure 40a). This cage assembly is the first example for a supramolecular cage mediated by boron-nitrogen dative bonds that is stable and exists as a discrete species in solution. Isothermal Titration Calorimetry (ITC) has been carried out to determine the thermodynamic association constants for the formation of the cage. The obtained values indicate that the rigid preorganization of the reactive sites in both components induce chelate cooperativity for the cage formation. Temperature dependent NMR studies indicate the reversible cage opening at high temperatures and reassembly upon cooling to room temperature (Figure 40b). The dissociation of cage **114** at higher temperatures can be rationalized by calculation of association constants and simulations of mole fractions for all the relevant species at different temperatures based on the ITC data. As another stimulus, pH-dependent dissociation and reformation of the cage has been investigated. The high fidelity and thermodynamic stability of this model cage establishes boron-nitrogen dative bond-based assemblies as a novel class for solution-stable cages with the possibility of purposely controlling the assembly in a reversible fashion. As an outlook, cages with larger cavities can be envisioned for the encapsulation of suitable guests accompanied by the benefit of selective release of molecular cargo by external stimuli.
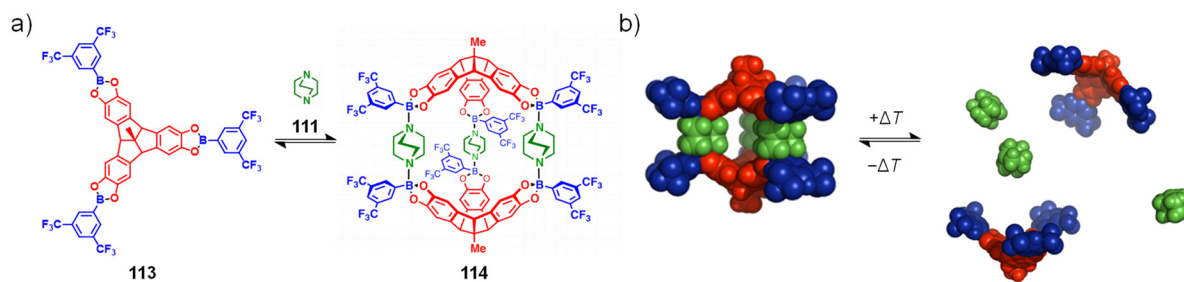
Figure 40 | Stimuli-responsive organic cage: **a)** a well-defined, monodisperse self-assembled [2+3]-cage based on boron-nitrogen dative bonds; **b)** temperature dependent switching between the cage assembly and the individual molecular units.

The spatial control of functionalities for self-assembled systems depends on the functionalization of the molecular building blocks and both exohedrally and endohedrally modified cages are accessible following this approach. In this regard, two new divergent building units have been designed and synthesized in the second part of the thesis.

On one hand, a novel and versatile protocol for the introduction of one terminal alkyne unit at the apical position of the TBTQ scaffold has been presented. This apically functionalized TBTQ **115** can now be synthesized in gram quantities from readily available starting materials (Scheme 37a). While synthesizing this compound, a mild two-step deprotection sequence was developed with an exchange of the methoxy groups to more labile triethylsilyl groups followed by the complete removal of the silyl groups under acidic condition thus leading to the formation of triscatechol derivative **123** (Scheme 37b). Since this transformation does not require the protection of the terminal alkyne prior to demethylation of the methoxy groups, this procedure proves to be a very useful protocol for methoxy deprotection in presence of labile alkyne groups. Postsynthetic modifications *via* the azide-alkyne Huisgen cycloaddition or Sonogashira cross-coupling at the alkyne moiety exemplarily showcase two of the most versatile ways of attaching a great variety of readily available molecules at the apical position of the TBTQ scaffold. This strategy now provides the desired spatial control of the functionality for self-assembled architectures, while the catechol groups take part in molecular self-assembly.

On the other hand, an elegant route for the synthesis of *meta*-diboronic acid **130** possessing a pyridyl group in 2-position has been documented (Scheme 37c). Since this diboronic acid has two independently addressable functional groups, namely boronic acid and pyridyl group, it is an ideal molecular building block for the formation of functionalized self-assembled systems.

a)

b)

c)
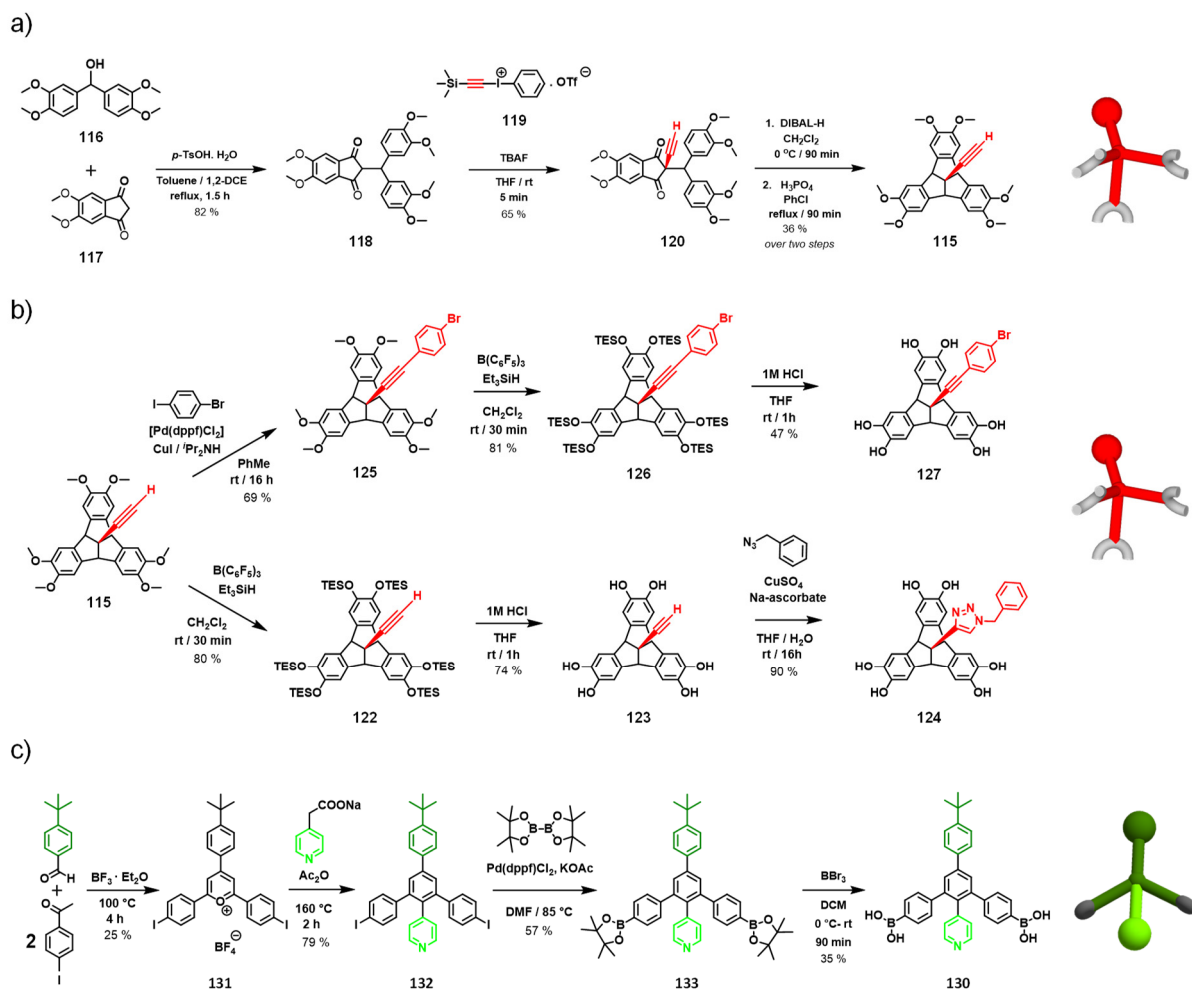
Scheme 37 | Molecular building blocks with divergent functionalities: **a)** the synthesis of an apically functionalized TBTQ derivative; **b)** the deprotection of the methoxy groups and modular post-synthetic modification of the apical alkyne group of the TBTQ scaffold; **c)** the synthesis of a ditopic *m*-terphenyl diboronic acid building block with intraannular functionalization.

Scheme 37 provides an overview over the modular synthetic routes to important molecular building blocks. The synthesis of **115** has obvious advantages not only in terms of ease of scalability but also the versatility of functional groups that can be anchored at the apical position. Furthermore, the attachment of the apical alkyne group and the formation of the TBTQ backbone are not inextricably wedded to the C-C cross-coupling of **116** and **117** in this route. Hence, depending on the functional groups of the coupling partners, a wide variety of TBTQ derivatives can be achieved with different functionalities on each of the three aromatic rings of the TBTQ scaffold along with apical functionalization. In the context of *meta*-diboronic acids, the concave or convex functionality can be modified by changing the small individual molecular units without the requirement of altering the synthetic sequence described for diboronic acid **130**. Such general adaptability of the synthetic procedure provides a unique opportunity to synthesize a diverse array of functionalized *meta*-diboronic acids as needed.

In the third part of this thesis, these now available building blocks have been implemented in initial investigations regarding cage formation. Two isostructural boronate ester based [2+3]-organic cages of the same shape, but with different functionality at the periphery have been synthesized by the co-condensation of apically functionalized TBTQ derivatives **123** and **127** with diboronic acids **100** (Scheme 38). These are the first examples of boronate ester-based organic cages with modular external functionalities.
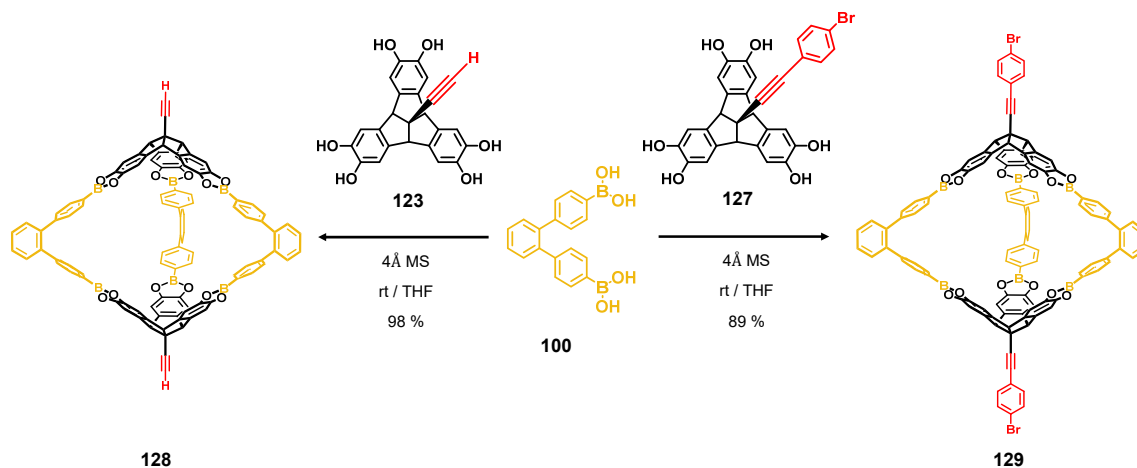
Scheme 38 | The boronate ester based covalent organic cages of the same trigonal bipyramidal shape but with different exohedral functionalities.

Finally, in the quest of spatial control of functionalities on both interior and exterior of organic cages, co-condensation of TBTQ **123** with diboronic acid **130** was performed. Unfortunately, the cage formation did not occur due to boron-nitrogen dative bonds between boronate esters and pyridyl units of **130**. Hence, pyridyl groups of **130** were protonated by addition of acid, which disrupted the formation of the undesired boron-nitrogen bonds and allowed the condensation to proceed smoothly. However, the insolubility of the precipitate obtained after the condensation poses difficulties in the characterization of the final cage structure. Since the spectral signature of the reaction over time evidently suggests a hint towards the formation of the intended cage, it is worth addressing the issue of solubility of the final product to fulfil the goal of forming cage compounds with both external and internal functionalities. In this context, the general synthetic route (Scheme 37c) that has been established for the synthesis of **130** can easily be applied to synthesize *meta*-diboronic acids with desired concave functionalities such as carboxylic acid or aldehyde to avoid any complication regarding the solubility of the final cage assembly. Afterwards, the newly synthesized diboronic acids can, in principle, be condensed with TBTQ **123** to synthesize organic cage compounds with both endohedral and exohedral functionalization.

CHAPTER 5

●

Zusammenfassung

Im Rahmen dieser Arbeit sollten funktionale organische Käfige durch einen gezielten Aufbau aus entsprechend funktionalisierten Bausteinen erhalten werden. Einerseits wurden dabei Auf- und Abbau eines Käfigs basierend auf dativen Bor-Stickstoff-Bindungen durch externe Parameter wie Temperatur oder pH-Wert beeinflusst. Andererseits ermöglichte der Einbau von neu neuentwickelten funktionalen molekularen Bauelementen wie apikal funktionalisierten TBTQ-Derivaten und 2-substituierten *meta*-Diboronsäuren in die Käfiggerüste die notwendige räumliche Kontrolle über die Funktionalitäten kovalent organischer Käfigverbindungen.

Im ersten Teil dieser Arbeit wurden dative Bor-Stickstoff-Bindungen für die Synthese des wohldefinierten bipyramidalen [2+3]-Käfigs **114** aus Tribenzotriquinacen-Trisboronsäureester **113** und 1,4-Diazabicyclo[2.2.2]octan **111** ausgenutzt (Abbildung 40a). Dieses Aggregat ist das erste Beispiel für einen supramolekularen Käfig, der durch dative Bor-Stickstoff-Bindungen aufgebaut ist und als stabile und diskrete Spezies in Lösung existiert. Die thermodynamischen Assoziationskonstanten für die Bildung des Käfigs wurden durch Isothermale Titrationskalorimetrie (ITC) bestimmt. Die erhaltenen Werte zeigen, dass die starre Vororganisation der reaktiven Gruppen in beiden Komponenten eine Chelatkooperativität für die Käfigbildung induziert. Temperaturabhängige NMR-Untersuchungen zeigen die reversible Käfigöffnung bei hohen Temperaturen und die Rückgewinnung des Käfigs bei Abkühlung auf Raumtemperatur (Abbildung 40b). Die Dissoziation des Käfigs **114** bei höheren Temperaturen wurde durch eine Berechnung der temperaturabhängigen Assoziationskonstanten und Molenbrüche für alle relevanten Spezies auf der Basis der ITC-Daten nachvollzogen. Als zusätzlicher Stimulus wurde die pH-abhängige Dissoziation und Assoziation des Käfigs untersucht. Die ausgesprochene Reversibilität und hohe thermodynamische Stabilität dieses Modellsystems etabliert Aggregate auf der Basis von dativen Bor-Stickstoff-Bindungen als eine neue Klasse von lösungsstabilen Käfigen, deren Auf- und Abbau reversibel gesteuert werden kann. In Zukunft sind dabei Käfige mit größeren Hohlräumen vorstellbar, die den Einschluss und die stimuli-responsive Freisetzung von geeigneten Gästen ermöglichen sollten.
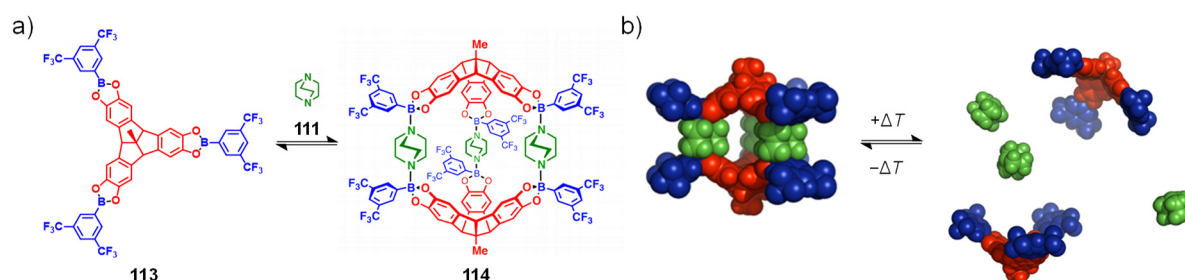
Abbildung 40 | Stimuli-responsive organische Käfige: **a)** ein wohldefinierter, monodisperser, selbstorganisierter [2+3]-Käfig **114** auf der Basis von dativen Bor-Stickstoff-Bindungen; **b)** temperaturabhängiges Schalten zwischen dem Käfig und den einzelnen molekularen Einheiten.

Die räumliche Kontrolle von Funktionalitäten in selbstorganisierten Systemen hängt von der Funktionalisierung der molekularen Bausteine ab, wobei sowohl exo- als auch endohedral modifizierte Käfige über einen derartigen Ansatz zugänglich sein sollten. In diesem Zusammenhang wurden im zweiten Teil der Arbeit zwei neue divergente Bausteine entworfen und synthetisiert.

Zunächst wurde ein neues und vielseitig anwendbares Synthese-Protokoll für die Einführung einer terminalen Alkineinheit an der apikalen Position des TBTQ-Gerüstes entwickelt. Das apikal funktionalisierte TBTQ-Derivat **115** kann nun im Gramm-Maßstab aus einfach zugänglichen Ausgangsverbindungen dargestellt werden (Schema 37a). Für die Synthese dieser Verbindung wurde weiterhin eine milde, zweistufige Entschützungs-Sequenz entwickelt, in der zunächst die Methoxygruppen zu labileren Triethylsilylgruppen umgesetzt wurden, die anschließend unter sauren Bedingungen vollständig zum Triscatechol **123** entfernt wurden (Schema 37b). Da diese Transformation keine Schützung des terminalen Alkins erfordert, könnte sich dieses Verfahren als eine sehr nützliche Vorschrift für die Demethylierung von Methoxygruppen in Gegenwart von labilen Alkinen erweisen. Postsynthetische Modifikationen mit Hilfe von Azid-Alkin-Huisgen-Cycloadditionen oder Sonogashira-Kreuzkupplungen an der Alkin-Einheit illustrieren beispielhaft das Potential, über diese Zwischenstufe eine Vielzahl von leicht zugänglichen Molekülen an der apikalen Position des TBTQ-Gerüstes anzubringen. Diese Strategie ermöglicht nun die gewünschte räumliche Kontrolle über die Funktionalität von selbstorganisierten Architekturen, während die Catechol-Einheiten für die molekulare Selbstorganisation eingesetzt werden.

Weiterhin wurde ein eleganter Weg zur Synthese der *meta*-Diboronsäure **130** mit einer Pyridylgruppe in 2-Position entwickelt (Schema 37c). Auch diese Verbindung weist mit den Boronsäuren und der Pyridylfunktion zwei unabhängig voneinander adressierbare Gruppen auf, was sie zu einem idealen molekularen Baustein für die Bildung von funktionalisierten selbstorganisierten Systemen macht.
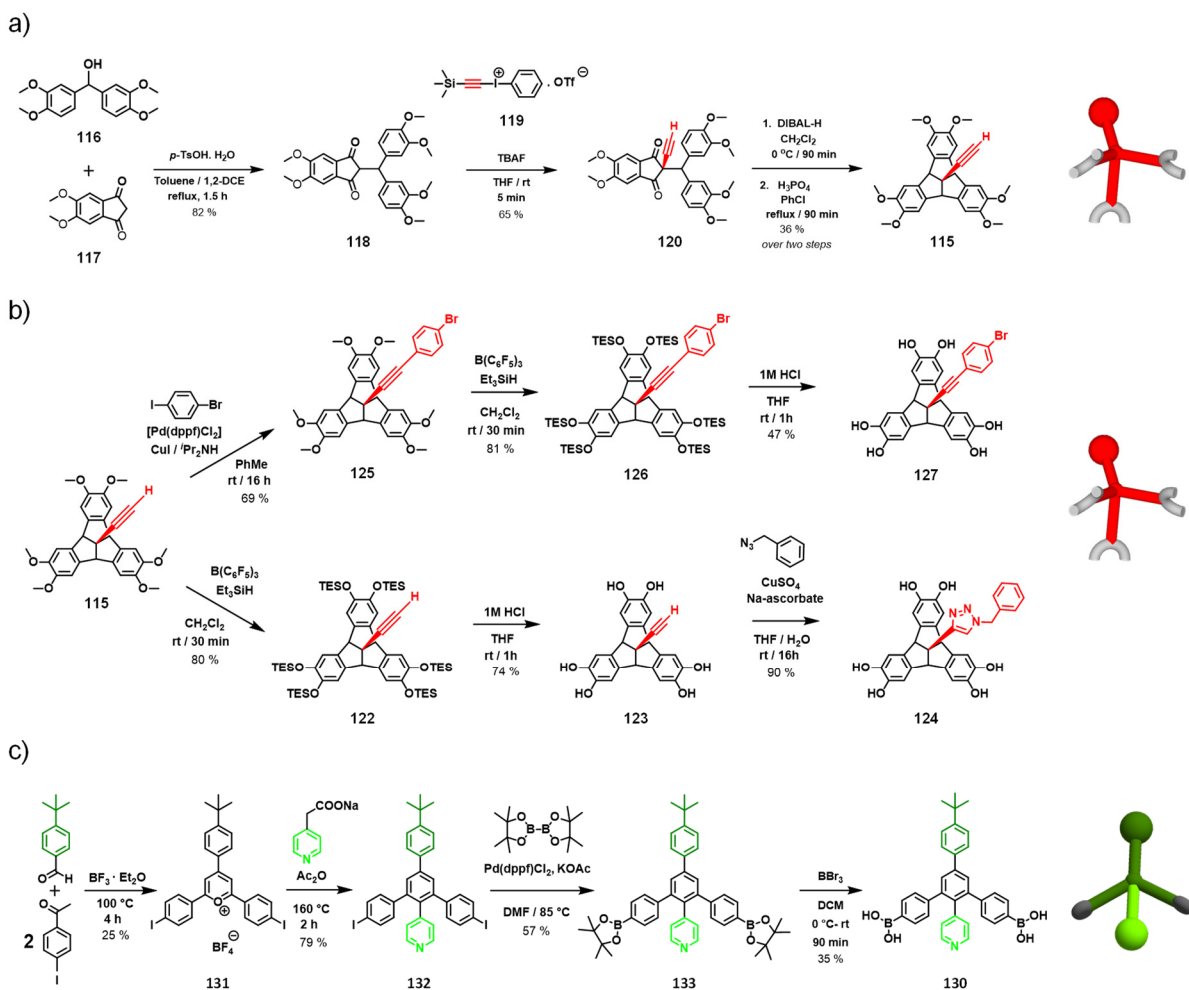

Schema 37 | Molekulare Bausteine mit divergenten Funktionalitäten: **a)** Synthese eines apikal funktionalisierten TBTQ-Derivats; **b)** Entschützung der Methoxygruppen und modulare postsynthetische Modifikation der apikalen Alkingruppe des TBTQ-Gerüsts; **c)** Synthese eines ditopischen *meta*-Terphenyl-Diboronsäure-Bausteins mit intraannularer Funktionalisierung.

Schema 37 gibt einen Überblick über die modularen Syntheserouten zu den wichtigsten im Rahmen dieser Arbeit entwickelten molekularen Bausteinen. Die Synthese von **115** ist dabei nicht nur aufgrund der einfachen Skalierbarkeit, sondern auch in Bezug auf die Vielfalt an funktionellen Gruppen, die an der apikalen Position verankert werden können, sehr vorteilhaft.

Weiterhin sind die Vorstufen für den Aufbau des TBTQ-Gerüsts nicht nur auf die beiden Methoxy-Derivate **116** und **117** beschränkt. Vielmehr sind in Abhängigkeit der Substituenten an den Kopplungspartnern auch eine Vielzahl von weiteren TBTQ-Derivaten mit unterschiedlichen Funktionalitäten an jedem der drei aromatischen Ringe des TBTQ-Gerüsts zusammen mit der apikalen Funktionalisierung denkbar. Für die *meta*-Diboronsäuren können sowohl der konkave als auch konvexe Substituent durch Variation der niedermolekularen Vorstufen modifiziert werden, ohne dass die für die Diboronsäure **130** beschriebene grundlegende Synthese-Sequenz verändert werden muss. Dieses modulare Syntheseverfahren sollte nun einen einzigartigen Zugang zu einer Vielzahl an funktionalisierten *meta*-Diboronsäuren liefern.

Im dritten Teil dieser Arbeit wurden diese nun vorhandenen Bausteine in ersten Untersuchungen zu organischen Käfigen umgesetzt. Zwei isostrukturelle [2+3]-Boronsäureester-Käfige mit gleicher Form, aber unterschiedlicher peripherer Funktionalität konnten durch die Co-Kondensation der apikal funktionalisierten TBTQ-Derivate **123** und **127** mit der *ortho*-Diboronsäure **100** synthetisiert werden (Schema 38). Dies sind die ersten Beispiele für organische Boronsäureester-Käfige mit modularer externer Funktionalisierung.
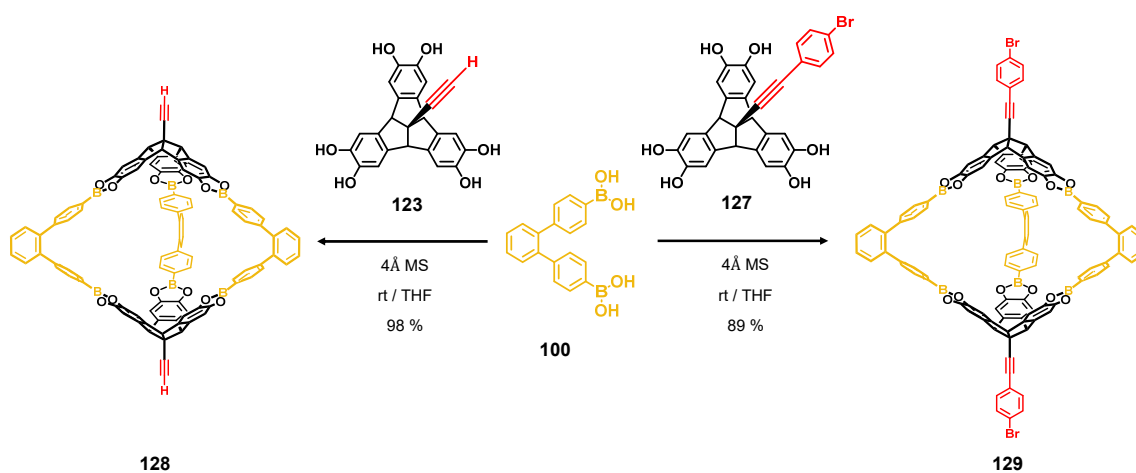
Schema 38 | kovalent organische Käfige auf der Basis von Boronsäureestern mit identischer trigonal-bipyramidaler Form aber unterschiedlichen exohedralen Funktionalitäten.

Schlussendlich wurde mit dem Ziel einer gleichzeitigen inneren und äußeren Funktionalisierung von organischen Käfigen die Co-Kondensation von TBTQ **123** und der *meta*-Diboronsäure **130** untersucht. Leider wurde in diesem Fall eine erfolgreiche Käfigbildung durch dative Bor-Stickstoff-Bindungen zwischen den Boronsäureestern und den Pyridyl-

Einheiten von **130** verhindert. Daher wurden diese Pyridylgruppen durch Säure-Zugabe protoniert, was die Bildung der unerwünschten Bor-Stickstoff-Bindungen unterdrückte und stattdessen Boronsäureester-Kondensationen ermöglichte. Allerdings erwies sich die Charakterisierung des nach der Reaktion erhaltenen Niederschlags aufgrund seiner geringen Löslichkeit als äußerst schwierig. Da spektroskopische Untersuchungen während des Reaktionsverlaufs jedoch auf eine zunehmende Umsetzung zur finalen Käfigstruktur hindeuteten, sollte dieser Weg in weiteren Studien für Bausteine mit höherer Löslichkeit weiterverfolgt werden. Im Erfolgsfall sollten so Käfige mit sowohl externer als auch interner Funktionalisierung zugänglich werden. In diesem Zusammenhang ist der für die Synthese von **130** etablierte allgemeine Syntheseweg (Schema 37c) vorteilhaft, um *meta*-Diboronsäuren mit konkaven Substituenten wie Carbonsäuren oder Aldehyden zu synthetisieren, für die die Löslichkeit in organischen Lösungsmitteln genau eingestellt werden kann. Anschließend sollten die neu synthetisierten Diboronsäuren mit TBTQ **123** umgesetzt werden, um organische Käfigverbindungen mit sowohl endohedraler als auch exohedraler Funktionalisierung zu erhalten.

CHAPTER 6

●

Experimental Section

6.1 Materials and Methods

All chemicals were purchased from commercial suppliers ALFA AESAR, MERCK, ACROS and SIGMA ALDRICH and were used without further purification. The solvents were distilled prior to use. Dichloromethane, toluene and tetrahydrofuran were dried by using the solvent purification system "PureSolv MD 5" from INNOVATIVE TECHNOLOGY.

Column chromatography: Glass-columns were individually packed with silica gel (grain-size 4-63 μm; MERCK).

TLC-sheets: Silica gel 60 F_{254} TLC-aluminium foils (MERCK).

NMR spectroscopy: NMR spectra were recorded on BRUKER AVANCE 400 and BRUKER AVANCE DMX 600 spectrometers. Chemical shifts are indicated in ppm in relation to the particular internal standard (^{1}H-NMR: 7.26 ppm for $CDCl_3$, 5.32 ppm for CD_2Cl_2, 3.31 ppm for MeOD, 1.72 ppm for THF-d_8; ^{13}C-NMR: 77.16 ppm for $CDCl_3$, 53.84 ppm for CD_2Cl_2, 49.00 ppm for MeOD, 25.31 ppm for THF-d_8). Signal multiplicities are denoted as s (singlet), d (doublet), t (triplet), q (quartet) and m (multiplet). Processing of the raw data was performed with the program Topspin 3.0.[128]

Mass spectrometry (MALDI): Mass spectra were recorded on an Autoflex II BRUKER spectrometer. As matrix, a DCTB - *trans*-2-[3-(4-*t*-Butylphenyl)-2-methyl-2-propenylidene] malononitrile - was used.

Elemental Analysis (%): Analyses were performed on an Elementar CHNS 932 analyzer.

Isothermal Titration Calorimetry (ITC): ITC-measurements were recorded on a VP-ITC instrument from MicroCal.

X-Ray Diffraction Analysis: Single crystals were mounted on a 100 μm MiTeGen MicroLoop using perfluorinated polyalkylether. Single crystal X-ray diffraction data were collected on a Bruker D8 Quest Kappa diffractometer with a Photon100 CMOS detector and multi-layered mirror monochromated CuK_α radiation. The images were processed with the Bruker software packages and equivalent reflections were merged. The data were corrected for absorption effects using semi-empirical methods from equivalents. Corrections for Lorentz and polarization effects were applied. The structures were solved by direct methods, refined with the SHELXTL software package[129] and expanded using Fourier techniques. All non-hydrogen atoms were refined anisotropically. Hydrogen atoms were assigned to geometrically idealized positions and were included in structure factor calculations.

6.2 Synthesis and Characterization

2-(Bis-(3,4-dimethoxyphenyl)methyl)-5,6-dimethoxy-1*H*-indene-1,3(2*H*)-dione **108**[71], phenyl(trimethylsilylethynyl)iodonium triflate **119**,[111] TBTQ **58b**,[13c] 4-(5'-(4-(*tert*-butyl)phenyl)-4,4''-diiodo-[1,1':3',1''-terphenyl]-2'-yl)pyridine **132**[119] and the reference boronate ester **112**[39] were synthesized according to known literature procedures.

Trisboronate ester 113:
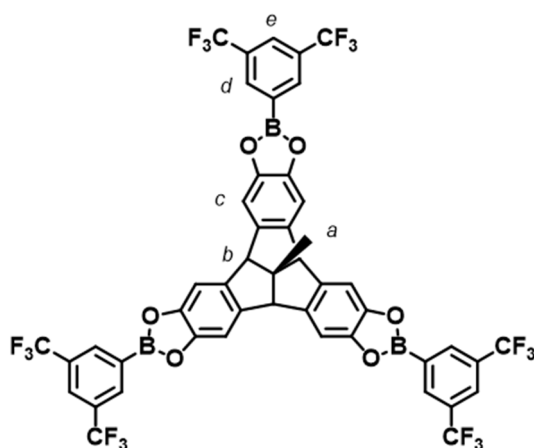
Chemical Formula: C$_{47}$H$_{21}$B$_3$F$_{18}$O$_6$
Molecular Weight: 1056.08 g mol^{-1}

Hexahydroxy-TBTQ **58b** (18.3 mg, 46.9 μmol, 1 eqv) and 3,5-bis(trifluoromethyl)phenyl boronic acid **110** (36.2 mg, 14.0 μmol, 3 eqv) were dissolved in a mixture of acetonitrile and

methanol (10 mL/1 mL). The flask was connected to a Dean-Stark apparatus attached with a reflux condenser. The solution was refluxed at 100 °C for two hours until the volume of the solution reached 2 mL in the flask. After cooling to room temperature, the off-white precipitate was filtered through a Whatman 0.45 μm filter paper and washed with acetonitrile (2×1 mL). The solid was dried under high vacuum for two hours to give trisboronate ester **113** (31.0 mg, 29.3 μmol, 63 %).

^{1}H NMR (400 MHz, CDCl$_3$, rt): δ = 8.48 (s, 6 H, H_d), 8.05 (s, 3 H, H_e), 7.41 (s, 6 H, H_c), 4.57 (s, 3 H, H_b), 1.79 (s, 3 H, H_a) ppm.

^{13}C NMR (101 MHz, CDCl$_3$, rt): δ = 148.39, 140.31, 134.87, 131.86, 126.00, 124.74, 122.03, 108.67, 63.26, 63.11, 27.73 ppm.

MS (MALDI, DCTB, positive): m/z = 1056.17 [M]$^+$.

2-(Bis-(3,4-dimethoxyphenyl)methyl)-2-ethynyl-5,6-dimethoxy-1H-indene-1,3(2H)-dione 120:
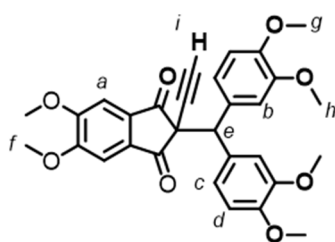
Chemical Formula: C$_{30}$H$_{28}$O$_8$
Molecular Weight: 516.55 g mol^{-1}

A 250 mL round bottom Schlenk flask was charged with **118** (2.27 g, 4.61 mmol, 1 eqv) and put through three vacuum/N$_2$ flushing cycles. Afterwards, dry THF (150 mL) was added. To this yellow solution, TBAF (1M in THF, 6.91 mL, 6.91 mmol, 1.5 eqv) was added. The obtained orange solution was stirred for five minutes followed by the addition of **119** (2.70 g, 5.99 mmol, 1.3 eqv) in one portion resulting in immediate color change to dark yellow. After stirring for five minutes under N$_2$, the solution was quenched by addition of water (150 mL). The dark yellow solution was extracted with CH$_2$Cl$_2$ (3×200 mL). The organic phases were washed with brine and dried over Na$_2$SO$_4$. After evaporation of the solvent, the crude oil was purified by flash column chromatography (silica, Et$_2$O/hexane 6:1, 8:1, 10:1 as eluents) to give **120** as a yellowish solid (1.67 g, 3.23 mmol, 65 %).

¹H-NMR (400 MHz, CDCl$_3$, rt): δ = 7.20 (s, 2H, H_a), 7.14 (d, 2H, J = 1.9 Hz, H_b), 6.95 (dd, 2H, J = 8.4, 2.0 Hz, H_c), 6.67 (d, 2H, J = 8.4 Hz, H_d), 4.88 (s, 1H, C-H_e), 3.96 (s, 6H, H_f), 3.83(s, 6H, H_h), 3.78 (s, 6H, H_g), 2.29 (s, 1H, H_i) ppm.

¹³C-NMR (101 MHz, CDCl$_3$, rt): δ = 195.73, 156.44, 148.31, 141.78, 136.56, 132.01, 122.06, 113.08, 110.71, 103.71, 79.17, 75.43, 57.58, 56.85, 56.42, 55.86, 55.78 ppm.

MS (MALDI-TOF, DCTB): m/z = 516.1 [M]$^+$.

Anal. Calcd. for C$_{30}$H$_{28}$O$_8$·0.5C$_4$H$_{10}$O: C, 69.43; H, 6.01; found: C, 69.52; H, 6.02.

2-(bis(3,4-dimethoxyphenyl)methyl)-2-ethynyl-5,6-dimethoxy-2,3-dihydro-1*H*-indene-1,3-diol 121:
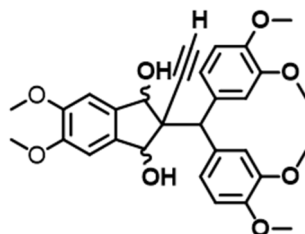
Chemical Formula: C$_{30}$H$_{32}$O$_8$
Molecular Weight: 520.58 g mol^{-1}

Under N$_2$ atmosphere in a 500 mL Schlenk flask, **120** (3.00 g, 5.42 mmol, 1.0 eqv) was dissolved in dry CH$_2$Cl$_2$ (250 mL) and the flask was subjected to cooling in an ice-bath at 0 °C. Afterwards, DIBAL-H (1M in THF, 23.2 mL, 23.2 mmol, 4.3 eqv) was added dropwise over a period of 30 minutes. Subsequently, the solution was brought to room temperature and stirred under N$_2$ for one hour. The reaction was quenched by addition of water (100 mL) and the obtained suspension was stirred for ten minutes. The intermediate colorless precipitate was dissolved after addition of aqueous HCl (1.2 M, 100 mL). The organic layer was separated and the water phase was extracted with CH$_2$Cl$_2$ (3×50 mL). The combined organic phases were washed with saturated aqueous solution (2 x 50 mL) of K$_2$CO$_3$ and brine (100 mL) and dried over Na$_2$SO$_4$. The crude product (3.10 g) was obtained as colorless precipitate after solvent removal and directly used as a mixture of diastereomers without further purification.

MS (MALDI-TOF, DCTB): m/z = 520.2 [M]$^+$.

TBTQ 115:
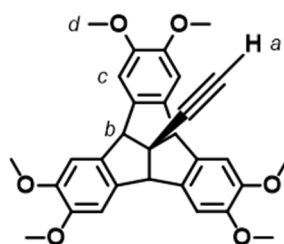
Chemical Formula: $C_{30}H_{28}O_6$
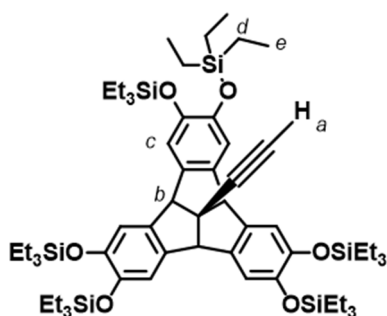Molecular Weight: 484.55 g mol^{-1}

In a 500 mL 3-necked round-bottom flask, orthophosphoric acid (1.56 mL) was added to chlorobenzene (100 mL) and refluxed at 140 $^\circ$C for 30 minutes under vigorous stirring. Subsequently, a solution of crude **121** (3.10 g, 5.95 mmol) in chlorobenzene (300 mL) was added to the refluxing solution dropwise through a dropping funnel. Afterwards, the solution was refluxed for another hour. A dark violet precipitate appeared at the bottom of the flask and the color of the solution changed from dark yellow to dark red. The solution was brought to room temperature and a saturated aqueous solution (200 mL) of K_2CO_3 was added. The mixture was extracted with CHCl$_3$ (3×100 mL). The combined organic phases were washed with brine (100 mL) and dried over Na_2SO_4 followed by evaporation of the solvent to obtain a dark brown residue. The crude product was purified by flash column chromatography on silica (hexane/EtOAc = 2:1, 1:1, 1:2 as eluents) and the yellowish product collected was recrystallized from EtOH to furnish **115** (1.03 g, 2.13 mmol, 36 % over two steps) as colorless single crystals.

¹H-NMR (400 MHz, CDCl$_3$, rt): δ = 6.87 (s, 6H, H_c), 4.90 (s, 3H, H_b), 3.87 (s, 18H, H_d), 2.58 (s, 1H, H_a), ppm.

¹³C-NMR (101 MHz, CDCl$_3$, rt): δ = 149.57, 136.13, 107.07, 90.33, 72.69, 64.60, 58.93, 56.40 ppm.

MS (MALDI-TOF, DCTB): m/z = 484.2 [M]$^+$.

Anal. Calcd. for $C_{30}H_{28}O_6 \cdot 0.5C_2H_6O \cdot 1.5H_2O$: C, 69.65; H, 6.41; found: C, 69.26; H, 6.45.

TBTQ 122:

Chemical Formula: $C_{60}H_{100}O_6Si_6$
Molecular Weight: 1085.96 g mol^{-1}

A 100 mL round bottom Schlenk flask was charged with **115** (400 mg, 0.748 mmol, 1.0 eqv) and put through three vacuum/N_2 flushing cycles. Afterwards, dry CH_2Cl_2 (50 mL) and triethylsilane (1.35 g, 11.6 mmol, 15.5 eqv) were added. Then, a solution of trispentafluorophenylborane (21.2 mg, 0.041 mmol, 0.05 eqv) in dry CH_2Cl_2 was added to the reaction mixture under N_2. Bubbles of gas (methane) evolved out of the solution and the color of the solution changed from colorless to yellow to finally yellowish orange. After 30 minutes, trimethylamine (0.1 mL) was added and color changed again to yellow. The solution was filtered through celite pad and the filtrate was evaporated to dryness to obtain a crude colorless solid which was washed by distilled MeOH to obtain **122** as a pure colorless solid (646 mg, 0.595 mmol, 80 %).

^{1}H-NMR (400 MHz, CDCl$_3$, rt): δ = 6.71 (d, 6H, J = 0.5 Hz, H_c), 4.72 (s, 3H, H_b), 2.55 (s, 1H, H_a), 0.97 (t, 54H, J = 7.9 Hz, H_e), 0.73 (q, 36H, J = 7.9 Hz, H_d) ppm.

^{13}C-NMR (101 MHz, CDCl$_3$, rt): δ = 146.70, 137.17, 115.39, 91.37, 72.05, 64.03, 59.17, 6.83, 5.25 ppm.

MS (MALDI-TOF, DCTB): m/z = 1084.6 [M]$^+$.

Anal. Calcd. for C$_{60}$H$_{100}$O$_6$Si$_6$: C, 66.36; H, 9.28; found: C, 66.14; H, 9.11.

TBTQ 123:
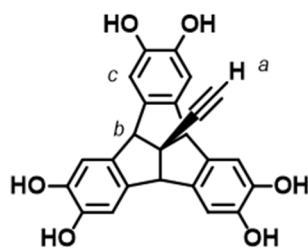
Chemical Formula: $C_{24}H_{16}O_6$
Molecular Weight: 400.39 g mol^{-1}

A 50 mL round bottom flask was charged with **122** (250 mg, 0.23 mmol, 1 eqv) and distilled THF (15 mL) was added. To this solution, aqueous HCl (1.0 M, 3.45 mL, 3.45 mmol, 15 eqv) was added and the reaction mixture was stirred for one hour at room temperature. Afterwards, water (20 mL) was added and the mixture was extracted with EtOAc (3×50 mL). The combined organic phases were dried over Na_2SO_4 and the solvent was evaporated to get a crude product. Afterwards, MeOH (20 mL) was added and the solution was filtered. The filtrate was evaporated to obtain a colorless solid. The crude product was then washed with CH_2Cl_2 (3×10 mL) to obtain **123** as colorless powder (77.2 mg, 0.193 mmol, 74 %).

^{1}H-NMR (400 MHz, MeOD, rt): δ = 6.77 (d, 6H, J = 0.4 Hz, H_c), 4.59 (s, 3H, H_b), 2.84 (s, 1H, H_a) ppm.

^{13}C-NMR (101 MHz, MeOD, rt): δ = 146.21, 136.97, 111.26, 92.15, 72.91, 65.45, 59.94 ppm.

MS (MALDI-TOF, DCTB): m/z = 400.1 [M]$^+$, 651.2 [M+DCTB+H]$^+$, 901.4 [M+2DCTB+H]$^+$.

Anal. Calcd. for $C_{24}H_{16}O_6 \cdot 3H_2O$: C, 63.43; H, 4.88; found: C, 63.34; H, 4.89.

TBTQ 124:
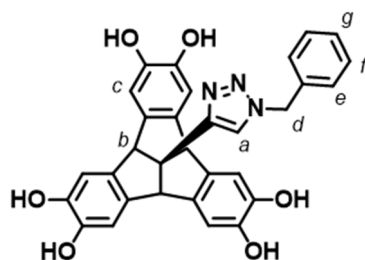
Chemical Formula: $C_{31}H_{23}N_3O_6$
Molecular Weight: 533.54 g mol^{-1}

TBTQ **123** (20.0 mg, 0.050 mmol, 1.0 eqv) and benzyl azide (13.3 mg, 0.1 mmol, 2.5 eqv) were dissolved in THF (5 mL). Sodium ascorbate (0.5 mmol, 0.5 mL of freshly prepared 1M solution in water) was added, followed by the addition of copper(II) sulfate (1.6 mg, 0.01 mmol, in 1 mL of water). Then, the solution was stirred overnight for 18 hours under N_2 at room temperature. Water (10 mL) was added and the mixture was extracted with EtOAc (3×10 mL), dried over Na_2SO_4, and evaporated to dryness. After washing the residue with CH_2Cl_2 (3×5 mL), pure **124** was obtained as a colorless powder (23.2 mg, 0.043 mmol, 90 %).

^{1}H-NMR (400 MHz, MeOD, rt): δ = 7.89 (s, 1H, H_a), 7.36-7.28 (m, 5H, $H_{e,f,g}$), 6.81 (s, 6H, H_c), 5.53 (s, 2H, H_d), 4.68 (s, 3H, H_b) ppm.

^{13}C-NMR (101 MHz, MeOD, rt): δ = 158.00, 146.18, 137.47, 136.87, 129.99, 129.48, 129.03, 121.61, 111.39, 66.17, 64.34, 54.92 ppm.

MS (MALDI-TOF, DCTB): m/z = 534.1 [M+H]$^+$.

Anal. Calcd. for $C_{31}H_{23}N_3O_6 \cdot 3H_2O$: C, 63.37; H, 4.97; N, 7.15; found: C, 64.73; H, 5.39; N, 6.28.

TBTQ 125:
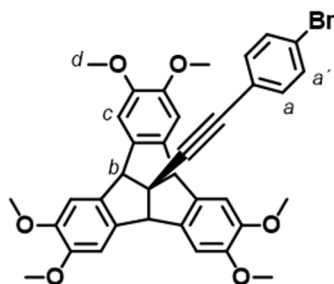
Chemical Formula: $C_{36}H_{31}BrO_6$
Molecular Weight: 639.54 g mol^{-1}

In a Schlenk tube, 1-bromo-4-iodobenzene (43.8 mg, 0.103 mmol, 1.1 eqv), Pd(dppf)Cl$_2$ (3.02 mg, 4.1 µmol, 0.04 eqv), CuI (0.786 mg, 4.1 µmol, 0.04 eqv) and diisopropylamine (2.5 mL) were dissolved in dry toluene (5 mL) under N$_2$ atmosphere and degassed by three freeze-pump-thaw cycles. In another Schlenk tube, **115** (50.0 mg, 0.094 mmol, 1 eqv) was dissolved in dry toluene (5 mL) and also degassed by three freeze-pump-thaw cycles. Afterwards, the solution of **115** was slowly added dropwise to the first Schlenk tube. After complete addition, the reaction mixture was stirred overnight for 16 hours under N$_2$. The solution was quenched by addition of HCl solution (2M, 20 mL) and extracted with Et$_2$O (2×30 mL). The organic extract was washed with saturated aqueous solution (30 mL) of K$_2$CO$_3$ while additional EtOAc (20 mL) was added for a better separation of the organic and water layers. Then, the combined organic layers were washed with brine, dried over Na$_2$SO$_4$ and evaporated to dryness. To the residue, Et$_2$O (50 mL) was added. After separation of the precipitate (Glaser product), the filtrate was evaporated to obtain a yellowish residue. This crude product was purified by flash column chromatography (silica, hexane/EtOAc = 1:1 to EtOAc as eluents) and the yellowish product collected was dissolved in the minimum amount of Et$_2$O followed by addition of hexane to furnish pure **125** as a colorless precipitate (41.2 mg, 0.064 mmol, 69 %).

^{1}H-NMR (400 MHz, CD$_2$Cl$_2$, rt): δ = 7.43 (d, 2H, J = 8.7 Hz, $H_{a'}$), 7.28 (d, 2H, J = 8.7 Hz, H_a), 6.90 (s, 6H, H_c), 4.96 (s, 3H, H_b), 3.83 (s, 18H, H_d) ppm.

^{13}C-NMR (101 MHz, CD$_2$Cl$_2$, rt): δ = 150.04, 136.28, 133.29, 131.86, 123.07, 122.22, 107.56, 97.12, 83.92, 64.84, 59.89, 56.54 ppm.

MS (MALDI-TOF, DCTB): m/z = 638.1, 640.1 [M]$^+$.

**Anal.** Calcd. for C$_{36}$H$_{31}$BrO$_6$·1.5C$_4$H$_{10}$O: C, 67.20; H, 6.18; found: C, 67.18; H, 6.01.

TBTQ 126:
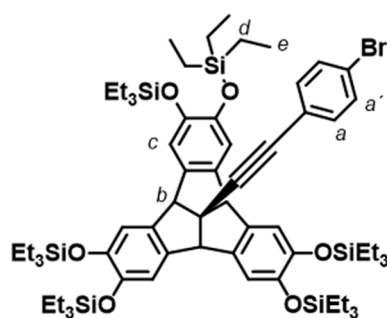
Chemical Formula: $C_{66}H_{103}BrO_6Si_6$

Molecular Weight: 1240.96 g mol^{-1}

A 100 mL round bottom Schlenk flask was charged with **125** (200 mg, 0.313 mmol, 1.0 eqv) and put through three vacuum/N$_2$ flushing cycles. Afterwards, dry CH$_2$Cl$_2$ (25 mL) and triethylsilane (1.09 g, 9.39 mmol, 30.0 eqv) were added. Then, a solution of trispentafluorophenylborane (32.2 mg, 0.063 mmol, 0.2 eqv) in dry CH$_2$Cl$_2$ (20 mL) was added to the reaction mixture under N$_2$. Bubbles of gas (methane) evolved out of the solution. Color of the solution changed from colorless to yellowish orange. After 30 minutes, trimethylamine (0.2 mL) was added and color changed to light yellow. The solution was filtered through a celite pad and the filtrate was evaporated to obtain a yellow oily crude product. To this oily crude product, MeOH (30 mL) was added and the emulsion was sonicated for seven minutes. Afterwards, this suspension was centrifuged to obtain **126** as a pure colorless precipitate (314 mg, 0.253 mmol, 81 %).

^{1}H-NMR (400 MHz, CD$_2$Cl$_2$, rt): δ = 7.42 (d, 2H, J = 8.8 Hz, $H_{a'}$), 7.28 (d, 2H, J = 8.8 Hz, H_a), 6.77 (d, 6H, J = 0.6 Hz, H_c), 4.80 (s, 3H, H_b), 0.98 (t, 54H, J = 8.0 Hz, H_e), 0.75 (q, 36H, J = 8.0 Hz, H_d) ppm.

^{13}C-NMR (101 MHz, CD$_2$Cl$_2$, rt): δ = 147.18, 137.34, 133.28, 131.86, 123.14, 122.16, 115.64, 97.77, 83.67, 64.30, 30.28, 6.86, 5.44 ppm.

MS (MALDI-TOF, DCTB): m/z = 1240.6, 1241.6 [M]$^+$.

TBTQ 127:
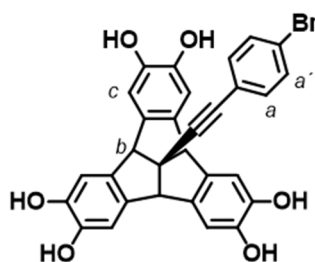
Chemical Formula: $C_{30}H_{19}BrO_6$
Molecular Weight: 555.38 g mol^{-1}

A 50 mL round bottom flask was charged with **126** (308 mg, 0.23 mmol, 1 eqv) and distilled THF (20 mL) was added. To this solution, aqueous HCl solution (3.72 mL, 3.72 mmol, 15 eqv) was added and the reaction mixture was stirred for one hour at room temperature. Initially, the color of the solution was yellow and it gradually changed to light red. Afterwards, water (20 mL) was added and the mixture was extracted with EtOAc (3×30 mL). The combined organic phases were dried over Na$_2$SO$_4$ and solvent was evaporated to get crude brown oily product. Afterwards, MeOH (20 mL) was added and the solution was filtered. The filtrate was evaporated to obtain a dark-red oily precipitate. The crude product was then washed with CH$_2$Cl$_2$ (5×10 mL) to obtain **127** as a slightly red powder (61 mg, 0.11 mmol, 47 %).

^{1}H-NMR (400 MHz, MeOD, rt): δ = 7.44 (d, 2H, J = 8.7 Hz, $H_{a'}$), 7.30 (d, 2H, J = 8.7 Hz, H_a), 6.80 (d, 6H, J = 0.4 Hz, H_c), 4.68 (s, 3H, H_b) ppm.

^{13}C-NMR (101 MHz, MeOD, rt): δ = 146.27, 136.97, 134.13, 132.60, 124.42, 122.67, 111.30, 98.83, 83.90, 65.47, 60.71 ppm.

MS (MALDI-TOF, DCTB): m/z = 554.1, 556.1 [M]$^+$.

4-(5'-(4-(*tert*-butyl)phenyl)-4,4''-bis(4,4,5,5-tetramethyl-1,3,2-dioxaborolan-2-yl)-[1,1':3',1''-terphenyl]-2'-yl)pyridine 133:

Chemical Formula: C$_{45}$H$_{51}$B$_2$NO$_4$
Molecular Weight: 691.53 g mol^{-1}
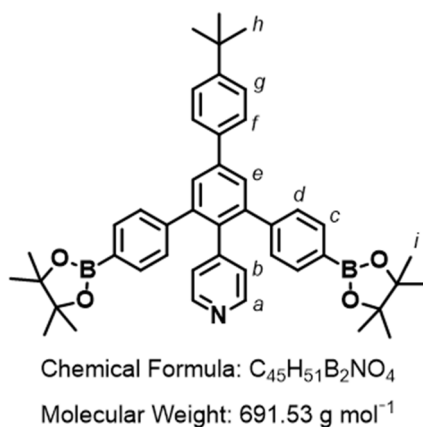
A 50 mL round bottom Schlenk flask was charged with **132** (200 mg, 0.290 mmol, 1.0 eqv), bis(pinacolato)diboron (430 mg, 1.70 mmol, 6.0 eq), Pd(dppf)Cl$_2$ (40 mg, 0.06 mmol, 0.2 eqv), potassium acetate (340 mg, 3.50 mmol, 12 eq) and was put through three vacuum/N$_2$ flushing cycles. Afterwards, dry DMF (8 mL) was added and the reaction mixture was heated to 85 °C for three hours under N$_2$. The reaction mixture was quenched by addition of water (50 mL) and extracted with diethyl ether (3×100 mL). The combined organic extract was washed with brine (100 mL) and dried over Na$_2$SO$_4$. After evaporation of the solvent, crude brown oily precipitate was purified by flash column chromatography (silica, DCM to MeOH/DCM 1:100, 2:100, 5:100 as eluents) to give **133** as a yellowish solid (115 mg, 0.166 mmol, 57 %).

^{1}H-NMR (400 MHz, CD$_2$Cl$_2$, rt): δ = 8.18 (d, 2H, J = 6.0 Hz, H_a), 7.67 (s, 2H, H_e), 7.64 (d, 2H, J = 8.7 Hz, H_f), 7.57 (d, 4H, J = 8.1 Hz, H_c), 7.50 (d, 2H, J = 8.7 Hz, H_g), 7.13 (d, 4H, J = 8.1 Hz, H_d), 6.82 (d, 2H, J = 6.0 Hz, H_b), 1.36 (s, 9H, H_h), 1.31 (s, 24H, H_i) ppm.

^{13}C-NMR (101 MHz, CD$_2$Cl$_2$, rt): δ = 155.31, 151.50, 148.92, 148.32, 144.28, 142.48, 141.23, 137.31, 135.37, 134.54, 129.60, 128.58, 127.10, 126.33, 84.20, 34.88, 31.43, 25.04 ppm.

MS (MALDI-TOF, DCTB): *m/z* = 691.4 [M]$^+$, 692.4 [M+H]$^+$.

(5'-(4-(*tert*-butyl)phenyl)-2'-(pyridin-4-yl)-[1,1':3',1''-terphenyl]-4,4''-diyl)diboronic acid 130:
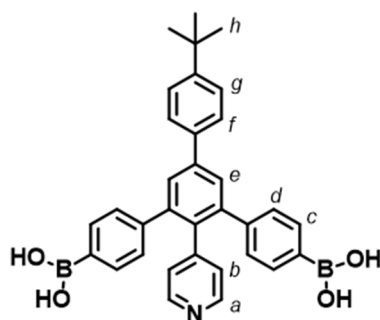
Chemical Formula: $C_{33}H_{31}B_2NO_4$
Molecular Weight: 527.23 g mol^{-1}

Under N_2 atmosphere in a 50 mL round bottom Schlenk flask, **133** (180 mg, 0.26 mmol, 1.0 eqv) was dissolved in dry dichloromethane (15 mL) and the flask was subjected to cooling in an ice-bath. Afterwards, a solution of boron tribromide (580 mg, 2.30 mmol, 9.0 eqv) in dry dichloromethane (10 mL) was added dropwise over a period of 15 minutes. Subsequently, the solution was brought to room temperature and stirred under N_2 for one hour. The reaction was quenched by addition of water (100 mL) extracted with EtOAc (3×100 mL), dried over Na_2SO_4 and evaporated to dryness. After washing the crude product first with CH_2Cl_2 (3×50 mL) and then with MeOH (3×50 mL), pure **130** was obtained as a colorless solid (48 mg, 0.09 mmol, 35 %).

1H-NMR (400 MHz, THF-d_8/D_2O, rt): δ = 8.10 (d, 2H, J = 6.0 Hz, H_a), 7.65 - 7.61 (8H, $H_{e,f,c}$), 7.47 (d, 2H, J = 8.6 Hz, H_g), 7.04 (d, 4H, J = 8.2 Hz, H_d), 6.80 (d, 2H, J = 6.0 Hz, H_b), 1.32 (s, 9H, H_h) ppm.

13C-NMR (101 MHz, THF-d_8-D_2O, rt): δ = 151.63, 149.22, 149.20, 143.71, 143.54, 141.88, 138.21, 135.97, 134.77, 129.66, 128.91, 127.76, 127.60, 126.69, 35.24, 31.72 ppm.

MS (MALDI-TOF, DCTB): m/z = 527.2 $[M]^+$, 528.2 $[M+H]^+$.

5'-(4-(*tert*-butyl)phenyl)-2'-(pyridin-4-yl)-[1,1':3',1''-terphenyl]-4,4''-diol 135:
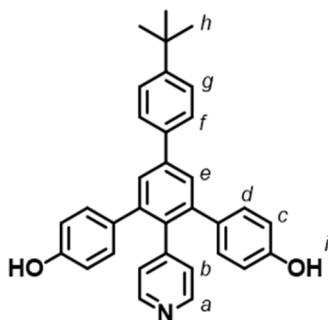
Chemical Formula: $C_{33}H_{29}NO_2$
Molecular Weight: 471.60 g mol^{-1}

A 100 mL round bottom flask was charged with **133** (110 mg, 0.16 mmol, 1 eqv) and sodium periodate (205 mg, 0.96 mmol, 6.0 eqv). After addition of distilled water (10 mL) and THF (20 mL), the suspension was stirred at room temperature for 15 minutes. Afterwards, aqueous HCl (1M, 0.3 mL, 0.3 mmol) was added and the reaction mixture was stirred overnight at room temperature. Water (30 mL) was added and the mixture was extracted with EtOAc (3×50 mL). The combined organic phases were dried over Na_2SO_4. After evaporation of the solvent, the crude product was purified by flash column chromatography (silica, acetone/*n*-hexane 1:1 as eluent) to give **135** as a colorless solid (39 mg, 0.08 mmol, 50 %).

¹H-NMR (400 MHz, THF-d$_8$, rt): δ = 8.16 (d, 2H, J = 6.0 Hz, H_a), 8.16 (s, 2H, H_i), 7.63 (d, 2H, J = 8.7 Hz, H_f), 7.57 (s, 2H, H_e), 7.48 (d, 2H, J = 8.7 Hz, H_g), 6.89 (d, 4H, J = 8.6 Hz, H_c), 6.78 (d, 2H, J = 6.0 Hz, H_b), 6.55 (d, 4H, J = 8.6 Hz, H_d) 1.35 (s, 9H, H_h) ppm.

¹³C-NMR (101 MHz, THF-d$_8$, rt): δ = 157.59, 151.20, 149.57, 149.09, 143.16, 138.61, 136.24, 133.24, 131.67, 130.68, 128.52, 127.55, 127.53, 126.48, 115.47, 35.17, 31.67 ppm.

MS (MALDI-TOF, DCTB): m/z = 472.2 [M+H]$^+$.

[2+3]-cage 128:
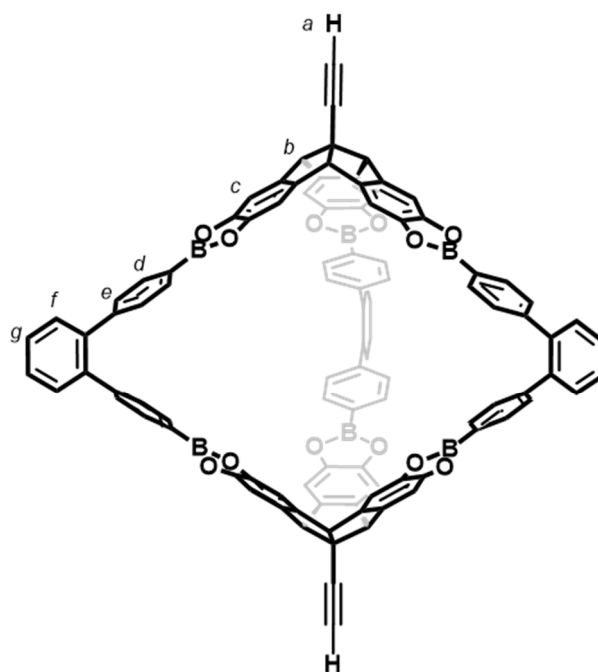
Chemical Formula: $C_{102}H_{56}B_6O_{12}$
Molecular Weight: 1538.42 g mol^{-1}

Into an NMR tube, TBTQ **123** (3.309 mg, 8.265 μmol, 2.0 eqv) and diboronic acid **100** (3.941 mg, 12.40 μmol, 3.0 eqv) were dissolved in 0.6 ml deuterated THF and molecular sieves 4 Å were added. The progress of the reaction was followed by ^{1}H-NMR spectroscopy. After four days, ^{1}H-NMR spectrum showed quantitative formation of cage **128**. Afterwards, the solvent was evaporated and dried under vacuum to obtain cage **128** as a colorless precipitate (12.4 mg, 8.02 μmol, 98 %).

^{1}H-NMR (400 MHz, THF-d$_8$, rt): δ = 7.78 (d, 12H, J = 7.6 Hz, H_d), 7.46 (s, 12H, H_c), 7.44-7.35 (m, 12H, $H_{f,g}$), 7.26 (d, 12H, J = 7.6 Hz, H_e), 5.00 (s, 6H, H_b), 3.02 (s, 2H, H_a) ppm.

^{13}C-NMR (101 MHz, THF-d$_8$, rt): δ = 149.81, 146.77, 141.95, 139.27, 134.95, 130.99, 130.28, 128.28, 125.44, 108.59, 90.61, 74.67, 65.24, 59.27 ppm.

MS (MALDI-TOF, DCTB): m/z = 1538.6 [M]$^+$.

[2+3]-cage 129:
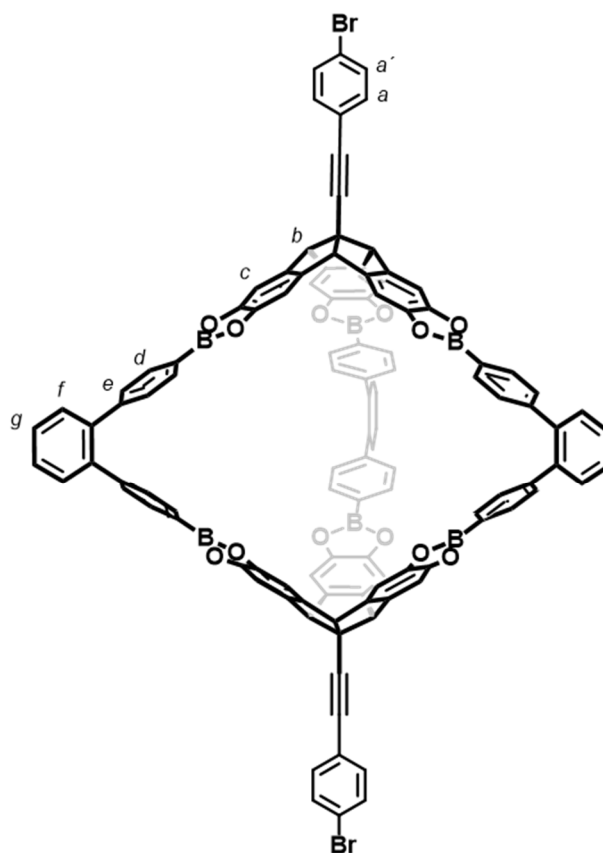
Chemical Formula: $C_{114}H_{62}B_6Br_2O_{12}$

Molecular Weight: 1848.4 g mol^{-1}

Into an NMR tube, TBTQ **127** (4.58 mg, 8.25 µmol, 2.0 eqv) and diboronic acid **100** (3.94 mg, 12.4 µmol, 3.0 eqv) were dissolved in 0.7 ml deuterated THF and molecular sieves 4 Å were added. The progress of the reaction was followed by ^{1}H-NMR spectroscopy. After two days, the solution was separated and freshly dried molecular sieves 4 Å were added. After four days, the solution was transferred into an NMR tube and 0.2 mL deuterated DCM was added to it. ^{1}H-NMR spectrum showed the formation of cage **129**. After evaporation of the solvent, cage **129** was obtained as an amorphous precipitate (13.6 mg, 7.36 µmol, 89 %).

^{1}H-NMR (400 MHz, THF-d$_8$/CD$_2$Cl$_2$ 2:1, rt): δ = 7.79 (d, 12H, J = 8.1 Hz, H_d), 7.42-7.31 (m, 32H, $H_{a,a',c,f,g}$), 7.24 (d, 12H, J = 8.1 Hz, H_e), 5.08 (s, 6H, H_b) ppm.

MS (MALDI-TOF, DCTB): m/z = 1847.4, 1848.4, 1849.4 [M]$^+$.

References

[1] E. Dexler, *Engines of Creation*, Anchor Press/Doubleday, Garden City, N.Y. , **1986**.

[2] G. M. Whitesides, B. Grzybowski, *Science* **2002**, *295*, 2418–2421.

[3] M. Boncheva, G. M. Whitesides, *MRS Bull.* **2011**, *30*, 736–742.

[4] L. Catti, Q. Zhang, K. Tiefenbacher, *Chem. Eur. J.* **2016**, *22*, 9060–9066.

[5] A. Galan, P. Ballester, *Chem. Soc. Rev.* **2016**, *45*, 1720–1737.

[6] C. Schmuck, *Angew. Chem. Int. Ed.* **2007**, *46*, 5830–5833.

[7] a) W.-Y. Sun, M. Yoshizawa, T. Kusukawa, M. Fujita, *Curr. Opin. Chem. Biol.* **2002**, *6*, 757–764; b) L. J. Prins, D. N. Reinhoudt, P. Timmerman, *Angew. Chem. Int. Ed.* **2001**, *40*, 2382–2426; c) H. Adams, C. A. Hunter, K. R. Lawson, J. Perkins, S. E. Spey, C. J. Urch, J. M. Sanderson, *Chem. Eur. J.* **2001**, *7*, 4863–4877; d) K. Müller-Dethlefs, P. Hobza, *Chem. Rev.* **2000**, *100*, 143–168.

[8] Y. Jin, C. Yu, R. J. Denman, W. Zhang, *Chem. Soc. Rev.* **2013**, *42*, 6634–6654.

[9] L. Cademartiri, K. J. Bishop, *Nat. Mater.* **2015**, *14*, 2–9.

[10] a) E. Sheepwash, N. Luisier, M. R. Krause, S. Noé, S. Kubik, K. Severin, *Chem. Commun.* **2012**, *48*, 7808–7810; b) N. Luisier, K. Bally, R. Scopelliti, F. T. Fadaei, K. Schenk, P. Pattison, E. Solari, K. Severin, *Cryst. Growth Des.* **2016**, *16*, 6600–6604.

[11] D. N. Reinhoudt, M. Crego-Calama, *Science* **2002**, *295*, 2403–2407.

[12] D. Kuck, A. Schuster, R. A. Krause, J. Tellenbröker, C. P. Exner, M. Penk, H. Bögge, A. Müller, *Tetrahedron* **2001**, *57*, 3587–3613.

[13] a) F. Beuerle, S. Klotzbach, A. Dhara, *Synlett* **2016**, *27*, 1133–1138; b) D. Beaudoin, F. Rominger, M. Mastalerz, *Angew. Chem. Int. Ed.* **2016**, *55*, 15599–15603; c) J. Vile, M. Carta, C. G. Bezzu, N. B. McKeown, *Polym. Chem.* **2011**, *2*, 2257.

[14] a) S. Klotzbach, T. Scherpf, F. Beuerle, *Chem. Commun.* **2014**, *50*, 12454–12457; b) S. Klotzbach, F. Beuerle, *Angew. Chem. Int. Ed.* **2015**, *54*, 10356–10360.

[15] B. V. Prasad, M. E. Hardy, T. Dokland, J. Bella, M. G. Rossmann, M. K. Estes, *Science* **1999**, *286*, 287–290.

[16] a) J. L. Atwood, L. R. MacGillivray, *Nature* **1997**, *389*, 469–472; b) C. A. Hunter, *J. Am. Chem. Soc.* **1992**, *114*, 5303–5311; c) R. S. Meissner, J. Rebek Jr., J. Demendoza, *Science* **1995**, *270*, 1485–1488; d) T. R. Cook, Y. R. Zheng, P. J. Stang, *Chem. Rev.* **2013**, *113*, 734–777.

[17] a) M. E. Briggs, A. I. Cooper, *Chem. Mater.* **2017**, *29*, 149–157; b) G. Zhang, M. Mastalerz, *Chem. Soc. Rev.* **2014**, *43*, 1934–1947; c) S. Lee, A. Yang, T. P.

Moneypenny, II, J. S. Moore, *J. Am. Chem. Soc.* **2016**, *138*, 2182–2185; d) J. W. Sadownik, E. Mattia, P. Nowak, S. Otto, *Nat. Chem.* **2016**, *8*, 264–269.

[18]   Q. Zhang, K. Tiefenbacher, *Nat. Chem.* **2015**, *7*, 197–202.

[19]   N. Ponnuswamy, F. B. Cougnon, J. M. Clough, G. D. Pantoş, J. K. Sanders, *Science* **2012**, *338*, 783–785.

[20]   J. D. Badjić, A. Nelson, S. J. Cantrill, W. B. Turnbull, J. F. Stoddart, *Acc. Chem. Res.* **2005**, *38*, 723–732.

[21]   a) O. M. Yaghi, M. O'Keeffe, N. W. Ockwig, H. K. Chae, M. Eddaoudi, J. Kim, *Nature* **2003**, *423*, 705–714; b) B. F. Hoskins, R. Robson, *J. Am. Chem. Soc.* **1989**, *111*, 5962–5964; c) H. Furukawa, K. E. Cordova, M. O'Keeffe, O. M. Yaghi, *Science* **2013**, *341*, 1230444.

[22]   a) M. Yoshizawa, J. K. Klosterman, M. Fujita, *Angew. Chem. Int. Ed.* **2009**, *48*, 3418–3438; b) T. K. Ronson, S. Zarra, S. P. Black, J. R. Nitschke, *Chem. Commun.* **2013**, *49*, 2476–2490; c) K. S. Chichak, S. J. Cantrill, A. R. Pease, S. H. Chiu, G. W. Cave, J. L. Atwood, J. F. Stoddart, *Science* **2004**, *304*, 1308–1312.

[23]   F. Würthner, *Nat. Chem.* **2014**, *6*, 171–173.

[24]   M. R. Jones, N. C. Seeman, C. A. Mirkin, *Science* **2015**, *347*, 1260901.

[25]   a) K. Harris, D. Fujita, M. Fujita, *Chem. Commun.* **2013**, *49*, 6703–6712; b) R. Chakrabarty, P. S. Mukherjee, P. J. Stang, *Chem. Rev.* **2011**, *111*, 6810–6918; c) M. M. Smulders, I. A. Riddell, C. Browne, J. R. Nitschke, *Chem. Soc. Rev.* **2013**, *42*, 1728–1754.

[26]   M. Mastalerz, *Angew. Chem. Int. Ed.* **2010**, *49*, 5042–5053.

[27]   a) F. Hof, S. L. Craig, C. Nuckolls, J. Rebek Jr., *Angew. Chem. Int. Ed.* **2002**, *41*, 1488–1508; b) D. Ajami, L. Liu, J. Rebek Jr., *Chem. Soc. Rev.* **2015**, *44*, 490–499.

[28]   J. H. Jordan, B. C. Gibb, *Chem. Soc. Rev.* **2015**, *44*, 547–585.

[29]   a) S. Geller, *J. Chem. Phys.* **1960**, *32*, 1569–1570; b) M. A. Dvorak, R. S. Ford, R. D. Suenram, F. J. Lovas, K. R. Leopold, *J. Am. Chem. Soc.* **1992**, *114*, 108–115.

[30]   H. Höpfl, *J. Organomet. Chem.* **1999**, *581*, 129–149.

[31]   a) H. Höpfl, N. Farfán, *J. Organomet. Chem.* **1997**, *547*, 71–77; b) V. Barba, R. Villamil, R. Luna, C. Godoy-Alcántar, H. Höpfl, H. I. Beltran, L. S. Zamudio-Rivera, R. Santillan, N. Farfán, *Inorg. Chem.* **2006**, *45*, 2553–2561; c) M. Sánchez, H. Höpfl, M. E. Ochoa, N. Farfán, R. Santillan, S. Rojas-Lima, *Chem. Eur. J.* **2002**, *8*, 612–621.

[32]   M. Hutin, G. Bernardinelli, J. R. Nitschke, *Chem. Eur. J.* **2008**, *14*, 4585–4593.

[33]   a) K. Kataoka, T. D. James, Y. Kubo, *J. Am. Chem. Soc.* **2007**, *129*, 15126–15127; b) K. Kataoka, S. Okuyama, T. Minami, T. D. James, Y. Kubo, *Chem. Commun.* **2009**, 1682–1684.

[34]   E. Galbraith, A. M. Kelly, J. S. Fossey, G. Kociok-Köhn, M. G. Davidson, S. D. Bull, T. D. James, *New J. Chem.* **2009**, *33*, 181–185.

[35]   N. Christinat, R. Scopelliti, K. Severin, *Chem. Commun.* **2004**, 1158.

[36]   a) K. Severin, *Coord. Chem. Rev.* **2003**, *245*, 3–10; b) K. Severin, *Chem. Commun.* **2006**, 3859–3867.

[37]   N. Christinat, R. Scopelliti, K. Severin, *J. Org. Chem.* **2007**, *72*, 2192–2200.

[38]   B. Icli, E. Solari, B. Kilbas, R. Scopelliti, K. Severin, *Chem. Eur. J.* **2012**, *18*, 14867–14874.

[39]   N. Christinat, R. Scopelliti, K. Severin, *Chem. Commun.* **2008**, 3660–3662.

[40]   a) M. Grosche, E. Herdtweck, F. Peters, M. Wagner, *Organometallics* **1999**, *18*, 4669–4672; b) M. Fontani, F. Peters, W. Scherer, W. Wachter, M. Wagner, P. Zanello, *Eur. J. Inorg. Chem.* **1998**, 1453–1465.

[41]   N. Christinat, E. Croisier, R. Scopelliti, M. Cascella, U. Röthlisberger, K. Severin, *Eur. J. Inorg. Chem.* **2007**, *2007*, 5177–5181.

[42]   E. Sheepwash, V. Krampl, R. Scopelliti, O. Sereda, A. Neels, K. Severin, *Angew. Chem. Int. Ed.* **2011**, *50*, 3034–3037.

[43]   a) J. Cruz-Huerta, D. Salazar-Mendoza, J. Hernández-Paredes, I. F. Hernandez Ahuactzi, H. Höpfl, *Chem. Commun.* **2012**, *48*, 4241–4243; b) D. Salazar-Mendoza, J. Guerrero-Alvarez, H. Höpfl, *Chem. Commun.* **2008**, 6543–6545; c) J. Cruz-Huerta, G. Campillo-Alvarado, H. Höpfl, P. Rodríguez-Cuamatzi, V. Reyes-Márquez, J. Guerrero-Álvarez, D. Salazar-Mendoza, N. Farfán-García, *Eur. J. Inorg. Chem.* **2016**, *2016*, 355–365; d) D. Salazar-Mendoza, J. Cruz-Huerta, H. Höpfl, I. F. Hernández-Ahuactzi, M. Sanchez, *Cryst. Growth Des.* **2013**, *13*, 2441–2454.

[44]   B. Icli, E. Sheepwash, T. Riis-Johannessen, K. Schenk, Y. Filinchuk, R. Scopelliti, K. Severin, *Chem. Sci.* **2011**, *2*, 1719.

[45]   M. Stępień, *Synlett* **2013**, *24*, 1316–1321.

[46]   H. Langhals, M. Rauscher, J. Strübe, D. Kuck, *J. Org. Chem.* **2008**, *73*, 1113–1116.

[47]   a) J. W. Steed, P. C. Junk, J. L. Atwood, M. J. Barnes, C. L. Raston, R. S. Burkhalter, *J. Am. Chem. Soc.* **1994**, *116*, 10346–10347; b) S. Mizyed, P. E. Georghiou, M. Bancu, B. Cuadra, A. K. Rai, P. Cheng, L. T. Scott, *J. Am. Chem. Soc.* **2001**, *123*, 12770–12774.

[48] W. R. Xu, G. J. Xia, H. F. Chow, X. P. Cao, D. Kuck, *Chem. Eur. J.* **2015**, *21*, 12011–12017.

[49] a) X. Liu, Y. Liu, G. Li, R. Warmuth, *Angew. Chem.* **2006**, *118*, 915–918; b) D. Xu, R. Warmuth, *J. Am. Chem. Soc.* **2008**, *130*, 7520–7521.

[50] S. B. Nimse, T. Kim, *Chem. Soc. Rev.* **2013**, *42*, 366–386.

[51] M. J. Hardie, *Chem. Soc. Rev.* **2010**, *39*, 516–527.

[52] G. Crini, *Chem. Rev.* **2014**, *114*, 10940–10975.

[53] Y. T. Wu, J. S. Siegel, *Chem. Rev.* **2006**, *106*, 4843–4867.

[54] a) S. Shimizu, N. Kobayashi, *Chem. Commun.* **2014**, *50*, 6949–6966; b) C. G. Claessens, D. González-Rodríguez, M. S. Rodríguez-Morgade, A. Medina, T. Torres, *Chem. Rev.* **2014**, *114*, 2192–2277.

[55] D. Kuck, *Chem. Rev.* **2006**, *106*, 4885–4925.

[56] R. B. Woodward, T. Fukunaga, R. C. Kelly, *J. Am. Chem. Soc.* **1964**, *86*, 3162–3164.

[57] D. Kuck, *Angew. Chem. Int. Ed.* **1984**, *23*, 508–509.

[58] D. Beaudoin, F. Rominger, M. Mastalerz, *Angew. Chem. Int. Ed.* **2017**, *56*, 1244–1248.

[59] A. Dhara, F. Beuerle, *Chem. Eur. J.* **2015**, *21*, 17391–17396.

[60] a) T. Wang, Y. F. Zhang, Q. Q. Hou, W. R. Xu, X. P. Cao, H. F. Chow, D. Kuck, *J. Org. Chem.* **2013**, *78*, 1062–1069; b) J. Wei, Z. M. Li, X. J. Jin, X. J. Yao, X. P. Cao, H. F. Chow, D. Kuck, *Chem. Asian J.* **2015**, *10*, 1150–1158.

[61] a) B. Bredenkötter, S. Henne, D. Volkmer, *Chem. Eur. J.* **2007**, *13*, 9931–9938; b) P. E. Georghiou, L. N. Dawe, H. A. Tran, J. Strübe, B. Neumann, H. G. Stammler, D. Kuck, *J. Org. Chem.* **2008**, *73*, 9040–9047; c) T. Wang, Z. Y. Li, A. L. Xie, X. J. Yao, X. P. Cao, D. Kuck, *J. Org. Chem.* **2011**, *76*, 3231–3238; d) S. Henne, B. Bredenkötter, A. A. Dehghan Baghi, R. Schmid, D. Volkmer, *Dalton Trans.* **2012**, *41*, 5995–6002; e) B. Bredenkötter, M. Grzywa, M. Alaghemandi, R. Schmid, W. Herrebout, P. Bultinck, D. Volkmer, *Chem. Eur. J.* **2014**, *20*, 9100–9110.

[62] H. W. Ip, C. F. Ng, H. F. Chow, D. Kuck, *J. Am. Chem. Soc.* **2016**, *138*, 13778−13781.

[63] J. G. Brandenburg, S. Grimme, P. G. Jones, G. Markopoulos, H. Hopf, M. K. Cyranski, D. Kuck, *Chem. Eur. J.* **2013**, *19*, 9930–9938.

[64] D. Kuck, T. Lindenthal, A. Schuster, *Chem. Ber. Recl.* **1992**, *125*, 1449–1460.

[65] G. Markopoulos, L. Henneicke, J. Shen, Y. Okamoto, P. G. Jones, H. Hopf, *Angew. Chem. Int. Ed.* **2012**, *51*, 12884–12887.

[66] a) M. Mastalerz, D. Beaudoin, F. Rominger, *Synthesis* **2015**, *47*, 3846–3848; b) D. Kuck, *Pure Appl. Chem.* **2006**, *78*.

[67] J. Tellenbröker, D. Kuck, *Beilstein J. Org. Chem.* **2011**, *7*, 329–337.

[68] E. U. Mughal, D. Kuck, *Org. Biomol. Chem.* **2010**, *8*, 5383–5389.

[69] A. Schuster, D. Kuck, *Angew. Chem. Int. Ed.* **1991**, *30*, 1699–1702.

[70] a) R. Haag, B. r. Ohlhorst, M. Noltemeyer, A. Schuster, D. Kuck, A. de Meijere, *J. Chem. Soc., Chem. Commun.* **1993**, 1727; b) D. Kuck, A. Schuster, B. Ohlhorst, V. Sinnwell, A. Demeijere, *Angew. Chem. Int. Ed.* **1989**, *28*, 595–597; c) R. Haag, D. Kuck, X.-Y. Fu, J. M. Cook, A. de Meijere, *Synlett* **1994**, *1994*, 340–342; d) R. Haag, B. Ohlhorst, M. Noltemeyer, R. Fleischer, D. Stalke, A. Schuster, D. Kuck, A. de Meijere, *J. Am. Chem. Soc.* **1995**, *117*, 10474–10485.

[71] M. Harig, B. Neumann, H.-G. Stammler, D. Kuck, *Eur. J. Org. Chem.* **2004**, *2004*, 2381–2397.

[72] a) J. Tellenbröker, D. Kuck, *Angew. Chem. Int. Ed.* **1999**, *38*, 919–922; b) L. Zhou, T. X. Zhang, B. R. Li, X. P. Cao, D. Kuck, *J. Org. Chem.* **2007**, *72*, 6382–6389.

[73] J. Strübe, B. Neumann, H. G. Stammler, D. Kuck, *Chem. Eur. J.* **2009**, *15*, 2256–2260.

[74] W. R. Xu, H. F. Chow, X. P. Cao, D. Kuck, *J. Org. Chem.* **2014**, *79*, 9335–9346.

[75] a) W. X. Niu, T. Wang, Q. Q. Hou, Z. Y. Li, X. P. Cao, D. Kuck, *J. Org. Chem.* **2010**, *75*, 6704–6707; b) T. Wang, Q. Q. Hou, Q. F. Teng, X. J. Yao, W. X. Niu, X. P. Cao, D. Kuck, *Chem. Eur. J.* **2010**, *16*, 12412–12424; c) D. Beaudoin, F. Rominger, M. Mastalerz, *Eur. J. Org. Chem.* **2016**, *2016*, 4470–4472.

[76] W. Greschner, B. Neumann, H. G. Stammler, H. Gröger, D. Kuck, *Angew. Chem. Int. Ed.* **2015**, *54*, 13764–13768.

[77] C. A. Dullaghan, G. B. Carpenter, D. A. Sweigart, D. Kuck, C. Fusco, R. Curci, *Organometallics* **2000**, *19*, 2233–2236.

[78] Y. Kirchwehm, A. Damme, T. Kupfer, H. Braunschweig, A. Krueger, *Chem. Commun.* **2012**, *48*, 1502–1504.

[79] E. U. Mughal, D. Kuck, *Chem. Commun.* **2012**, *48*, 8880–8882.

[80] H.-W. Ip, H.-F. Chow, D. Kuck, *Org. Chem. Front.* **2017**, *4*, 817–822.

[81] D. Kuck, A. Schuster, C. Fusco, M. Fiorentino, R. Curci, *J. Am. Chem. Soc.* **1994**, *116*, 2375–2381.

[82] A. G. Slater, A. I. Cooper, *Science* **2015**, *348*, 988–997.

[83] P. A. Wright, *Microporous Framework Solids* RSC Publishing, Cambridge, **2008**.

[84] a) M. Kondo, T. Yoshitomi, H. Matsuzaka, S. Kitagawa, K. Seki, *Angew. Chem. Int. Ed.* **1997**, *36*, 1725–1727; b) A. K. Cheetham, G. Férey, T. Loiseau, *Angew. Chem. Int. Ed.* **1999**, *38*, 3268–3292.

[85]   A. P. Côté, A. I. Benin, N. W. Ockwig, M. O'Keeffe, A. J. Matzger, O. M. Yaghi, *Science* **2005**, *310*, 1166–1170.

[86]   A. Thomas, *Angew. Chem. Int. Ed.* **2010**, *49*, 8328–8344.

[87]   P. M. Budd, B. S. Ghanem, S. Makhseed, N. B. McKeown, K. J. Msayib, C. E. Tattershall, *Chem. Commun.* **2004**, 230–231.

[88]   R. G. Taylor, C. G. Bezzu, M. Carta, K. J. Msayib, J. Walker, R. Short, B. M. Kariuki, N. B. McKeown, *Chem. Eur. J.* **2016**, *22*, 2466–2472.

[89]   M. Mastalerz, I. M. Oppel, *Angew. Chem. Int. Ed.* **2012**, *51*, 5252–5255.

[90]   T. Tozawa, J. T. Jones, S. I. Swamy, S. Jiang, D. J. Adams, S. Shakespeare, R. Clowes, D. Bradshaw, T. Hasell, S. Y. Chong, C. Tang, S. Thompson, J. Parker, A. Trewin, J. Bacsa, A. M. Slawin, A. Steiner, A. I. Cooper, *Nat. Mater.* **2009**, *8*, 973–978.

[91]   a) A. Avellaneda, P. Valente, A. Burgun, J. D. Evans, A. W. Markwell-Heys, D. Rankine, D. J. Nielsen, M. R. Hill, C. J. Sumby, C. J. Doonan, *Angew. Chem. Int. Ed.* **2013**, *52*, 3746–3749; b) Z. Wu, S. Lee, J. S. Moore, *J. Am. Chem. Soc.* **1992**, *114*, 8730–8732; c) C. Zhang, C. F. Chen, *J. Org. Chem.* **2007**, *72*, 9339–9341.

[92]   C. Zhang, Z. Wang, L. Tan, T. L. Zhai, S. Wang, B. Tan, Y. S. Zheng, X. L. Yang, H. B. Xu, *Angew. Chem. Int. Ed.* **2015**, *54*, 9244–9248.

[93]   J. Zhang, Y. Li, W. Yang, S. W. Lai, C. Zhou, H. Liu, C. M. Che, Y. Li, *Chem. Commun.* **2012**, *48*, 3602–3604.

[94]   S. J. Rowan, S. J. Cantrill, G. R. L. Cousins, J. K. M. Sanders, J. F. Stoddart, *Angew. Chem. Int. Ed.* **2002**, *41*, 898–952.

[95]   a) G. Zhang, O. Presly, F. White, I. M. Oppel, M. Mastalerz, *Angew. Chem. Int. Ed.* **2014**, *53*, 1516–1520; b) S. D. Bull, M. G. Davidson, J. M. van den Elsen, J. S. Fossey, A. T. Jenkins, Y. B. Jiang, Y. Kubo, F. Marken, K. Sakurai, J. Zhao, T. D. James, *Acc. Chem. Res.* **2013**, *46*, 312–326.

[96]   K. Ono, K. Johmoto, N. Yasuda, H. Uekusa, S. Fujii, M. Kiguchi, N. Iwasawa, *J. Am. Chem. Soc.* **2015**, *137*, 7015–7018.

[97]   a) M. J. Bojdys, M. E. Briggs, J. T. Jones, D. J. Adams, S. Y. Chong, M. Schmidtmann, A. I. Cooper, *J. Am. Chem. Soc.* **2011**, *133*, 16566–16571; b) T. Hasell, J. L. Culshaw, S. Y. Chong, M. Schmidtmann, M. A. Little, K. E. Jelfs, E. O. Pyzer-Knapp, H. Shepherd, D. J. Adams, G. M. Day, A. I. Cooper, *J. Am. Chem. Soc.* **2014**, *136*, 1438–1448; c) T. Mitra, X. Wu, R. Clowes, J. T. Jones, K. E. Jelfs, D. J. Adams, A. Trewin, J. Bacsa, A. Steiner, A. I. Cooper, *Chem. Eur. J.* **2011**, *17*, 10235–10240; d) K. E. Jelfs, X. Wu, M. Schmidtmann, J. T. Jones, J. E. Warren, D. J. Adams, A. I. Cooper, *Angew.*

Chem. Int. Ed. **2011**, *50*, 10653–10656; e) P. Skowronek, B. Warżajtis, U. Rychlewska, J. Gawroński, *Chem. Commun.* **2013**, *49*, 2524–2526; f) S. Jiang, J. Bacsa, X. Wu, J. T. Jones, R. Dawson, A. Trewin, D. J. Adams, A. I. Cooper, *Chem. Commun.* **2011**, *47*, 8919–8921; g) S. Hong, M. R. Rohman, J. Jia, Y. Kim, D. Moon, Y. Kim, Y. H. Ko, E. Lee, K. Kim, *Angew. Chem. Int. Ed.* **2015**, *54*, 13241–13244; h) S. Jiang, J. T. Jones, T. Hasell, C. E. Blythe, D. J. Adams, A. Trewin, A. I. Cooper, *Nat. Commun.* **2011**, *2*, 207; i) J. T. Jones, T. Hasell, X. Wu, J. Bacsa, K. E. Jelfs, M. Schmidtmann, S. Y. Chong, D. J. Adams, A. Trewin, F. Schiffman, F. Cora, B. Slater, A. Steiner, G. M. Day, A. I. Cooper, *Nature* **2011**, *474*, 367–371; j) J. T. Jones, D. Holden, T. Mitra, T. Hasell, D. J. Adams, K. E. Jelfs, A. Trewin, D. J. Willock, G. M. Day, J. Bacsa, A. Steiner, A. I. Cooper, *Angew. Chem. Int. Ed.* **2011**, *50*, 749–753; k) H. Ding, Y. Yang, B. Li, F. Pan, G. Zhu, M. Zeller, D. Yuan, C. Wang, *Chem. Commun.* **2015**, *51*, 1976–1979; l) Y. Jin, B. A. Voss, A. Jin, H. Long, R. D. Noble, W. Zhang, *J. Am. Chem. Soc.* **2011**, *133*, 6650–6658; m) Y. Jin, Y. Zhu, W. Zhang, *CrystEngComm* **2013**, *15*, 1484–1499; n) P. Kieryk, J. Janczak, J. Panek, M. Miklitz, J. Lisowski, *Org. Lett.* **2016**, *18*, 12–15; o) M. W. Schneider, I. M. Oppel, M. Mastalerz, *Chem. Eur. J.* **2012**, *18*, 4156–4160.

[98]   a) Q. Wang, C. Yu, H. Long, Y. Du, Y. Jin, W. Zhang, *Angew. Chem. Int. Ed.* **2015**, *54*, 7550–7554; b) Q. Wang, C. Zhang, B. C. Noll, H. Long, Y. Jin, W. Zhang, *Angew. Chem. Int. Ed.* **2014**, *53*, 10663–10667; c) Q. Wang, C. Yu, C. Zhang, H. Long, S. Azarnoush, Y. Jin, W. Zhang, *Chem. Sci.* **2016**, *7*, 3370–3376.

[99]   M. W. Schneider, I. M. Oppel, A. Griffin, M. Mastalerz, *Angew. Chem. Int. Ed.* **2013**, *52*, 3611–3615.

[100] P. S. Reiss, M. A. Little, V. Santolini, S. Y. Chong, T. Hasell, K. E. Jelfs, M. E. Briggs, A. I. Cooper, *Chem. Eur. J.* **2016**, *22*, 16547–16553.

[101] N. Giri, C. E. Davidson, G. Melaugh, M. G. Del Pópolo, J. T. A. Jones, T. Hasell, A. I. Cooper, P. N. Horton, M. B. Hursthouse, S. L. James, *Chem. Sci.* **2012**, *3*, 2153.

[102] N. Giri, M. G. Del Pópolo, G. Melaugh, R. L. Greenaway, K. Ratzke, T. Koschine, L. Pison, M. F. Gomes, A. I. Cooper, S. L. James, *Nature* **2015**, *527*, 216–220.

[103] P. Thordarson, *Chem. Soc. Rev.* **2011**, *40*, 1305–1323.

[104] a) S. W. Benson, *J. Am. Chem. Soc.* **1958**, *80*, 5151–5154; b) W. F. Bailey, A. S. Monahan, *J. Chem. Educ.* **1978**, *55*, 489–493; c) D. M. Bishop, K. J. Laidler, *J. Chem. Phys.* **1965**, *42*, 1688–1691; d) G. Ercolani, C. Piguet, M. Borkovec, J. Hamacek, *J. Phys. Chem. B* **2007**, *111*, 12195–12203.

[105] P. Barczyński, Z. Dega-Szafran, A. Katrusiak, W. Perdoch, M. Szafran, *J. Mol. Struct.* **2009**, *938*, 283–290.

[106] *Spartan ´14*, Wavefunction, Inc.

[107] *Python Software Foundation.* **Python Language Reference, version 2.7.**, Available at http://www.python.org.

[108] L. K. S. von Krbek, C. A. Schalley, P. Thordarson, *Chem. Soc. Rev.* **2017**, *46*, 2622–2637.

[109] C. A. Hunter, H. L. Anderson, *Angew. Chem. Int. Ed.* **2009**, *48*, 7488–7499.

[110] a) M. Ochiai, M. Kunishima, Y. Nagao, K. Fuji, M. Shiro, E. Fujita, *J. Am. Chem. Soc.* **1986**, *108*, 8281–8283; b) D. Fernández González, J. P. Brand, J. Waser, *Chem. Eur. J.* **2010**, *16*, 9457–9461.

[111] S. Nicolai, S. Erard, D. F. González, J. Waser, *Org. Lett.* **2010**, *12*, 384–387.

[112] M. Ochiai, T. Ito, Y. Takaoka, Y. Masaki, M. Kunishima, S. Tani, Y. Nagao, *J. Chem. Soc., Chem. Commun.* **1990**, 118.

[113] a) M. F. Lappert, B. Prokai, *J. Organomet. Chem.* **1964**, *1*, 384–400; b) A. Suzuki, *Pure Appl. Chem.* **1986**, *58*; c) J. R. Blackborow, *J. Organomet. Chem.* **1977**, *128*, 161–166.

[114] P. Schröder, T. Förster, S. Kleine, C. Becker, A. Richters, S. Ziegler, D. Rauh, K. Kumar, H. Waldmann, *Angew. Chem. Int. Ed.* **2015**, *54*, 12398–12403.

[115] C. Mitsui, H. Tanaka, H. Tsuji, E. Nakamura, *Chem. Asian J.* **2011**, *6*, 2296–2300.

[116] J. E. Nuñez, A. Natarajan, S. I. Khan, M. A. Garcia-Garibay, *Org. Lett.* **2007**, *9*, 3559–3561.

[117] V. Gevorgyan, J.-X. Liu, M. Rubin, S. Benson, Y. Yamamoto, *Tetrahedron Lett.* **1999**, *40*, 8919–8922.

[118] G. Markiewicz, A. Jenczak, M. Kołodziejski, J. J. Holstein, J. K. M. Sanders, A. R. Stefankiewicz, *Nat. Commun.* **2017**, *8*, 15109.

[119] S. Höger, S. Rosselli, A. D. Ramminger, V. Enkelmann, *Org. Lett.* **2002**, *4*, 4269–4272.

[120] T. Zimmermann, G. W. Fischer, *J. Prakt. Chem.* **1987**, *329*, 975–984.

[121] K. Chen, S. Zhang, P. He, P. Li, *Chem. Sci.* **2016**, *7*, 3676–3680.

[122] T. Ishiyama, M. Murata, N. Miyaura, *J. Org. Chem.* **1995**, *60*, 7508–7510.

[123] a) J. R. Falck, M. Bondlela, S. K. Venkataraman, D. Srinivas, *J. Org. Chem.* **2001**, *66*, 7148–7150; b) S. J. Coutts, J. Adams, D. Krolikowski, R. J. Snow, *Tetrahedron Lett.* **1994**, *35*, 5109–5112.

[124] G. H. Bertrand, V. K. Michaelis, T. C. Ong, R. G. Griffin, M. Dincă, *Proc. Natl. Acad. Sci. U. S. A.* **2013**, *110*, 4923–4928.

[125] P. Rodríguez-Cuamatzi, R. Luna-García, A. Torres-Huerta, M. I. Bernal-Uruchurtu, V. Barba, H. Höpfl, *Cryst. Growth Des.* **2009**, *9*, 1575–1583.

[126] J. D. Larkin, J. S. Fossey, T. D. James, B. R. Brooks, C. W. Bock, *J. Phys. Chem. A* **2010**, *114*, 12531–12539.

[127] a) N. A. Yakelis, R. G. Bergman, *Organometallics* **2005**, *24*, 3579–3581; b) H. Nishida, N. Takada, M. Yoshimura, T. Sonoda, H. Kobayashi, *Bull. Chem. Soc. Jpn.* **1984**, *57*, 2600–2604.

[128] *Topspin 3.0, Bruker*, available at http://www.bruker.com.

[129] G. M. Sheldrick, *Acta Crystallogr. C Struct. Chem.* **2015**, *71*, 3–8.

[130] a) P. Vandersluis, A. L. Spek, *Acta Crystallogr. A* **1990**, *46*, 194–201; b) A. L. Spek, *Acta Crystallogr. D Biol. Crystallogr.* **2009**, *65*, 148–155.

Appendix

Crystallographic Data

Crystal data and refinement details for diketone 120:

Suitable crystals for X-ray diffraction were grown from slow evaporation of 1/1 *n*-hexane/Et$_2$O solutions overnight.

Crystal data and refinement details for TBTQ 115:

Suitable crystals for X-ray diffraction were obtained by recrystallization from EtOH. The refinement showed residual electron density that could not be modeled satisfactorily. Therefore, the corresponding electron density was removed by using the SQUEEZE routine of Platon[130].

Details about the Squeezed Material:
```
loop_
  _platon_squeeze_void_nr
  _platon_squeeze_void_average_x
  _platon_squeeze_void_average_y
  _platon_squeeze_void_average_z
  _platon_squeeze_void_volume
  _platon_squeeze_void_count_electrons
  _platon_squeeze_void_content
  1  0.000  0.250  0.125     358     92 ''
  2  0.000  0.750  0.875     358     92 ''
  3  0.500  0.250  0.375     358     92 ''
  4  0.500  0.750  0.625     358     92 ''
 _platon_squeeze_void_probe_radius          1.20
 _platon_squeeze_details                 ?
```

The unit cell contains solvent molecules which are distributed over four voids. The solvent accessible voids with a volume of 358 Å^3 and an electron count of 92 are attributed to incorporated disordered ethanol molecules that could not be modeled satisfactorily. The remaining structure could be refined nicely.

Table A1. *Crystal data and structure refinement for diketone **120**.*

Empirical formula $C_{30}H_{28}O_8 \cdot C_4H_{10}O$

Formula weight   553.58 g mol^{-1}

Temperature   100(2) K

Wavelength   1.54178 Å

Crystal system   Triclinic

Space group $P\overline{1}$ (Nr. 2)

Unit cell dimensions   a = 10.6280(4) Å   a = 74.4890(10) °

   b = 11.3725(4) Å   b = 88.2680(10) °
   c = 13.4594(5) Å   g = 65.9900(10) °

Volume   1426.20(9) Å^3

Z   2

Density (calculated)   1.289 g cm^{-1}

Absorption coefficient   0.769 mm^{-1}

F(000)   586

Crystal size   0.409 x 0.282 x 0.160 mm^3

Θ range for data collection   3.421 to 72.196°

Index ranges $-13 \leq h \leq 13, -14 \leq k \leq 14, -16 \leq l \leq 16$

Reflections collected   22240

Independent reflections   5606 [R_{int} = 0.0240]

Completeness to Θ = 67.679°   99.7%

Absorption correction   Semi-empirical from equivalents

Max. and min. transmission   0.7536 and 0.6768

Refinement method   Full-matrix least-squares on F^2

Data / restraints / parameters   5606 / 0 / 371

Goodness-of-fit on F^2 1.044

Final R indices [$I > 2(\sigma(I)$] R_1 = 0.0396, wR_2 = 0.1005

R indices (all data) R_1 = 0.0416, wR_2 = 0.1023

Largest diff. peak and hole   0.528 and -0.551 e Å^{-3}

*Table A2. Crystal data and structure refinement for TBTQ **115**.*

Empirical formula $C_{30}H_{28}O_6$

Formula weight   484.52 g mol^{-1}

Temperature   100(2) K

Wavelength   1.54178 Å

Crystal system   Tetragonal

Space group $I4_1/a$ (Nr. 88)

Unit cell dimensions   a = 31.7190(10) Å,   a = 90°
   b = 31.7190(10) Å,   b = 90°
   c = 10.8097(4) Å,   g = 90°

Volume   10875.6(8) Å^3

Z 16

Density (calculated)   1.184 g cm^{-1}

Absorption coefficient   0.668 mm^{-1}

F(000)   4096

Crystal size   0.194 x 0.062 x 0.047 mm^3

Θ range for data collection   2.786 to 74.767°

Index ranges $-39 \leq h \leq 39, -39 \leq k \leq 39, -11 \leq l \leq 13$

Reflections collected   77846

Independent reflections   5576 [R_{int} = 0.0420]

Completeness to Θ = 67.679°   100.0%

Absorption correction   Semi-empirical from equivalents

Max. and min. transmission   0.7538 and 0.6990

Refinement method   Full-matrix least-squares on F^2

Data / restraints / parameters   5576 / 0 / 343

Goodness-of-fit on F^2 1.033

Final R indices [$I > 2(\sigma(I)$] R_1 = 0.0346, wR_2 = 0.0885

R indices (all data) R_1 = 0.0409, wR_2 = 0.0928

Largest diff. peak and hole   0.244 and -0.166 e Å^{-3}

Analytical Data
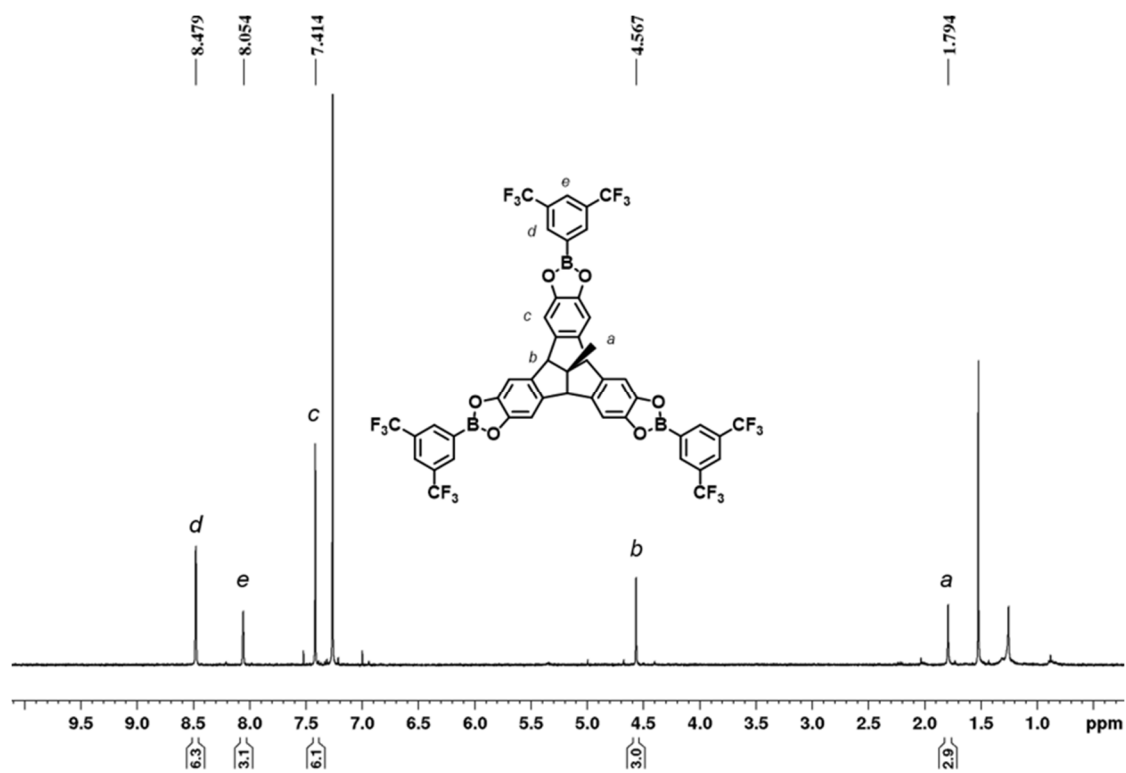
Figure A1 | ^{1}H-NMR (400 MHz, CDCl$_3$, rt) spectrum of **113.**
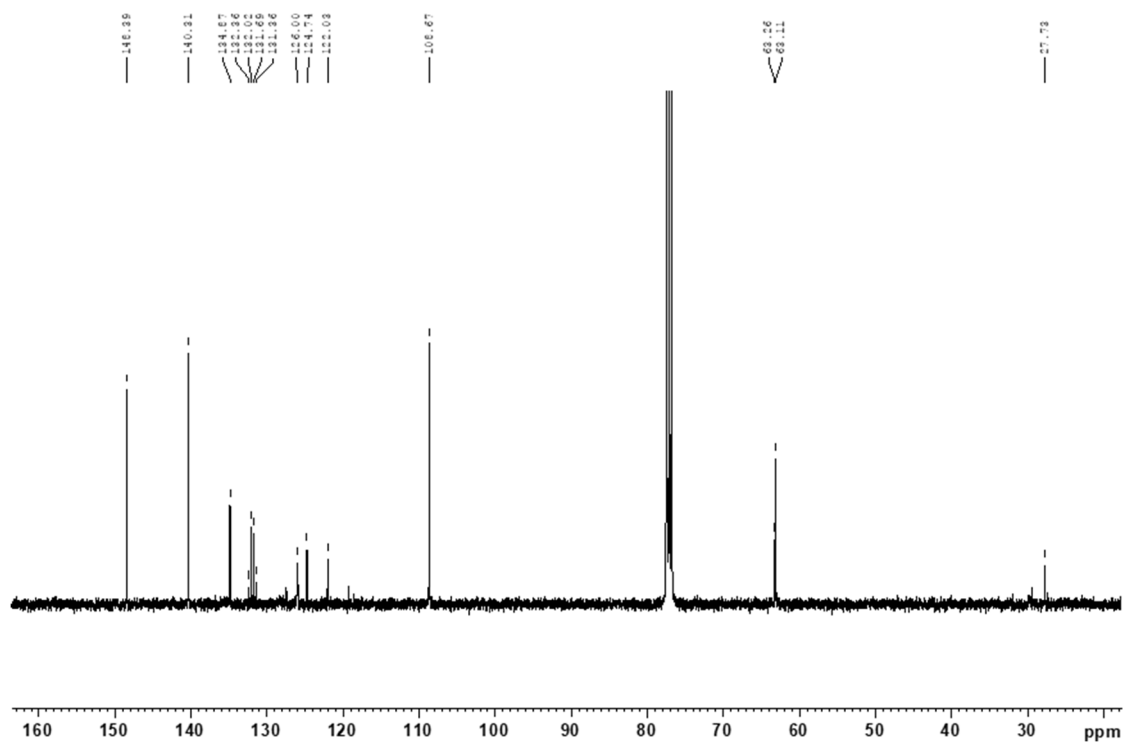
Figure A2 | ^{13}C-NMR (101 MHz, CDCl$_3$, rt) spectrum of **113.**
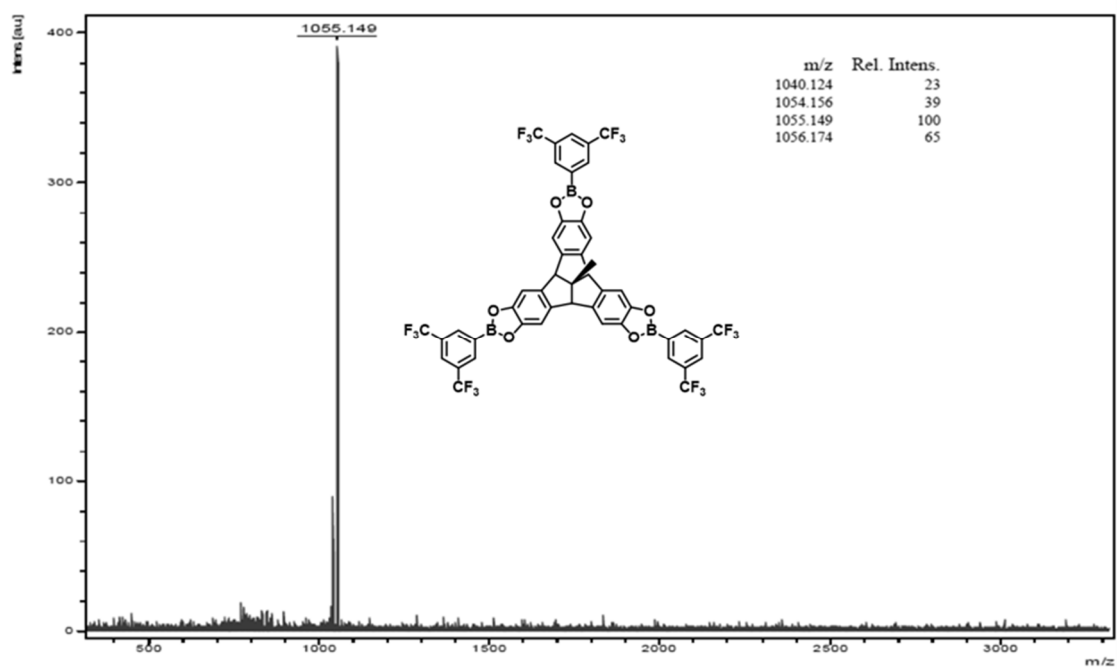
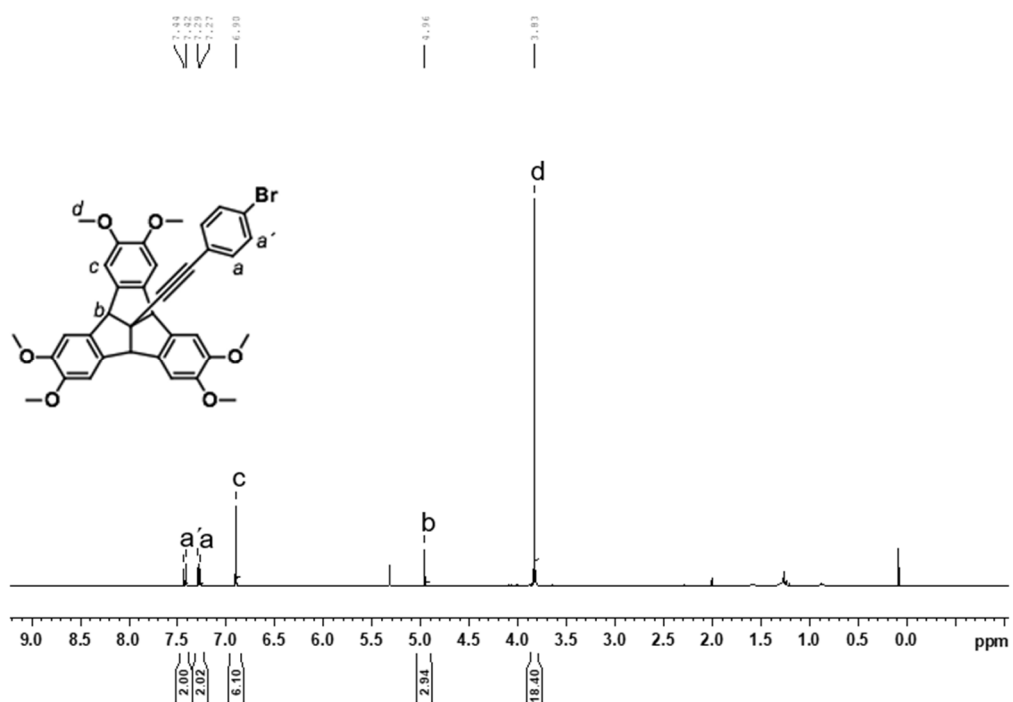**Figure A3** | MALDI-TOF mass spectrum (DCTB, CHCl₃) of **113**.
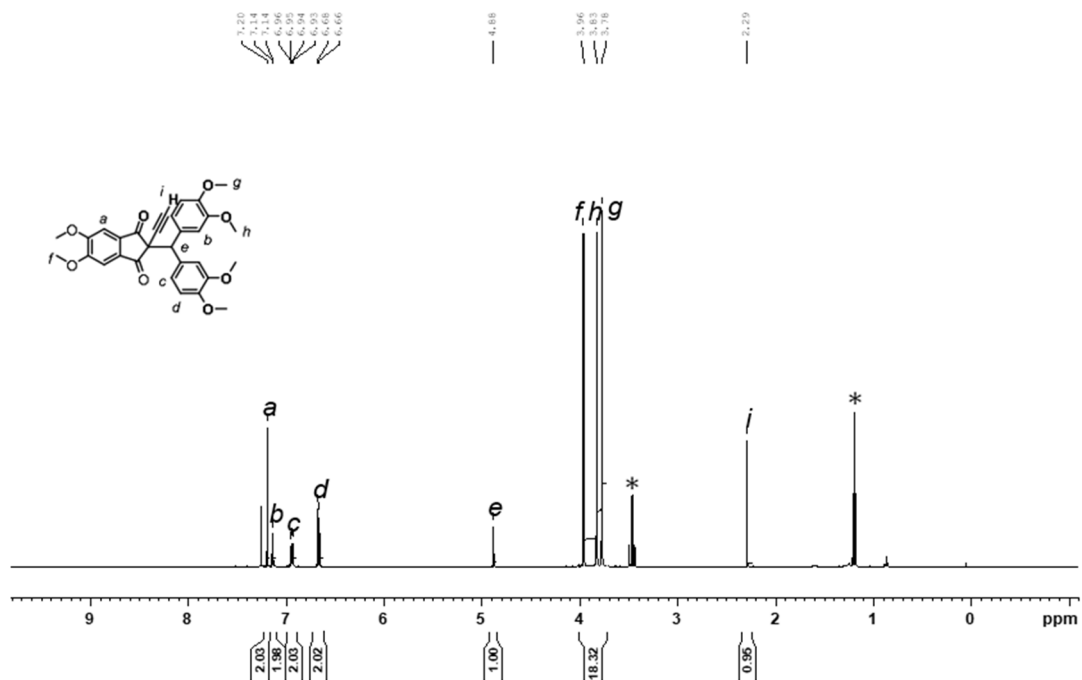
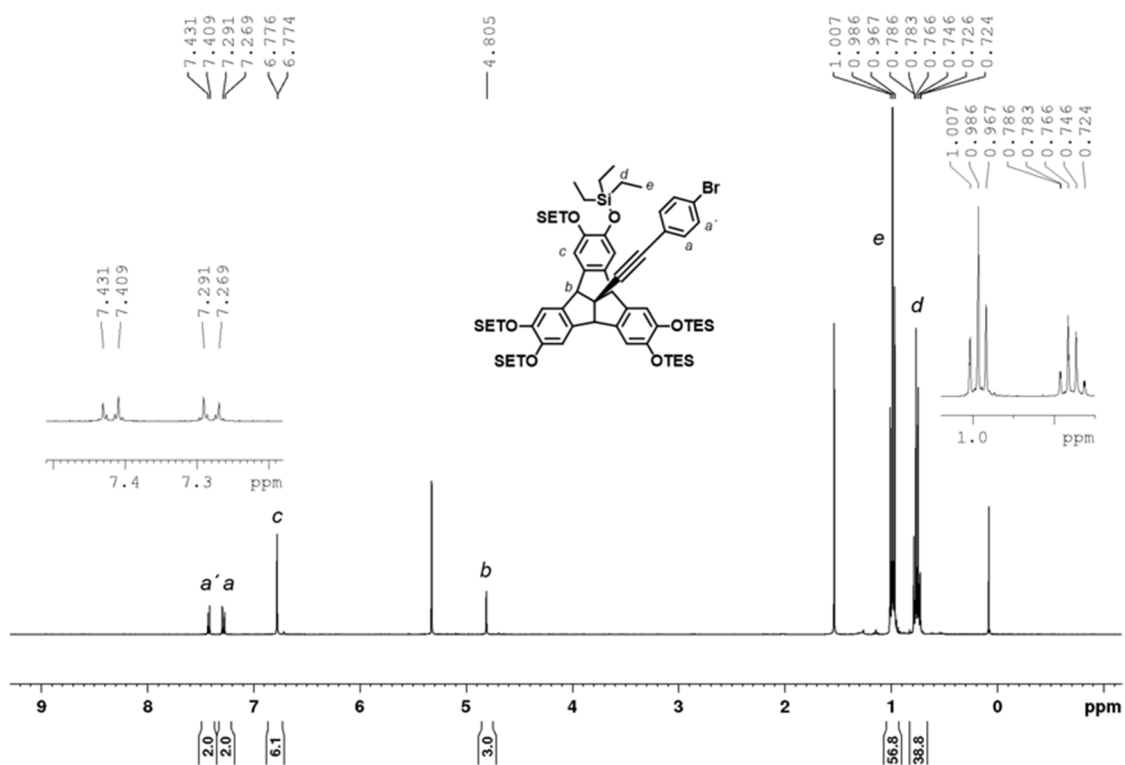**Figure A4** | ¹H-NMR (400 MHz, CDCl₃, rt) spectrum of **120.**
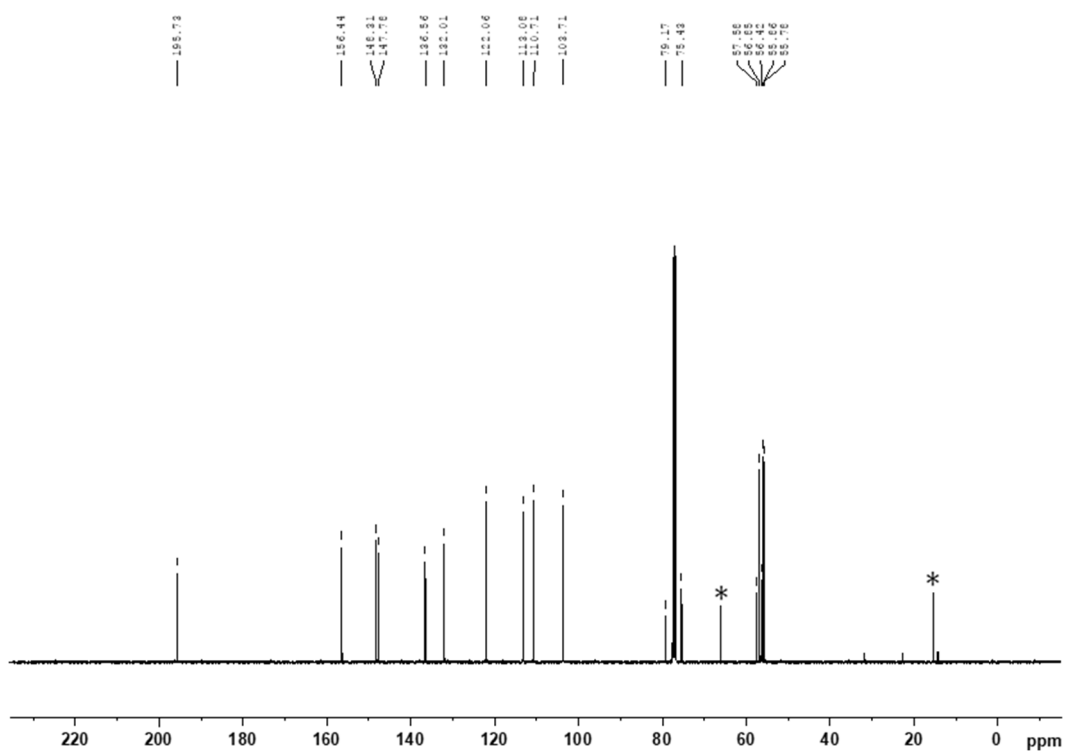
Figure A5 | ^{13}C-NMR (101 MHz, CDCl$_3$, rt) spectrum of **120**.

m/z	Rel. Intens.
500.257	17
515.141	25
516.141	100
517.151	30
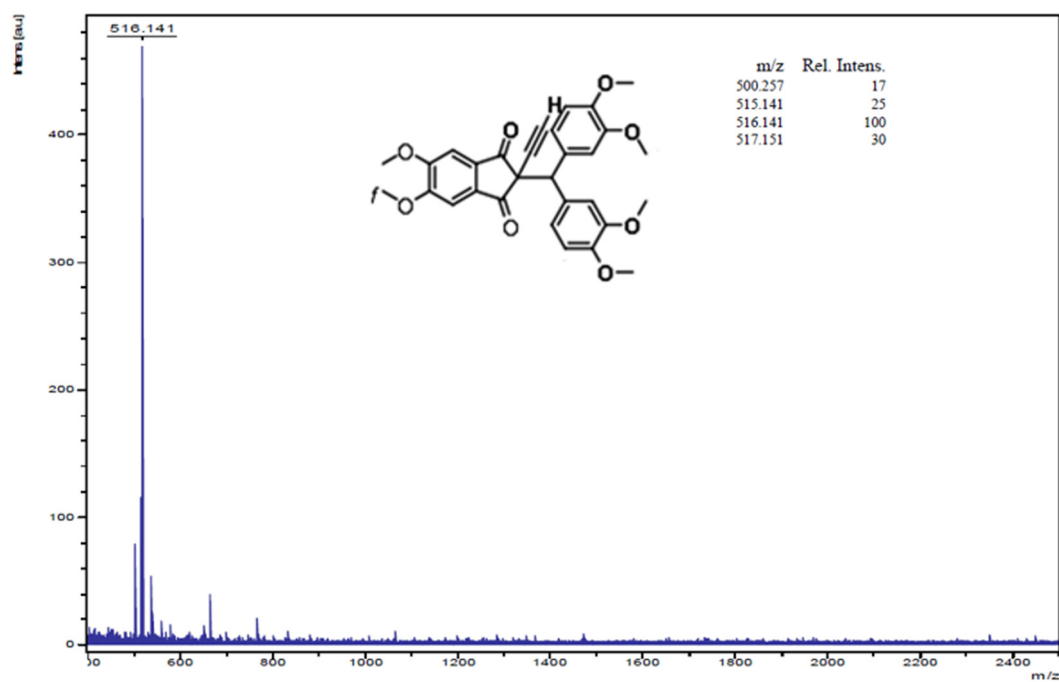
Figure A6 | MALDI-TOF mass spectrum (DCTB) of **120**.

Figure A7 | ¹H-NMR (400 MHz, CD₂Cl₂, rt) spectrum of **121.**

Figure A8 | MALDI-TOF mass spectrum (DCTB) of **121.**
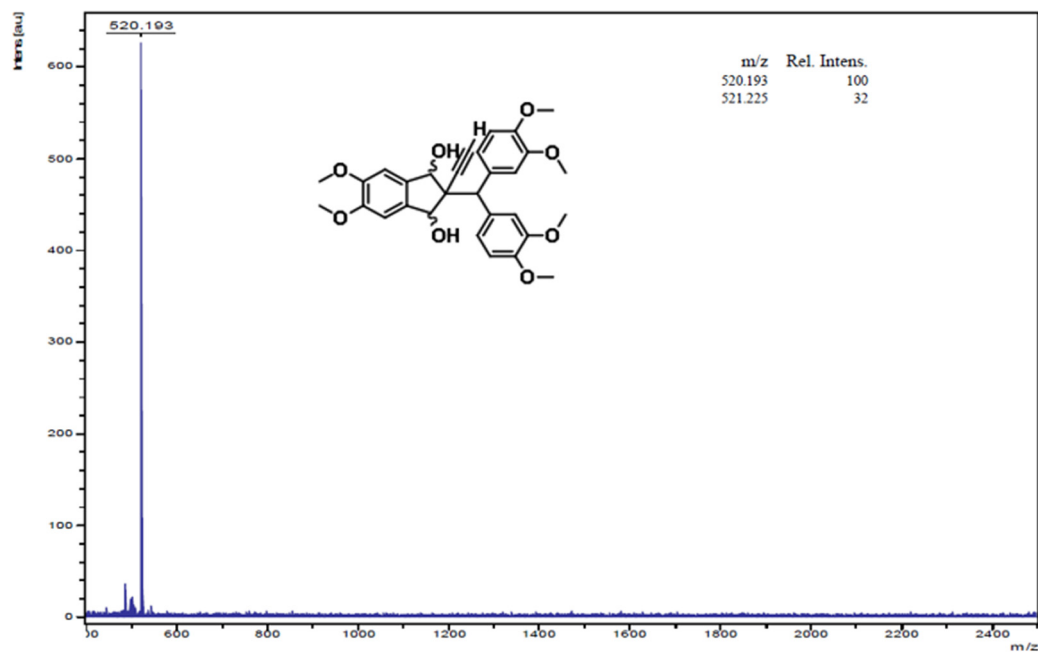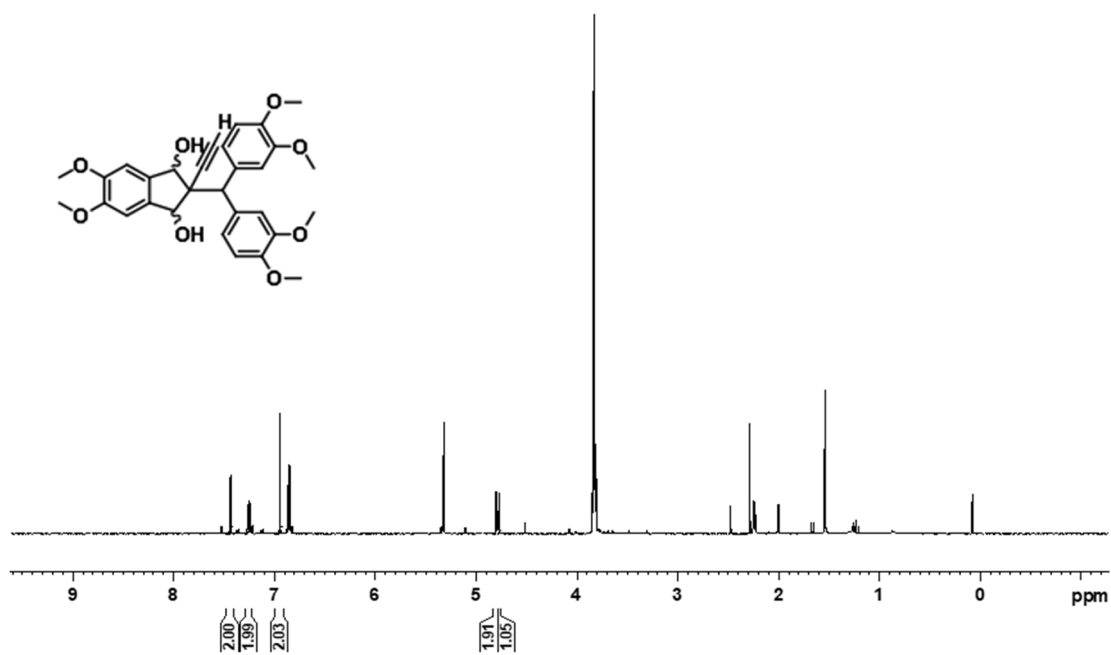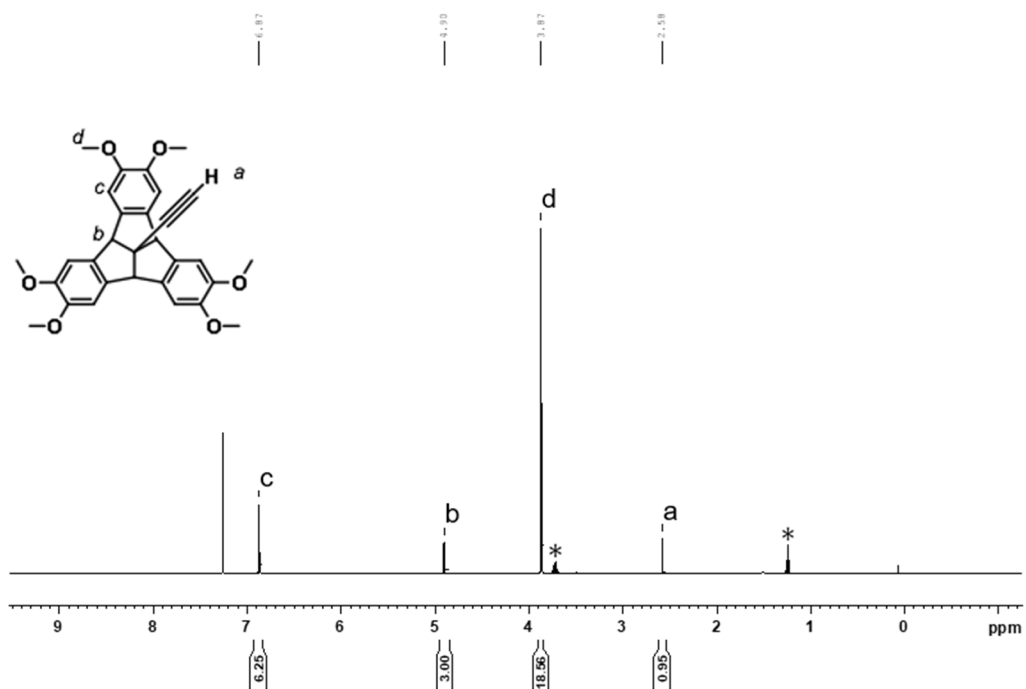
Figure A9 | ^{1}H-NMR (400 MHz, CDCl$_3$, rt) spectrum of **115**. $*$ indicates EtOH
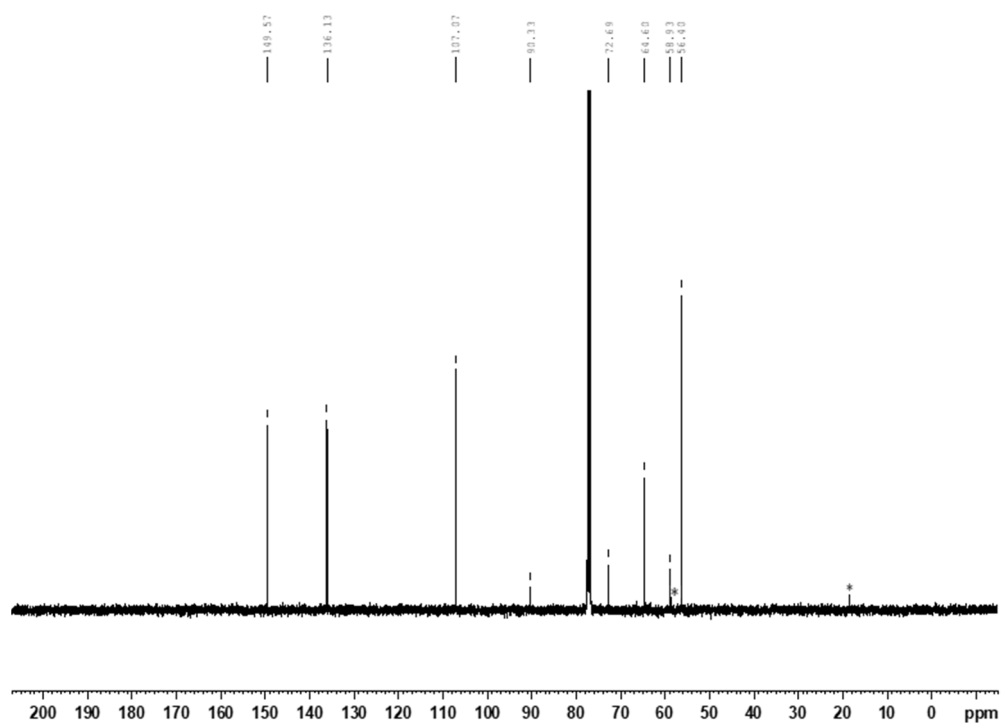
Figure A10 | ^{13}C-NMR (101 MHz, CDCl$_3$, rt) spectrum of **115**. $*$ indicates EtOH
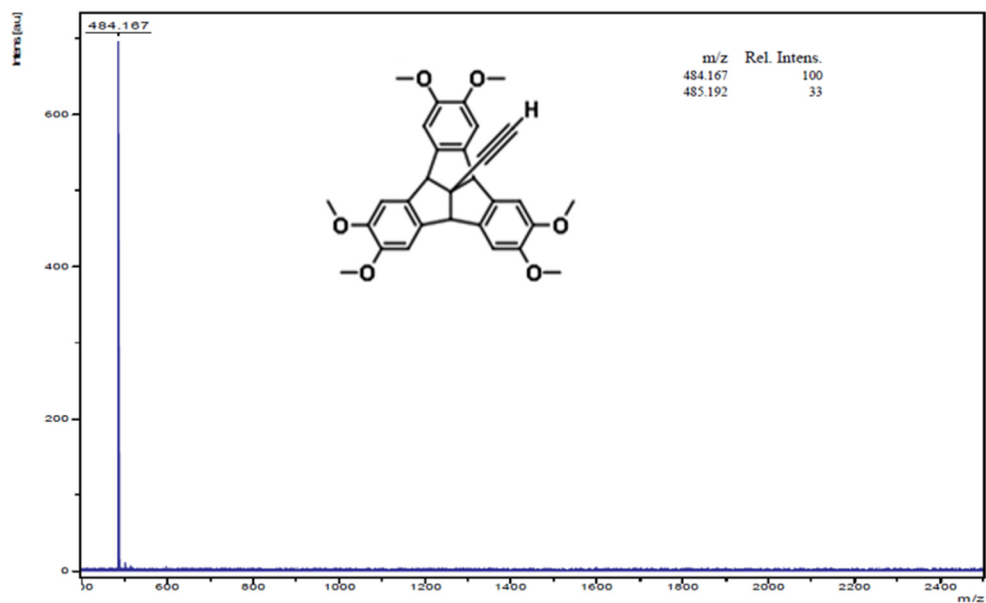
Figure A11 | MALDI-TOF mass spectrum (DCTB) of **115**.
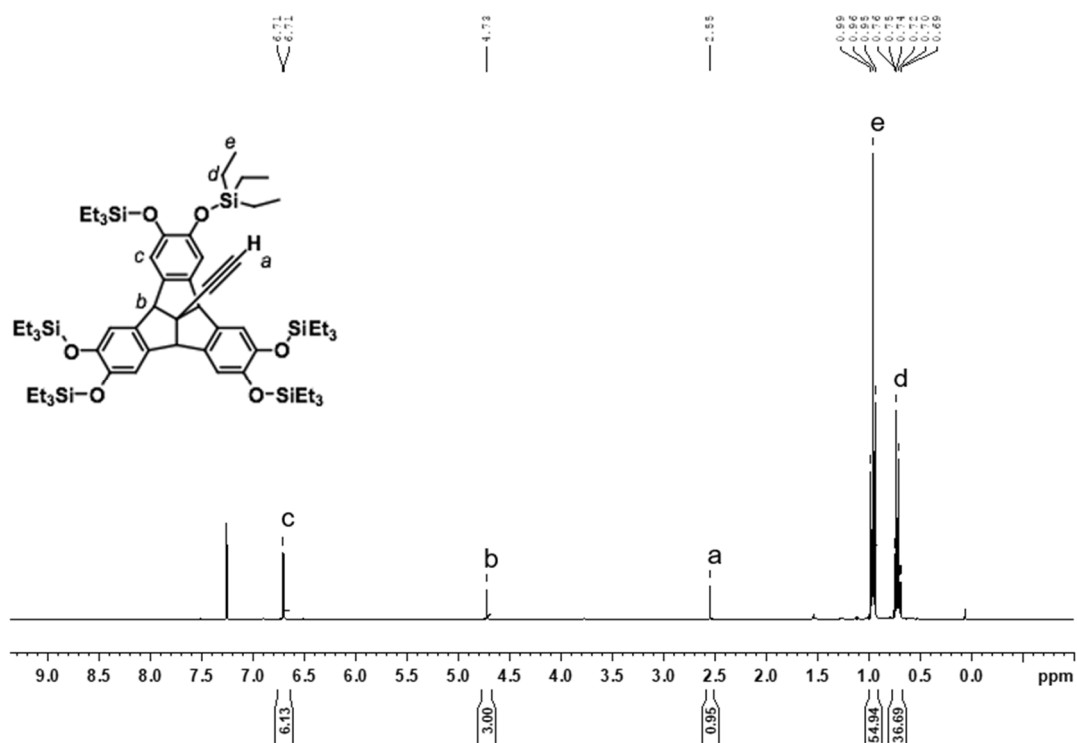
Figure A12 | ¹H-NMR (400 MHz, CDCl₃, rt) spectrum of **122**.
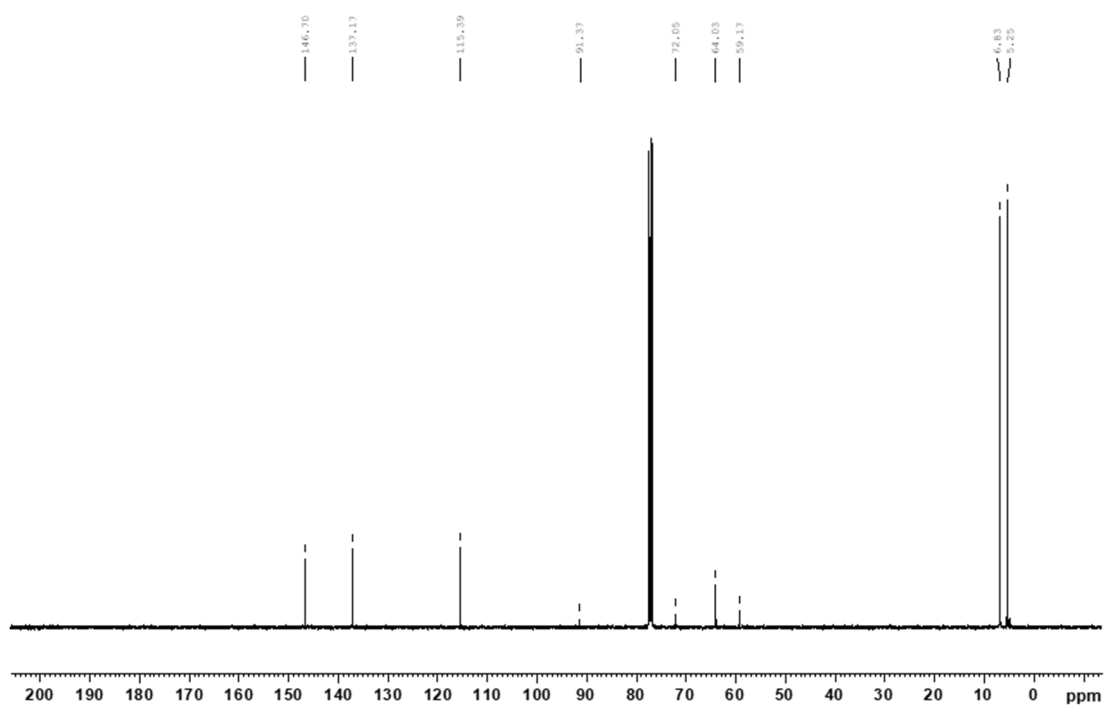
Figure A13 | ^{13}C-NMR (101 MHz, CDCl$_3$, rt) spectrum of **122**.

m/z	Rel. Intens.
984.518	8
985.525	9
1004.475	11
1005.486	10
1006.482	12
1084.601	100
1085.615	97
1086.631	67
1087.639	37
1088.640	15
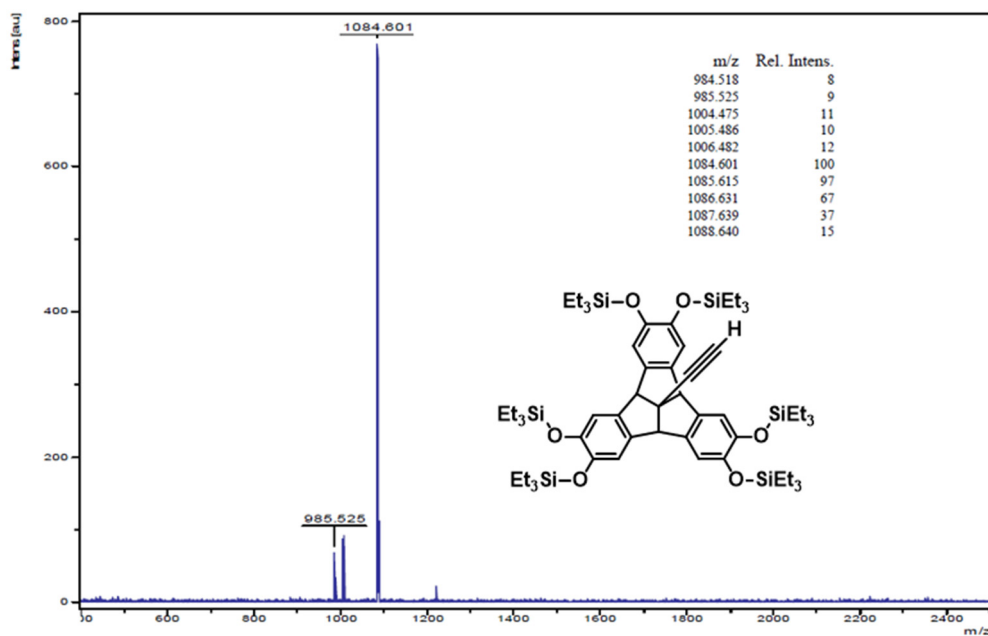
Figure A14 | MALDI-TOF mass spectrum (DCTB) of **122**.
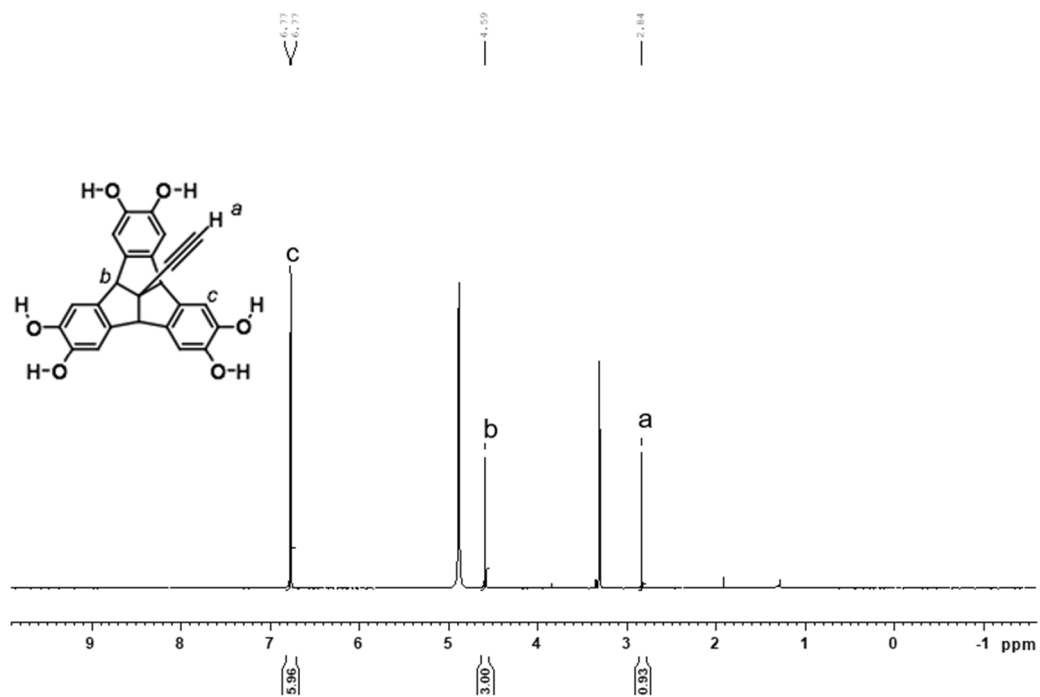
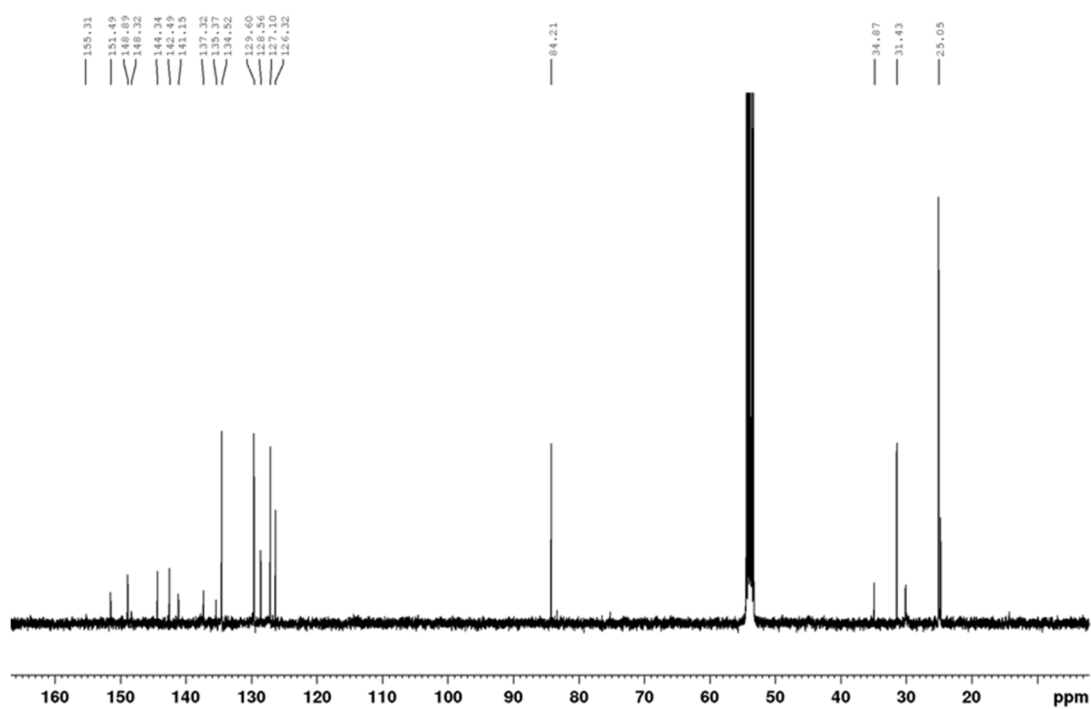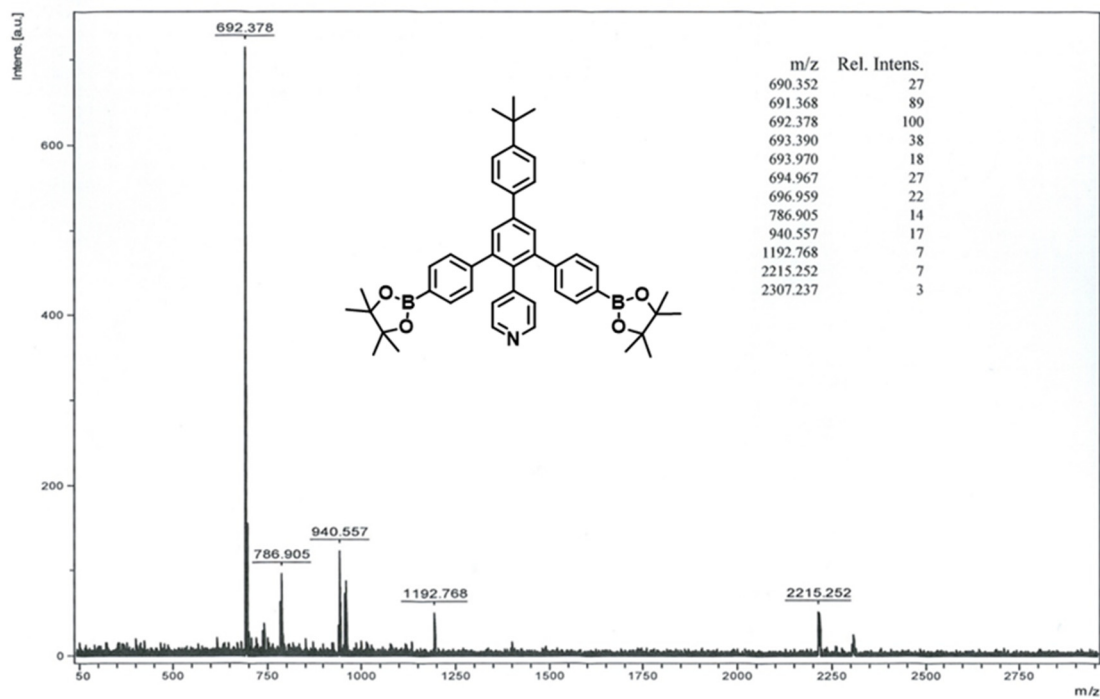**Figure A15** | ¹H-NMR (400 MHz, MeOD, rt) spectrum of **123**.
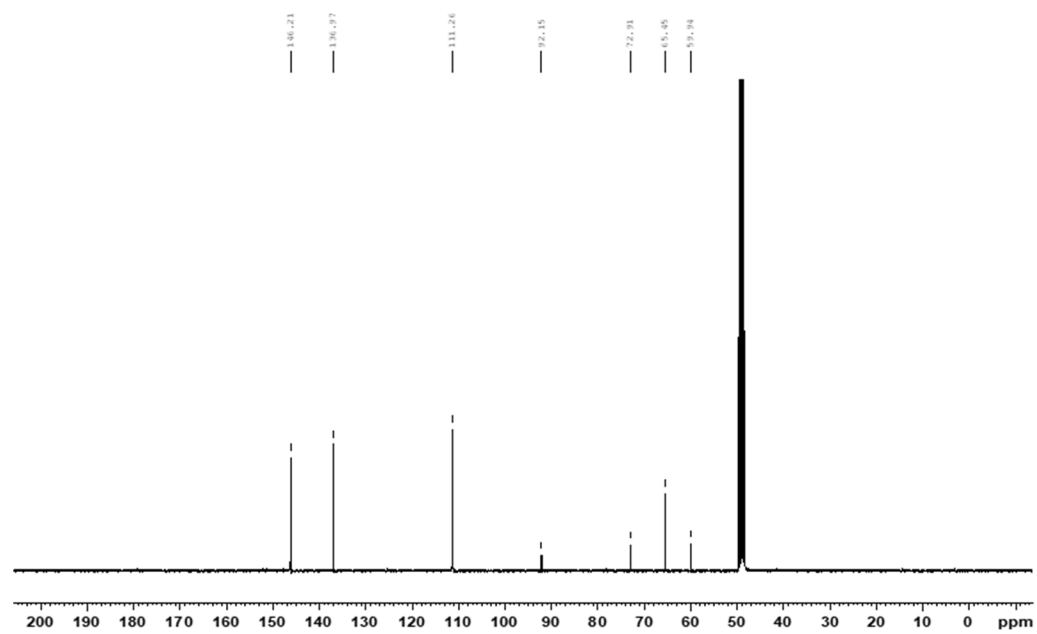
Figure A16 | ¹³C-NMR (101 MHz, MeOD, rt) spectrum of **123**.
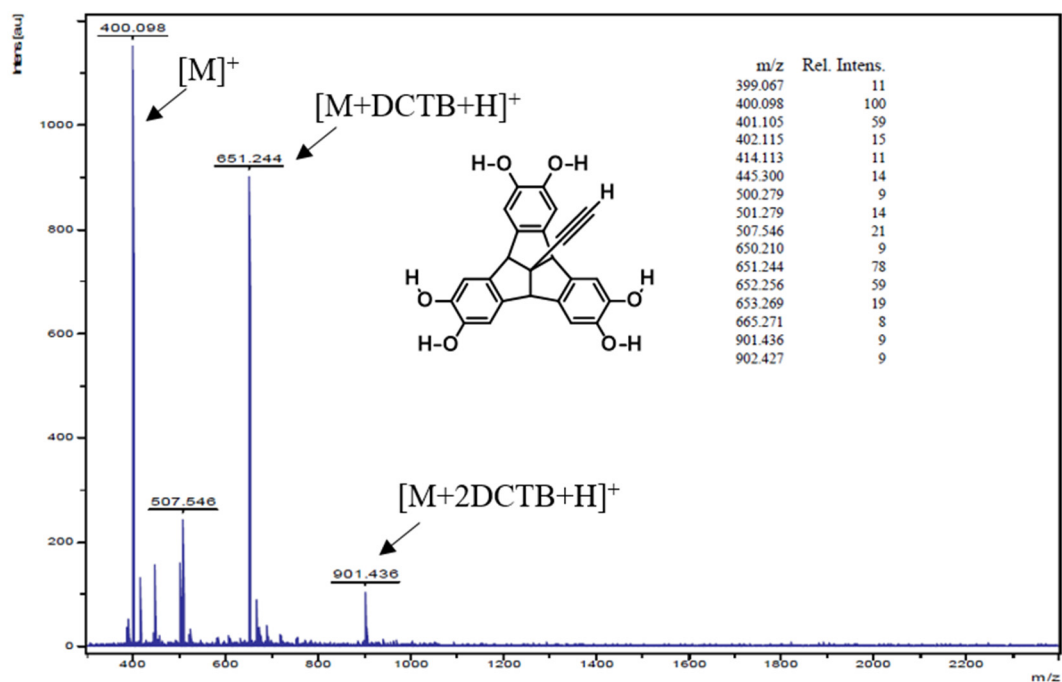
Figure A17 | MALDI-TOF mass spectrum (DCTB) of **123**.
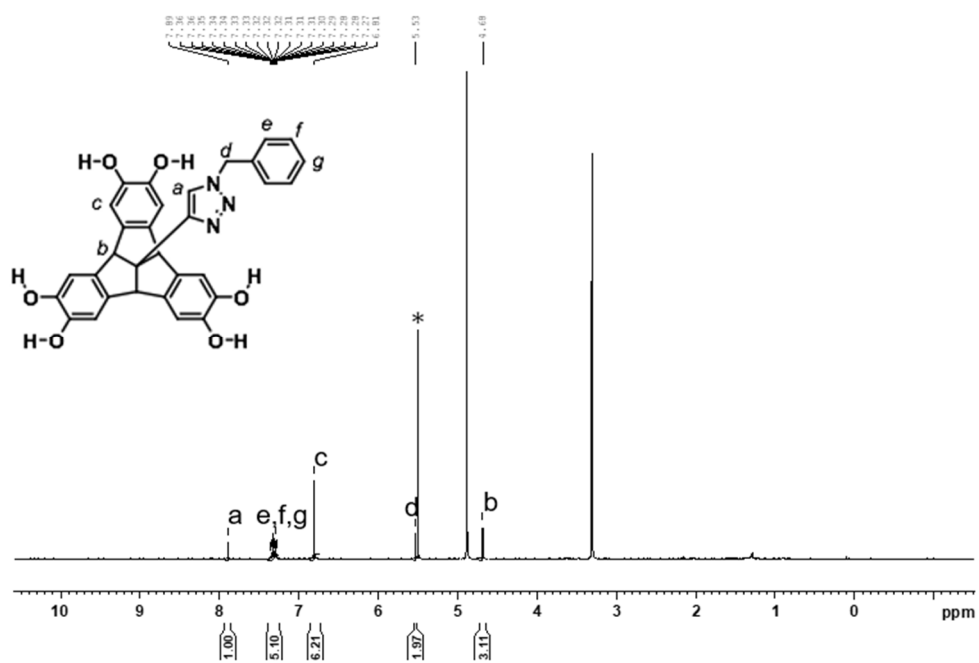
**Figure A18 |** ¹H-NMR (400 MHz, MeOD, rt) spectrum of **124**. ∗ indicates dichloromethane
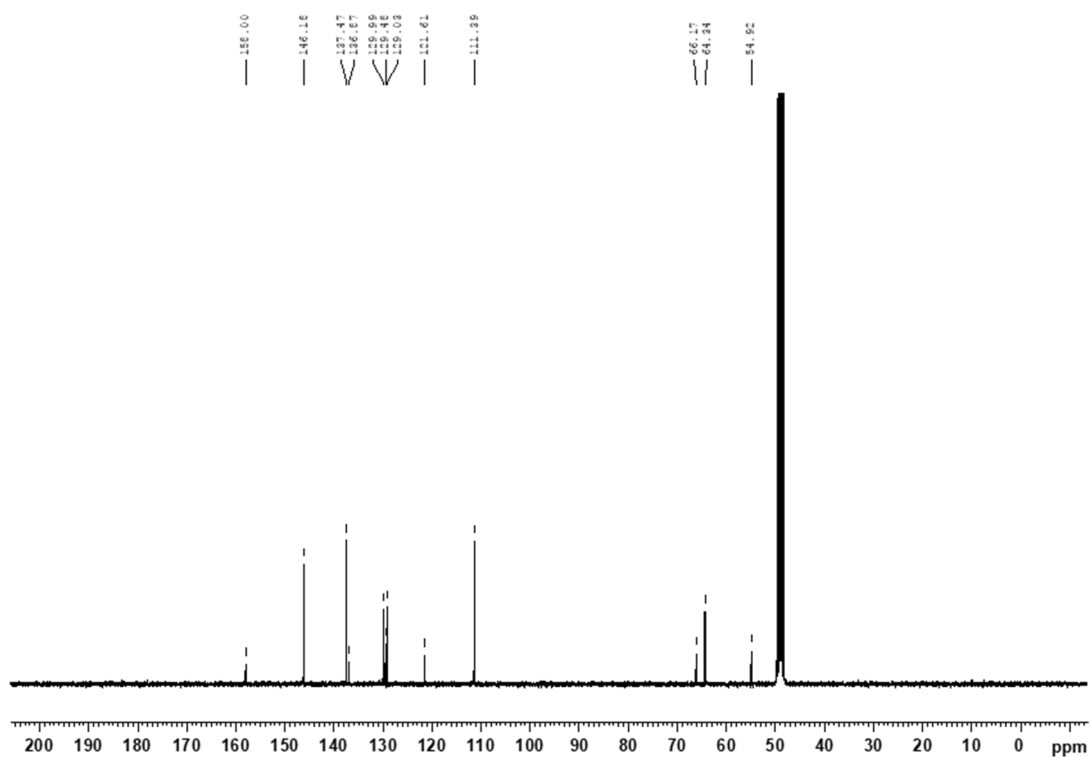
Figure A19 | ^{13}C-NMR (101 MHz, MeOD, rt) spectrum of **124**.

m/z	Rel. Intens.
445.275	53
507.527	17
532.143	15
533.134	89
534.139	100
535.146	42
1085.668	18
1270.690	15
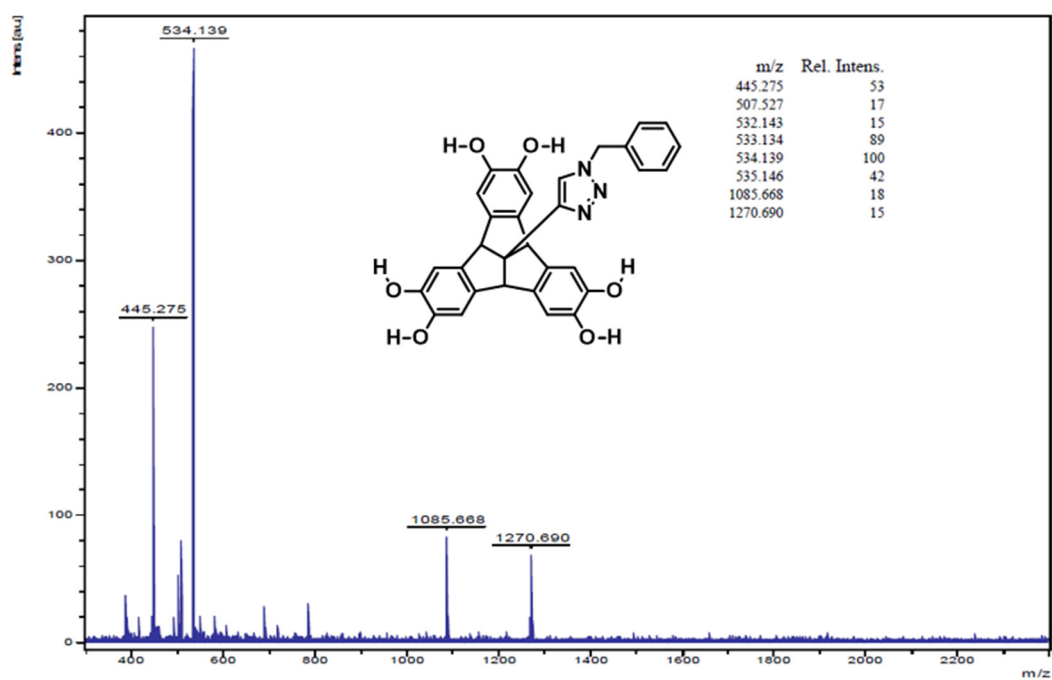
Figure A20 | MALDI-TOF mass spectrum (DCTB) of **124**.

Figure A21 | ^{1}H-NMR (400 MHz, CD$_2$Cl$_2$, rt) spectrum of **125**.
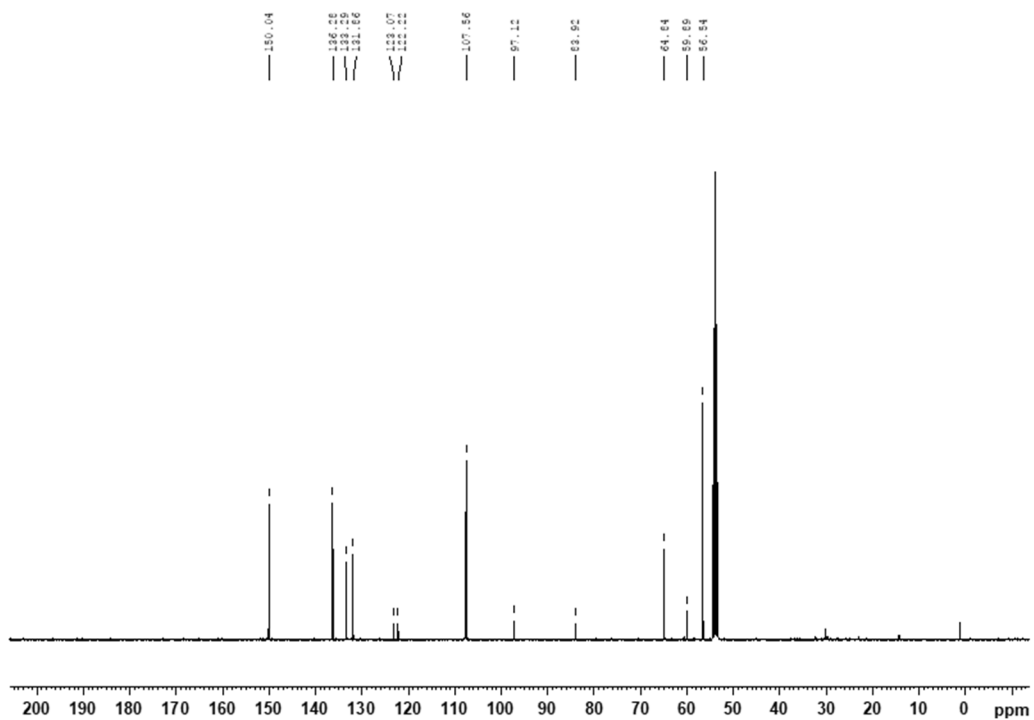
Figure A22 | ^{13}C-NMR (101 MHz, CD$_2$Cl$_2$, rt) spectrum of **125**.
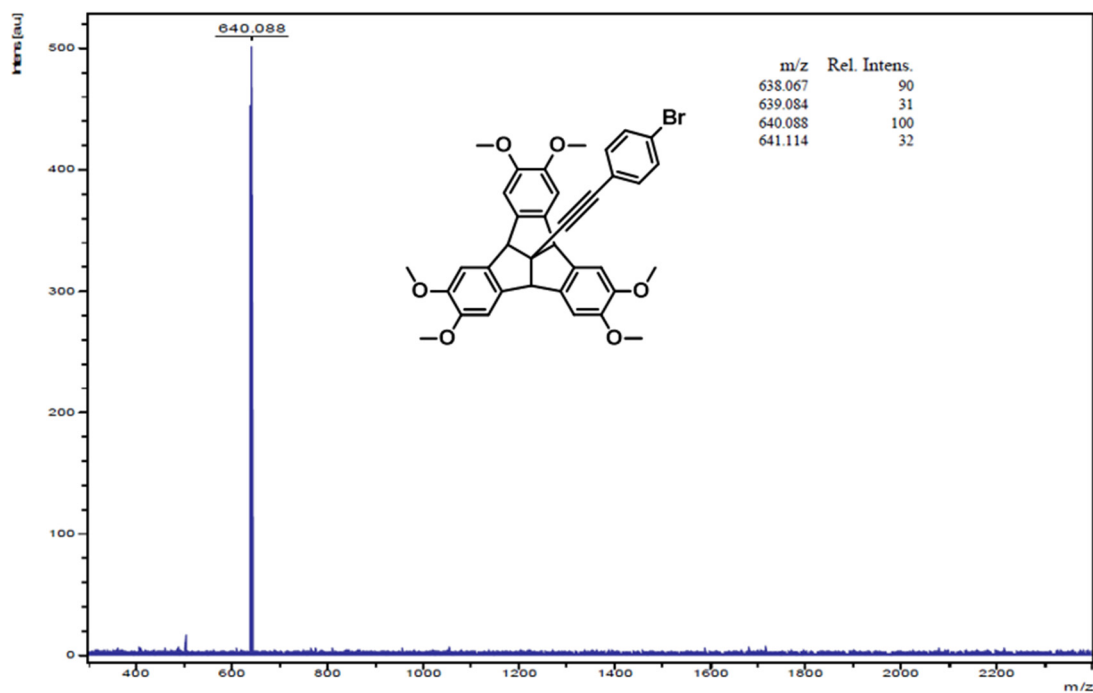
Figure A23 | MALDI-TOF mass spectrum (DCTB) of **125**.

Figure A24 | ^{1}H-NMR (400 MHz, CD$_2$Cl$_2$, rt) spectrum of **126.**
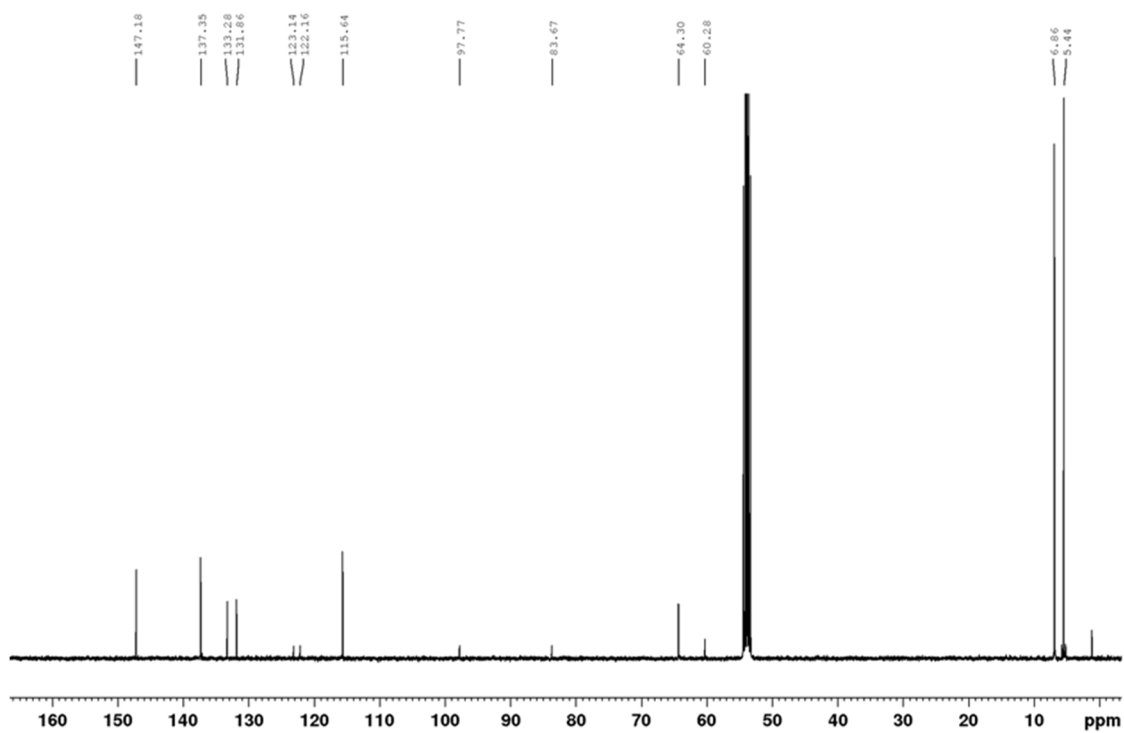
Figure A25 | ^{13}C-NMR (101 MHz, CD$_2$Cl$_2$, rt) spectrum of **126**.
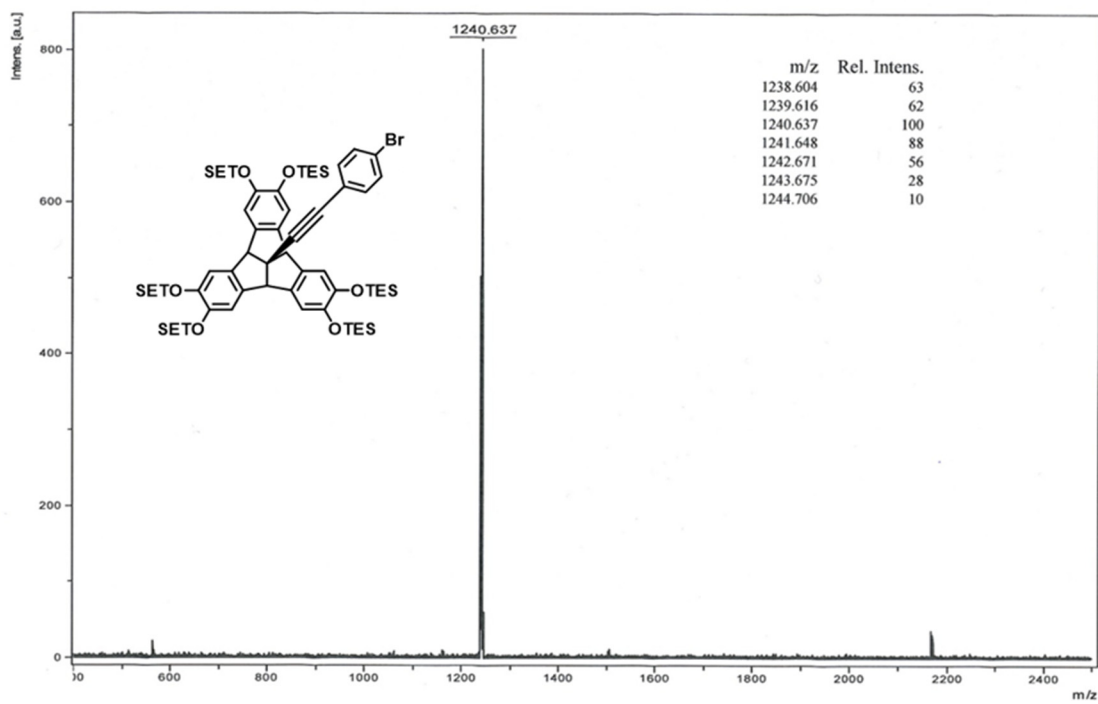
Figure A26 | MALDI-TOF mass spectrum (DCTB) of **126**.
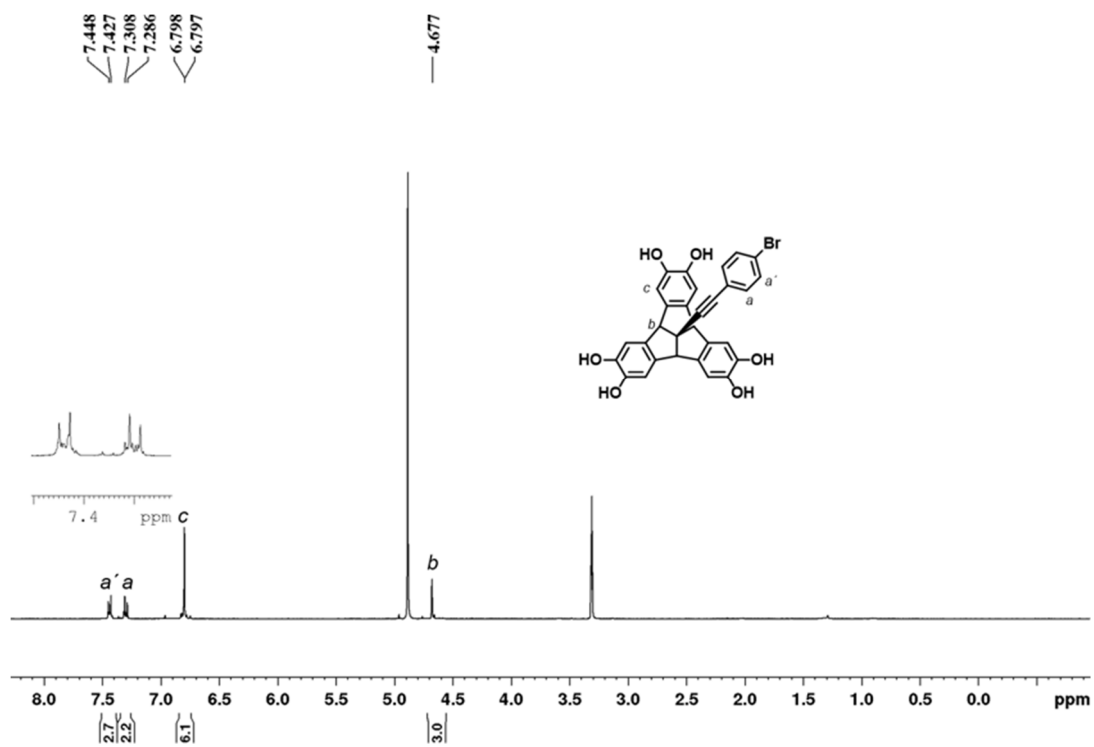
Figure A27 | ^{1}H-NMR (400 MHz, MeOD, rt) spectrum of **127**.
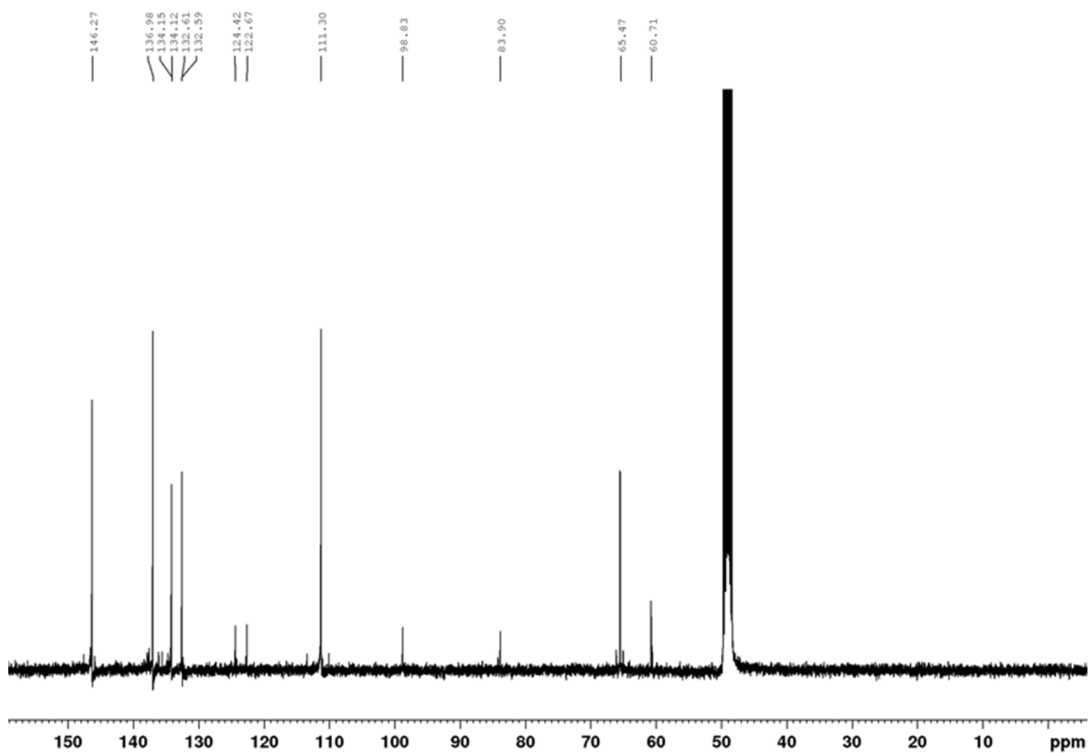
Figure A28 | ^{13}C-NMR (101 MHz, MeOD, rt) spectrum of **127**.
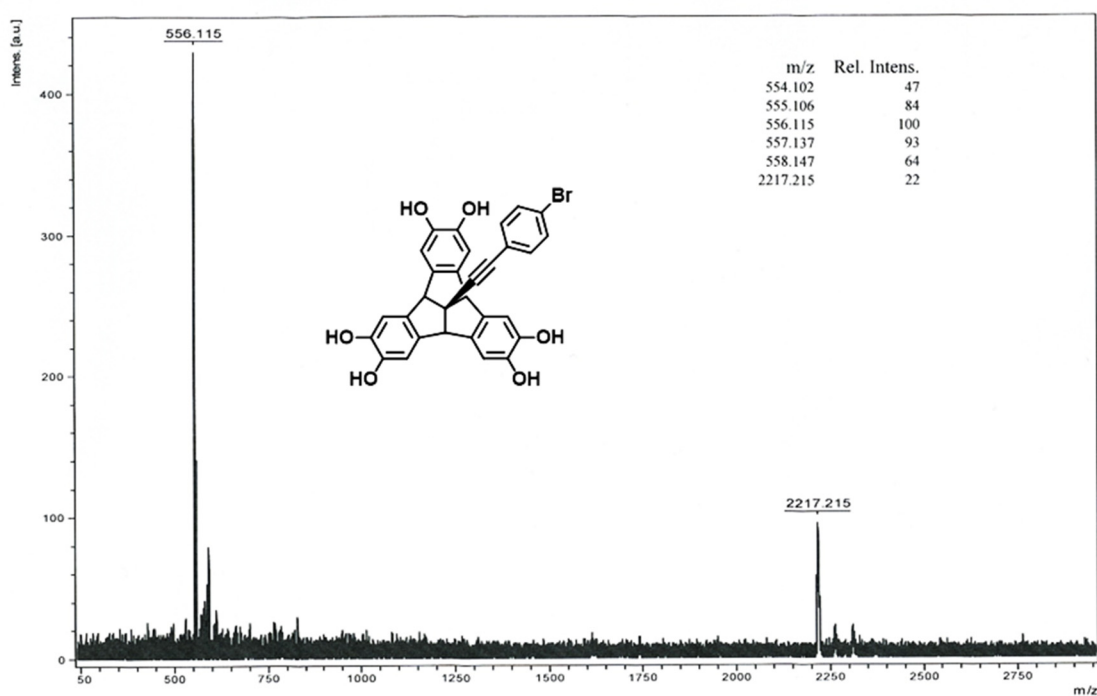
Figure A29 | MALDI-TOF mass spectrum (DCTB) of **127**.
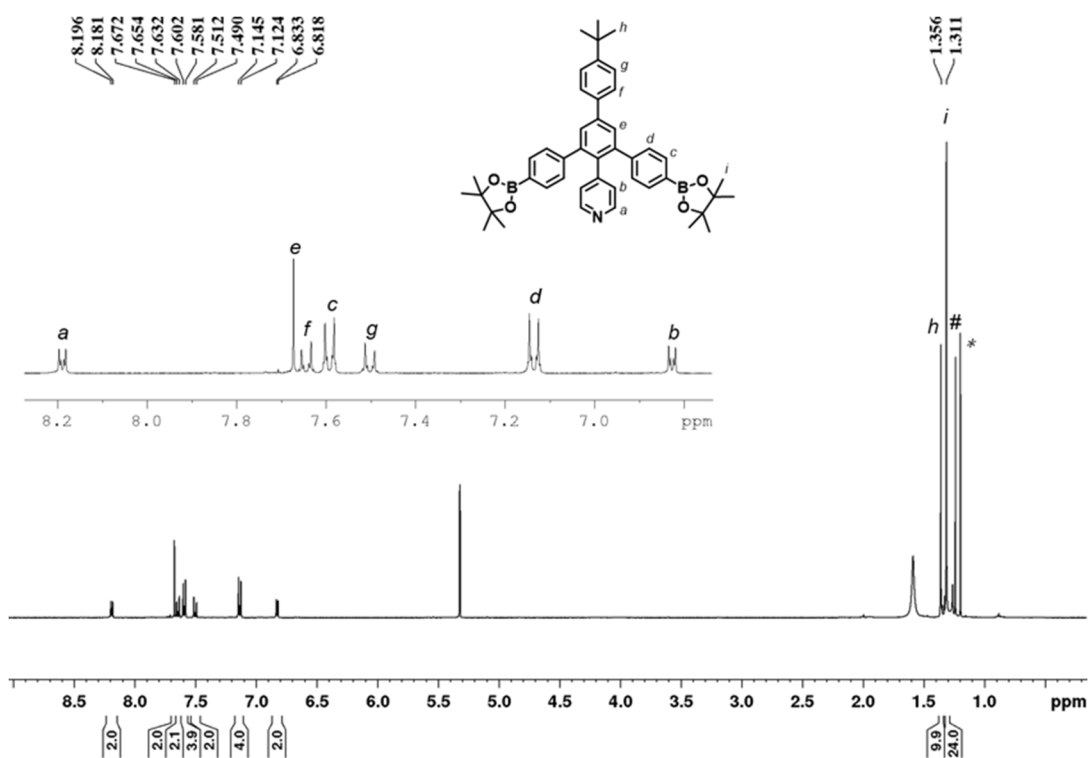
Figure A30 | ^{1}H-NMR (400 MHz, CD$_2$Cl$_2$, rt) spectrum of **133**. # = tert-butanol, * = B$_2$(pin)$_2$

Figure A31 | ^{13}C-NMR (101 MHz, CD$_2$Cl$_2$, rt) spectrum of **133**.

Figure A32 | MALDI-TOF mass spectrum (DCTB) of **133**.
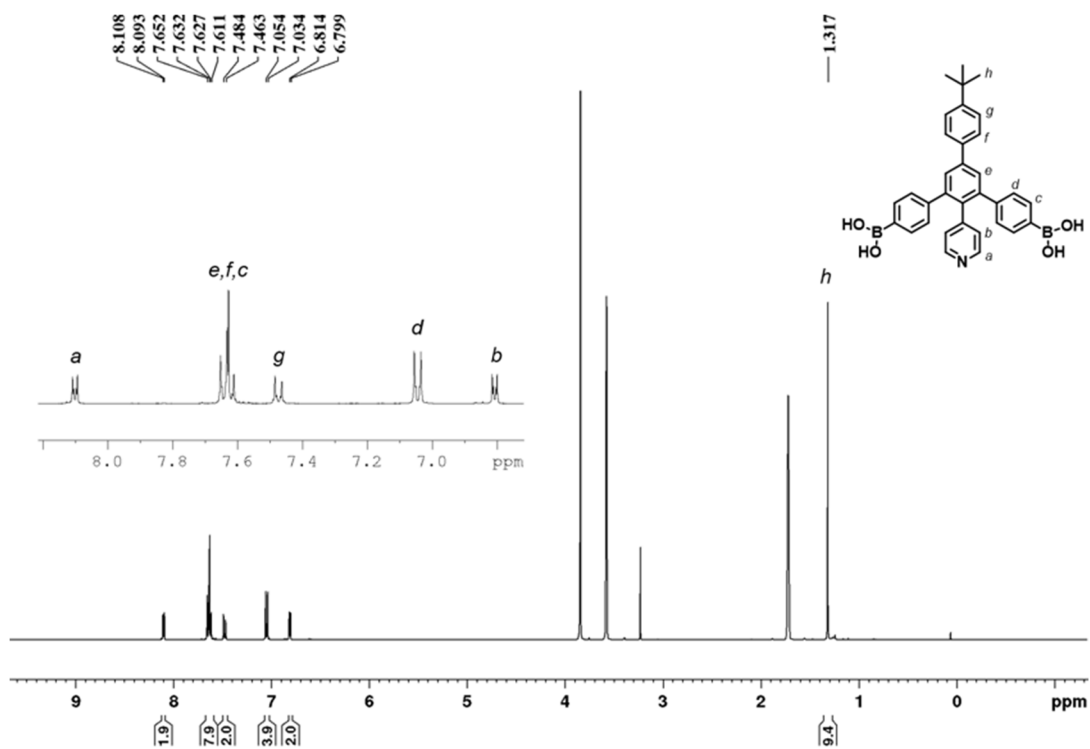
Figure A33 | ^{1}H-NMR (400 MHz, THF-d$_8$-D$_2$O, rt) spectrum of **130**.
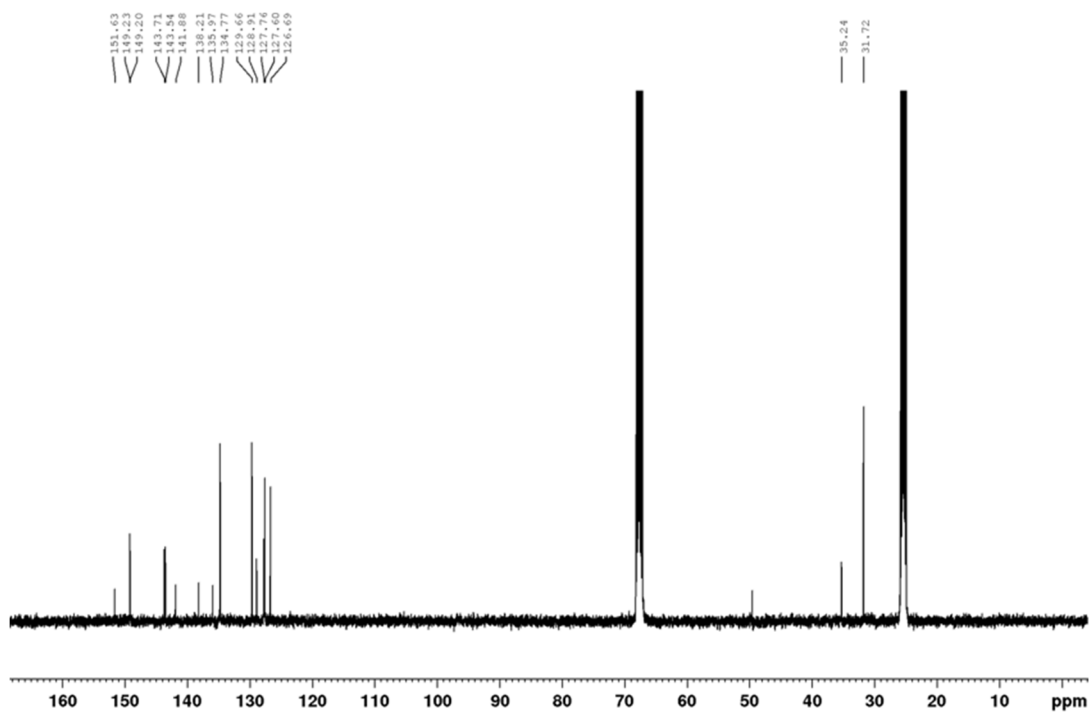
Figure A34 | ^{13}C-NMR (101 MHz, THF-d$_8$-D$_2$O, rt) spectrum of **130**.
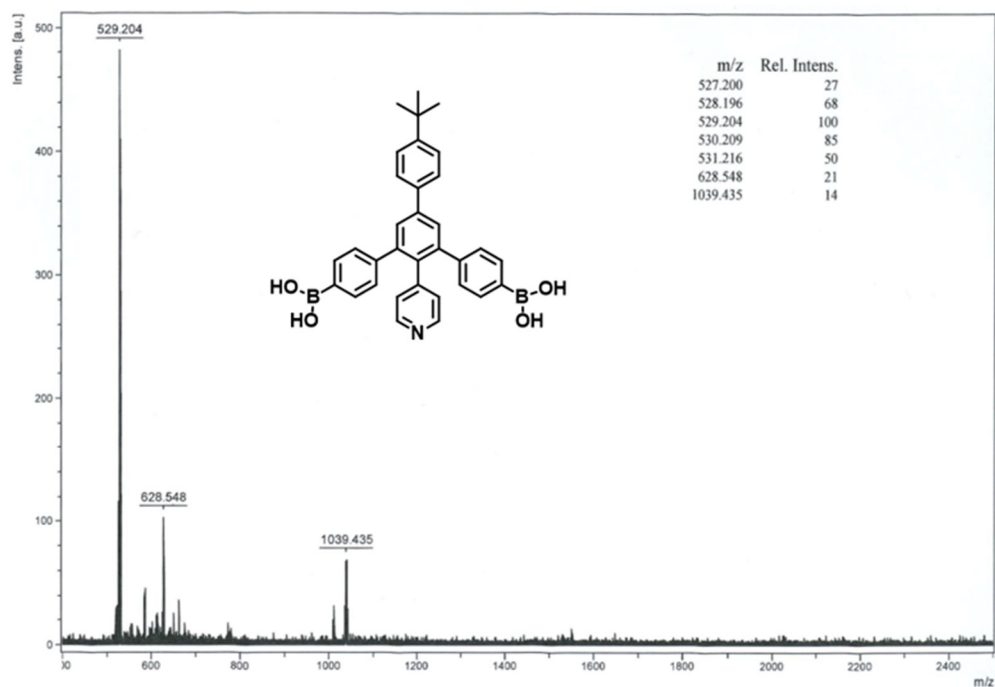
Figure A35 | MALDI-TOF mass spectrum (DCTB) of **130**.
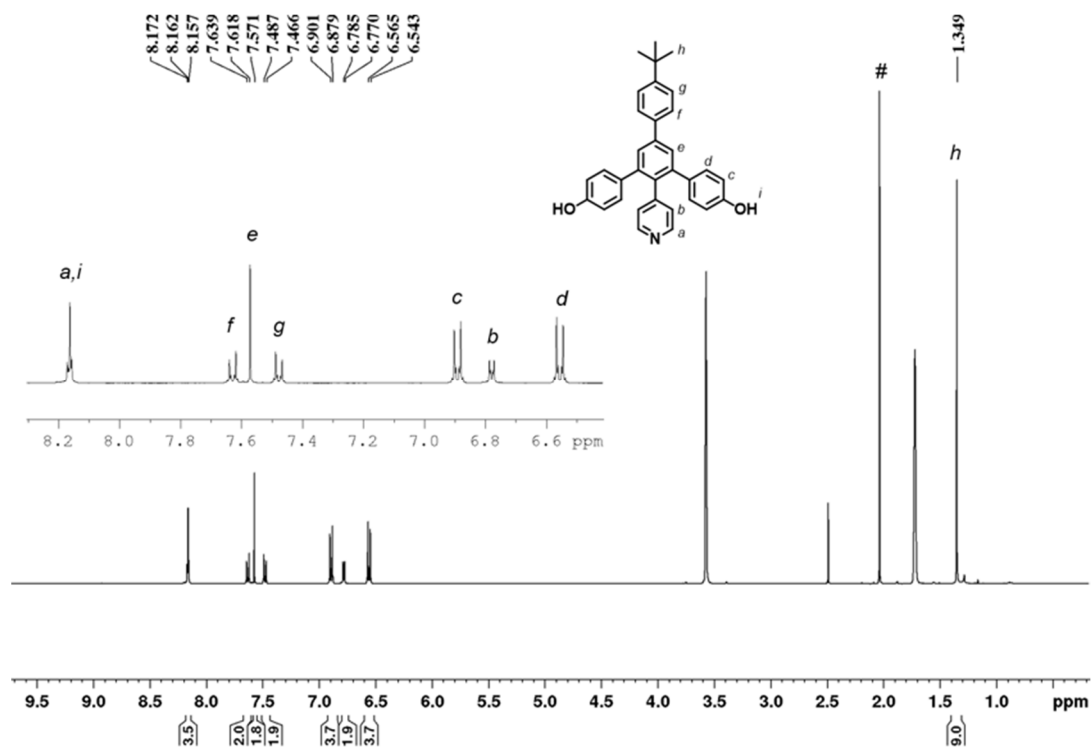
Figure A36 | ^{1}H-NMR (400 MHz, THF-d$_8$, rt) spectrum of **135**. # = acetone
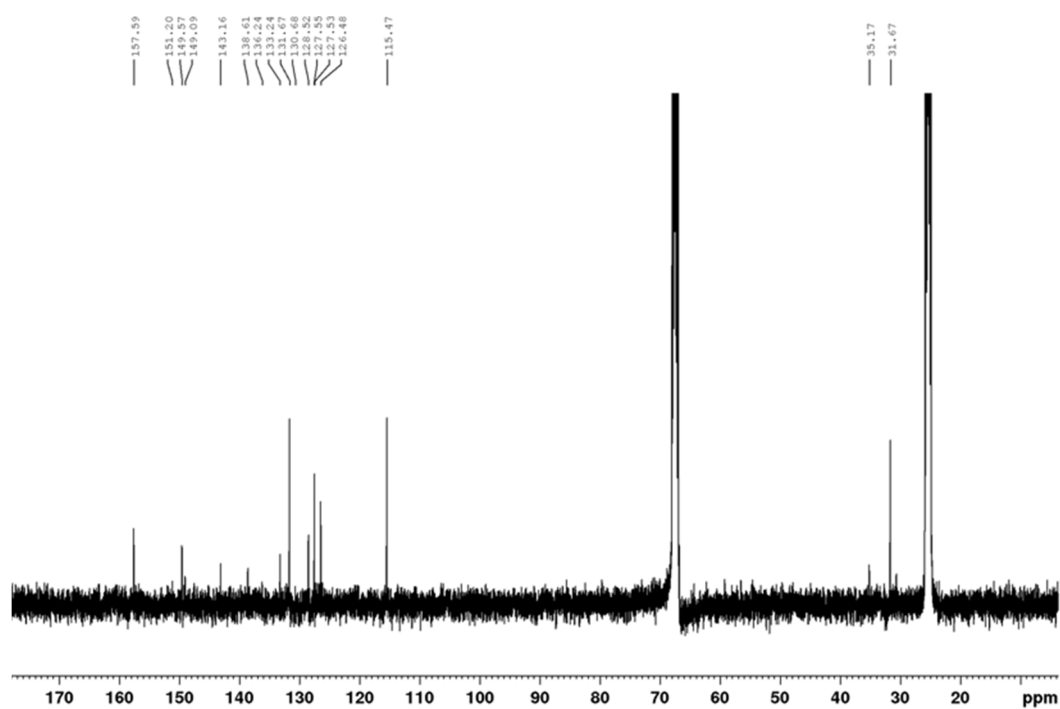
Figure A37 | ^{13}C-NMR (101 MHz, THF-d$_8$, rt) spectrum of **135**.

m/z	Rel. Intens.
471.078	7
472.152	100
472.785	9
473.193	76
474.222	27
542.191	13
598.060	6
720.237	6
722.281	16
723.301	6
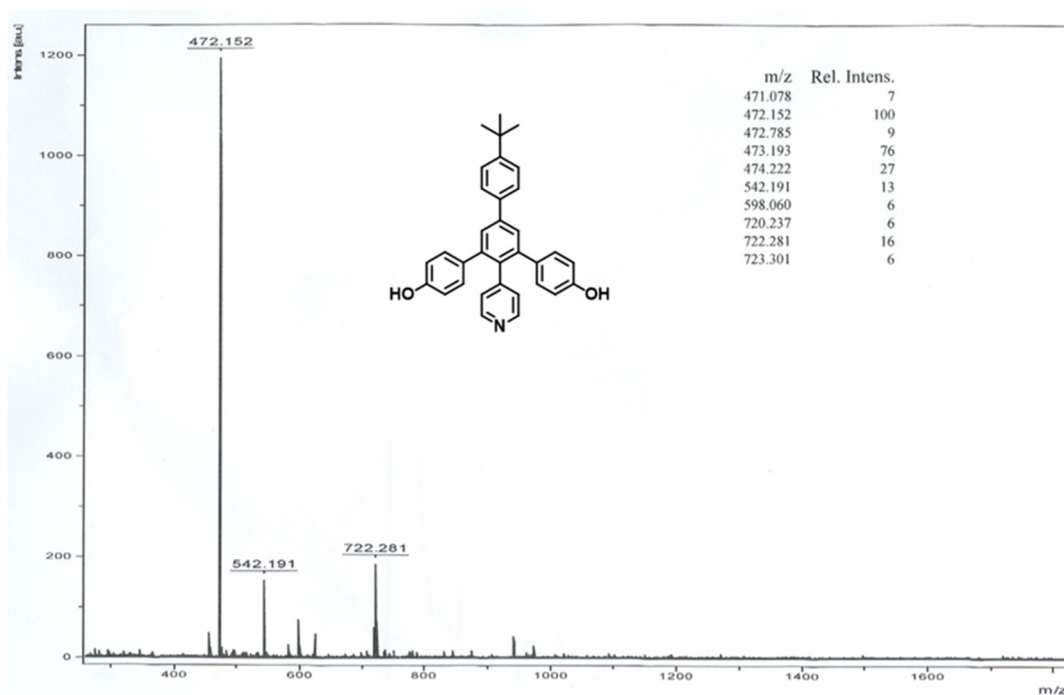
Figure A38 | MALDI-TOF mass spectrum (DCTB) of **135**.
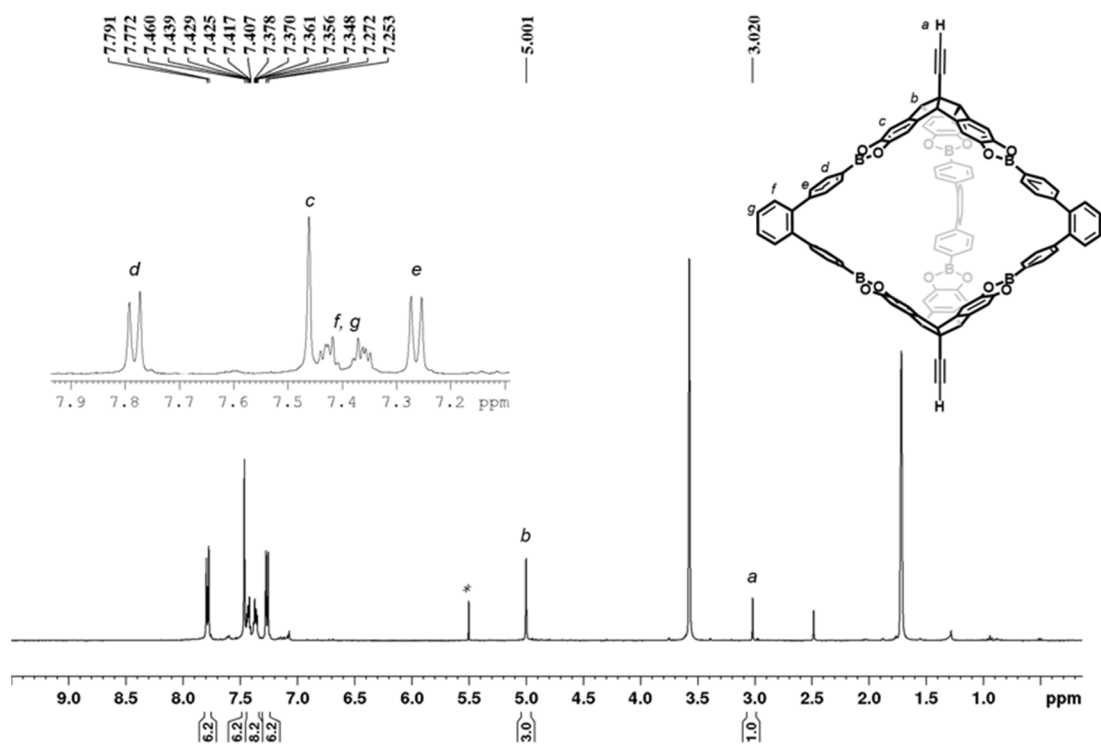
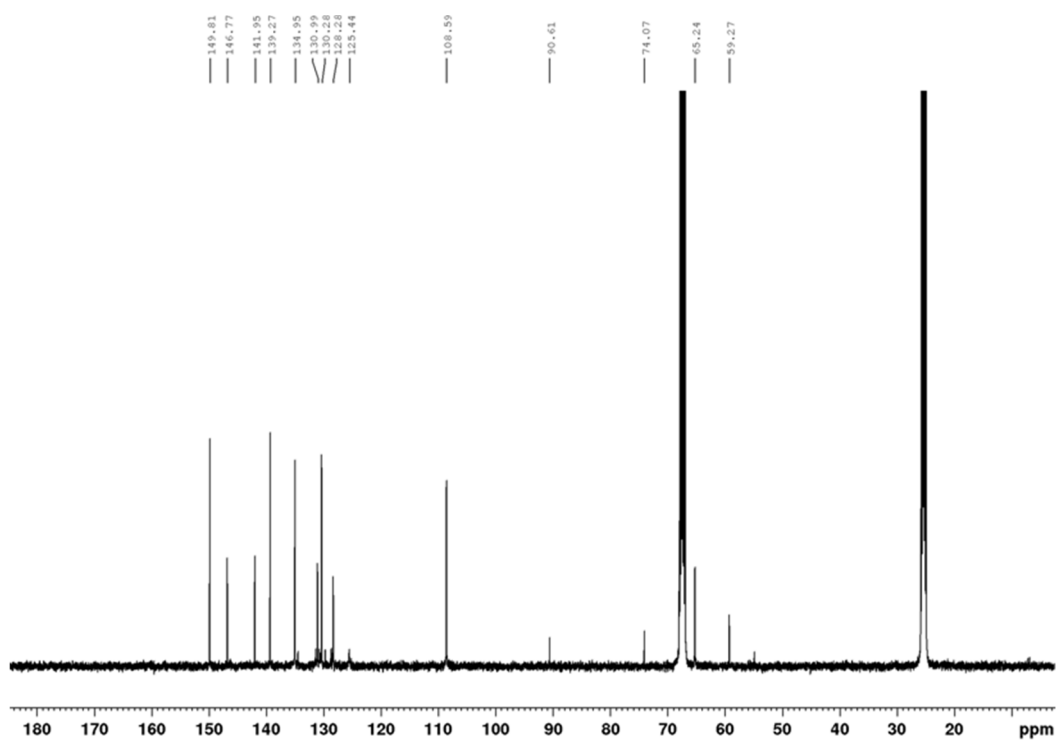**Figure A39** | ^{1}H-NMR (400 MHz, THF-d$_8$, rt) spectrum of **128**. $*$ = dichloromethane

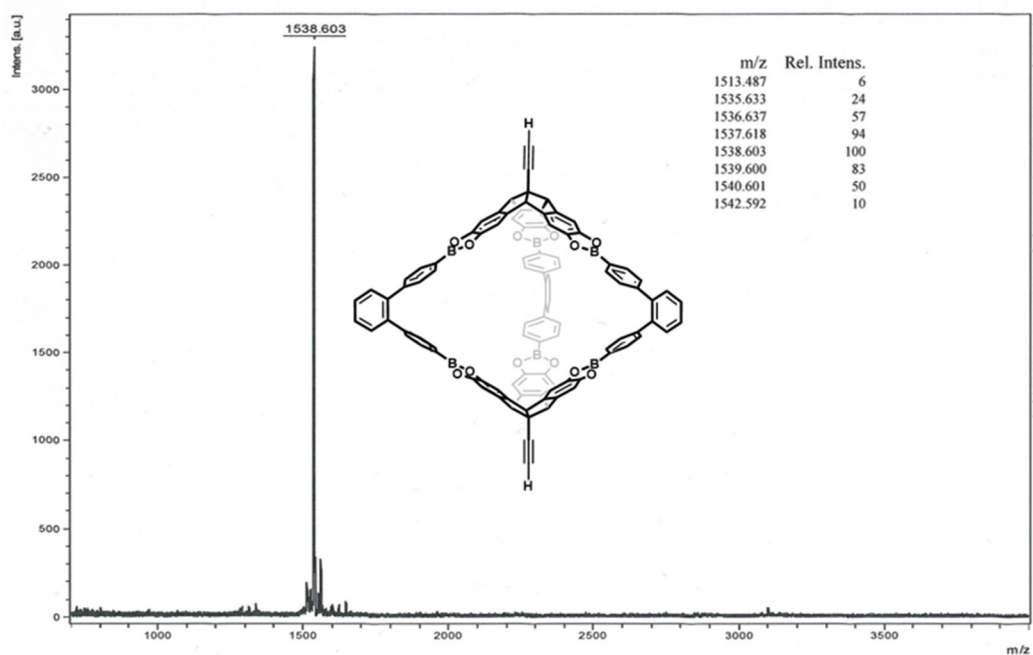**Figure A40** | ^{13}C-NMR (101 MHz, THF-d$_8$, rt) spectrum of **128**.
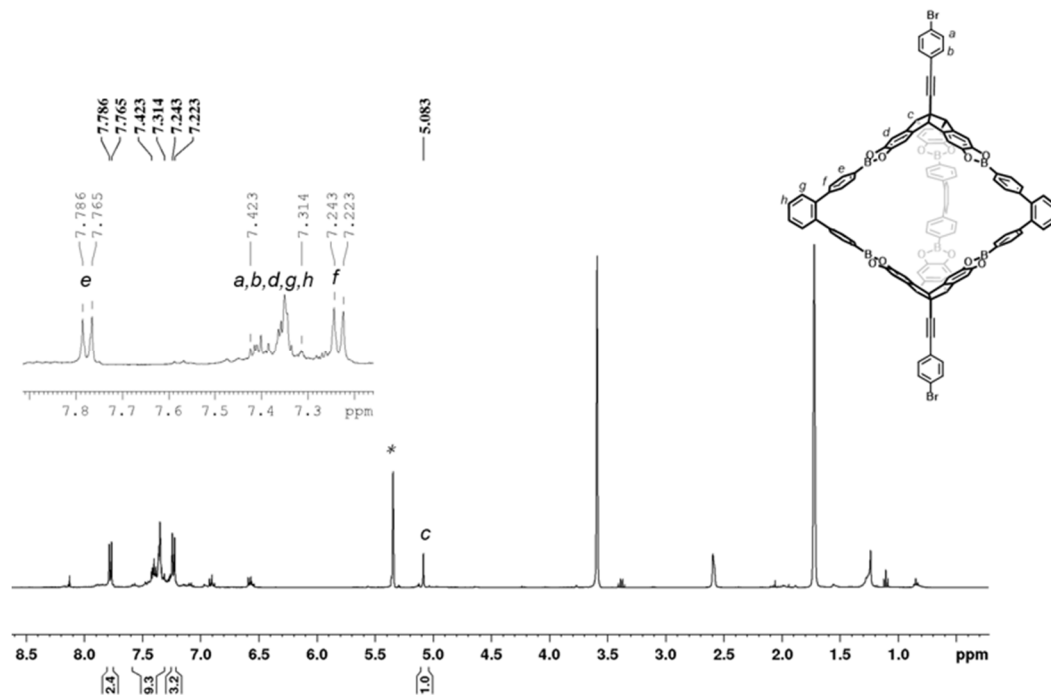
Figure A41 | MALDI-TOF mass spectrum (DCTB) of **128**.

Figure A42 | ¹H-NMR (400 MHz, THF-d₈, rt) spectrum of **129**. ∗ = residual dichloromethane peak from CD₂Cl₂
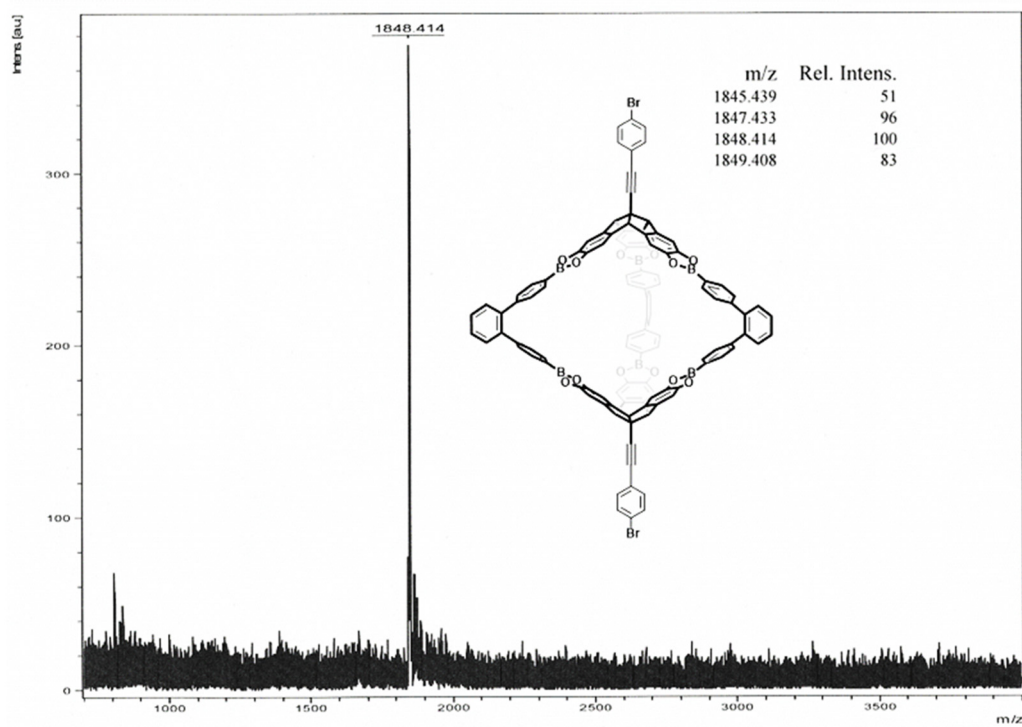
Figure A43 | MALDI-TOF mass spectrum (DCTB) of **129**.

Titration Data

^{1}H-NMR Spectroscopy

For the model system, CDCl$_3$ stock solutions of boronate ester **112** (9.89×10^{-3} M) and **111** (9.89×10^{-3} M) were prepared. Thirty ^{1}H-NMR spectra were measured varying concentration of **111**. Total volume of solution for each ^{1}H-NMR spectrum was 0.60 mL. Consecutive spectra were taken with an increment of 0.02 mL solution of **111**.
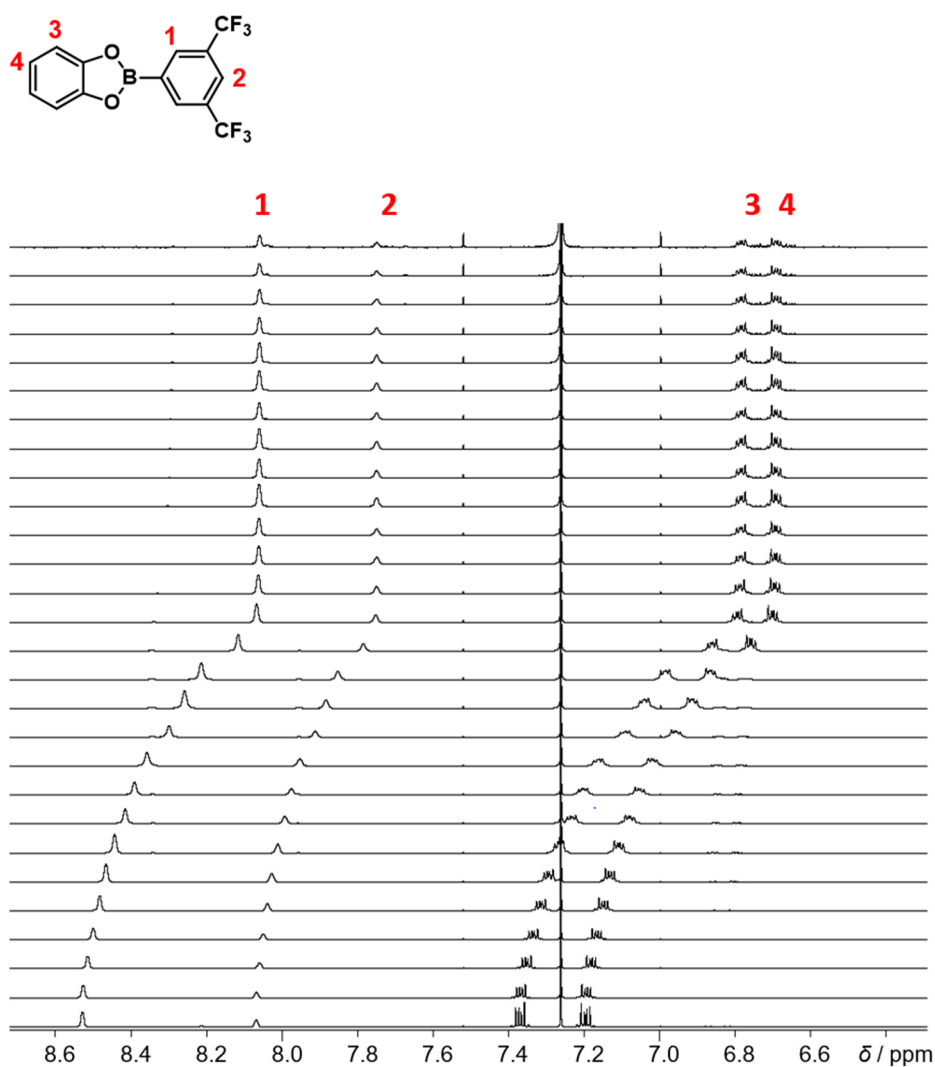
Figure A44 | ^{1}H-NMR (400 MHz, CDCl$_3$, rt) spectra for titration of boronate ester **112** with **111** (increasing from bottom to top).

For the supramolecular cage formation, CDCl₃ stock solutions of trisboronate ester **113** (1.204×10^{-3} M) and **111** (1.204×10^{-3} M) were prepared. Eleven ¹H-NMR spectra were measured varying the ratio between **113** and **111**, *e.g.* for **B2.0 D3.0** ¹H-NMR spectrum, 0.2 mL of 1.204×10^{-3} M **113** and 0.3 mL of 1.204×10^{-3} M **111** were mixed together in an NMR tube and ¹H-NMR spectrum was measured.

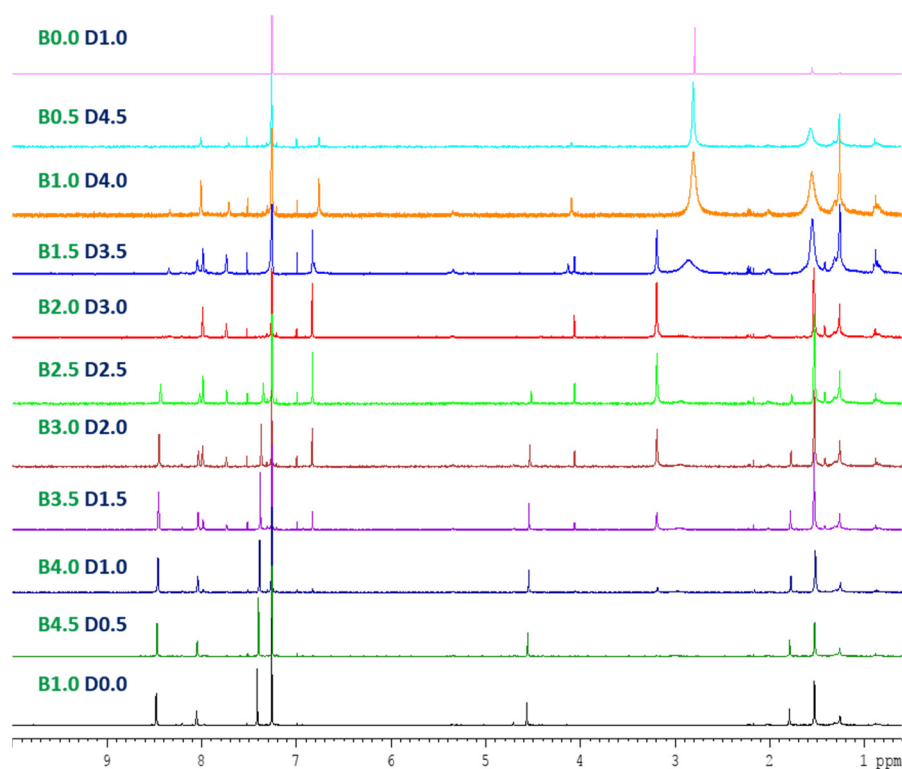| Boronate ester **113**	DABCO **111**	¹H-NMR
1.0	0.0	**B1.0 D0.0**
4.5	0.5	**B4.5 D0.5**
4.0	1.0	**B4.0 D1.0**
3.5	1.5	**B3.5 D1.5**
3.0	2.0	**B3.0 D2.0**
2.5	2.5	**B2.5 D2.5**
2.0	3.0	**B2.0 D3.0**
1.5	3.5	**B1.5 D3.5**
1.0	4.0	**B1.0 D4.0**
0.5	4.5	**B0.5 D4.5**
0.0	1.0	**B0.0 D1.0**

Figure A45 | ¹H-NMR (400 MHz, CDCl₃, rt) spectra for titration of trisboronate ester **113** with **111** (increasing from bottom to top).

Isothermal Titration Calorimetry (ITC)

ITC of model system [$(112)_n \cdot (111)$] was performed by stepwise injection of 2 µL solution of **112** (20.2 mM in CDCl$_3$) at a rate of 0.5 µL/s into the calorimeter cell containing a solution of **111** (1.43 mL, 1.08 mM in CDCl$_3$) at 293 K. The time spacing between consecutive injections was 120 seconds.

Figure A46 | Isothermal Titration Calorimetry (ITC) of model system [$(112)_n \cdot (111)$].

The formation of supramolecular cage **114** was investigated by stepwise injection of 2 µL solution of **111** (2.2244 mM in CHCl₃) at a rate of 0.5 µL/s into the calorimeter cell containing a solution of **113** (1.43 mL, 0.1033 mM in CHCl₃) at 293 K. The time spacing between consecutive injections was 100 seconds in order to achieve chemical and thermal equilibria before next injection.
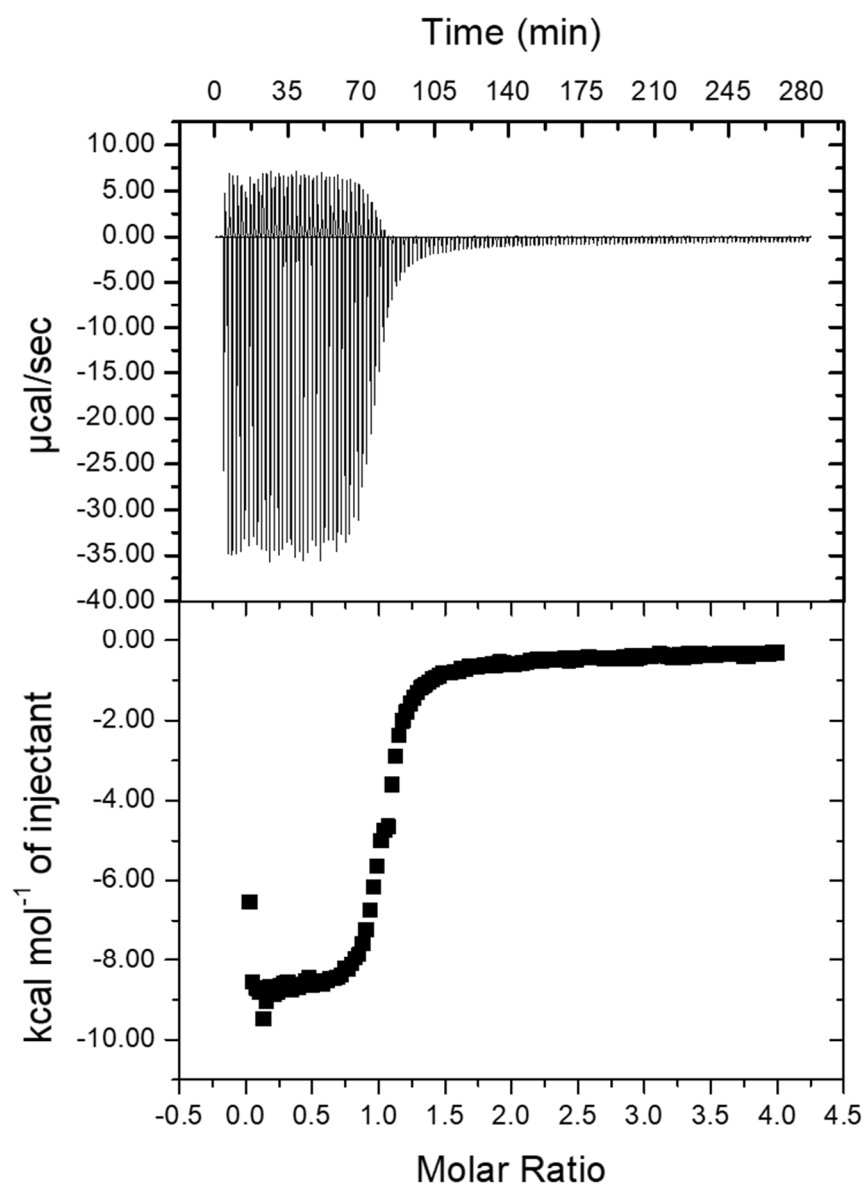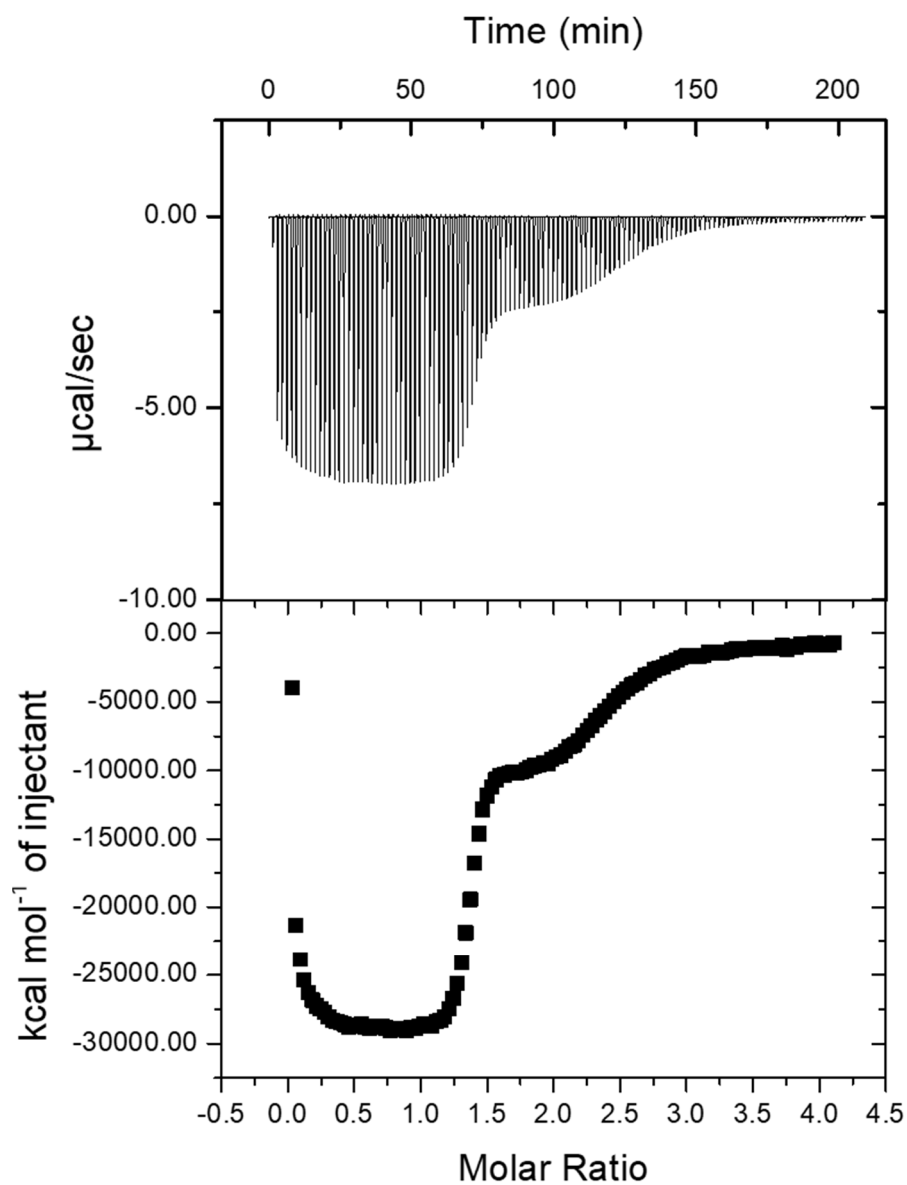

Figure A47 | Isothermal Titration Calorimetry (ITC) for supramolecular cage **114**.

Acknowledgements

First and foremost, I count myself extremely lucky to get an opportunity to work in the research group of Priv.-Doz. Dr. Florian Beuerle. I would like to thank him for his enthusiasm, guidance and for keeping his door open for any discussion throughout my PhD. I would also like to thank Prof. Dr. Frank Würthner not only for letting me share the laboratory equipment and the lab-space with his group but also for providing his support and valuable suggestions for my research projects.

I would like to acknowledge the financial support by the Fonds der Chemischen Industrie and the Collaboratory Research Network "Solar Technologies Go Hybrid" of the Bavarian Ministry of Science, Research and the Arts for funding my research projects.

I would like to express my sincere gratitude to Ana-Maria Krasue and Dr. David Schmidt for the single crystal X-ray analysis, Dr. Michael Grüne, Elfriede Ruckdeschel and Juliane Adelmann for carrying out DOSY and temperature dependent NMR measurements.

I would also like to thank Dr. Michael Büchner, Fritz Dadrich and Antje Heckmann for measuring the mass spectra, Liselotte Michels and Sabine Timmroth for performing the elemental analyses, Bernd Brunner for the IT service, all the staffs of chemical store (Engin Bala, Regina Klarmann-Röder, Bianca Lange, Mario Meckel and Joachim Wlaka), Jonathan Landeck for the glassblowing work, Christiana Toussaint, Eleonore Klaus and Anette Krug for the administrative support. I am grateful to Dr. Matthias Stolte, Dr. Chantu R. Saha-Möller and Dr. David Schmidt for their useful advice in group meetings and providing assistance to safety-related issues in the laboratory.

I am also thankful to Annike Weißenstein and Dr. Jana Gershberg for helping me get familiar with the technical details of ITC measurements. I also appreciate the synthetic support I have got from practical students (Julian, Friedrich, Ben, Joshua, Theresa and Heiko), bachelor students (Anna, Tim and Sebastian) and Lisa, a former technical staff in the Beuerle group.

I would like express my gratitude to Dr. Peter Frischmann, a former post-doc in the Würthner group who I had fruitful scientific discussions with at the start of my PhD. Those discussions spurred the idea of my first research project, *i.e.* utilizing boron-nitrogen dative bonds for the formation of supramolecular self-assemblies. I am also grateful to Prof. Dr. Linda Shimizu, a former guest professor in the Würthner group for some important suggestions especially regarding oral presentations of my research.

I have had the pleasure to interact with many bachelor, master, PhD students and post-docs of the Würthner group and the former Fernández group during my PhD. I would like to thank all of them for their help and advice in both chemistry and non-chemistry-related issues. Special thanks go to the members of the Beuerle group: Andreas, Steffi, Bappa, Lisa and Viki for their friendly assistance and keeping a nice lab atmosphere. I owe a debt of gratitude to Dr. David Bialas for thorough correction of the thesis and improving the draft immensely. I would like to thank Dr. Andreas Kraft for making some corrections of the thesis and Dr. Vincenzo Grande for providing many tips while I was writing my PhD thesis.

I also cherish the moments of social activities (such as `Stammtisch´, Saturday night-dinner) arranged by different group members which made my stay in Würzburg entertaining and enjoyable. I am very grateful to Alhama, Tobi, Eva, Jayesh, Valentin, David, Shubhendu, Debottam, Pramod and Arnab for helping me troubleshooting issues in life outside the lab and keeping my sanity intact.

Last but not least I would like to thank my parents and grandmother for their unconditional love and for always believing in me.